EVALUATION OF MECHANICAL PROPERTIES OF ENGINEERED CEMENTITIOUS COMPOSITE FOR EXTERIOR BEAM-COLUMN JOINTS UNDER REVERSED CYCLIC LOADING

SHWAN HUSSAIN SAID

THESIS SUBMITTED IN FULFILLMENT OF THE REQUIREMENT FOR THE DEGREE OF DOCTOR OF PHELOSOPHY

FACULTY OF ENGINEERING
UNIVERSITY OF MALAYA
KUALA LUMPUR

2016

UNIVERSITY OF MALAYA

ORIGINAL LITERARY WORK DECLARATION

Name of Candidate: **Shwan Hussain Said**

Registration/Matric No: **KHA110041**

Name of Degree: **Doctor of Philosophy**

Title of Thesis: **Evaluation of Mechanical Properties of Engineered Cementitious Composite for Exterior Beam-Column Joints under Reversed Cyclic Loading**

Field of Study: **Structural Engineering**

I do solemnly and sincerely declare that:

(1) I am the sole author/writer of this Work;
(2) This Work is original;
(3) Any use of any work in which copyright exists was done by way of fair dealing and for permitted purposes and any excerpt or extract from, or reference to or reproduction of any copyright work has been disclosed expressly and sufficiently and the title of the Work and its authorship have been acknowledged in this Work;
(4) I do not have any actual knowledge nor do I ought reasonably to know that the making of this work constitutes an infringement of any copyright work;
(5) I hereby assign all and every rights in the copyright to this Work to the University of Malaya ("UM"), who henceforth shall be owner of the copyright in this Work and that any reproduction or use in any form or by any means whatsoever is prohibited without the written consent of UM having been first had and obtained;
(6) I am fully aware that if in the course of making this Work I have infringed any copyright whether intentionally or otherwise, I may be subject to legal action or any other action as may be determined by UM.

Candidate's Signature Date:

Subscribed and solemnly declared before,

Witness's Signature Date:

Name:

Designation:

ABSTRACT

This thesis describes the experimental program and results of three different stages of a study. The first stage is concerned with the strength, deformation and toughness characteristics of engineered cementitious composite (ECC) slabs cast with three different polymer fibers namely polyvinyl alcohol (PVA) fibers, polypropylene (PP) fibers and polyethylene (PE) fibers. Results showed significant increase in flexural strength, ductility and toughness for both PVA and PE slabs by increasing the reinforcing index, with unpromising results for PP slabs.

The second stage of the project involved testing ECC I-shaped samples under direct tension using two different polymer fibers such as PVA and PE fibers to evaluate the direct tensile stress-strain relationship of ECC. Results showed that the cut-off point for ECC-PVA direct tension I-shaped samples occurred at reinforcing index equals to 527 while the cut-off point for ECC PE samples is apparent at the reinforcing index of 474.

The third stage includes casting and testing of fourteen full scale RC exterior beam-column joints to evaluate their performance under cyclic loading. The ECC beam-column joint showed significant improvement in the ultimate shear and moment capacities, as well as in the ductility and damage tolerance compared to the normal concrete (NC) joint. In addition, the ECC-PE beam-column joint showed an increase in the ultimate shear and moment capacities with better ductility and damage tolerance compared to ECC-PVA beam-column joint. Moreover, the usage of higher reinforcing index of fibers in ECC beam-column joint improved the ultimate shear and moment capacities with better ductility and crack propagation. Installation of one lateral steel hoop in the ECC joint zone showed noticeable improvement in the ultimate shear and moment capacities as well as in ductility and damage tolerance compared to ECC joints without steel hoops.

The shear strength factor (λ) is proposed by ACI 352R-02 to evaluate the nominal shear stress developed in the Type 2 joint. Based on the experimental results, the λ value is evaluated for all beam-column specimens in this study ranged from 1.01 to 1.36 for PVA joints, while for PE joints ranged from 1.05 to 1.67, compared to the ACI proposed value of 1.

ABSTRAK

Tesis ini memperihalkan program dan hasilkerja dari 3 tahap kajian. Kajian tahap pertama adalah berkenaan sifat kekuatan, ubahbentuk dan ketahanan papak komposit simen dijuruterakan (EEC) yang dituang dengan tiga jenis seratan polimer, iaitu seratan *'polyvinyl alcohol'* (PVA), seratan "*polypropylene'* (PP) dan seratan *'polyethylene'* (PE). Hasil ujikaji menunjukkan peningkatan kekuatan lenturan, kemuluran dan ketahanan yang bermakna, untuk kedua-dua papak dari PVA dan PE; dengan meningkatkan indeks pengkuatan, dengan hasilkerja yang sangat menggalakkan untuk papak-papak PP.

Tahap kedua projek ini adalah menguji sampel-sampel bentuk-I EEC dalam keadaan tegang terus, menggunakan dua jenis seratan polimer seperti PVA dab PE. Ini adalah untuk menilai hubungan tegasan-terikan EEC. Hasil ujikaji menunjukkan titik potong untuk sampel EEC-PVA dalam kenaan daya tegang terus berlaku pada tahap indeks pengkuatan 527, manakala titik potong untuk sampel EEC-PE dilihat pada tahap indeks pengkuatan 474.

Tahap ketiga termasuk tuangan dan ujikaji 14 skil penuh sampel konkrit bertetulang sambungan rasuk-tiang luar, untuk menilai prestasi dalam bebanan berkitar. Sambungan rasuk-tiang EEC menunjukkan peningkatan bermakna untuk ricih dan keupayaan lentur muktamad, dengan termasuk peningkatan kemuluran dan toleransi kerosakan berbanding dengan sambungan rasuk-tiang ECC-PVA. Tambahan lagi, penggunaan indeks pengkuatan serat yang tinggi bagi sambungan rasuk-tiang EEC memperbaiki ricih dan keupyaan lentur muktamad dengan menambah baik kemuluran dan peningkatan retak. Pemasangan satu gelung keluli di kawasan sambungan EEC menunjukkan peningkatan ketara pada ricih dan keupayaan lentur muktamad, termasuk

peningkatan kemuluran dan toleransi kerosakan, berbanding dengan sambungan EEC yang tidak mempunyai gelungan keluli.

Faktor kekuatan ricih (λ) adalah dicadangkan oleh ACI 352R-02, untuk menilai tegasan ricih nominal dalam sambungan Jenis -2. Berdasarkan hasil ujikaji, nilai λ didapati untuk semua sampel rasuk-tiang dalam kajian ini, adalah dalam julat 1.05 hingga 1.36 untuk PVA dan 1.05 hingga 1.67 untuk PE, berbanding dengan nilai 1.0, yang dicadangkan oleh ACI.

ACKNOWLEDGEMENT

In the name of **ALLAH**, the author praises and thanks **ALLAH** Almighty who gave him the capability and patience to finalize this research.

The author would like to express his sincere gratitude to his dear supervisors Prof. Dr. Hashim Abdul Razak and Ir. Dr. Ismail Othman for their support, assistance, and valuable guidance throughout the research. Their valuable opinions have been so useful for completing this work.

The author also would like to thank University of Malaya for providing financial support through IPPP fund and HIR research grant.

The author also expresses his thanks to the staff of Civil Engineering Department in the Faculty of Engineering for their assistance to finalize this work. They did not hesitate to provide whatever is necessary to facilitate the requirement of research.

The author

2016

TABLE OF CONTENT

LIST OF FIGURES

LIST OF TABLES

LIST OF SYMBOLS

A_g = Gross area of column section

A_{sv} = cross sectional area of joint links

B = binder (i.e. cement + fly ash)

b_c = width of the column section

$b_c^{"}$ = core dimension of tied column, outside to outside edge of the links

b_j = effective width of joint

C = internal compression force (Figure 3.19)

C_m = Portland cement

d = diameter of the fiber

d_b = the effective depth of the beam

d_c = effective depth of the column section

d_n = denier of polymer fibers

d_r = diameter of steel bars

dx = (dtex) the mass of polymer fibers in grams per 9000 meters

E_c = modulus of elasticity of concrete

E_s = modulus of elasticity of steel

f_c' = compressive strength of concrete cylinders

$\frac{f_f}{f_t}$ = flexural strength to tensile strength ratio

f_y = yield stress nof steel bars

f_{yv} = yield strength of the hoops

G = gravel (coarse aggregate)

h_b = total height of the beam section

h_c = total height of the column section

I_5, I_{10}, I_{20} ….. I_T and I_S = different kinds of toughness indices

jd_b = the distance between the internal compression and tension force resultants in the beam section

L = the distance between the acting point of applied load and the center of the joint

l = length of the fiber

l_{ch} = material characteristic length

M = the design bending moment

M_j = ultimate moment capacity of the joint

N = axial force on column

P = applied ultimate load at the acting point of the beam

$R_{S,T}$ = the residual strength factor between two indices I_T and I_S

S = sand (fine aggregate)

s_v = spacing of the hoops

T = tension force resultant

V = the design shear force

V_c = lateral shear force developed at the tip of the column

V_f = volume content of fibers

V_{jh} = ultimate shear force in the joint zone

v_{jh} = ultimate shear strength of the joint

$\propto$ and β = the angle measured between M-L and M-N directions

ϵ_1 and ϵ_2 = principal strain values in the joint zone

ϵ_a, ϵ_b and ϵ_c = strain value in L, M and N direction, respectively

$\Delta_1$and $\Delta_1^{/}$ = the elongation values on the diagonal of joint

$\Delta_2$and $\Delta_2^{/}$ = the shortness values on the opposite diagonal of the joint

ψ_1 and ψ_2 = shear rotation on the vertical and horizontal side of joint

γ = shear strength factor depends on the type of beam-column joint based on English units

γ_{sh} = total shear rotation of the joint

λ = shear strength factor depends on the type of beam-column joint based on SI units

δ = the deflection value at first crack

LIST OF ABBREVIATIONS

ACI 352R 02: Recommendations for Design of Beam-Column Connections in Monolithic Reinforced Concrete Structures

A.R: aspect ratio of the fiber

ASCE: *American Society of civil engineers*

ASTM*: American Society for Testing and Materials*

ASTM C1018: Standard Test Method for Flexural Toughness and First-Crack Strength of Fiber-Reinforced Concrete

BS: British standards

ECC: Engineered cementitious composite

E modulus: Modulus of elasticity

Eurocode: European code

FA: fly ash

FRC: fiber reinforced concrete

FRP: Fiber-reinforced polymer

GFRP: Glass fiber-reinforced polymer

GGBS: ground granulated blast-furnace slag

HPFRCC: high performance fiber reinforced cementitious composite

HSC: High-strength concrete

LVDT: linear variable differential transducer

JCI*: Japan Concrete Institute*

JSCE: Japan Society of Civil Engineers

MFS: Melamine formaldehyde sulfonate

NC: Normal concrete

NZS: New Zealand standards

PCS_m: Post cracking strength at (m) deflection value

PDDA: performance Driven Design Approach

PE: polyethylene fibers

PP: Polypropylene fibers

PVA: Poly vinyl alcohol fibers

RC: Reinforced concrete

R.I: Reinforcing index

RSGs: rosette strain gauges

SCC: Self-compacting concrete

SFRC: Steel fiber reinforced concrete

S.G: specific gravity

SP: superplasticizer

T.I: toughness index

CHAPTER 1: INTRODUCTION

1.1 High-Performance Fiber Reinforced Cementitious Composites (HPFRCC)

As reported in literature, fiber reinforced concrete (FRC) is concrete in which fibers were added to enhance its capacity in flexure, tension, shear, abrasion, fatigue, freezing and thawing cycles as well as to improve the concrete resistance against cracks, shrinkage and penetration of aggressive liquids in order to enhance its toughness and durability. In FRC, different kinds of fibers were used such as iron wires, granular iron wastes, annular steel fibers and slurry infiltrated fibers. The tensile stress-strain relationship for FRC exhibits linearity up to first crack stage; beyond this stage the curve follows softening behavior i.e. descends steadily up to failure with localized development of crack (Batson et al., 1972; A.E. Naaman, 1985; Pakotiprapha et al., 1974; Rajagopalan et al., 1974; Swamy et al., 1974).

High- performance fiber reinforced cementitious composites (HPFRCC) are the modified and recent class of FRC from which the tensile stress-strain relationship exhibits strain-hardening behavior with multiple cracking, characterized with reduced spacing and width of cracks with higher strain value (Liao et al., 2007). The maximum stress attained by HPFRCC after the first crack point is called the post-cracking strength, and is shown in Figure 1.1. This is the unique property through which the HPFRCCs can be differentiated from other types of FRC (A. E. Naaman, 2007). To prepare this kind of material, it is convenient to provide high fiber content, or fibers with high aspect ratio (V. C. Li, 2008). Krenchel & Stang (1989) showed that the HPFRCCs can be prepared using continuous aligned fibers. Reinhardt et al. (2003) demonstrated that the continuous fiber reinforcement can be prepared by using textile materials in the concrete. In the most recent years, two new types of HPFRCCs have appeared; the first is called Ductal which is characterized by high tensile strength (about

12 MPa) and a normal strain 0.02-0.06%. In contrast to Ductal, engineered cementitious composite (ECC) is the second type of HPFRCC, and it is characterized by normal tensile strength of 4-6MPa and higher ductility of 3-7% (V. C. Li, 2002).

1.2 Engineered cementitious composite (ECC)

Engineered cementitious composite (ECC), or bendable concrete, or self-healing concrete, is a class of improved HPFRCC, which was introduced in the early 90's (V. C. Li, 2008). It is characterized with a tensile strain-hardening and multiple-cracking behavior (Lepech & Li, 2008). In contrast to normal concrete, ECC has a tensile strain capacity which ranges from 3 to 7% compared to a value of 0.01% for normal concrete (V. C. Li, 2002). The tensile strength value for ECC is around 4-6MPa with compressive strength about 30-80MPa based on mix design, and compressive strain capacity of 0.4-0.65%. In order to attain an extremely high ductile ECC with the addition of small fiber content i.e. 2% or less, it is recommended to achieve the underlying principles stated thus. Firstly, elimination of the usage of coarse aggregates (Li & Kanda, 1998.) and the use of fine silica sand with maximum particle size of 200 microns (Fischer et al., 2003). Secondly, the addition of discrete short fibers having diameter of several tens of microns. Thus, filament polymeric fibers are the most suitable fibers having such a diameter.

Micromechanical material design is the most convenient approach employed to prepare high bendable composite. It is the micromechanical model employed to describe the formation of synergistic mechanical interactions between the fiber, matrix and interface, as well as to develop the microstructure of the composite (V. C. Li, 1993). These properties allow ECC to sustain tensile, flexural and shear loads as well as to enhance its ductility (V. C. Li, 2002). Its tensile stress-strain relationship is analogous to that of a ductile metal. At compression behavior, and due to the absence of coarse aggregates in ECC, the elastic stiffness would be reduced and the elastic modulus would be lesser

than that of normal concrete resulting in more strain when it attains its compressive strength. The softening tail of compressive stress-strain relationship will descend in a gradual manner more than the normal concrete that is, less inclined to achieve higher deformation. Figure 1.2 shows the difference in the behavior of compressive stress-strain relationship of the fibrous composites and normal concrete.

The ductile behavior allows ECC to create numerous closely spaced microcracks with very specific width. Due to its microcracking behavior, ECC is highly durable, that is, corrosion resistant and resistant to the penetration of aggressive liquids (Maalej & Li, 1995). ECC has the property of self-healing, whereby the unreacted cementitious particles after cracking exposed to hydration, create a cementitious product, which will extend and fill the cracks having specific widths (Minard, 2009).

There are several kinds of ECC such as lightweight ECC (Wang & Li, 2003), self-compacting ECC (Kong et al., 2003a, 2003b), sprayable ECC (shotcrete ECC) (Kim et al., 2003) and extruded ECC (Shao & Shah, 1997). Different types of applications for ECC have been implemented in Japan, Korea, Switzerland, Australia and USA in different construction works (M. Li & Li, 2012), such as repairing and retrofitting of older reinforced concrete structures (The Mitaka Dam and earth retaining wall in Japan were repaired using ECC), in shear elements exposed to cyclic loading, protectable cover for steel bars in beams against corrosion, in precast shear panels against seismic loads, in coupling beams (coupling beams were cast with ECC in GlorioRoppongi building and Nabeaure Yokohama Tower in Japan) (V. C. Li, 2006) and in the joint core of beam-column connections for sustaining large shear forces and deformations.

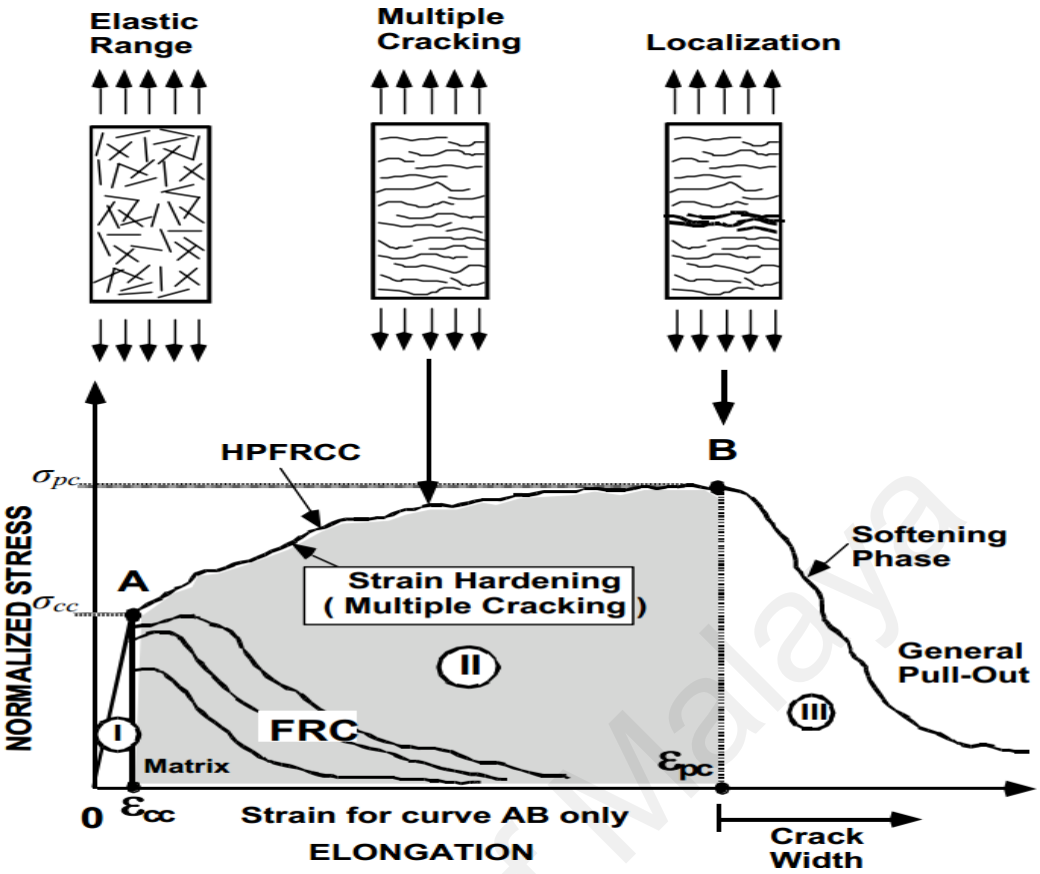

Figure 1.1: Idealized tensile stress-strain relations for FRC and HPFRCC (Naaman & Reinhardt, 1996)

1.3 Evolution of beam-column joints

Since the 1970s, structural engineers have been paying more attention to the main role of beam-column joints in reinforced concrete structures exposed to earthquake attacks. Interests emphasized on structural needs, detailing and design of beam-column joints due to the numerous wide observations of joint failure during latest earthquakes (Cheung et al., 1993).

Beam-column joint is the weakest and the most critical region in reinforced concrete structures due to its structural location of sustaining different kinds of horizontal and vertical loads, as well as redistributing and transferring the loads to the foundation. During an earthquake, if the joint zone was not detailed adequately, the beam-column joints would be the most vulnerable regions susceptible to the damage and this will lead to the collapse of the structure (Hanson & Connor, 1967; Yurdakul et al., 2013).

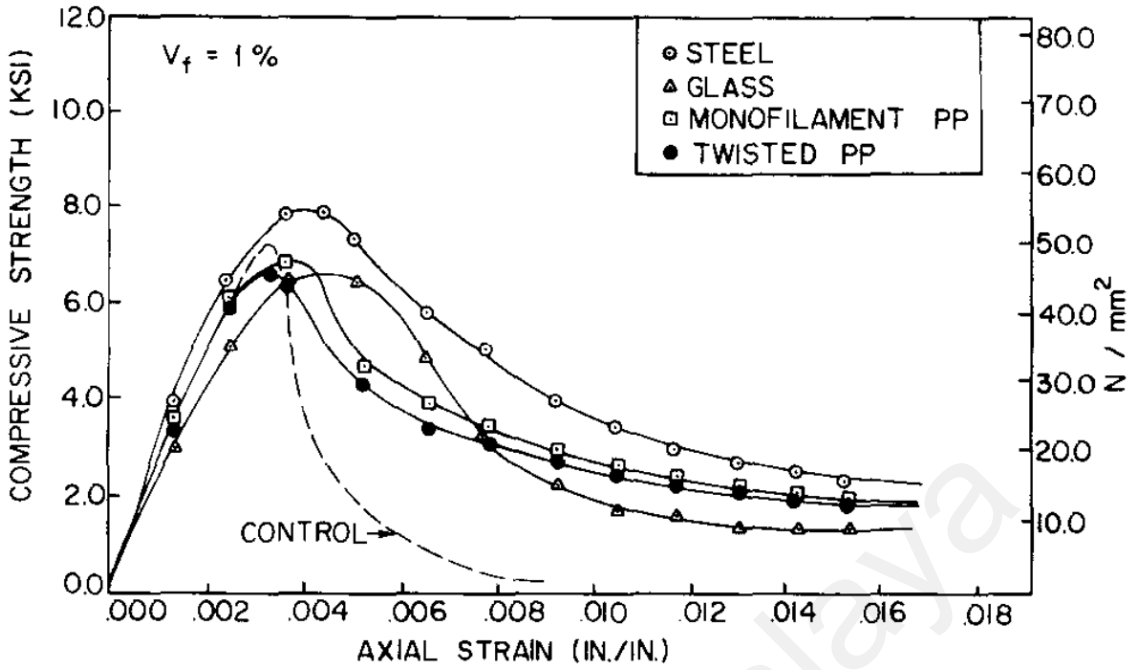

Figure 1.2: Typical stress-strain relationship for fiber reinforced mortar in compression (Fanella & Naaman, 1985)

The first research work on the seismic behavior of beam-column joints was conducted in 1967 (Hanson & Connor, 1967). Many studies in New Zealand on beam-column joints have started to emerge since 1971, especially in the University of Canterbury and Auckland (Cheung et al., 1993).

Many catastrophic earthquakes occurred worldwide, as shown in Figure 1.3, such as Mexico City earthquake in 1985, Chi-Chi earthquake in Taiwan in 1999, Kocaeli and Duzce earthquake at the Marmara region in Turkey in 1999, Wenchuan earthquake in China in 2008 and Abruzzo earthquake in Italy in 2009. As a result, collapse of several multi-story buildings occurred. For concrete structures exposed to cyclic loading such as earthquakes, they need to attain ductile behavior in beam-column joints. The majority of the structural collapses could be attributed to the negative performance of beam-column joint due to low material quality, inadequate joint detailing and lateral stiffness.

Mexico City, 1985 Kocaeli and Duzce, Turkey 1999

Chi-Chi, Taiwan, 1999

Wenchuan, China, 2008 Abruzzo, Italy, 2009

Figure 1.3: Failure of beam-column joints in different earthquakes (Engindeniz, 2008; S. Park, 2010)

The plastic hinges occurred at the end of columns and near the joints for most of the damaged buildings. Closely spaced transverse reinforcement is required to provide the adequate ductility and shear strength. However, due to reinforcement congestion within joint zone during casting of the concrete and due to lack in rheology and homogeneity,

as well as the difficulties of reinforcement placement led to defect caused by a lack of workmanship. Through the invention of FRC and HPFRCC, it was found that it is suitable to reduce the transverse reinforcement and replace the normal concrete (NC) with fibrous concrete within the joint zone and reduce all the difficulties previously mentioned. Numerous researches were carried out, and the experimental results showed that the usage of SFRC in beam-column joints could increase the shear strength and ductility, and could also be an alternative solution for minimizing the density of transverse reinforcement. However, insufficient researches were done to investigate the behavioral effect of ECC in the beam-column joint subjected to cyclic loads.

1.4 Importance of engineered cementitious composite (ECC)

The substitution of normal concrete (NC) in reinforced concrete members with ECC could improve the tensile strength, flexural strength, shear strength, deformation characteristics, ductility, energy absorption ability and toughness significantly. Due to the superior property of ECC by filling small voids, it is also intended to repair the old-damaged structures such as building, dams and retaining walls by filling the severe wide cracks. Strain-hardening property of ECC restricts the cracks from widening and thus, reduces the penetration of detrimental liquids into the structures which leads to the protection of the steel bars from corrosion.

The multiple cracking behavior of ECC effectively develops the energy absorption ability and prevents the potential of disastrous collapse of structures under anticipated catastrophes such as earthquakes (Pan et al., 2012). The ECC cracked structures can manage themselves by self-healing property of ECC, i.e. the unreacted cementitious particles can hydrate and form hardened particles that would expand and fill into the cracks. The usage of ECC would be for the structures usually exposed to seismic loading. Due to the high cost of ECCs, and to make them more economical and cost efficient, it is suggested that the ECCs would be utilized in the critical zones within the

structure such as coupling beams and beam-column joints. The main advantages of using ECC in beam-column joints can be briefly explained as follows:

1. Increase in the flexural and shear strength of the joint.
2. Increase in the bond strength between the beam longitudinal steel bars and ECC which leads to a reduction in the development lengths of longitudinal steel bars.
3. Reduction or elimination of the transverse shear reinforcement in joint zone which leads to mitigation of the congestion of reinforcement and facilitation in the casting process.
4. The ECC beam-column joints could convert the structure to extremely damage-tolerant, i.e. highly deformable structure without any sudden or brittle failure under seismic loading.
5. Increase in the toughness and ductility as well as the enhancement of the energy absorption ability.

1.5 Problem statement

Based on the points mentioned in the previous section, it is important to specify the problem statement in this thesis as follows:

1. Due to the high ductility and toughness of ECC previously mentioned, it is suitable to present a new definition for ECC material analogous to the definition stated in ASTM C1018 (Standard Test Method for Flexural Toughness and First-Crack Strength of Fiber-Reinforced Concrete) of fibrous concrete by casting and testing small ECC slabs under flexural loading.

2. The production of ECC is successfully based on the microstructure requirements of its components to achieve the micromechanical considerations such as the synergistic tailoring of the mechanical interactions between polymeric fiber, cementitious matrix and interfacial surface. The achievement of the conditions above leads to attain the

main definition of strain-hardening under direct tension test. The past studies on ECC are lacking the exact amount of polymer fibers to produce ECC. To attain this definition, it is necessary to identify the exact polymer fiber content in ECC (or identify the reinforcing index of the incorporated polymer fibers).

3. Beam-column joint is the most critical region in the reinforced concrete strictures. During earthquake attack, the beam-column joints would be the most first vulnerable regions susceptible to the damage. Consequently, the transverse reinforcement is required to provide the adequate ductility and shear strength in the joint zone. However, due to the reinforcement congestion within joint zone, the concrete mix encounters lack in rheology and homogeneity. Therefore, it is suitable to reduce the transverse reinforcement and replace the conventional concrete by fibrous concrete such as steel fiber reinforced concrete (SFRC).

Many researches and experimental works have been conducted using SFRC in the beam-column joints. On the other hand, the application of SFRC in beam-column joints led to several problems such as lack in rheology and homogeneity and the balling phenomenon of steel fibers observed during the mixing process, in case of extra fibers addition. Moreover, many difficulties encountered to produce SFRC with strain-hardening behavior.

Attempts by researchers focused on finding a new soft cementitious material as promising alternative to the SFRC characterized by the strain-hardening behavior using appropriate amount of fibers. Eventually, the ECC was identified as an appropriate alternative which serves in solving many difficulties of applying SFRC. However, the application of ECC in beam–column joints has not been extensively studied.

For all the points stated above, this thesis will address these points within an extensive program of experimental work.

1.6 Objectives

The proposed thesis aims at attaining the following objectives:

1. To determine the effective type of fiber for producing engineered cementitious composites with improved capacity, ductility and toughness

2. Evaluating the direct tensile stress-strain relationship for ECC using two kinds of polymer fibers and identifying the cut-off point of ECC based on the basic definition of ECC, by evaluating the strain-hardening behavior of ECC mixtures using different reinforcing indices.

3. To evaluate the structural performance in terms of failure modes, crack propagation, capacity and deformation of ECC beam-column joint.
4. Estimating the energy absorption ability and stiffness degradation of beam-column joint to identify the ductility and damage tolerance of the joint.
5. Evaluating the shear strength factor (λ) for beam-column joint, based on the experimental results, using the equation proposed by the ACI 352R-02 to evaluate the nominal shear stresses developed in the Type 2 joint zone.

1.7 Scope of work

This thesis focuses on three experimental studies. Firstly, a study was conducted to evaluate the flexural strength and deformation characteristics, and toughness indices of twenty-one ECC slabs. Moreover, it is convenient to identify the active kinds of polymer fibers which are successfully able to produce ECC with strain hardening behavior. Three different polymer fibers which are PVA, PE and polypropylene fibers, with two different aspect ratios for each of PVA and PE fibers, and one aspect ratio for (PP) fibers were used in this study. For each aspect ratio, five fiber volume contents were used. Secondly, a study was conducted to evaluate the direct tensile behavior of sixteen I-shaped ECC specimens. Two kinds of fibers which are PVA and PE fibers,

with two different aspect ratios for each kind of fibers were used in this study. For each aspect ratio, four fiber volume contents were used. This stage is considerably substantial to determine the fiber content (or the reinforcing index value) sufficient to produce the ECC which attains the basic definition of high performance fiber reinforced cementitious composites (HPFRCC). This stage is considered as a preparatory work for the third stage which is fundamental for this study.

Thirdly, based on the findings from the previous study, full-scale exterior beam–column joint specimens were cast and prepared for the main experimental study conducted to evaluate the performance of reinforced concrete exterior ECC beam-column joints under reversed cyclic loading. Two beam-column joint specimens were prepared for testing using normal concrete (NC), with and without lateral steel hoops.

The NC specimen with lateral steel hoops was designed according to the seismic requirements provided in the ACI 352R-02 (352R-02, 2002). In addition, the same kind of fibers and aspect ratios as in the second study were used with four reinforcing indices for each kind of fibers to prepare eight ECC beam-column joint specimens without any lateral steel hoops in the joint zone. Regarding the inclusion of lateral steel hoops in the joint zone, two ECC beam-column joint specimens were prepared (by fixing the fiber content and aspect ratio) from each kind of fibers including one hoop and two hoops in the joint zone, respectively.

The study of beam-column joint is based on the following parameters:

a. The inclusion of ECC in the joint zone
b. Type of fiber: two types of polymer fibers, polyvinyl alcohol (PVA) and polyethylene (PE) are used in the third-stage study.
c. Reinforcing index of polymer fibers.
d. The inclusion of lateral steel reinforcement (or hoops) in NC joint zone
e. The inclusion and amount of lateral steel hoops in ECC joint zone.

1.8 Thesis layout

An extensive experimental work, a mathematical analysis, and a Microsoft Excel program were implemented to attain the main objectives of this study.

The work in this thesis was presented in five chapters:

Chapter one includes a general introduction, definition and evolution of FRC, HPFRCCs, importance of ECC, problem statement, objectives and scope of study.

Chapter two includes a review on literature regarding the properties, production and evolution of ECC, review on the main parameters affecting the exterior beam-column joints, review on beam-column joints with normal concrete, with steel fibrous concrete, or with engineered cementitious composite, with or without lateral steel hoops.

Chapter three includes the full detail of the experimental program of three stages. The chapter also includes material properties, table of parameters, mix proportions, mixing process, setup details, testing process and illustrative images for each stage of work.

Chapter four includes the results displayed such as comparing among the curves and among values in tables commencing from the first stage until the end of third stage and the relation between the stages. Also, it includes a clear discussion for each plotted curve or table.

Chapter five includes the most important conclusions obtained from the thesis results, novelties and contribution, and suggestions for future studies.

CHAPTER 2: LITERATURE REVIEW

2.1 Introduction

This chapter includes two types of previous studies, the first study is relevant to the mechanical properties, micromechanical behavior and mix design of engineered cementitious composites (ECC); the second study is relevant to the parameters influencing the strength and deformation characteristics of exterior beam-column joints as well as different approaches proposed by the authors to evaluate the shear stresses developed at the exterior beam-column joints under seismic or cyclic loading.

2.2 Properties and applications of engineered cementitious composites (ECC)

An experimental work was carried out by Ward & Li (1991) to investigate the effect of beam size and fiber contents on the flexural load-deflection curve of mortar reinforced with steel or synthetic fibers. Several flexural parameters were introduced in this study to describe the brittleness of material such as material characteristic length (l_{ch}) and flexural strength to tensile strength ratio (f_f/f_t). The results showed that as the l_{ch} or f_f/f_t gets higher and the depth of beam gets lower, the mortar becomes more ductile. Furthermore, for higher fibers content, higher flexural strength and energy absorption were obtained. However, the flexural strength decreases when the depth of beam increases.

Balaguru et al. (1992) conducted an experimental study to evaluate the flexural toughness of steel fiber reinforced concrete (SFRC). Results showed that the indices at higher deflection, such as I_{50} and I_{100} are good indicators and should be computed for the evaluation of FRC. Hooked-end fibers with fiber content in the range of 0.385 to 0.77% are adequate for presenting better toughness and ductility, whereas the length of fibers ranging from 30 to 60 mm does not influence the toughness. In order to improve the toughness in high strength concrete, higher fiber content is therefore required. Also,

1.54% of steel fibers are needed in mix containing 20% silica fume to obtain significant ductility.

An analytical model has been proposed by Maalej & Li (1994) to predict the flexural strength of fiber cementitious composites. The dominant factors in this model are the mechanical parameters of fiber composite and specimen geometry. Good agreement has been attained between the predicted model and the experimental data obtained from literature.

Banthia & Trottier (1995) discussed the disadvantages of the existing procedures of evaluating the flexural toughness of FRC. The researchers discussed in particular, the ASTM procedure with focus on the difficulty of accuracy in locating the first-crack point, and the acquisition of an inaccurate computation of the first crack area. The researchers also examined the JSCE procedure and concluded that such approach must compute the area till the deflection value of span/150 is achieved. This value is arbitrary and is not selected according to the serviceability limitations. A technique of evaluating the flexural toughness of FRC by calculating the post cracking strength values (PCS_m) at any selected deflection value was then proposed. This introduced technique specifies the peak load point on the load–deflection curve instead of determining the first-crack point.

Maalej & Li (1995) produced an improved design for the durability of reinforced concrete flexural members using ECC. With ECC, the crack widths under service loads of reinforced concrete members can be limited to extremely specific values. Moreover, ECC can prevent liquids from penetrating into the concrete and reinforcements.

Shao & Shah (1997) explored the mechanical properties of PVA fiber reinforced cement composites fabricated by extrusion process and revealed that higher fiber content, larger aspect ratio, and greater cement contents induce higher flexural strength, larger deflection at ultimate load, and higher elastic modulus.

Li, V. C. (1998) presented several application studies on ECCs in the University of Michigan, USA. They involved the use of ECCs in shear structural elements under seismic loading, such as in beam–column connection, retrofitting of shear wall, as a protection cover against corrosion for steel bars in beams, and as a rehabilitation material in structural frames.

Li, V. C. (1998) pointed to a study presented by Mishra, (1995) which interested in the use of ECC in the plastic hinging zone which is subjected to seismic hysteresis loops. Results indicate that the ECC hinging zone using polyethylene (PE) fibers, exhibits energy absorption capacity of about 2.8 times of the normal concrete. The failure commences inside the hinging zone due to the reduced first crack strength of ECC. Finally, the study recommends that ECC is a promising material and that it is possible to use it in structures exposed to earthquake attacks.

A paper was submitted by Kamada & Li (2000) which addresses the preparation of interfacial surface between ECC layer and concrete substrate. In order to prevent the delamination or spalling in the interfacial zone of ECC and substrate concrete, experimental results revealed that the smooth surfaces are more effective than the rough surfaces to maintain a durable and intact structure. In contrast, (M. Li & Li, 2006) proved by experimental tests that ECC generates a poor bond with smooth surfaces due to the high fly ash content within its ingredients which produce lower chemical bond with concrete substrate. In addition, surface preparation is necessary by deep roughening on the concrete substrate surface and applying a thin layer of cement bond slurry on the roughened surface before the ECC casting.

Li, V. C. (2002) reviewed several researches in ECC. It is indicated that the superior ductility of ECC is accomplished by improving the microstructure of the composite taking into account the micromechanical considerations such as the synergistic tailoring of the mechanical interactions between polymeric fiber, cementitious matrix and

interfacial surface. Based on the micromechanical requirements, it is necessary to provide fibers with diameter less than 50 μm to perform strain-hardening behavior with small fiber volume content. There is a potential for manufacturing the steel fibers with such diameter but it became excessively expensive. In addition, the review study showed superior characteristics of ECC in damage tolerance, shear strength capacity, energy dispersion capacity, high durability due to crack width control, resistance to delamination and spalling and high deformability.

Li & Wang (2002) conducted a study to highlight the flexural behavior of ECC beams reinforced with glass fiber-reinforced polymer (GFRP). Results showed that using the same reinforcement details, ECC beams demonstrated an increase in ductility, deformation, flexural strength, shear resistance, and damage tolerance compared to high-strength concrete (HSC) beams. In addition, ECC beams without stirrups, exhibit higher shear resistance than HSC beams having shear reinforcements.

Fischer & Li (2002) studied the deformation behavior of steel reinforced ECC flexural members under reversed cyclic loading conditions. Based on the results of their investigation, the researchers posited that the ECC matrix itself cannot enhance the flexural strength and energy absorption capacity of such steel reinforced concrete member. Nevertheless, the synergistic interaction between the steel reinforcement and ductile ECC exhibits excessive energy absorption and flexural strength ability. The use of stirrup reinforcement may also be reduced because of the high shear capacity of ECC matrix and its high resistance against spalling after crack localization.

Li, V. C. (2003) made mention of the production cost of ECC. The additional cost of ECC is embodied in the use of polymer fibers, such as PVA, and the higher cement content. Polymer fibers are more expensive than steel fibers per unit weight. However, the specific density of polymer fibers is about six or seven times lower than that of steel fibers and the fiber amount added to the mixture is by volume not by weight to attain

the performance of cementitious composite. Additionally, the replacement of a part of cement content with fly ash also reduces the cost of ECC. Moreover, lowering the construction costs such as minimizing or eliminating shear reinforcement in structural constructions using ECC is coupled with the reduction of workers. Finally, the superior ductility of ECC increases the service life of structures and reduces the maintenance costs.

Fischer et al. (2003) believed that high performance fiber reinforced cement composites (HPFRCCs) with enhanced mechanical properties in terms of tensile strength and strain capacity typically necessitate moderate or high fiber volume fractions (>1%). The researchers showed that the micromechanics-based design framework for hardened ECC provides an upper limit for the maximum particles size of solids incorporated in the composite of d_{max}=200 μm while a lower limit for the PVA fiber volume fraction is V_f=2% to achieve strain hardening and multiple cracking behavior of ECC in the hardened state.

An experimental work was achieved by Kong et al. (2003a) for producing self-consolidating ECC-PVA which exhibits tensile strain-hardening behavior in the hardened state while maintaining self–consolidating properties in the fresh state. The rheological design approach is adopted to control the aggregation between cement particles and sedimentation behavior with a combination of a strong polyelectrolyte of melamine formaldehyde sulfonate (MFS) and non-ionic polymer. The authors suggested an effective formulation approach of fresh sedimentation mix to maximize its fluidity without segregation. With using V_f =2%, the results exhibited tensile strain up to 5%.

Fischer & Li (2003) conducted an experimental study on flexural load–deflection behavior of fiber-reinforced polymer (FRP), and reinforced ECC PVA members under reversed cyclic loading conditions. Results indicated that the interaction of elastic FRP reinforcement and ECC with ductile behavior leads to nonlinear elastic behavior of

load–deflection curve. Furthermore, compatible deformation between reinforcement and ECC results in high interfacial bond, removal of interfacial bond stress, elimination of relative interfacial slip and the prohibition of the composite failure by bond splitting and spalling of ECC cover. Finally, FRP reinforced ECC members did not possess meaningful energy absorption capacity compared to the conventional steel reinforced members.

Lepech & Li (2008) clarify, that the usage of only a small volume fraction PVA fibers (approximately 2%) has led to tight crack width and has reduced the weak planes due to the interaction between the fibers and cementitious matrix, which can be custom-tailored for micromechanics design. Essentially, the fibers create many microcracks with a very specific width, rather than a few large cracks (as in conventional concrete), which allows ECC to deform without disastrous failure.

Minard (2009) explained that the microcracking behavior of ECC leads to superior corrosion resistance due to the creation of small and numerous cracks that is difficult for aggressive liquids to penetrate and attack the reinforcing steel bars. The researchers demonstrated the concept of self-healing, that is, in the presence of water molecules, unreacted cement particles recently exposed to hydration reactions, and forming a number of hydrated products which expand and fill in the crack. In addition to preventing the transport of fluids, the mechanical properties of composite are regained.

Rathod et al. (2010) conducted a comparative study to evaluate the mechanical properties of Recon (polymer) and steel fiber reinforced ECC under tension, compression, shear, impact and flexure loads. Results obtained from experiments show that recon fibers give superior deformation performance under different types of loading with moderate strength enhancement. On the other hand, steel fibers are found to enhance the strength of ECC under all types of loading, but fail to provide the required deformation.

Neela (2010) investigated the flexural behavior of ballast FRP bar reinforced concrete members with polypropylene fibers. Results showed that the addition of PP fibers leads to an increase in shear strength, toughness, and compressive strain. The results also showed a reduction in compressive strength, deflection and the ductility of PP reinforced slabs. The amount of energy absorption for concrete slabs reinforced with PP fibers is equal to that of slabs without fibers.

Sravana et al. (2010) assessed the flexural behavior of glass filament fiber-reinforced self-compacting concrete (SCC) slabs. The results of their investigation showed that the inclusion of glass fibers in SCC did not improve the flexural strength of slabs. Moreover, microcracking was not observed in the slabs.

Singh et al. (2010) conducted an experimental study to investigate the effects of steel–polypropylene hybrid fibers on the compressive and flexural strengths and toughness of hybrid fiber reinforced concrete. The toughness was evaluated by applying different procedures, such as ASTM C1018, JCI, ASTM 1609/C 1609 M, and PCS_m technique. The results of the tests revealed that the best performance of all mechanical property tests was in proportion with hybrid fibers of 75%steel and 25% polypropylene, which is the most promising proportion. Such proportion performed a maximum increase in compressive and flexural strengths of 18% and 80%, respectively, over the plain concrete, and this proportion also achieved the highest flexural toughness results with all the procedures which are considered.

Pan et al. (2012) investigated the effect of mix proportion on flexural toughness of ECC with PVA fibers. The results indicated that the increment in water reducer results in reduced flexural capacity and toughness. Besides, the increase in fiber content should be over 2% in order to be able to develop a significant increase in flexural ductility and toughness due to the bridging of cracks. Moreover, higher amount of sand leads to

reduced ductility and toughness. Thus, the best ratio of sand to be used in ECC to obtain better flexural toughness and ductility is 0.2.

An experimental study made by Chen et al. (2013) to investigate the effect of ground granulated blast-furnace slag (GGBS) on the quasi-static compressive strength and dynamic load-carrying capacity of engineered cementitious composite ECC is presented. The GGBS was used as partial replacement for the fly ash (FA) in ECC with different levels. Results indicated that the quasi-static compressive strength and elastic modulus of GGBS-ECC decreased with the increase of GGBS content. The peak strain slightly increased with the increase of GGBS content indicating better ductility. In addition, it is revealed that the quasi-static compressive strength of GGBS-ECC was higher than that of ECC with fly ash. All GGBS-ECC samples indicated strain-hardening behavior in direct tensile test with strain capacity ranging between 1.5% and 2.7% which is lower than that for ECC with fly ash. Finally, as the replacement of fly ash with GGBS in ECC matrix improves the bearing capacity, it affects the ductility in a negative trend.

2.3 Parameters affecting reinforced concrete (RC) exterior beam-column joints

2.3.1 Headed reinforcement

Wallace (1997) and Wallace et al. (1998) presented an experimental work to evaluate the seismic behavior of reinforced concrete exterior beam-column joints under cyclic loading using headed reinforcement instead of 90 degrees standard hooks, as shown in Figure 2.1. Results showed that the specimens with headed bars improved the seismic performance of the joint as compared to the standard hooks due to the increased bond and mechanical strength developed between the surrounding concrete and headed reinforcement. In addition, the use of headed reinforcement leads to easier construction and minimum anchorage length of $12d_b$ embedded into the joint core. Moreover, it was found that the headed reinforcement in tension provided at least 4 times of the standard

hooked bar area. Chutarat & Aboutaha (2003) presented an experimental investigation on exterior beam-column joint specimens under seismic loading for transferring the location of plastic hinge away from column face by using headed bars within the joint zone. Results observed indicated that the use of headed bars to move the plastic hinge away from the face of column was successfully achieved. However, the joint must be detailed adequately to enhance its shear strength and thus, the headed bars would be capable of shifting the plastic hinge away from column face.

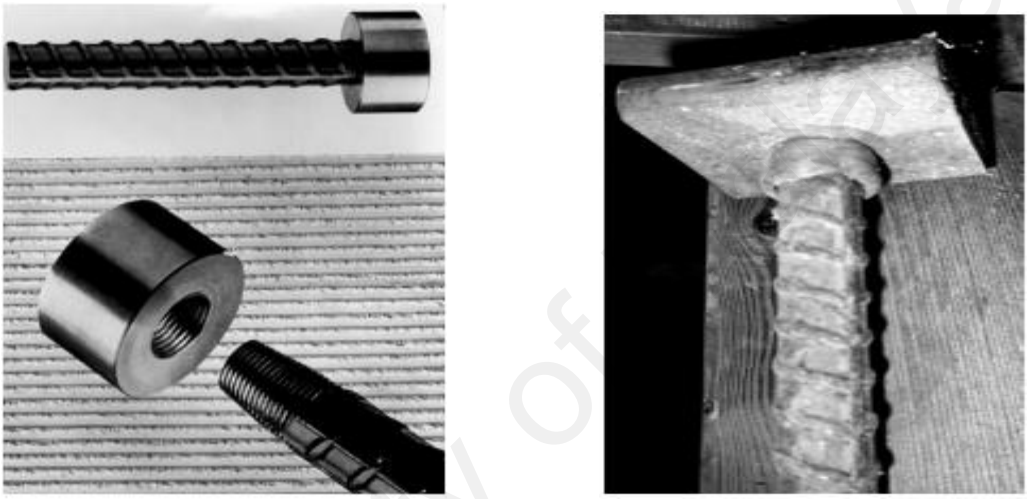

(a) (b)

Figure 2.1: Types of headed reinforcement used in beam-column joints (Wallace, 1997) and (Wallace et al., 1998)

2.3.2 Transverse shear reinforcement

Many researches were conducted to investigate the importance of transverse shear reinforcement (it may also be called hoops or links or stirrups) installed in beam-column joints.

Megget & Park (1971) conducted an experimental study to investigate the behavior of reinforced concrete exterior beam-column joints under seismic loading with low axial load on column. Results showed that the amount of steel hoops according to ACI code was insufficient to maintain the joint region intact during intense cyclic deformations caused by seismic motions due to inadequate amount of strength provided to resist the

shear force transferred across the joint as well as poor concrete confinement in joint core which leads to the rupture caused by cracking.

Fujii & Morita (1991) presented an experimental study to compare between the behavior of interior and exterior reinforced concrete beam-column joints under cyclic loading. Results revealed that the increase in amount of joint hoops did not improve the performance of both joints.

Bakir & Boduroglu (2002) conducted parametric studies on cyclically loaded exterior beam-column joints. The authors found that as the cyclic number of loading increases, the strain in the stirrups also increases.

An experimental investigation was presented by Tsonos et al. (1992) to study the seismic behavior and resistance of 20 exterior reinforced concrete beam-column joints tested under cyclic loading and reinforced with inclined bars. The beam-column prototypes were grouped into sets, each set consists of a specimen with conventionally reinforced joint i.e. without inclined reinforcing bars, and a specimen with joint reinforced with crossed inclined reinforcing bars as displayed in Figure 2.2. Results showed that the joints reinforced with crossed inclined bars possess higher strength, less deterioration at reaching the maximum capacity and higher ability of energy absorption than the conventionally reinforced joints. In addition, joints with inclined bars sustained horizontal shear stresses higher than those recommended in ACI committee R352. In contrast, the conventionally reinforced joints do not sustain shear stresses more than the ones which are recommended in ACI committee R352 (352R-02, 2002). Moreover, the inclusion of inclined steel bars presents a modern way for analyzing shear transfer.

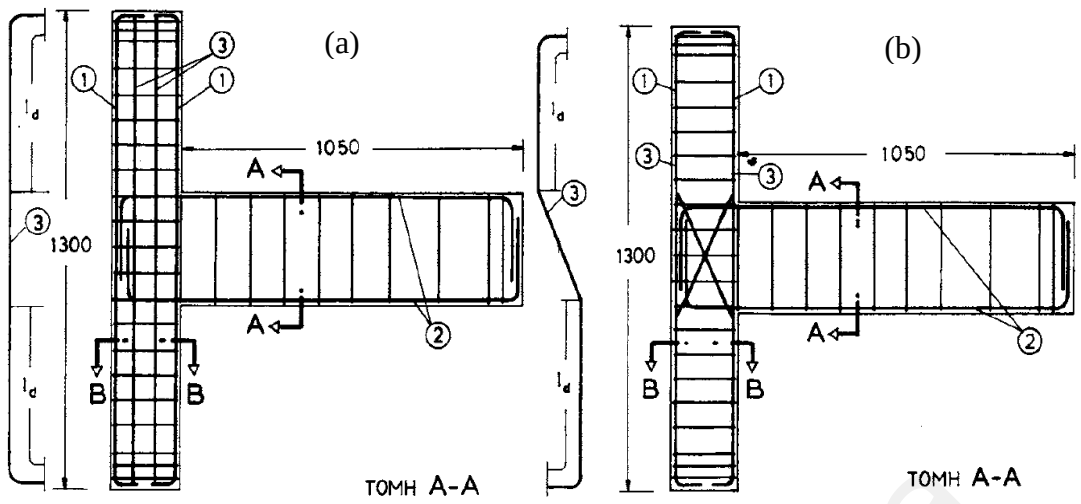

Figure 2.2: Reinforcement details of beam-column joint (a) conventionally reinforced (b) reinforced with crossed inclined bars (Tsonos et al., 1992)

An experimental study which was carried out by Filiatrault et al. (1994) included two exterior normal reinforced concrete (RC) beam-column joint specimens subjected to seismic loading. The first specimen was designed according to Building Code of Canada but it ignores any provision for seismic considerations (without transverse reinforcement in the joint). The second specimen was made by applying all the recommendations of code (including the transverse reinforcement). Results showed that a premature shear failure occurred in the joint for first specimen without any configuration of plastic hinge in the beam. The maximum strain recorded in the beam longitudinal bars was 3000 $\mu\varepsilon$ and the test ended at displacement ductility level of 2.5. A pinching effect of loops was observed and the specimen didn't attain its theoretical moment capacity. On the other hand, as the second specimen was being reinforced in accordance with the seismic recommendations of Canadian Code, there was a considerable strain deformations of 40,000 $\mu\varepsilon$ reached in the beam longitudinal reinforcement without any shear failure in the joint zone. The joint attained its theoretical moment capacity. The deterioration in the maximum load appeared after 2.5 of displacement ductility. The test ended at displacement ductility level of 4.

Parra-Montesinos & Wight (2000) presented an experimental study to investigate the seismic response of exterior RC column-to-steel beam connection exposed to reversed cyclic loads. The joint zone is constructed from steel (I) section beam frames into RC column. Results illustrate that the appropriate volume ratio of stirrups included in joint region is 0.9% to provide better confinement as well as to enhance the joint shear strength. The spacing between stirrups should not be greater than the smaller of $h_{col}/4$ and $h_{beam}/4$. Moreover, usage of steel fiber concrete (SFC) or ECC in joint zone will reduce or replace thoroughly the stirrups.

Murty et al. (2003) conducted an experimental study to investigate the effectiveness of transverse reinforcement in exterior RC beam-column joints prototypes exposed to earthquake excitation. Three details of transverse shear reinforcement were provided in Figure 2.3. The first detail is described with no inclusion of transverse reinforcement (example of non-seismic detail), the second detail is stirrups in the form of open hairclip-type reinforcement that extends into the beam coming from the face of column and the third detail is closed stirrups according to the ACI 318 limitations. Results indicate that the specimens of non-seismic reinforcement details which exposed to considerable joint shear stresses caused a severe joint failure before the attaching members' capacity was attained. On the other hand, the presence of joint transverse shear reinforcement like hairclips or closed ties increases the post cracking capacity as well as the energy absorption ability. The hairclip-type reinforcement is more effective.

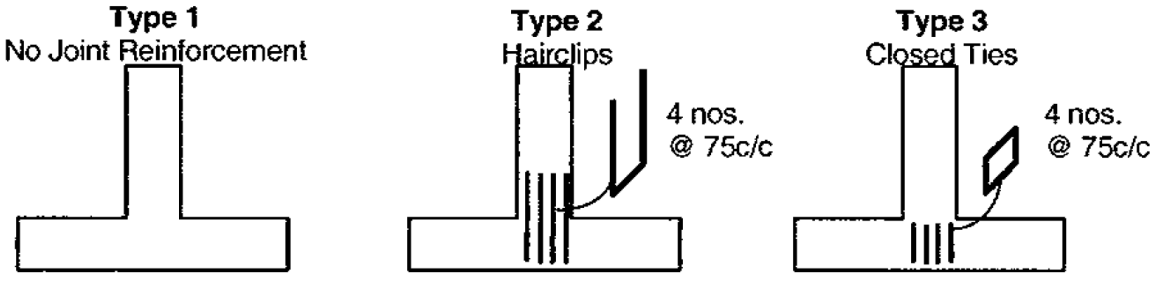

Figure 2.3: reinforcing details in joints (Murty et al., 2003)

Hwang et al. (2005) conducted an experimental program to investigate the effect of steel hoops on shear strength of exterior reinforced concrete (RC) beam-column joints subjected to earthquake loading. Results found that the steel hoops in the joint zone act as a tension tie and restrain the crack width. The presence of joint hoops can effectively protect the joint zone under earthquake loading from any destruction. The most reliable design for beam-column joint under cyclic reversals is providing the adequate number of steel hoops in the joint zone.

An experimental study was conducted by Alva et al. (2007) for evaluating the seismic behavior of RC beam-column joint assemblies under cyclic loading. Results showed that the increase in shear reinforcement from 2 to 4 stirrups in joint core enhanced the joint shear capacity to around 11%. Moreover, the increase in number of stirrups reduced the deflection and joint rotation at the same level of cycles and load i.e. increases the stiffness of joint.

Park & Mosalam (2010) came up with semi-empirical model to simulate the behavior of RC exterior beam-column joints without the transverse reinforcement exposed to cyclic loading. Experimental results were collected from two specimens and were compared with the results obtained from formulated model. Results indicate that the joint shear failure was the failure attributed to the yielding of longitudinal beam reinforcement of both specimens. The absence of transverse reinforcement in both specimens reduced the load capacity in both specimens.

Bedirhanoglu et al. (2010) conducted an experimental study to estimate the behavior of weak exterior beam-column joints subjected to cyclic loads. Three specimens were prepared with three different amounts of stirrups, one stirrup and two stirrups. The inclusion of stirrups has shown slimmer inclined cracks in joint zone, higher ultimate load capacity, higher strains and higher bond strength of longitudinal beam bars with concrete due to the higher confinement of concrete in the joint zone. All the mentioned

specimens reached the maximum drift ratio of 6% which means that the drift ratio is irrelevant to the inclusion of joint shear reinforcement.

Kuang & Wong (2011) achieved an experimental work carried out to evaluate the influence of horizontal stirrups inclusion in the joint zone on the seismic behavior of non-seismically designed exterior beam-column joints subjected to cyclic loading. As illustrated in Figure 2.4, three full-scale specimens were cast with three different shear reinforcement ratios of 0, 0.13% and 0.26% were considered in this study. Results have shown that the existence of horizontal stirrups in joint zone can significantly improve the seismic performance and increase the joint shear strength, as shown in Figure 2.5. It was discovered that the best ratio for stirrups inclusion in the joint zone is 0.4% and any additional stirrups is not effective. In addition, shear failure was the failure mode observed in the joint zone for all beam-column specimens before the beam reaches its ultimate flexural strength. The joints without horizontal stirrups failed at 70% of designed ultimate flexural strength. Inclusion of horizontal stirrups in the joint zone enhanced the ductility and energy absorption capacity of joint as well as increased the ultimate joint capacity to 85-90% of ultimate design capacity of beam.

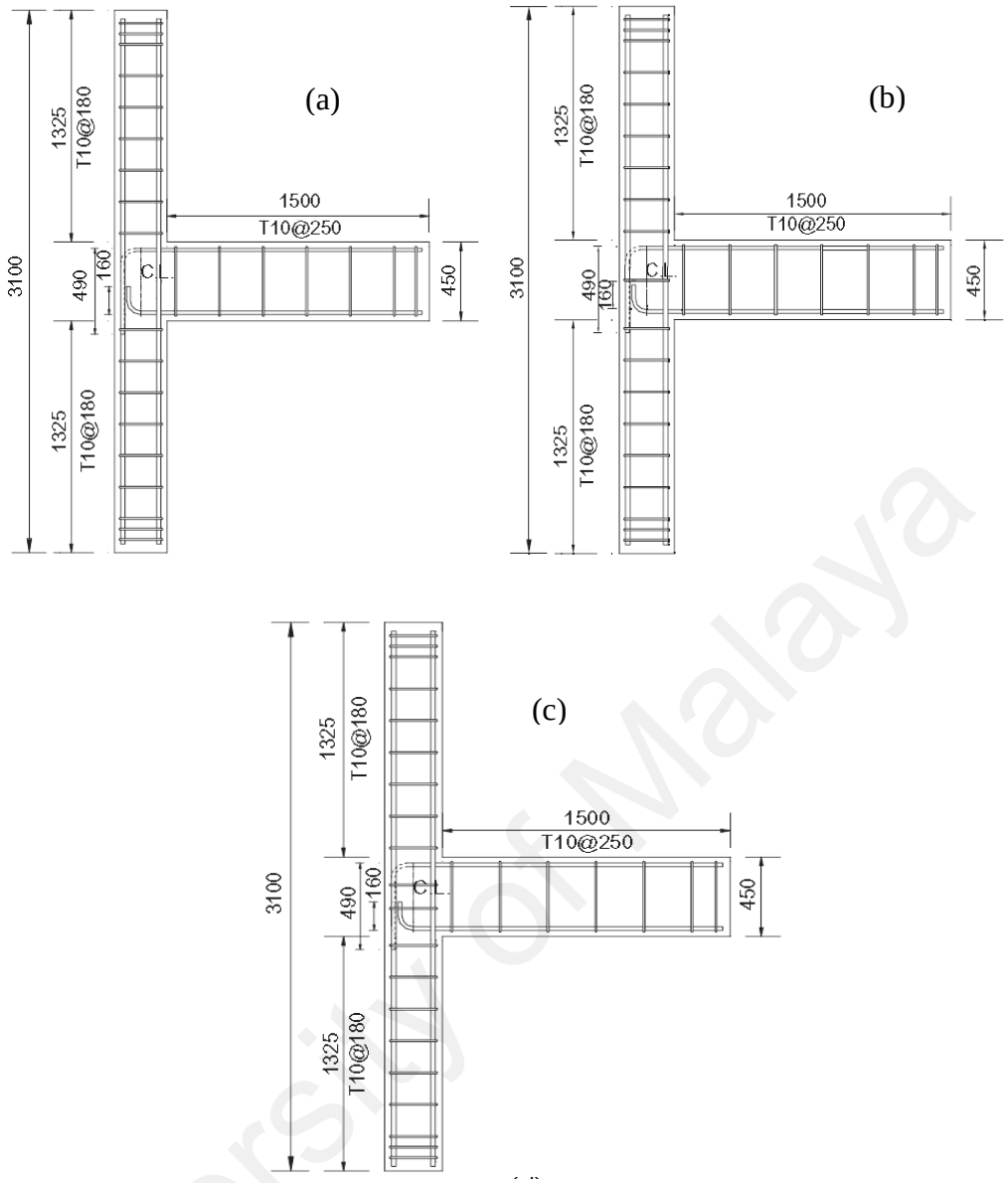

Figure 2.4: Various reinforcement details in beam-column joints (a) no stirrup (b) one stirrup (c) two stirrups (Wong & Kuang, 2008)

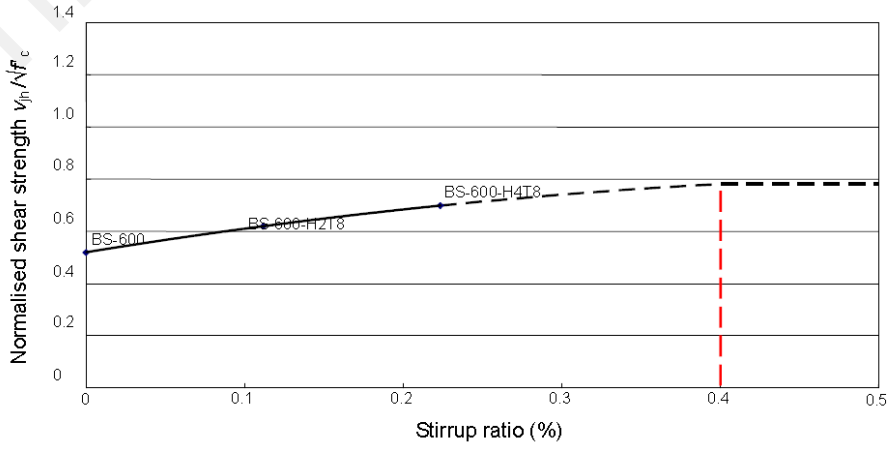

Figure 2.5: Effect of variation of stirrup ratio on shear strength of beam-column joints (Kuang & Wong, 2011)

2.3.3 Beam longitudinal steel reinforcement

An experimental program was conducted by Ha et al. (1992) to evaluate the response of reinforced concrete (RC) high-strength beam-column joints under cyclic loading. To improve the seismic behavior of the joints, additional extra intermediate longitudinal bars were penetrated inside the beam-column joint zone and tied to the main longitudinal beam reinforcement, as shown in Figure 2.6. Results have shown that the existence of such additional intermediate bars has successfully moved the location of beam plastic hinge away from the column face. Moreover, the additional bars increased the joint ultimate capacity by 14% and its energy absorption by 6% as compared to the conventional details of high strength joints.

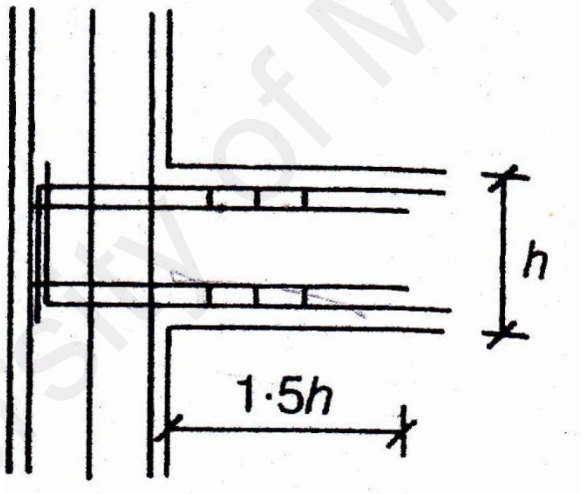

Figure 2.6: Additional intermediate bars were tied to the main longitudinal beam reinforcement (Ha et al., 1992)

Bakir & Boduroglu (2002) presented a parametric study to evaluate the factors affecting the shear strength of exterior RC beam-column joints exposed to cyclic loading. From the comparison between two beam-column joints, it was found that the higher the beam's longitudinal reinforcement ratio, the higher the joint shear strength. Moreover, the lower the beam's reinforcement ratio, the more the probability of yielding the

penetrated part of beam longitudinal reinforcement into the joint region which causes different joint crack patterns.

Results revealed from experimental tests conducted by Hwang et al. (2005) on RC exterior beam column joints by applying earthquake loading, that the beam's middle bars passing through the joint core cannot be used as shear reinforcement due to their contribution in beam flexure. On the other hand, results obtained from Bakir & Boduroglu (2002) indicated that as the beam's longitudinal bars increase, the joint shear strength increases as well.

2.3.4 Column axial load

Li & Kulkarni (2010) carried out some experiments and numerical analysis to estimate the behavior of RC exterior wide beam column joints under simulated earthquake load reversals. Results from finite element model displayed that the increase in column axial load up to 25% of its compression load capacity provides an increase of about 6 to 8% in joint shear strength. Any increase in axial load which is more than the ratio mentioned above, leads to an inverse effect of reduction in joint shear strength and stiffness.

Tests were conducted on two specimens by Yuan et al. (2013) to evaluate the effect of column axial load on the behavior of RC exterior ECC beam column joints subjected to cyclic loading. Both ECC specimens were very much identical, except for the fact that the column axial load for the first specimen was higher than the second specimen. Results showed that the ductility for the first specimen is higher than that of the second specimen due to the increased column load which restricts the propagation of cracks within the joint zone, and which leads to higher energy absorption capacity.

2.3.5 Column longitudinal steel reinforcement

A parametric study was presented by Bakir & Boduroglu (2002) revealed that the shear strength in exterior beam-column joint under cyclic loading is independent of column longitudinal reinforcement ratio whereas the shear strength in exterior beam-column joints under monotonic loading is relevant to the column longitudinal reinforcement ratio. Furthermore, results have shown from tests done by Park & Mosalam (2010) on exterior beam-column joints under cyclic loading, that the column middle bars didn't enhance the exterior joint shear strength, whereas results from experiments done on exterior beam-column joints under monotonic loading (Hegger et al., 2003) revealed that the increase in column longitudinal reinforcement enhanced the joint shear strength.

The effect of column longitudinal steel bars on seismic behavior of RC exterior beam-column joints was investigated by testing non-seismically designed beam-column joints by Wong & Kuang (2008). 0, 0.35 and 0.7% were the column's additional intermediate longitudinal reinforcement ratios considered in this study, as shown in Figure 2.7. From the tests carried out, results showed that the presence of additional intermediate longitudinal reinforcement in the column up to 0.8% and the presence of total column reinforcement up to 4% enhanced the joint shear strength and raised the ductility, as shown in Figure 2.8. In addition, any additional increase in the ratios mentioned in the column reinforcement, presents less improvement in joint shear strength, energy absorption ability, and ductility as compared to the reinforcement and detailing costs.

2.3.6 Beam-column depth ratio

A parametric study was conducted by Bakir & Boduroglu (2002) on cyclically loaded exterior beam-column joints. The authors proved that the joint shear strength is inversely proportional to the beam-column depth ratio through an empirical approach formulated by the authors, indicating that the joint shear strength is proportional to $(h_b/h_c)^{-0.61}$.

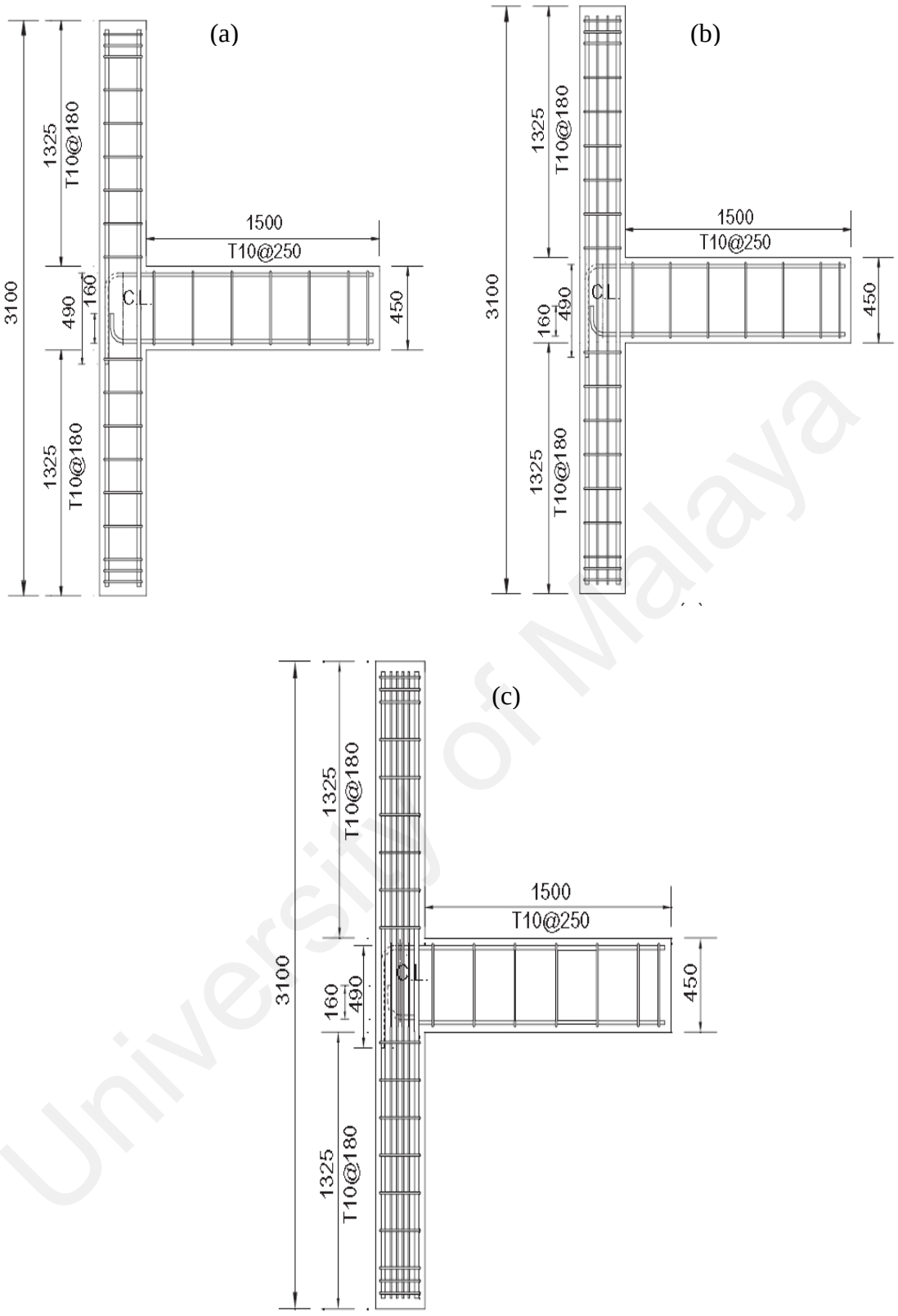

Figure 2.7: Variation of column longitudinal bars ratio in beam-column joints (a) 0% (b) 0.35% (c) 0.7% (Wong & Kuang, 2008)

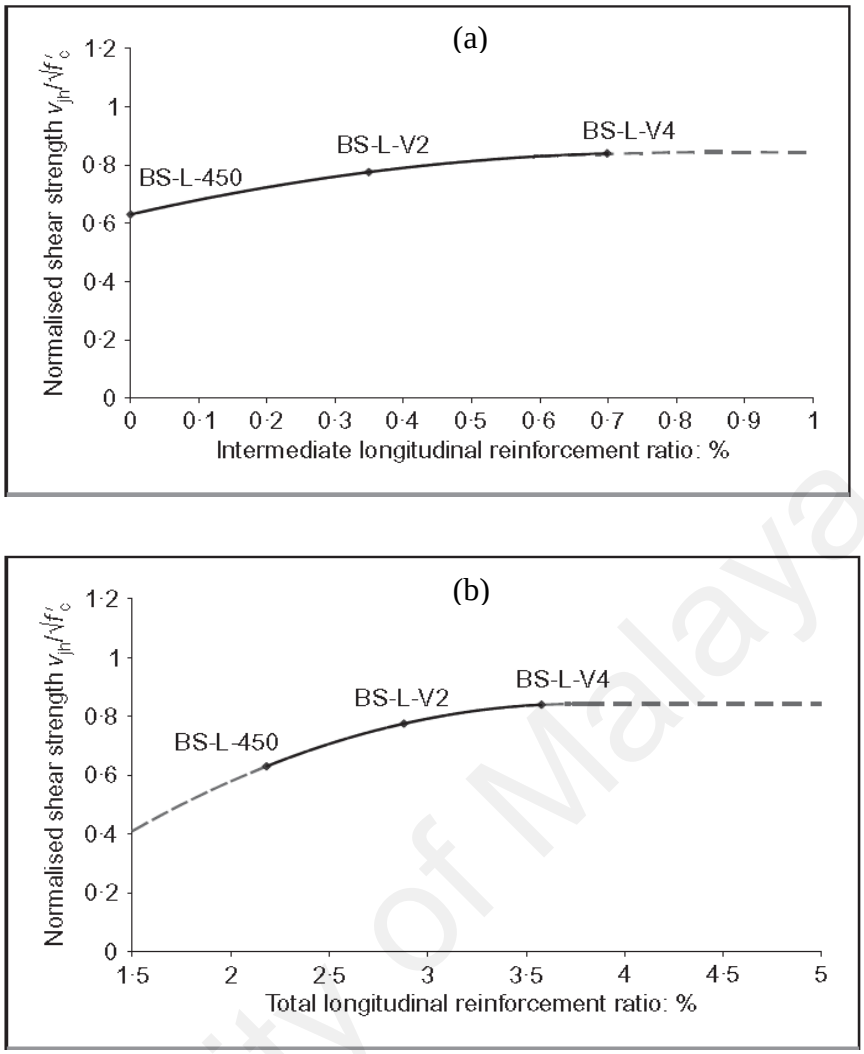

Figure 2.8: Effect of (a) intermediate column longitudinal bars ratio (b) total column longitudinal bars ratio (Wong & Kuang, 2008)

The effect of beam-column depth ratio is investigated experimentally by Wong & Kuang (2008), in non-seismically designed beam-column joints under cyclic loading. 1, 1.5 and 2 were the beam-column depth ratios considered in this study, as shown in Figure 2.9. Results shown in Figure 2.10 indicate that the best depth ratio was 1 and the specimen exhibit higher shear strength and better ductility. For beam-column depth ratio which equals to 1.5 and 2, the shear strength for joint decreases about 38 and 50%, respectively. Any increase in beam-column depth ratio over 2 does not reduce in joint shear strength.

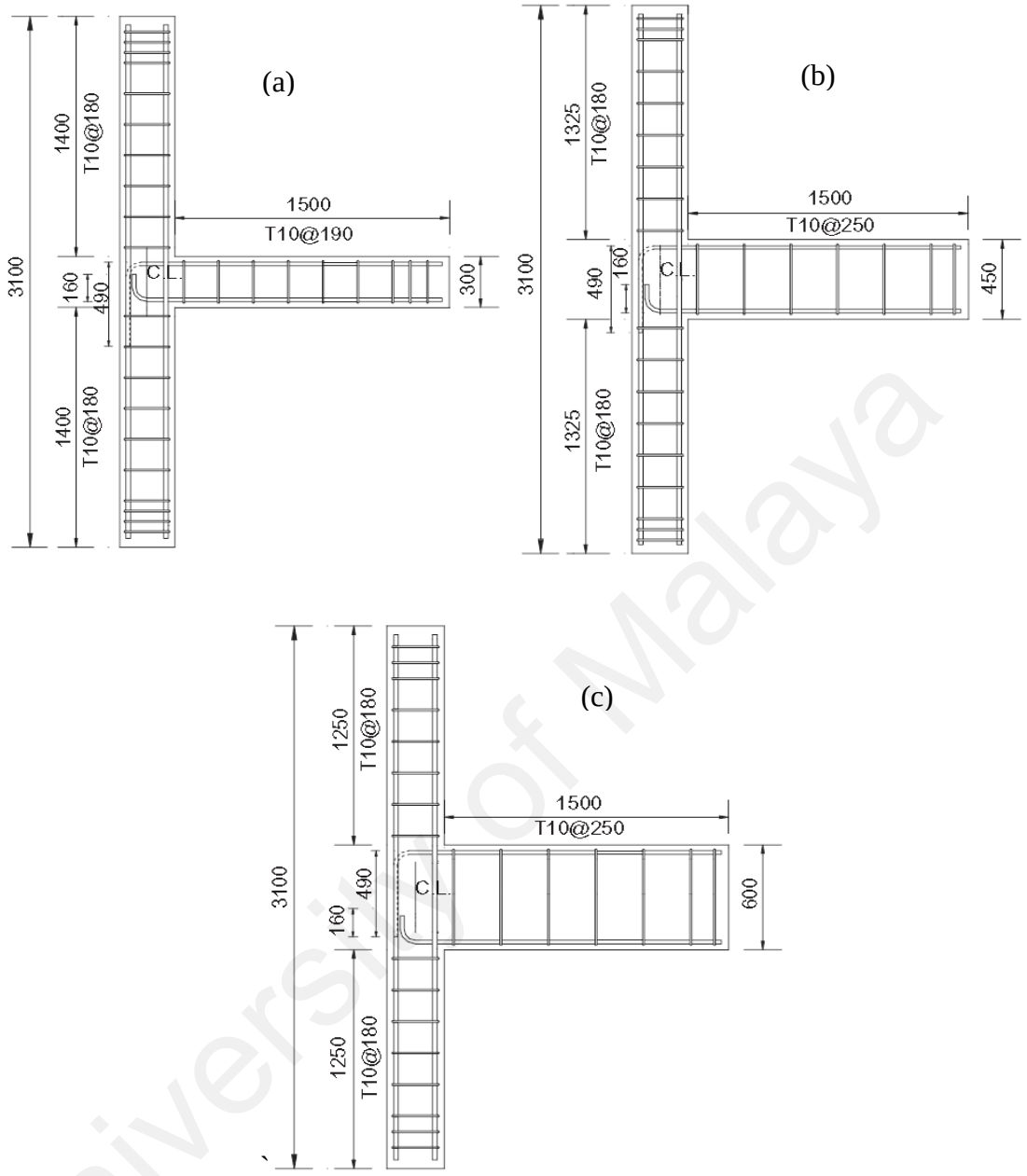

Figure 2.9: Reinforcing details and variation of beam-column depth ratio equals to (a) 1 (b) 1.5 (c) 2 in beam-column joints (Wong & Kuang, 2008)

2.3.7 Concrete grade

An experimental work was carried out by Ha et al. (1992) to assess the structural behavior of high-strength reinforced concrete (RC) exterior beam-column joints under cyclic loading. The results indicated that when the concrete strength increases, the joint stiffness deterioration will be faster due to the brittle failure nature of high-strength

concrete, which needs high rate of transverse reinforcement to reduce the joint deterioration severity. Moreover, a modified design method was presented to improve the reinforcing details of high-strength beam-column joint preventing the occurrence of diagonal cracking within the joint region and taking the probable beam plastic hinge away from the column face.

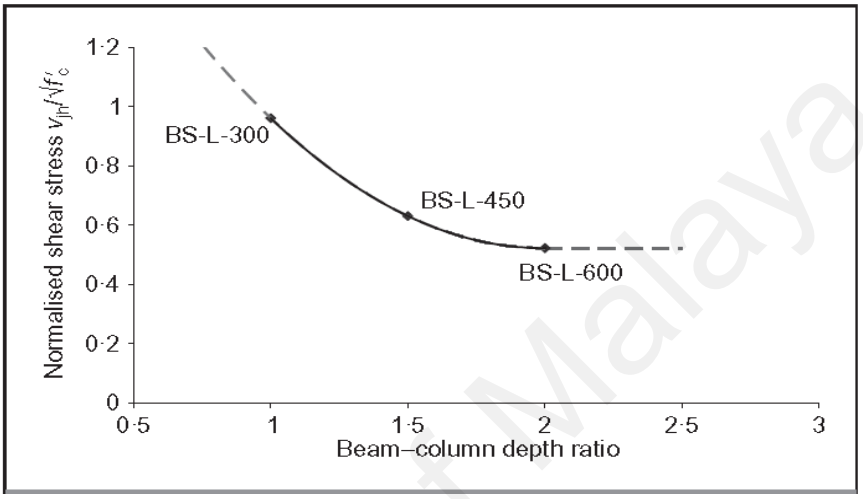

Figure 2.10: Effect of beam-column depth ratio on shear strength of beam-column joints ((Wong & Kuang, 2008)

Results gathered from an experimental study and investigated by Alva et al. (2007) on RC exterior beam-column joints under seismic loading, revealed that the increase in concrete compressive strength dominates the joint shear capacity more than the influence of stirrups existence and also affects the structural behavior of joint under cyclic loading.

2.3.8 Inclusion of steel fiber reinforced concrete (SFRC)

Henager (1977) conducted an experimental investigation to estimate the behavior of Steel fiber reinforced concrete (SFRC) exterior beam-column joints under seismic loading. Two beam-column joints were prepared for testing by inducing two major earthquake excitations. The first specimen was constructed by using normal concrete (NC) and placing stirrups in the joint zone according to the American seismic resistant design specifications (352R-02, 2002).

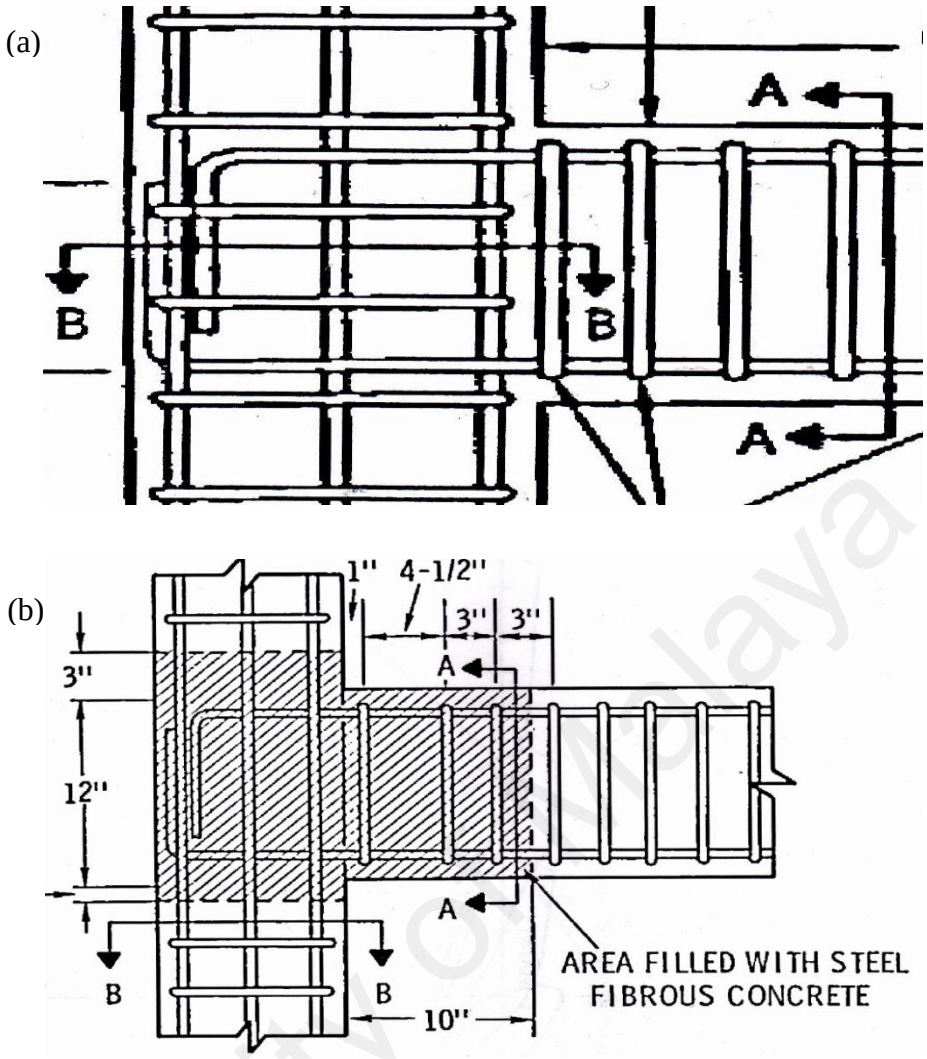

Figure 2.11: Beam-column joint (a) constructed by normal concrete and stirrups (b) replaced by steel fibrous concrete (Henager, 1977)

The second specimen was constructed by replacing the NC and stirrups with SFRC, as shown in Figure 2.11. Results showed that using SFRC in joint zone instead of stirrups and NC would increase ultimate capacity, ductility, stiffness, which better arrest the cracks and are more damage tolerant than the first specimen. Furthermore, the casting with SFRC would be easier and the fabrication of steel would be simpler and more economical, due to the absence of stirrups which mitigates the steel congestion and reduces the building costs to a large extent.

Craig et al. (1984) conducted an experimental study to highlight the behavior of SFRC exterior beam-column joints subjected to cyclic loading. The program included two

groups of beam-column joint prototypes. The first group of specimens was cast with SFRC including steel hooked-end fibers, whereas, the second group of specimens was cast with NC. Results showed that SFRC provided higher bond for steel bars, better confinement of concrete, less structural damage, and higher structural integrity than the NC joint. Besides, it was also proven that the inclusion of steel fibers in joint zone improved the shear strength, ultimate moment capacity, stiffness, energy absorption ability and ductility of the joint. In addition, multiple cracking behavior with smaller cracks width and spacing were observed in SFRC joints than those in NC joints.

Sood & Gupta (1987) studied the behavior of different types of SFRC beam-column joints such as cross, Tee and knee joints under cyclic fatigue loading. Results showed that the increase in steel fiber content enhanced the first cracking strength and decreased the crack width. Besides, the propagation of crack was delayed to a large extent, due to crack arresting mechanism in SFRC. Furthermore, SFRC joints gained a significant increase in the load capacity, stiffness, ductility and showed less deflection and rotation as compared to the NC joints at the same loading level. The replacement of stirrups and NC with SFRC in the joint zone leads to easier and simpler construction due to the reduction in reinforcement congestion. Finally, the use of steel fibers in concrete is rather restricted due to the high cost.

Experimental works carried out by Jiuru et al. (1992) to investigate the seismic behavior and shear strength of SFRC exterior and interior beam-column joints results showed that the steel fibers in concrete improved the shear strength, ductility and energy-absorption capacity of the beam-column joints. Moreover, the use of SFRC in the joint was able to reduce the reinforcement congestion and facilitates construction difficulties. SFRC mixture enhances the bond strength and develops the anchorage properties of steel bars.

Filiatrault et al. (1994) carried out an experimental program to study the seismic performance of SFRC exterior beam-column joints. Four full-scale RC beam-column

joints were constructed and tested under hysteresis loops of loading. As shown in Figure 2.12, both first and second specimens were cast by NC and designed according to the Building Code of Canada; the first specimen was non-seismically designed but the second specimen was designed according to seismic requirements of code. The third and fourth specimens were designed similar to first specimen, except that the concrete in the joint zone for both specimens was replaced by SFRC with fiber reinforcing index which equals to 60 and 160 respectively. In the third specimen, a gradual shear failure would occur due to the pulling out of steel fibers with increase in displacement ductility. The specimen attained 85% of its theoretical moment capacity. In the fourth specimen, and due to higher reinforcing index of fibers, the specimen showed higher shear strength in the joint, attained its theoretical moment capacity and insured a plastic hinge failure

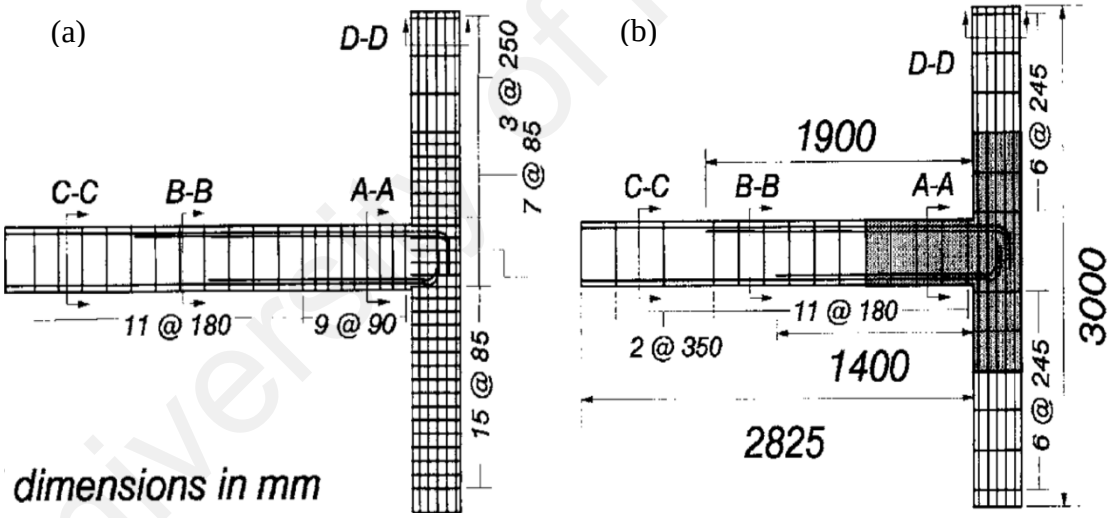

Figure 2.12: Beam-column joint (a) designed according to seismic requirements (b) designed non-seismically but replaced by SFRC in joint zone (Filiatrault et al., 1994)

in the beam. The seismic response for the fourth specimen is identical to the response of the second specimen. Moreover, the inclusion of SFRC in the joint zone eliminates any need to the transverse reinforcement. In addition, SFRC increased the joint shear strength and ductility, bridging the cracks and arresting the crack width. Finally, it was

proven that the higher the steel fiber reinforcing index, the better is the performance of the joint.

Bayasi & Gebman (2002) carried out an experimental study to reduce the lateral steel hoops in seismic exterior reinforced concrete beam-column joint through SFRC application. The authors clarified the fact that lateral steel hoops can be reduced when applying SFRC in joints. Such reduction can be interpreted as an increase of hoop spacing within the joint zone. Results showed that for steel fiber reinforcing index V_f (l/d) ranging between 100 and 160, the reduction in lateral steel hoops ranged between 0.3 and 1.1% which is equivalent to 50% and to more than 200% increase of hoop spacing. Moreover, such reduction in steel hoops is beneficial for reducing steel congestion in joints, reducing joint construction cost, and enhancing joint performance.

A study was conducted by Sarsam & Al-Azzawi (2010) to estimate the shear capacity of high-strength SFRC exterior beam-column joints. Literature has shown that the high strength concrete (HSC) in beam-column joints displays sudden or brittle mode of failure despite the presence of hoops in joint zone. Consequently, the inclusion of steel fibers in joint zone led to better integrity at failure. A larger number of smaller size and width of cracks were propagated within the joint zone and failed in a ductile behavior. For HSC joints, it is discovered that 1% of steel fiber content is the optimum percentage which can be incorporated to access the higher level of ductility and shear strength.

Gencoglu & Eren (2002) showed that the closely spaced transverse reinforcement is required by earthquake codes. However, placement of this reinforcement in joints always causes some casting difficulties. Furthermore, the use of SFRC in joints was intended to minimize the casting difficulties. Results of four full scale exterior beam-column specimens were tested under reversed cyclic loading revealed that the usage of SFRC in beam-column joints can be an alternative solution for minimizing the density of transverse reinforcement.

Ganesan et al. (2007) conducted an experimental study on ten high performance SFRC exterior beam column joint specimens tested under reversed cyclic loading. Results indicate that the inclusion of high performance SFRC in joint zone enhances the strength, ductility and stiffness, and is one of the possible alternative solutions for reducing the congestion of transverse reinforcement in beam-column joints.

Three exterior beam-column joint specimens were placed and tested under reversed cyclic loading by Perumal and Thanukumari (2011) using high strength concrete without considering the seismic design requirements. Three combinations of cocktail fibers were prepared to incorporate in the joint region such as 1.5% constant of steel fibers with 0, 0.2% and 0.4% of polypropylene (PP) fibers. Results indicate that the optimum percentage of cocktail fibers was for 1.5% steel fibers with 0.2% of PP fibers, which have more energy absorbing capacity, less joint rotation, more shear strength, more curvature ductility factor and less reinforcement strain.

Shakya et al. (2012) conducted an experimental program to apply the SFRC in exterior RC beam-column connections of rigid-framed railway bridges. The congestion of stirrups in the joint zone has led to many difficulties in fabricating and casting. The objective of this study therefore, is to mitigate the stirrups by applying SFRC in the joint region as a replacement to the stirrups. Results showed that the addition of 1.5% of steel fibers is the optimum amount required to reduce the stirrups in beam–column joints of railway rigid-framed bridges.

An experimental study was achieved by Thamilselvi (2012) to investigate the behaviour of exterior beam column joints using slurry infiltrated fiber concrete *(*SIFCON) and steel fiber reinforced concrete (SFRC) at the exterior beam-column joint. SIFCON and SFRC specimens were provided with half of steel hoops amount in the joint region. Results obtained were compared with conventional reinforced concrete joints subjected

to reversed cyclic lateral loading. Results found that a reduced crack width for SIFCON and SFRC joints compared to the conventional concrete joints with less number of cracks were noticed in the joint region in the case of SIFCON specimens. The load carrying capacity of SIFCON specimens was found to be greater than SFRC and Conventional specimens. Moreover, the stiffness of SIFCON specimens is 4 times more than the stiffness of SFRC specimen and 4.5 times more than the stiffness of conventional concrete. Besides, the energy absorption capacity for SFRC joints exceeds the SIFCON joints about 36%.

An experimental study was conducted by Ganesan et al. (2014) to study the effect of hybrid fibers on the strength and performance of exterior beam column joints subjected to reversed cyclic loads. A hybrid form of crimped steel fibers and polypropylene fibers were incorporated in high performance concrete of M_{60} grade. Addition of fibers improved the first crack load, ultimate load and ductility of the composite. The combination of 1% volume fraction of steel fibers and 0.15% volume fraction of polypropylene fibers showed better performance with respect to energy absorption capacity and stiffness degradation than the other compositions.

Experimental studies were conducted by Hemati et al. (2016) to assess the structural performance of high performance fiber reinforced cementitious composite (HPFRCC) frames. Results revealed that using HPFRCC materials, instead of normal concrete in RC frames, increased the ultimate load, ultimate deflection, ductility ratio, and plastic hinge characteristics of frames.

2.3.9 ECC inclusion

The application of ECC in beam–column joints has not been extensively studied (Fischer & Li, 2003; Mishra, 1995; Parra-Montesinos & Wight, 2000; Qudah & Maalej, 2014; Yuan et al., 2013; Zhang et al. 2015). Mishra (1995) found out that when the

beam–column connections was cast with ECC–PE and was subjected to hysteresis loops of loading, it led to higher energy absorption capacity. Using ECC in the beam–column joint, (Parra-Montesinos & Wight, 2000) showed that eliminating the lateral steel hoops in the joint mitigates construction difficulties.

An experimental investigation was conducted by Yuan et al. (2013) to estimate the seismic behavior of exterior beam-column joints which were subjected to simulated seismic loads. ECC was used as a replacement to the NC in the joint core to estimate the seismic effects of this material. All specimens were designed with respect to the principal of (strong component-weak joint). To show the effect of ECC inclusion, four specimens (S_1, S_2, S_3, S_4) were constructed and prepared for this study. S_1 and S_2 were constructed with NC without stirrups, and with two stirrups placed in the joint core respectively. S_3 and S_4 were constructed with ECC in the joint core without stirrups and with two stirrups placed in the joint core respectively. Test results showed that for S_1, the failure occurred in the joint zone by brittle shear failure due to the absence of stirrups. For S_2, the crack width within the joint zone was smaller than S_1 due to the existence of stirrups. The failure occurred with mixed mode of flexural yielding of beam longitudinal bars to brittle shear failure of concrete in the joint zone. S_3 exhibited a higher load capacity, better ductility and energy absorption capacity than S_1 and S_2, due to the ECC inclusion. Brittle shear failure was the failure mode observed in the joint core. S_4 showed enhanced higher load and higher ductility than S_3 due to the inclusion of two stirrups in addition to ECC in the joint core. The failure mode was the creation of flexural plastic hinge in the beam next to the column face.

An experimental study was carried out by Zhang et al. (2015) to apply the ECC in exterior RC beam-column connections of rigid-framed railway bridges. The over congestion of lateral steel hoops in the joint zone has led to many difficulties in fabricating and casting. The main objective in this study is how to reduce the steel

hoops by applying the ECC in the joint zone as a replacement to the lateral steel hoops. The polypropylene fibers were used to prepare the ECC. Results have shown that the ECC-PP is very effective and successfully compensates the effect of reduced amount of hoops in the beam–column joints of railway rigid-framed bridges.

2.3.10 GFRP reinforcement inclusion

Mady et al. (2011a) conducted an experimental program to evaluate the seismic behavior of exterior beam-column joints reinforced with glass fiber-reinforced polymer (GFRP) bars. The aim of this study is to show the advantages in the replacement of steel bars with such non-corrodible bars. GFRP bars are characterized by linear-elastic tensile stress-strain behavior up to failure. Three reinforcing details were applied in this study to prepare five beam-column prototypes for cyclic testing. The first specimen was detailed with steel bars and stirrups. Second specimen was detailed with GFRP bars and steel stirrups and the remaining specimens were detailed with totally GFRP bars and stirrups. Test results have shown that the beam-column specimens reinforced with GFRP bars can successfully sustain the cyclic reversals with non-excessive damage in the joint. In addition, for steel reinforced joint, a plastic hinge is localized in the face of column. For GFRP joints, a virtual plastic hinge was created away from column face and propagated over a longer length of the beam due to the large-elastic deformation facilities for GFRP. Moreover, the reduced value of E modulus for GFRP bars led to lower stiffness of joint specimen which exhibits higher amount of deformation as compared to the steel joints at the same drift level and reduces the ultimate shear capacity. Finally, the GFRP joints are able to dissipate energy more than the steel joints around 20%.

Mady et al. (2011b) presented an experimental study for analyzing and investigating full-scale exterior beam-column joints, fully reinforced with GFRP bars exposed to simulated seismic loading. The main parameter in this study was the beam longitudinal

reinforcement details by extending straight or bent bars into the joint zone and three specimens were prepared for testing. A straight bar as a beam reinforcement with a development length of 20 times the bar diameter ($20d_b$), were used for first specimen (G_1) while the third specimen (G_3) is the same as G_1 except that the depth of column is greater than G_1 with development length of $30d_b$. For the second specimen G_2, bend bars were used and embedded into the joint zone. The bend bars were spliced in a point near the joint face with a lap splice of $40d_b$. Results revealed that all the specimens satisfied the Canadian Code requirements, that is, the specimen passed the drift ratio of 2.5% before the failure occurred and fails with a flexural hinge in the beam with no shear splitting in joint. Figure 2.13 shows the loading history for testing with strain values measured in the GFRP bars. The specimen G_1 failed at 3% drift ratio due to slip anchorage of development length while $20d_b$ is insufficient. The specimen G_2 also failed at 3% drift ratio due to the slippage of lap splice. Specimen G_3 failed at a drift ratio of 5% with no slippage in the development length. It was deduced that the GFRP bars can be used and placed as a replacement to the steel bars in the exterior beam-column joints and could perform successfully high drift at the ratio of 5% under simulated seismic load, if they are detailed properly by limiting an embedment length not less than $30d_b$ in a situation whereby straight bars were used within joint region. Moreover, if lap splices were used with bent bars in GFRP beam, they must be in a length $\geq 40d_b$ to ensure highly sustained joint with no premature failure.

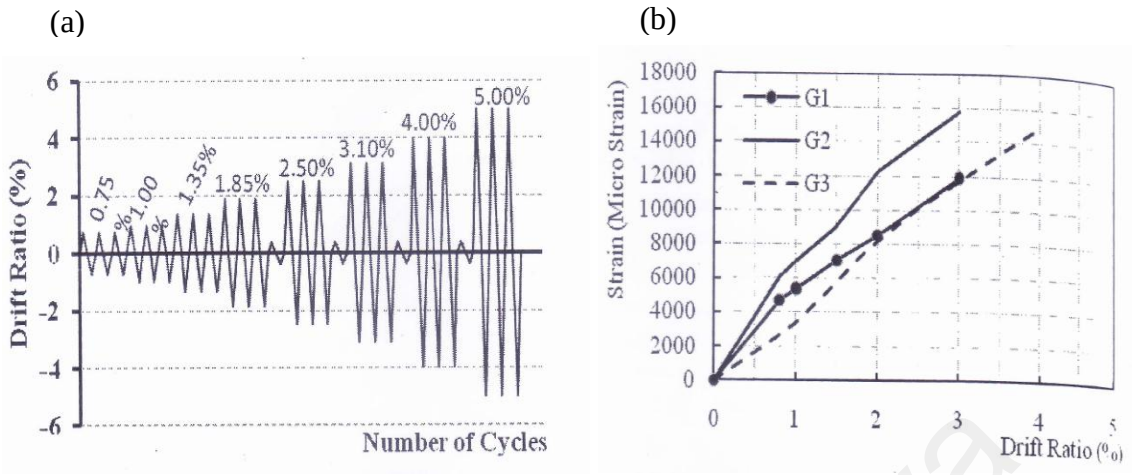

Figure 2.13: (a) Loading history (b) Strain values measured in beam longitudinal GFRP bars (Mady et al., 2011)

2.3.11 Development length and anchorage details

Experiments were carried out by Ha et al. (1992) to estimate the response of high-strength RC beam-column joints under hysteresis loops of loading. To prevent the diagonal cracks in the joints, a method was presented in Figure 2.14 to extend the longitudinal bars of beam diagonally inside the joint zone and to observe its effects on the joint. Results indicated that the formation of the diagonal anchorage into the joint zone prevented the development of diagonal cracking within the joint zone. However, the seismic behavior of such joints showed pinching effects owing to the sliding shear failure beside the beam-column interface.

Murty et al. (2003) carried out an experimental study to investigate the influence of reinforcement details in RC exterior beam-column joints exposed to earthquake simulation. As shown in Figure 2.15, four anchorage details of beam longitudinal bars were selected such as U-shape bent bar at the joint region (type P), standard ACI 90-degree hooks (type Q), both the top and bottom beam bars were anchored into the column with a development length (type R) and a detail of non-seismic frame i.e. tension bars at the joint region were anchored (type S). Results indicated that type Q and

R provided a significant behavior in sustaining shear stresses assessed by 45 to 79% higher than the values recommended in ACI code. Additionally, type R is the most excellent detail in the energy absorption as compared to the other types of anchorages.

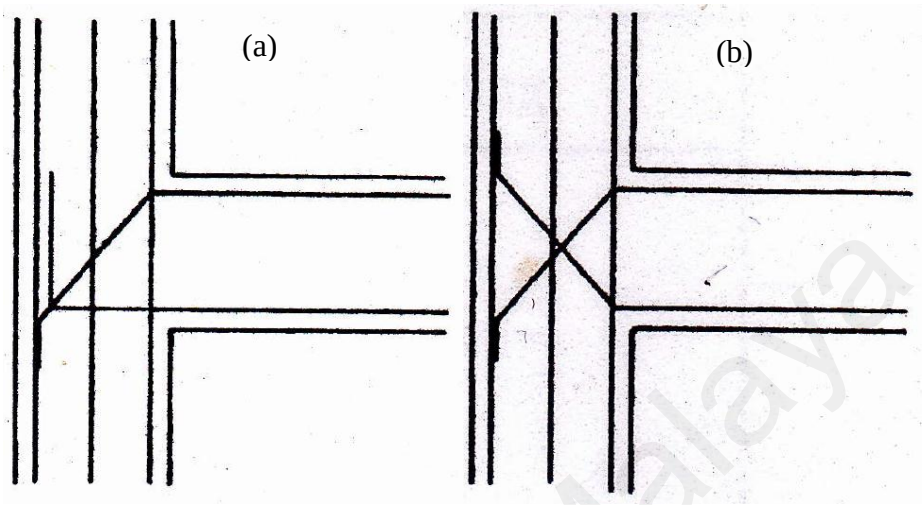

Figure 2.14: Diagonal anchorage of beam longitudinal bars inside the joint (Ha et al., 1992)

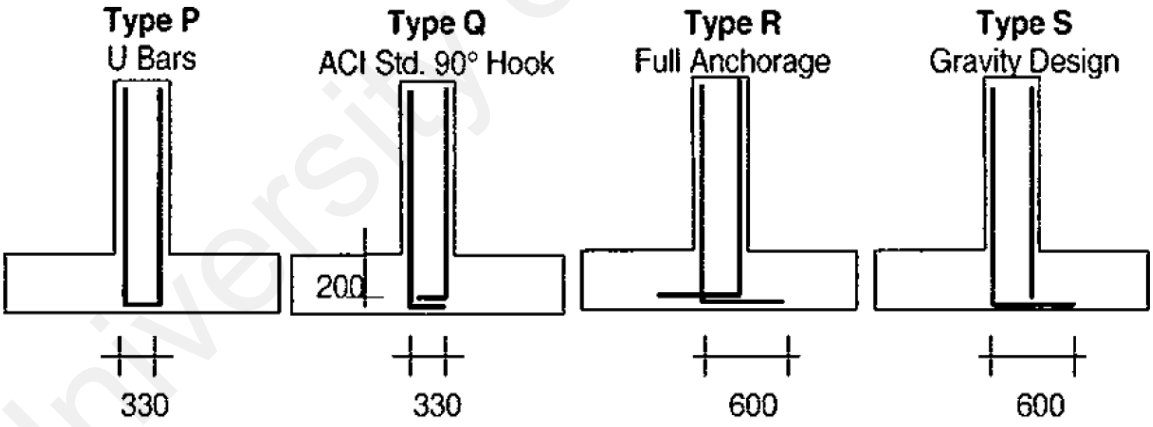

Figure 2.15: Anchorage details in beam-column joints (Murty et al., 2003)

Kuang & Wong (2006) carried out an experimental study to evaluate the effects of beam bar anchorage on seismic behavior of non-seismic designed exterior beam-column joints. As shown in Figure 2.16, five specimens were prepared for testing with different

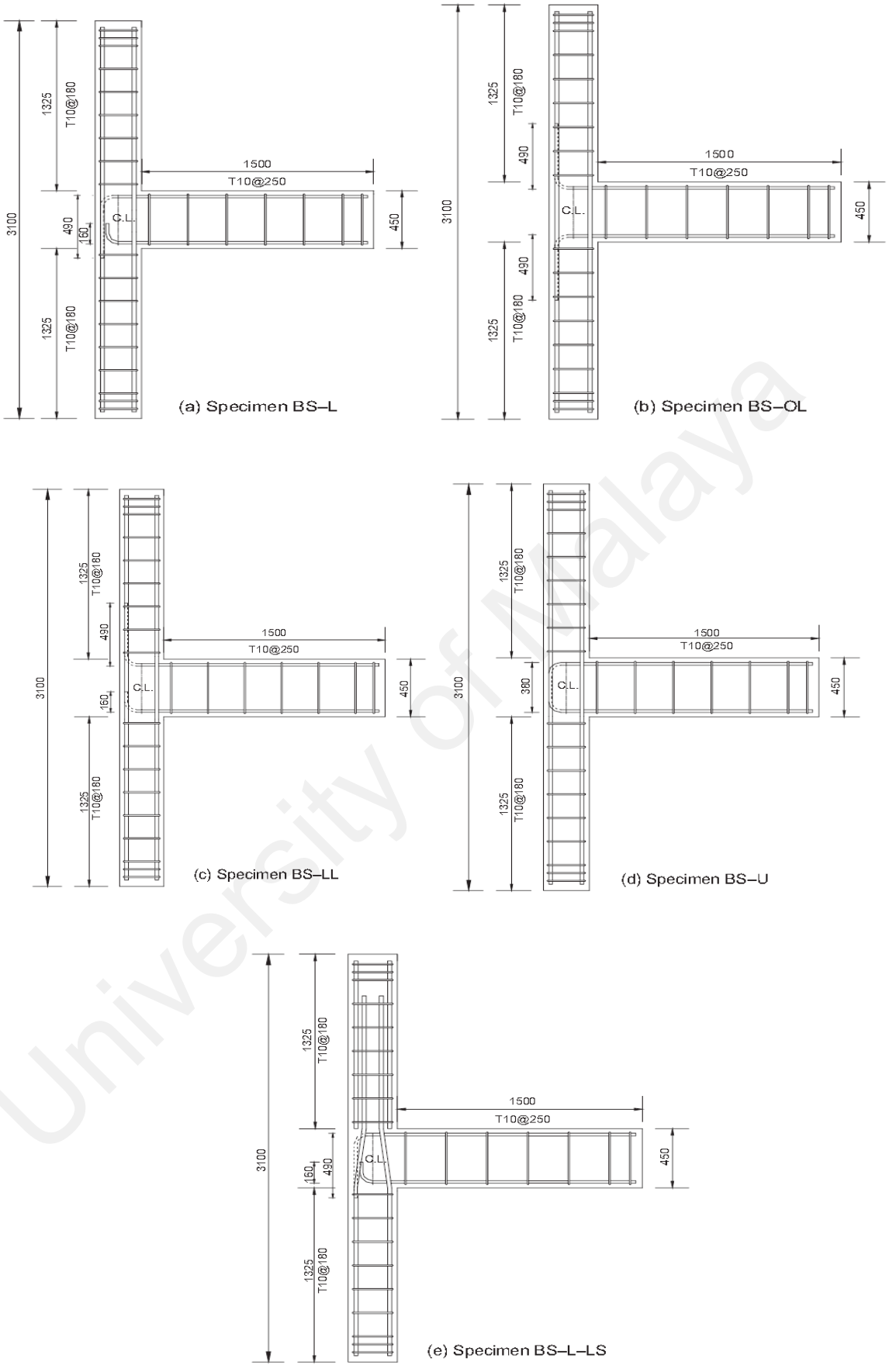

Figure 2.16: Specimens with different types of beam bar anchorage (Kuang & Wong, 2006)

types of anchorage such as higher and lower beam bars bent into the joint (type L), higher and lower beam bars bent away from the joint (type OL), upper bars bent away from the joint and lower bars bent into the joint (type LL), lap splices in form of U anchorage at the end region of beam (type U) and lap splices at the end region of upper column (type LS). Results showed that type OL and LL indicated lower shear strength and energy absorption capacity as compared to the other types. Therefore, these details should be avoided. In addition, the type U showed the best behavior under cyclic loading as it achieved 80% of designed flexural strength. In general, all specimens have shown shear failure in joint region at 50 to 70% of designed flexural capacity. Type LS has no any effect on the shear strength and the behavior of joints. Finally, the design codes of ACI 318-02, NZS 3101 and BS 8110 overestimated the shear strength of non-seismically detailed exterior joints while the Eurocode 2 considerably underestimated the joint shear strength in this study.

Chen et al. (2009) had conducted an experimental study to investigate the seismic behavior and strength of steel reinforced concrete beam-column joints. Regarding the development length parameter, results showed that the development length of beam's longitudinal bars has an evident effect on the crack pattern and joint shear strength. Thus, longer development length in beam-column joint results in high shear strength, and steeper diagonal cracks than those of shorter development length.

Bedirhanoglu et al. (2010) conducted an experimental study to estimate the behavior of weak beam-column joints subjected to cyclic loads. Nine beam-column specimens, were constructed with low-strength concrete (8.3 MPa), and plain steel bars were prepared in two groups for testing under cyclic loading. In the first group, the upper and lower beam longitudinal reinforcement was extended and bent 90 degree inside the joint core. In the second group, the specimens were similar to that in first group except that the upper and lower hooks were welded together in the joint core. Results showed that the flexural and

shear capacity of first group specimens didn't attain the expected limits due to the bond-slip failure of beam bar anchorages in the joint zone. For second group specimens, the average capacity was higher than the average capacity of first group with about 35%. However, this increase was unable to raise the beam and column strength to their expected strengths.

2.4 Prediction of shear strength in exterior beam-column joints

2.4.1 Analytical study

A new procedure was presented by Parker & Bullman (1997) for estimating the shear strength in RC exterior beam-column joints with and without lateral links based on the diagonal concrete strut concept, as shown in Figure 2.17. The procedure was verified by comparing the predicted results to the results of 12 exterior beam-column joints. Results showed good agreement between the predicted values and test results for specimens.

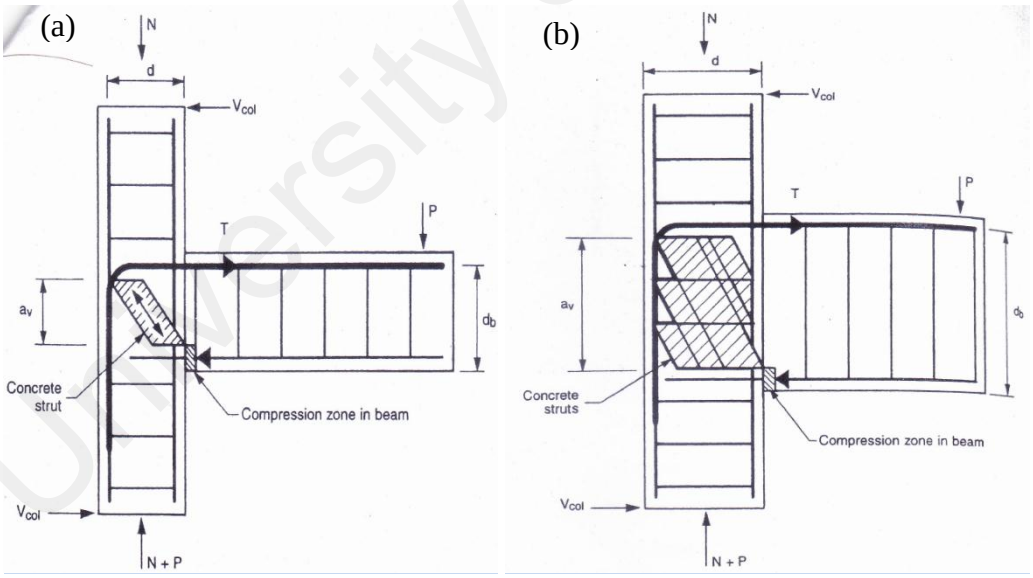

Figure 2.17: (a) Diagonal concrete strut and beam bars bent down into joint (b) role of links in beam-column joints (Parker & Bullman, 1997)

An analytical model has been proposed by Hwang & Lee (1999) for predicting shear strengths of exterior reinforced concrete beam-column joints exposed to seismic loading. The assumed strut-and-tie model is formed of diagonal, horizontal and vertical

mechanisms as illustrated in Figure 2.18. The diagonal mechanism is a diagonal compression strut force at the tilt angle of θ.

Hwang et al. (2005) have developed a model called (softened strut-and-tie, SST) to evaluate the shear strength of exterior beam-column joints subjected to seismic loading. The model satisfied the equilibrium, compatibility, and constitutive laws of cracked reinforced concrete. In addition, the model is based on the mechanism of force transmission in the joint zone, as shown in Figure 2.19.

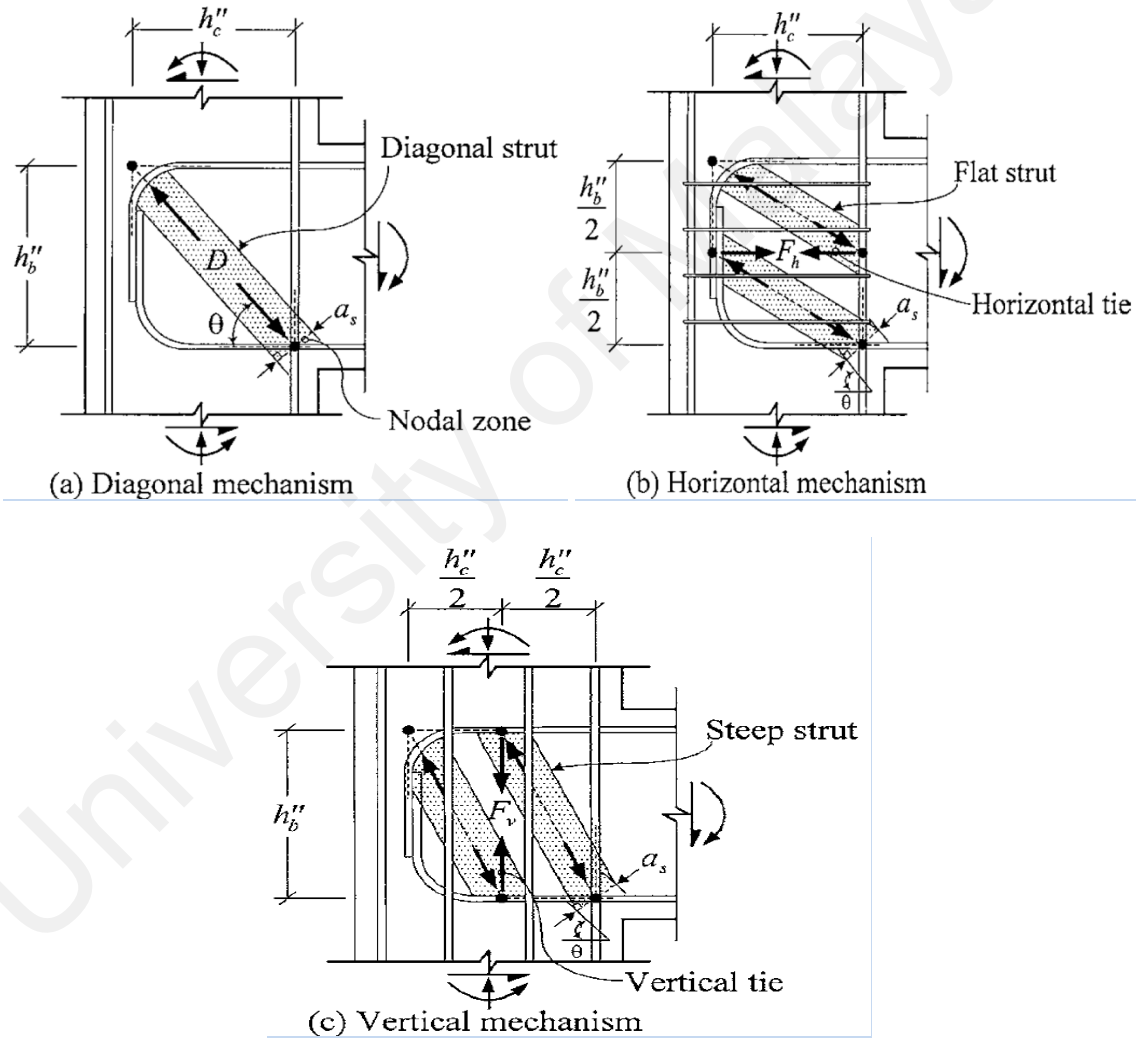

Figure 2.18: Assumption for transmission of shear forces in exterior beam-column joints (Hwang & Lee, 1999)

Park & Mosalam (2012) was concerned about investigating an analytical model to predict the shear strength of exterior RC beam-column joints without transverse

reinforcement. The proposed model was based on two inclined strut mechanisms in joint zone called ST1 and ST2 as shown in Figure 2.20, taking into account the variation effect of joint aspect ratio, beam reinforcement ratio and the gradual drop in bond strength between concrete and steel bars. In addition, the proposed model is valid for

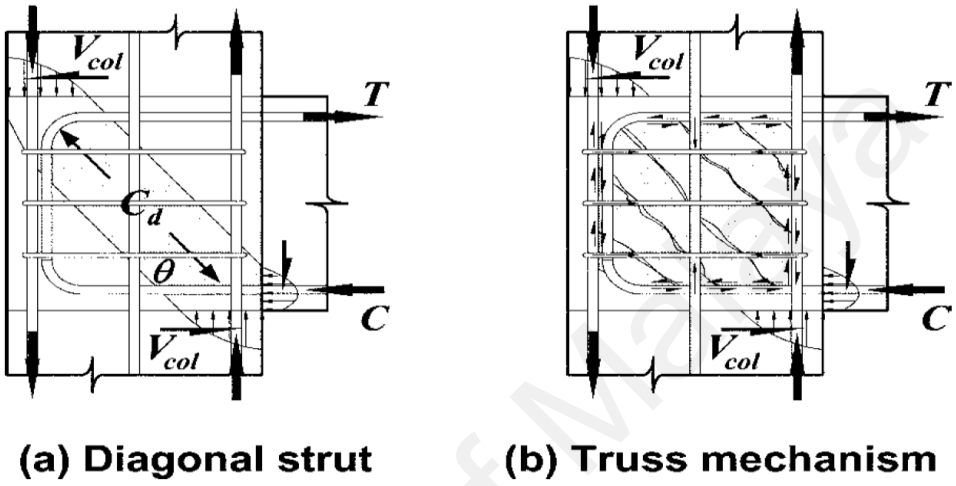

Figure 2.19: The mechanism of force transmission system in exterior beam-column joint (Hwang et al., 2005)

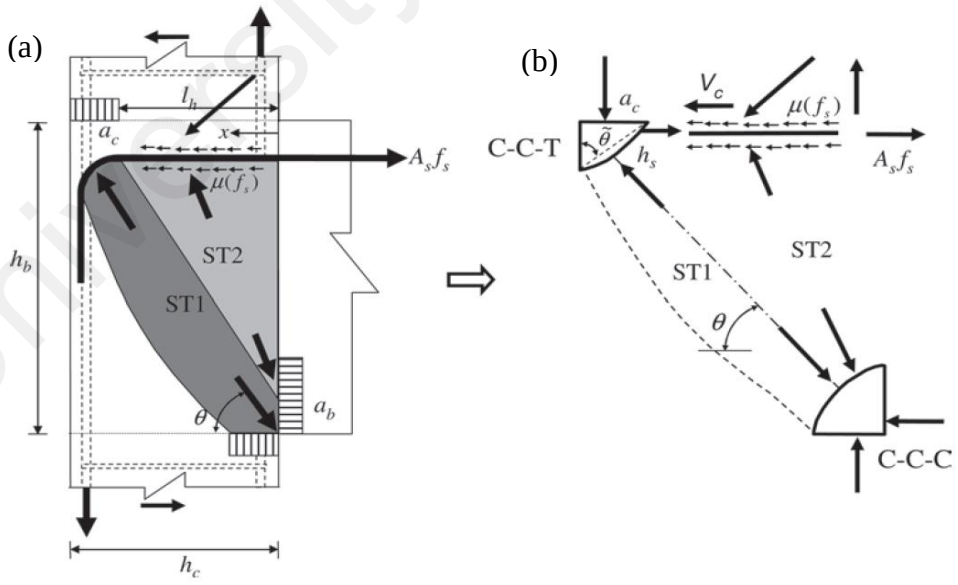

Figure 2.20: (a) Assumed dual strut-and-tie model (b) equilibrium condition in exterior beam-column joint (Park & Mosalam, 2012)

evaluating the joint moment-rotation relation. Moreover, the new model is verified by applying several experimental data of joint shear strength without transverse reinforcement for several published literature. Figure 2.21 shows the diagonal compression and tension zones in exterior RC beam-column joint (Murty et al., 2003) and Fig. 2.22 indicates forces acting at the interface of the joint.

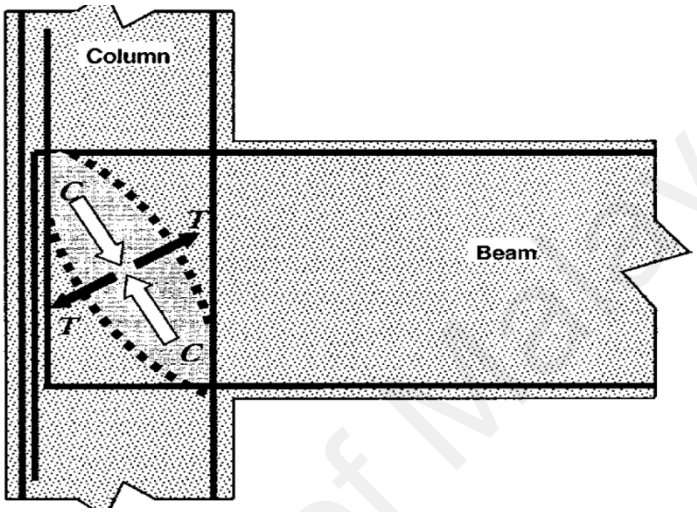

Figure 2.21: Diagonal compression and tension zones in exterior RC beam-column joint (Murty et al., 2003)

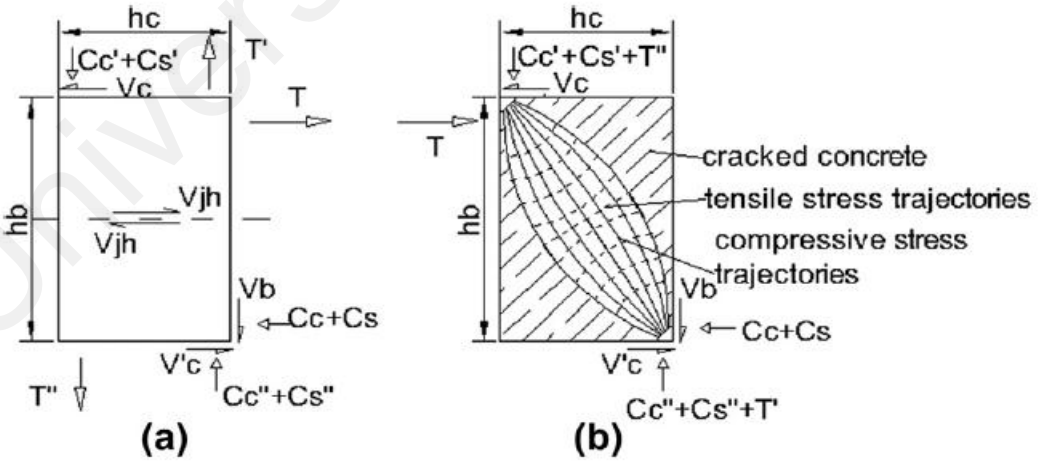

Fig. 2.22 (a) Forces acting at the interfaces of the joint with the beam and column elements and shear force V_{jh} at the horizontal cut at mid height of joint (b) compressive and tensile stresses trajectories assumed to develop within the joint at its ultimate limit state.(Kotsovou & Mouzakis, 2012)

2.4.2 Design approaches

2.4.2.1 ACI- ASCE committee 352

According to ACI- ASCE committee 352 (352R-02, 2002), the shear strength of beam-column joints exposed to seismic excitations can be estimated as

$V_j = 0.083\gamma\sqrt{f_c'}\, b_j h_c$ (in SI units) (Equation 2.1)

For the case of exterior beam-column joint, γ should be taken as 12. The last formula results in:

$V_{jh} = \sqrt{f_c'}\, b_j h_c$ (Equation 2.2)

The minimum transverse reinforcement amount of steel should be provided as a stirrup within the joint region against seismic or earthquake excitations, is calculated from the following formula:

$$A_{sv} = 0.3 \times \frac{s_v b_c^{"} f_c'}{f_{yv}} \left(\frac{A_g}{A_c} - 1\right) \quad \text{(Equation 2.3)}$$

2.4.2.2 NZS 3101:2006

The maximum nominal shear stress estimation according to the new Zealand code NZS 3101 (NZS3101, 2006), stated that (For beam column joint zones the larger of the nominal shear stresses calculated from the design shear forces in either the horizontal or vertical directions shall be equal to or less than the smaller of 0.2 f_c' or 10 MPa). The equation is formulated as follows:

$V_{jh} = 0.2 f_c'\, b_j h_c$

or $V_{jh} =$ 10 MPa whichever is smaller — (Equation 2.4)

2.4.2.3 BS 8110: 1997

The beam-column joint is considered according to BS 8110 (B/525 Technical Committee, 1997) considerations as that part of column specified within the depth of

beam. The shear strength is estimated by considering the joint which receives column axial load associated with transferred bending moment coming from the beam.

$$V_{jh} = \left(v_c + 1.33 \times 0.6 \frac{N}{A_g} \frac{Vh_c}{M}\right) b_c d_c + A_{sv} f_{yv} \left(\frac{d_c}{s_v}\right) \quad \text{(Equation 2.5)}$$

where

V_{jh} = Shear force at beam-column joint
M = the design bending moment
v_c = the design shear stress of concrete without reinforcement and axial load
A_g = gross area of column section
V = the design shear force
A_{sv} = cross sectional area of joint links
f_{yv} = yield strength of the links
f_c' = compressive strength of concrete cylinders
$b_c^{"}$ = core dimension of tied column, outside to outside edge of the links
b_c = width of the column section
d_c = effective depth of the column section
h_c = total height of column section
s_v = spacing of links
N = axial force on the column

2.5 Research gaps

The recent chapter addressed researches and experimental works dealt with the mechanical properties, strength and deformation characteristics, and toughness of steel fiber reinforced concrete (SFRC), dealt with the strength and deformation characteristics, mechanical properties, microcracking behaviour, micromechanical requirements, microstructure of ECC and commonly dealt with the main parameters affecting the exterior normal concrete (NC) beam-column joints exposed to cyclic or seismic loading without or with the inclusion of transverse reinforcement, researches dealt with exterior beam column joints replaced by SFRC and exterior beam-column joints replaced by ECC.

The main gaps are determined and recorded from the past studies, are presented in the following points:

1. The authors didn't assess the characteristics of ECC flexural toughness and compare it with the other fibrous composites. Also, the authors didn't assess the effect of type of polymer fibers in ECCs and compare among them. In addition, the authors didn't assess the effect of fiber content and aspect ratio (reinforcing index) on the flexural strength and deformation characteristics, and on the cut-off point of flexural strain-hardening behavior of ECC.

2. Due to the great importance of uniaxial tension capacity and deformation characteristics of ECC and its role in determining the applicability of ECC. The authors presented some experimental works regarding the tensile test using different kinds of polymer fibers. However, the authors didn't address the effect of fiber content and the fiber aspect ratio (effect of reinforcing index). The authors didn't compare among the different types of ECC based on type of polymer fibers used in fresh ECC. Besides, the authors didn't assess the cut-off point of tensile strain-hardening behavior of ECC.
3. Many experimental works in past studies were conducted to apply the SFRC in exterior beam-column joints under seismic or cyclic loading to enhance the shear capacity and ductility. However, there are only two research studies on the application of ECC in the exterior beam-column joints. The first study was conducted by Yuan et al. (2013) applying ECC-PVA, whereas the second study was conducted by Zhang et al. (2015) applying ECC-PP in the exterior beam-column joint zone.

The authors in both studies didn't evaluate the effect of type of fibers and reinforcing index of polymer fibers on the exterior beam-column joints. The authors also didn't evaluate the angular rotation, joint shear strength factor and estimation of factor of

safety in the ECC joint zone. The authors in the second study didn't assess the actual capacity and actual mode of failure in ECC joints as the principle of strong joint-weak beam was followed in the experimental work.

In this thesis, all the gaps aforementioned above will be addressed based on three stages of experimental work will be shown in Chapter 3.

CHAPTER 3: EXPERIMENTAL PROGRAM

3.1 Introduction

This chapter addresses the experimental program of three different stages in this project. The first stage is summarized by casting small slabs with ECC using three different polymer fibers, and then testing them for flexural strength and deformation characteristics. Accordingly, it was possible to identify the appropriate type of fiber which is applicable for producing cemetitious composite with strain hardening behavior.

The second stage of the experimental program was represented by casting and testing sixteen ECC I-shaped specimens under direct tensile loading, using two different kinds of polymer fibers to obtain the direct tensile stress-strain relationship. The main objective for this work is to assign the reinforcing index value, for each kind of fibers, at which the ECC is applicable. This stage is extremely necessary to assign the fiber content sufficient to produce the ECC which attains the basic definition of high performance fiber reinforced cementitious composites (HPFRCC). This stage is considered as a preliminary work to the third stage which is essential for this project.

The third stage includes casting and preparing fourteen full-scale reinforced concrete (RC) exterior beam-column joint specimens for testing under reversed cyclic loading. Two of them were cast with normal concrete, with and without inclusion of steel hoops in the joint zone. The other specimens were prepared by replacing the normal concrete with ECC in the joint zone using two different types of polymer fibers which are PVA and PE fibers. With each type of fibers, six ECC beam-column joint specimens were cast with different reinforcing indices and steel hoops inclusion. This stage also consists of measuring the load at the tip of the beam and the moment at the joint, measuring the strain amount at several points on beam longitudinal steel bars, measuring the principal strains in several points within the joint zone and measuring the rotation amount at the

center of the beam-column joint. The main parameters considered in this work are the inclusion of lateral steel hoops in the normal concrete joints, the inclusion of ECC in the joint zone, type of polymer fiber, reinforcing index and the inclusion of lateral steel hoops in the ECC joint zone.

3.2 ECC flexural specimens (first stage experimental program)

3.2.1 Experimental work

For this stage, timber moulds with dimensions of 590mmx220mmx25mm were constructed and prepared for the casting of ECC flexural specimens (ECC slabs) (Figure 3.1a). The ECC slabs were cured for 28 days inside a water tank at ambient laboratory temperature. The ECC mix ratios and weight of ingredients per $1m^3$ are illustrated in Table 3.1. The main parameters used with the ECC slabs are type of fiber, fiber content (V_f %) and aspect ratio (l/d), i.e. length/diameter of fiber. The mechanical properties of the polymer fibers are illustrated in Table 3.2. As shown in Table 3.3, 21 ECC slabs were cast and prepared for testing using three main types of polymer fiber, polyvinyl alcohol (PVA RECS15), polypropylene (PP Mono Tuf), and polyethylene (PE) fibers. For PVA RECS15, two different aspect ratios were used, A.R= 210 (length=8 mm) and A.R=316 (length= 12 mm) respectively, with five fiber volume contents, V_f = 1, 1.5, 2, 2.5 and 3% for each aspect ratio. For the PP Mono Tuf fibers, three specimens were cast with V_f = 1.5, 2, 2.5%. For the PE fibers, two different aspect ratios were used, A.R=316 (PE 4800D) and A.R=500 (PE 1600D) respectively, with fiber volume contents V_f =1, 1.5, 2 and 2.5% for each aspect ratio.

The cement type used in this work was Type I ordinary Portland cement (S.G.= 3.15), together with fine silica sand with maximum size of particles equals to 200 micron (S.G.= 2.65), and fly ash Type F (S.G.= 2.38). The binder is considered as the sum of the weight of the cement and fly ash. The superplasticiser (water reducing agent) used was Sika ViscoCrete1600. For each mix, the dry materials were mixed in a rotating

drum mixer for three minutes and then the water with SP was gradually added and mixed for another three minutes. Thereafter, the polymer fibers were slowly added with the rotation of the mixer to attain an appropriate workability of slump equals to 90–150mm (Figure 3.1 b and c). The testing of the ECC slabs was conducted within the period of 28 days, using an INSTRON-displacement-controlled compressive testing machine under four-point flexural loading with a displacement rate of 0.005 mm/s. The span of 540mm for the slab was equally divided into three parts. A linear

(a) (b)

(c) (d)

Figure 3.1: (a) Timber molds for slabs (b) slump test for ECC (c) Fresh ECC ready to cast (d) loading process in ECC slabs

variable differential transducer (LVDT) was fixed at the centre of the span for each slab to measure the deflection (Figure 3.1 d). Each test was continued until the load value reduced to less than 25% of the ultimate value.

Table 3.1: Mix proportion used in ECC specimens

Cement C/C	Sand S/C	Fly ash FA/C	Water W/B	(SP/B)%
1 (820)	0.8 (656)	0.25 (205)	0.37 (379.25)	0.3-0.35 (3.075-3.588)

Values given in parenthesis are given by weight in kg/m^3.
B - Binder i.e. cement and fly ash

Table 3.2: Mechanical Properties of polymer fibers*

Type of fiber	grade of fiber	Specific gravity	Length of fiber (mm)	Diameter of fiber (μm)	Aspect ratio (A.R) l/d	Elongation %	Tensile strength MPa	Modulus of elasticity MPa
PVA	RECS15-8	1.3	8	38	210	7	1600	42
PVA	RECS15-12	1.3	12	38	316	7	1600	42
PP	Mono-Tuf	0.91	12	48	250	10-20	350	21
PE	4800D	0.97	12	38	316	5-8	1950	39
PE	1600D	0.97	12	24	500	5-8	2700	82

*Based on manufacturer's data

3.2.2 Toughness estimation for ECC based on ASTM C1018

In order to estimate the flexural performance and the amount of energy absorption of ECC slabs, the ASTM C1018 (C1018, 1997) standard test method to determine the toughness and toughness indices for FRC was followed. Some relative values called "toughness indices" express the flexural performance and indicate the degree of ductility and energy absorption capacity up to a specified value of deflection and the ability of ECC slabs to deflect freely without any sudden failure. The evaluation of

Table.3.3: Specimens of ECC slabs with different polymer fibers

specimen	Symbol	Type of fiber	Fiber content %	Reinforcing index V_f*(l/d)
1	PVA_1	RECS15-8	1.0	210
2	PVA_2		1.5	316
3	PVA_3		2.0	421
4	PVA_4		2.5	527
5	PVA_5		3.0	631
6	PVA_6	RECS15-12	1.0	316
7	PVA_7		1.5	474
8	PVA_8		2.0	632
9	PVA_9		2.5	790
10	PVA_{10}		3.0	948
11	PP_1	Mono-Tuf	1.5	375
12	PP_2		2.0	500
13	PP_3		2.5	625
14	PE_1	4800D	1.0	316
15	PE_2		1.5	474
16	PE_3		2.0	632
17	PE_4		2.5	790
18	PE_5	1600D	1.0	500
19	PE_6		1.5	750
20	PE_7		2.0	1000
21	PE_8		2.5	1250

*Determined by volume

toughness indices depends on knowing the first-crack load and first-crack deflection values which necessitate determining them accurately on load-deflection curve. According to ASTM C1018 (C1018, 1997) definition, toughness index is the ratio of the area under load-deflection curve up to limited deflection value, to the area up to the deflection established at first crack as indicated in the following expression:

$$I_{T=}\frac{area\ under\ (load-deflection)\ curve\ up\ to\ limited\ deflection\ value}{area\ under\ (load-deflection)\ curve\ up\ to\ first\ crack\ deflection\ \delta} \qquad \text{(Equation 3.1)}$$

As shown in Figure 3.2, If T=5, the toughness index I_5 is equal to the ratio of area under the curve up to a deflection corresponding to three times the first crack deflection (3δ) (OACDBO area) to the area up to first crack deflection (OAB area). Similarly, the toughness indices I_{10} and I_{20} are calculated as the quotient of area under the load-deflection curve up to 5.5δ (OACEFDBO area) and 10.5δ (OACEGHFDBO area) to

the area up to the first crack deflection respectively. For brittle materials, the toughness index is equal to 1.

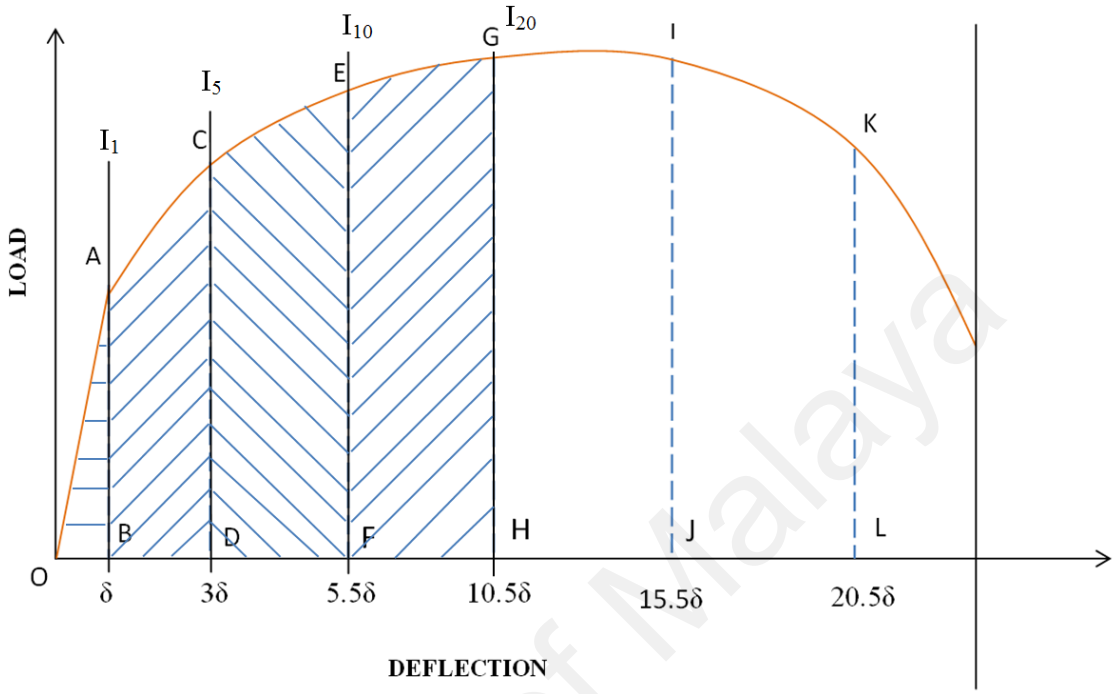

Figure 3.2: General definition of toughness indices (C1018, 1997)

The amount of area obtained under the load-deflection curve is a direct scale to the flexural toughness and the ability of ECC slab to absorb energy and to attain higher ductility. The higher amount of toughness (or area under load-deflection curve) is evaluated, the higher ductility and energy absorption capacity which results.

ASTM (C1018, 1997) allows for the evaluation of toughness indices I_{30}, I_{40} or more corresponding to area up to deflections $15.5\delta, 20.5\delta$ or more respectively. The higher the subscript T value of toughness index for testing beam or slab sample, the higher the flexural toughness and energy absorption capacity. The toughness index value I_T is a cumulative number of its predecessor I_S, (where T>S), plus the additional value determined from the area bounded between the corresponding deflection values for I_S and I_T. For elastic-perfectly plastic materials, I_5=5, I_{10}=10, I_{20}=20 and so on. In this

study and according to the load-deflection results, it is convenient to discuss the variation of toughness indices $I_{5,}$ $I_{10,}$ $I_{20,}$ I_{30} and I_{40} for PVA slabs. The toughness indices $I_{5,}$ I_{10}, I_{20}, I_{30} , $I_{40,}$ $I_{50,}$ …..until I_{100} for PE slabs may possibly be evaluated because of the high ductility and high deflection results.

Residual strength factor represents the amount of strength retained at the post-cracking stage within a specific interval as a percentage of the first crack strength. It is a measure of sustainability of beam or slab within a specific loading stage. The general formula for estimating the residual strength factor between two indices I_T and I_S as follows

$R_{S,T} = N(I_T - I_S)$ T>S (Equation 3.2)

where *N*= 100/ (T-S)

If S= 5 and T= 10 then N= 20 and $R_{5,10}$=20(I_{10}- I_5).

If S=10 and T=20 then N=10 and $R_{10,20}$=10(I_{20}- I_{10}) and so on

For brittle materials, the residual strength factor is equal to zero. However, for elastic-perfectly plastic materials, the R factors equal to 100. For PVA slabs, $R_{5,10}$, $R_{10,20}$, $R_{20,30}$ and $R_{30,40}$ were discussed and considered between the toughness indices I_5 and I_{10}, I_{10} and $I_{20,}$ I_{20} and I_{30}, I_{30} and I_{40}, respectively, while the residual strength factors $R_{5,10}$, $R_{10,20}$, $R_{20,30}$, $R_{30,40}$, $R_{40,50}$, until $R_{90,100}$ were evaluated for ECC PE slabs between the toughness indices I_5 and I_{10}, I_{10} and $I_{20,}$ I_{20} and I_{30}, I_{30} and I_{40}, I_{40} and I_{50}, until I_{90} and $I_{100,}$ respectively.

3.3 ECC direct tensile specimens (second stage experimental program)

3.3.1 Experimental work

For this stage, I-shaped steel molds were specially fabricated to cast and prepare I-shaped ECC specimens for direct tensile testing. The dimensions of the I-shaped mold are illustrated in Figure 3.3. As shown in Table 3.4, sixteen ECC specimens are cast and prepared for direct tensile testing using two types of polymer fibers, PVA RECS15 and

PE fibers. The I-shaped specimens were cured for 28 days inside a water tank at ambient laboratory temperature. The ECC mix proportions and the polymer fibers properties are illustrated in Tables 3.1 and 3.2 respectively.

For PVA RECS15, two different aspect ratios, A.R=210 (length=8mm) and A.R=316 (length=12mm), were used respectively, with four fiber volume contents, V_f =1.5, 2, 2.5 and 3% were used for each aspect ratio. For PE fibers, two different aspect ratios, A.R= 316 (PE 4800D) and A.R=500 (PE 1600D) were also used with four fiber volume contents, V_f = 1, 1.5, 2 and 2.5% for each aspect ratio, the mixing process and slump test for ECC was demonstrated in previous section, as shown in Figures 3.1 b and 3.1 c. The casting of I-shaped specimen was illustrated in Figure 3.4 a. For direct tensile ECC specimens, the aim of testing is to plot the tensile stress-strain relationship for various ECC specimens indicating the cut-off point of strain hardening behavior of ECC for the both kinds of polymer fibers and for different reinforcing indices. The testing was conducted using INSTRON displacement controlled tension testing machine, as shown in Figure 3.4b, with a displacement rate equals to 0.05 mm/min. The specimen was fixed in the machine via two steel grips which were fabricated for this purpose and fixed at the upper and lower points of the machine respectively upon specimen fixing. Two linear variable differential transducers (LVDT) were fixed via holders at both sides, one on each side of the specimen to measure the extension across the gauge during the loading process. The gauge length equals to 150mm located at the middle part of the specimen. The LVDTs are connected to a datalogger to record and store the data. Each test was continued until failure.

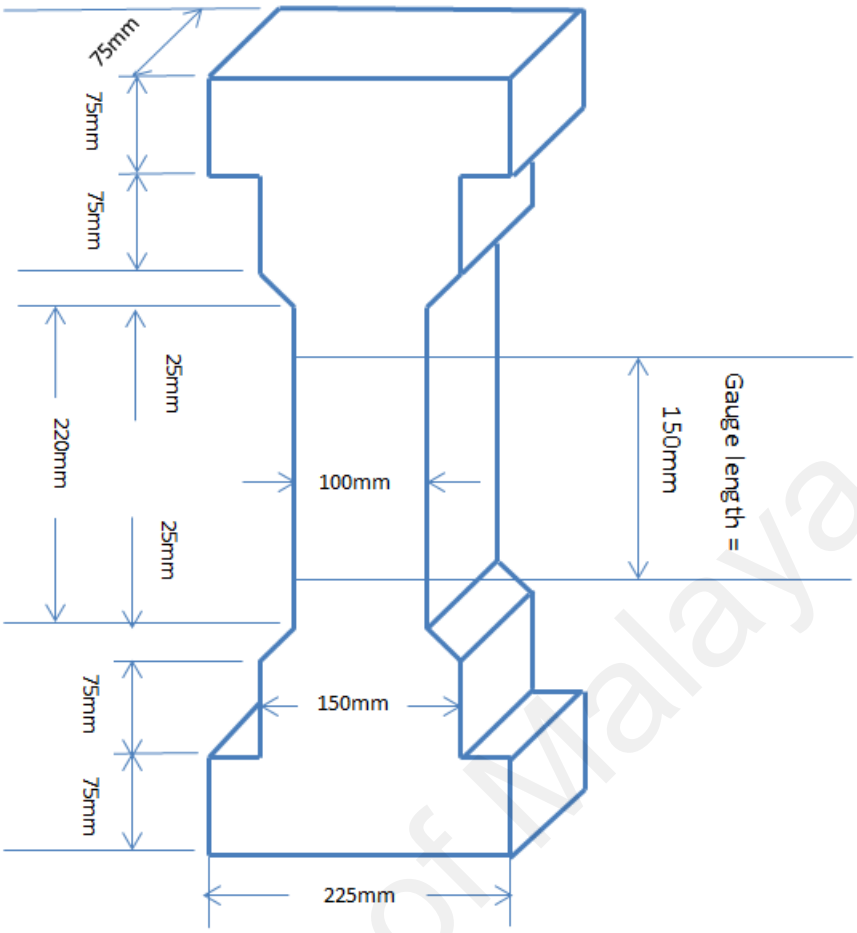

Figure 3.3: Direct tensile strength specimen, Shape and dimension

(a) (b)

Figure 3.4: (a) casting of I-shaped specimen (b) direct tensile testing of I-shaped specimen

3.3.2 Design of steel cages for tensile specimens

Direct tensile test was conducted with INSTRON machine by applying a pure axial tensile load through the vertical axis of specimen. After the development of the first crack and during the post cracking stage, it was revealed that the failure did not occur within the gauge length which is the narrowest part in the specimen. Major cracks occurred at the neck region of the specimen and widened gradually until failure occurred due to secondary tensile stresses developed at the neck region (Swaddiwudhipong et al., 2003; Zheng et al., 2001), as shown in Figure 3.5. The LVDTs within the gauge length were unable to record the significant readings during the loading process. For this reason, a steel cage was constructed and placed at each end of the specimen to transmit the crack development to the region within the web of specimen. The middle steel bars in the cage were extended into the specimen web to enhance the neck region and to prevent the occurrence of cracks within each of the ends, leaving a gauge length of 150mm only at the intermediate part of the specimen. Figure 3.6 shows the details of the cage bars, Figures 3.7a and 3.7b show the cage and cage placement in the mold.

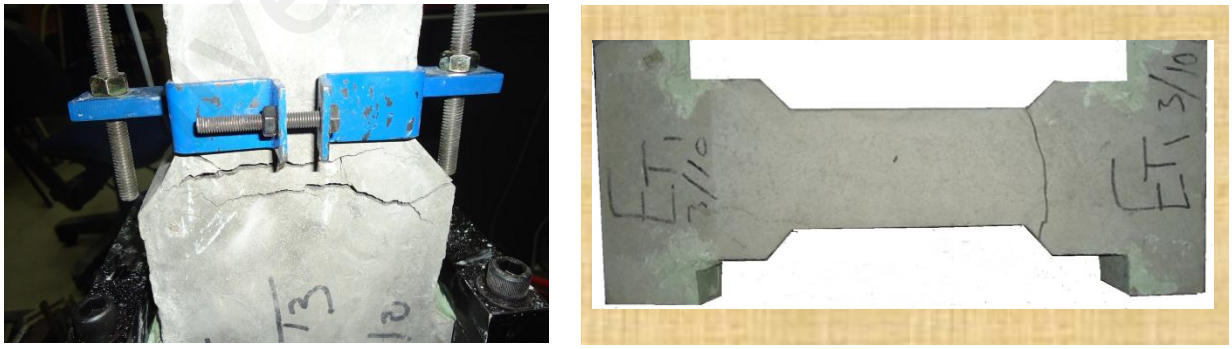

(a) (b)

Figure 3.5: Failure of direct tensile ECC specimens occurred in the neck

Table 3.4: Schedule for direct tensile ECC specimens

S	Tensile specimen symbol	Type of fiber	grade of fiber	Aspect ratio A.R	Fiber content V_f
1	$TPVA_1$	PVA	SECS15-8mm	211	1.5
2	$TPVA_2$				2.0
3	$TPVA_3$				2.5
4	$TPVA_4$				3
5	$TPVA_5$	PVA	SECS15-12mm	316	1.5
6	$TPVA_6$				2.0
7	$TPVA_7$				2.5
8	$TPVA_8$				3
9	TPE_1	PE	4800D	316	1
10	TPE_2				1.5
11	TPE_3				2.0
12	TPE_4				2.5
13	TPE_5	PE	1600D	500	1
14	TPE_6				1.5
15	TPE_7				2.0
16	TPE_8				2.5

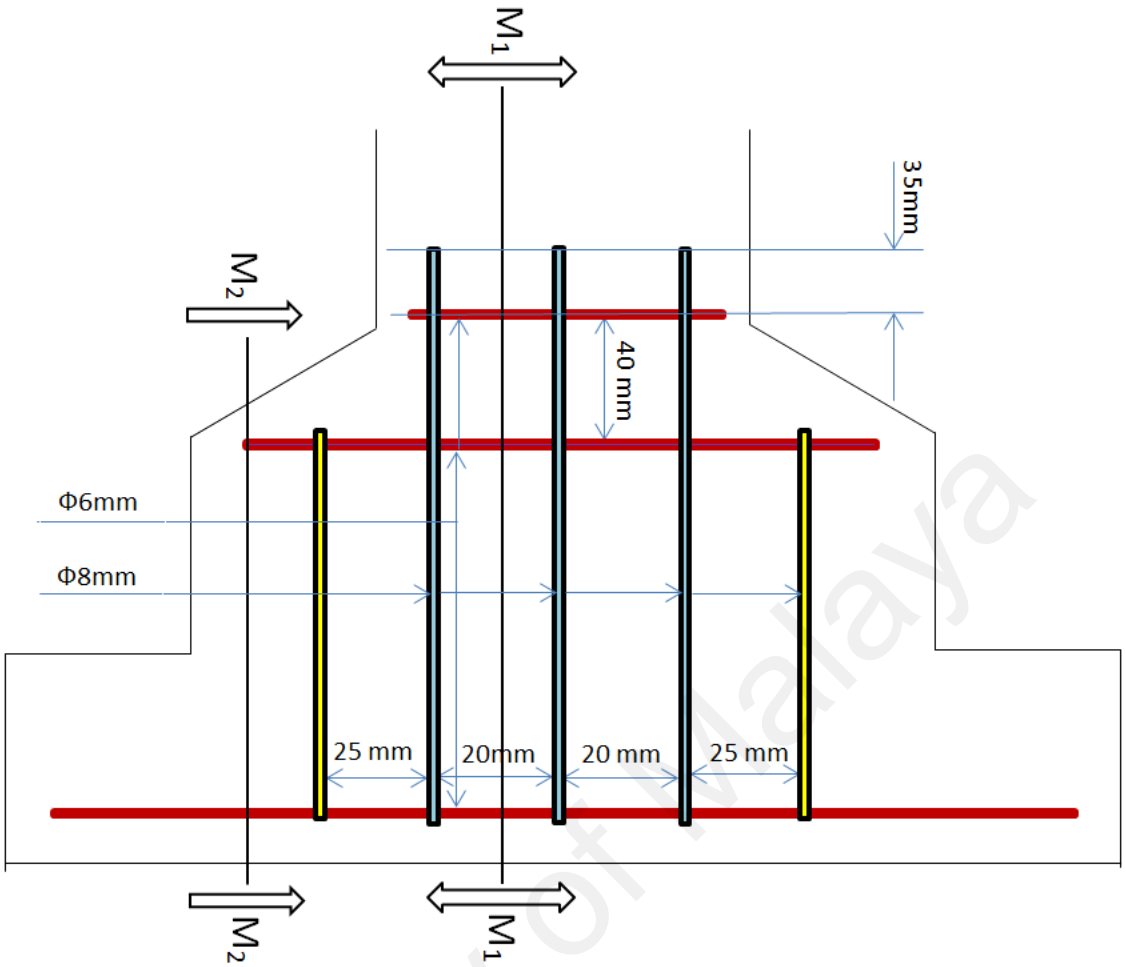

(a) Longitudinal section in the grip area of sample

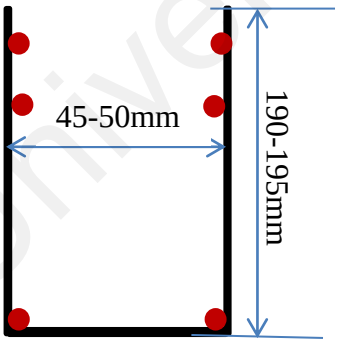

(b) Section $M_1 - M_1$

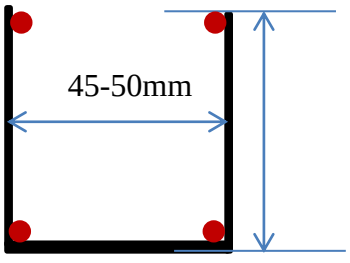

(c) Section $M_2 - M_2$

Figure 3.6: Details of the cage reinforcement

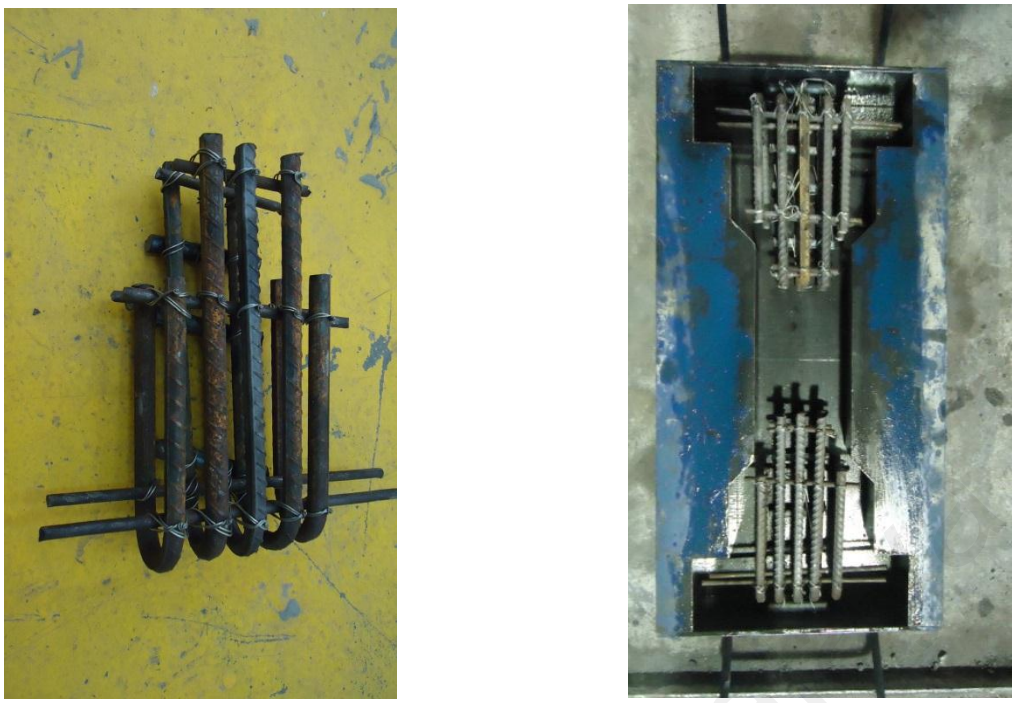

(a) (b)

Figure 3.7: (a) Steel cage (b) Placing of cages in mold

3.4 Exterior beam-column joint specimens (third stage experimental program)

3.4.1 Experimental work

At this stage, a steel mold was fabricated and prepared for casting the exterior beam–column joint specimens (T type joint specimens). The specimen consists of a 2.00 m high column and a 1.25 m long beam. The beam connects to the column as a cantilever at the middle region of the column height (as shown in Figure 3.8). The cross section height and width dimension for both column and beam is 250 mm and 170 mm, respectively. In terms of the design of the reinforcement details for the specimens, the concept of "strong component-weak joint" was applied to realize the behavior of joint and the mode of failure under cyclic excitation. The reinforcement details for all specimens are shown in Figure 3.9. The lateral steel hoops are installed for some of the specimens in the joint zone, as indicated in Table 3.6. Owing to the high cost of ECC mix production, the ECC mixture was placed within the joint zone only, as shown in

Figure 3.8, which is the most critical portion in the beam-column specimen and which is highly vulnerable to the seismic failure. The remaining parts of the specimen were cast with normal concrete. For this purpose, three steel gates were fabricated and placed in the mold to act as separators between the normal concrete and the ECC mix during the casting process, as shown in Figures 3.10 and 3.11.

3.4.2 Mix proportions

Table 3.5 shows the mix proportion for both normal concrete (NC) and ECC mixes. The NC mix is composed of ordinary Portland cement Type 1, silica sand from zone 2, according to the grading limits for fine aggregate, (BS 812), coarse aggregate with maximum size of 19 mm, fly ash Type F to improve workability, and superplasticizer (SP) from Sika ViscoCrete1600. The ECC mix consists of the same type of cement described above, fine silica sand with maximum size particles of 200 μm, fly ash Type F, same SP mentioned above, and finally PVA or PE filament fibers, with specified amount of fiber content and aspect ratio.

Table 3.5: Mix proportion used in beam-column specimens

Type of mix	Cement C/C	Sand S/C	Gravel G/C	Fly ash FA/C	Water W/B	(SP/B)%
Normal concrete NC	1 (360)	2 (720)	3 (1080)	0.125 (90)	0.47 (171)	0.2 (0.81)
Engineered cementitious composite ECC	1 (820)	0.8 (656)	-	0.25 (205)	0.37 (379.25)	0.3-0.35 (3.075-3.588)

B - Binder i.e. cement and fly ash
( ) - by weight in kg/m^3

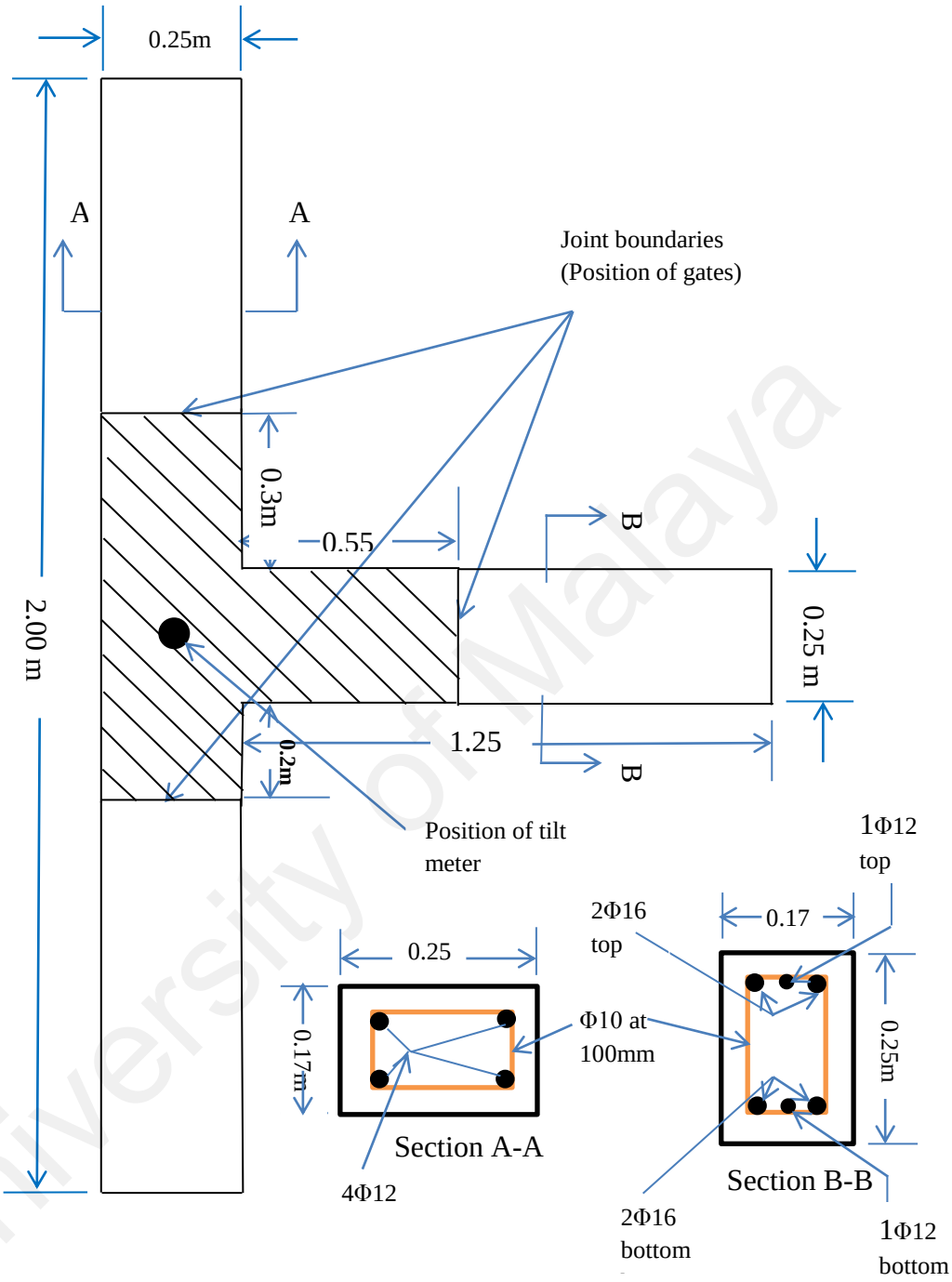

Figure 3.8: Beam-column specimen, reinforcing details and dimensions

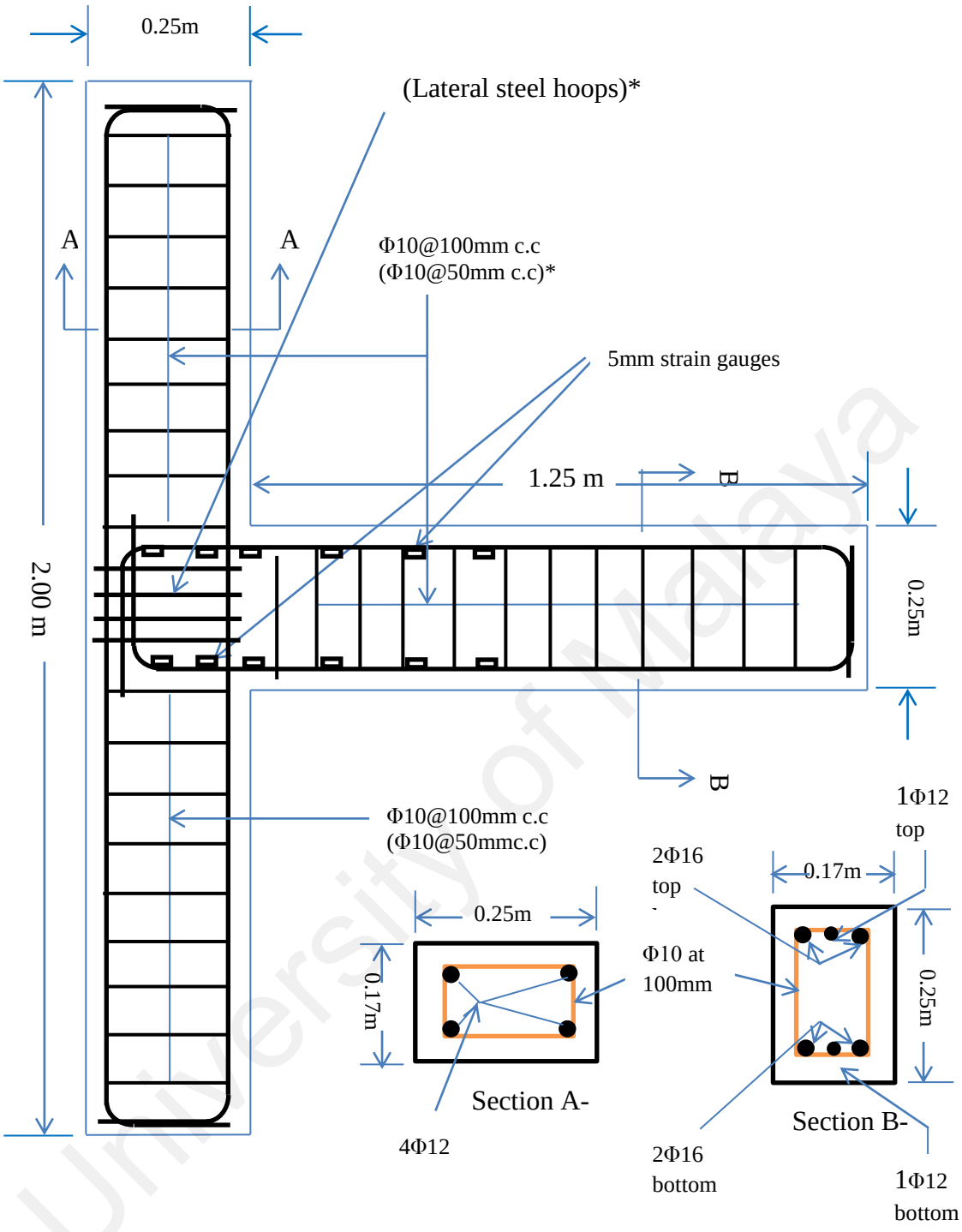

( )*In case of seismically designed type 2 joint

Figure 3.9: Overall details of beam-column specimen

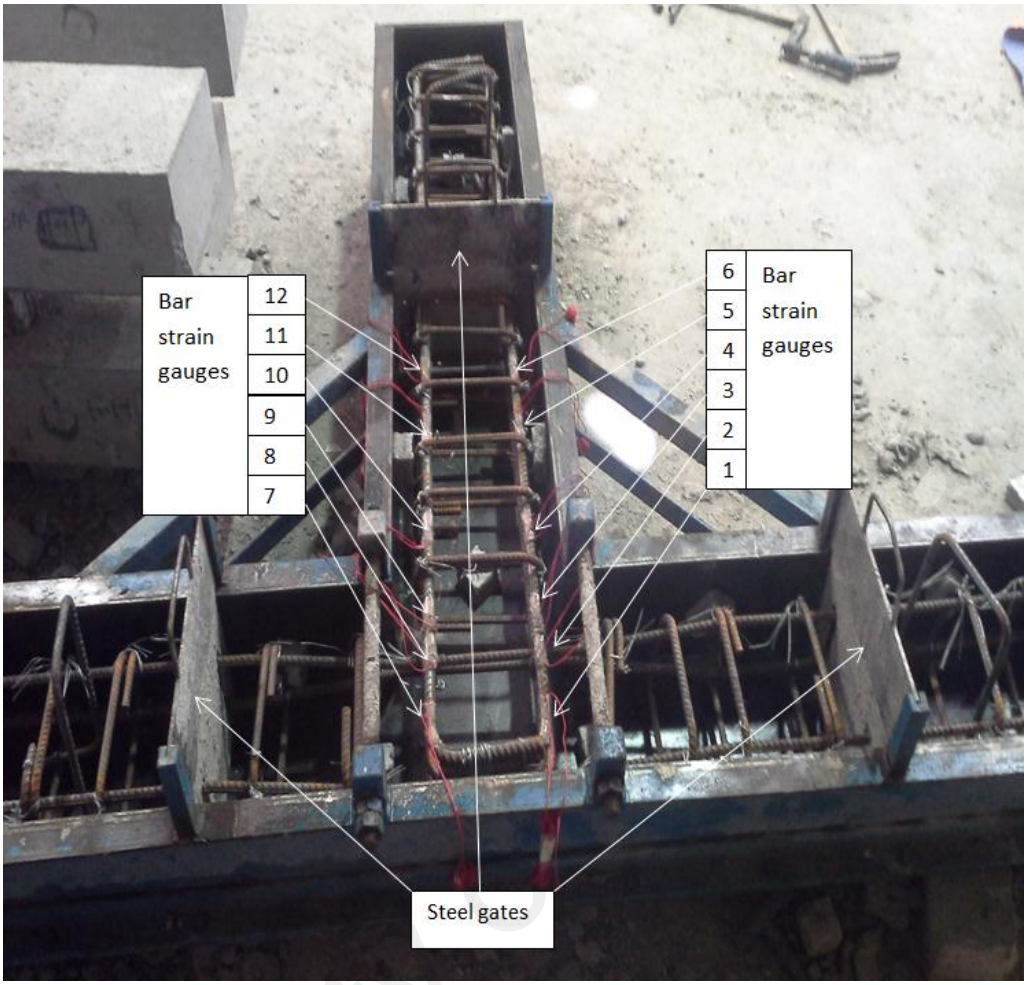

Figure 3.10: Strain gauges location on the longitudinal bars and the location of the gates inside the mold

3.4.3 Mixing process

The mixing process for the NC specimen was done by adding all the dry materials inside a drum mixer and mixing them for three minutes. Subsequently, all the water was gradually added into the mixer and the SP was then added based on the mix design. The mixing process continued for five minutes to obtain the proper workability. After getting a homogenous mix, the casting process started by supplying the fresh concrete to the steel mold with three layers of concrete. Each layer was compacted with internal vibrator and the external surface of the specimen was trowelled. The same procedure above was applied to the ECC specimen except that the steel gates were placed inside

the mold (Figure 3.10) and the mixing process was applied on two mixes at the same time by preparing two drum mixers. After adding the SP into the ECC mix, the PVA, or PE fibers were gradually supplied in small batches into the mixer. The mixing process continued for ten minutes to obtain a homogenous and good workable ECC mix. The casting and compaction process for both mixes were carried out at the same time (Figure 3.11). At the end of casting, the steel gates were removed and the boundaries of both mixes were carefully vibrated again.

The curing process began 24 hours after casting upon demoulding and continued for 28 days by covering the specimen with several layers of sponge and spraying the sponges daily with water until the designed strength was obtained.

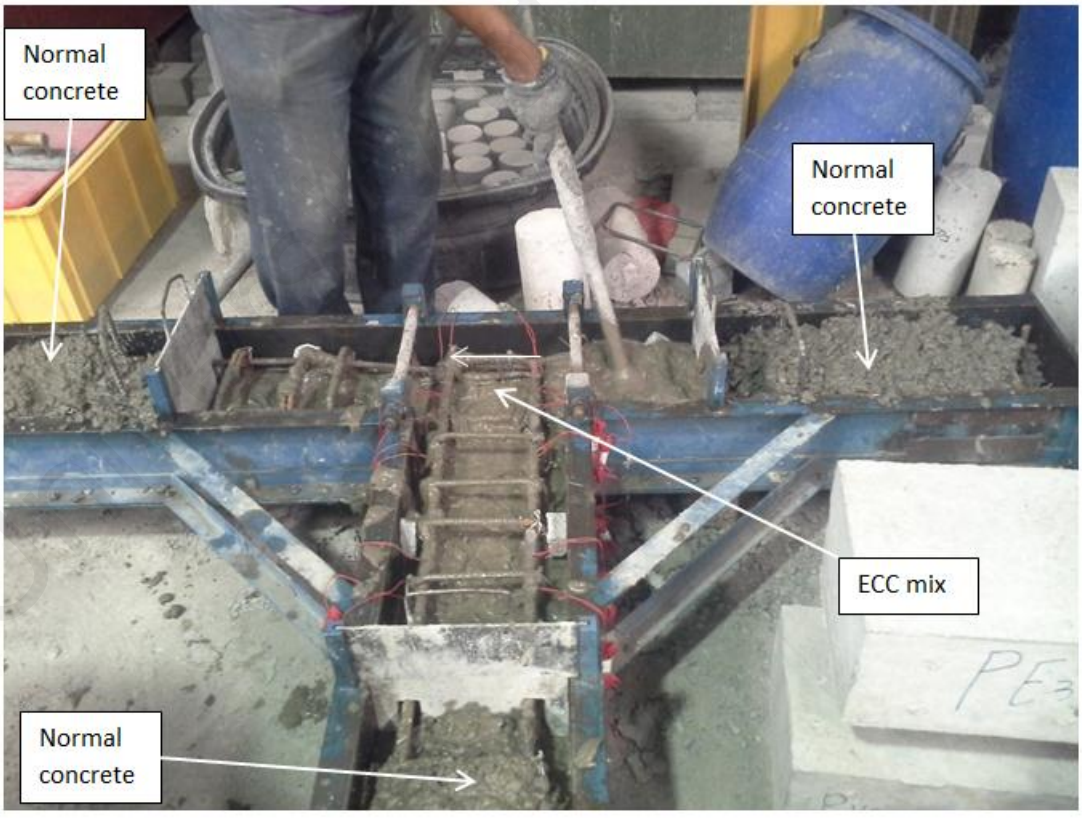

Figure 3.11: Casting process of ECC beam-column specimen

(a)

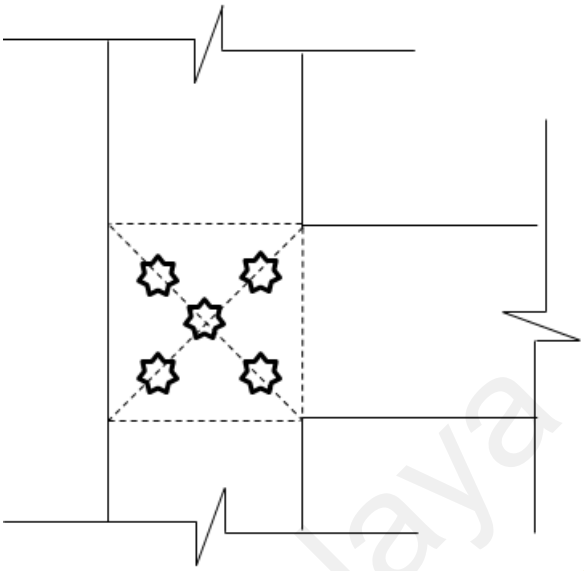

(b)

(c)

Figure 3.12: (a) 60mm rosette strain gauge (b) and (c) location of rosette strain gauges on the diagonals within the joint zone

3.4.4 Preparations for testing

12 Strain gauges of 5mm length was installed on the beam steel bars before casting, 6 on each bar at the top and bottom of the beam longitudinal axis, 2 gauges installed inside the joint zone, 1 at the junction point of the beam and column and another 3 inside the beam zone near the face of the column, as shown in Figures 3.9 and 3.10. After finishing the curing of the specimen, 5 rosette strain gauges (RSGs) of 60mm length were installed on the diagonals of the joint zone by a special kind of adhesive called PS ZI 10F with an accurate procedure followed for this purpose, as shown in Figure 3.12.

A tilt meter was installed at the center of the joint zone, as shown in Figure 3.8, to measure the amount of rotation developed at the center of joint zone during the loading cycles, as shown in Figure 3.13.

LVDT of 300 mm travel length was installed at the tip of the cantilever beam to measure the deflection during the testing process, as shown in Figure 3.13.

3.4.5 Testing process

As shown in Figure 3.13, the beam–column specimen was positioned and fixed orthogonally in a steel testing frame by placing the lower end of the column between two L-shaped steel attachments and tightened together with four steel threaded shafts, two at each side of the column. Before the onset of testing the column was subjected to a constant axial load of about 175 kN corresponding to 20% of the column axial load capacity until the completion of test by a hydraulic jack of 1000 kN capacity. The hydraulic jack with a load cell together attached and centered at the upper end of the steel testing frame, as shown in Figure 3.13. The jack was controlled by a hydraulic system to control the applied load, as shown in Figure 3.14.

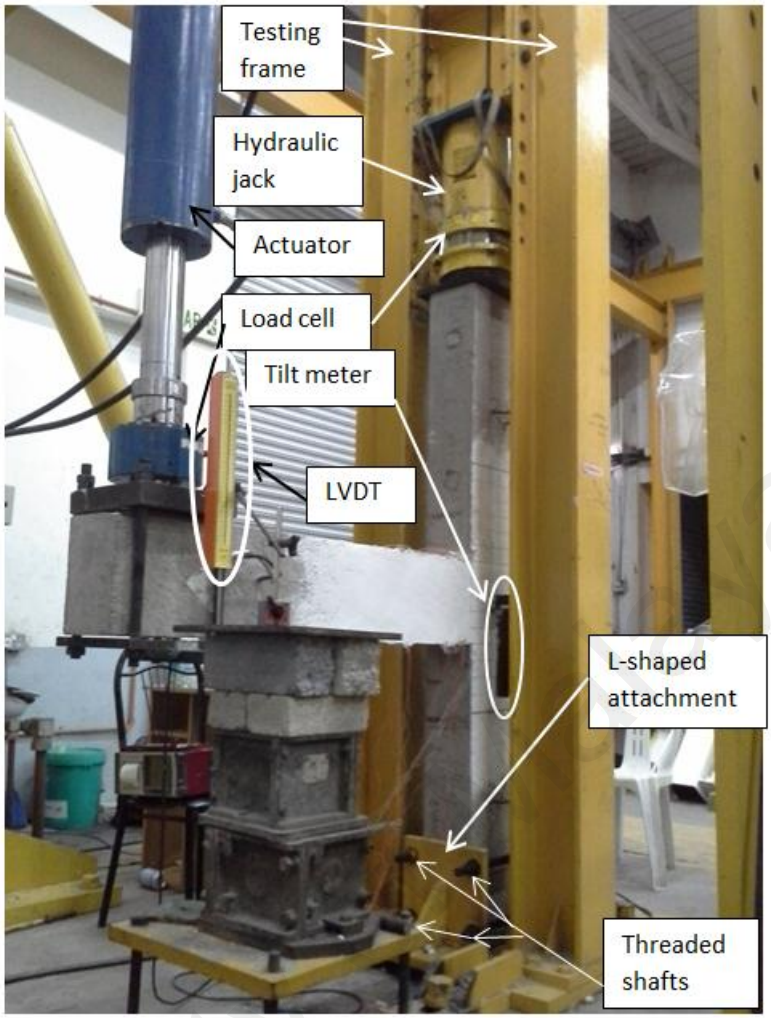

Figure 3.13: Testing process of beam-column joint

The cyclic action was simulated by a cyclic loading applied by a 250 kN actuator installed at the tip of the cantilever beam about 1.1 m from the face of the column. The upper end of the actuator was attached to a highly resistant steel frame while the lower end was attached and fixed to the tip of the cantilever beam with steel plates and threaded shafts. A dual-action 450 kN load cell was installed under the actuator to record the load applied by the actuator (Figure 3.13). The actuator was controlled by a hydraulic system to regulate the actuator motion and the direction of motion, as shown in Figure 3.14.

All strain gauges, RSGs, load cells and LVDT were connected to a datalogger which records and collects the data. The tilt meter was connected to a PC (personal computer)

to record the rotation values and the acquired data stored using PC-based data acquisition software, as shown in Figure 3.15.

During the testing process, the cracks propagation within the beam and joint zone were observed and recorded by a specialized technician during the testing process until the failure in structural lab, as shown in Figure 3.16. After finishing the testing, a new specimen is prepared by skilled workers for fixing after dismantling of the tested specimen, as shown in Figure 3.17.

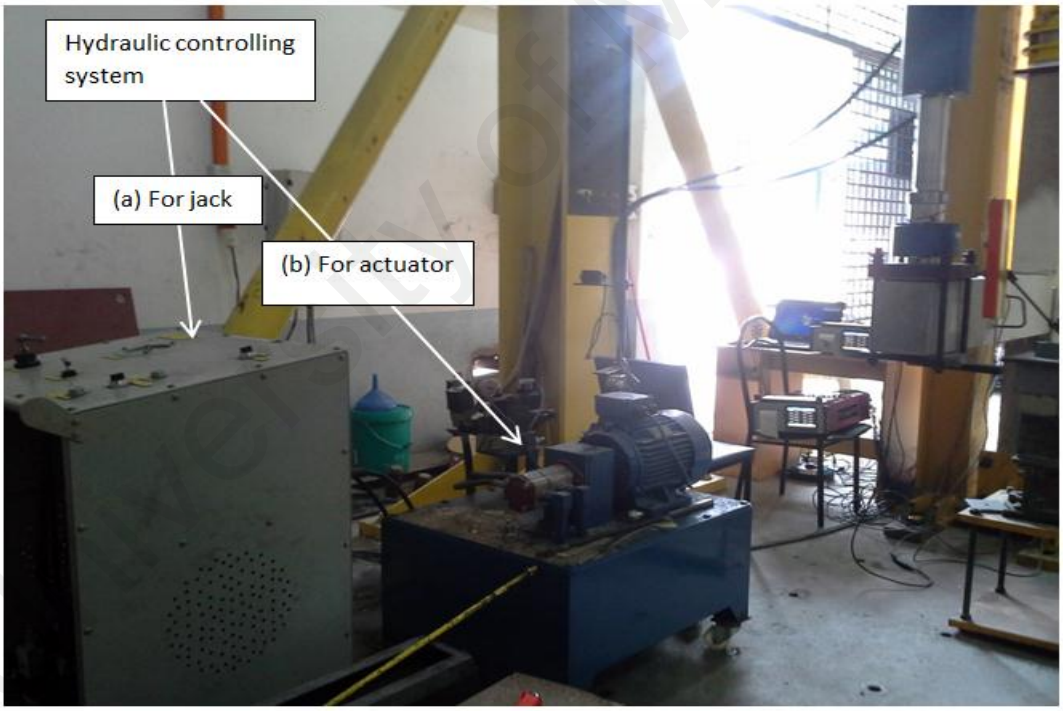

Figure 3.14: Hydraulic controlling system (a) for jack (b) for actuator

Figure 3.15: Data storage system

Figure 3.16: Observation of cracks propagation within the testing process

Figure 3.17: Fixing and dismantling of beam-column specimen

3.4.6 Loading history

The loading was applied to the beam–column specimen according to the cyclic loading history shown in Figure 3.18, starting with a small drift ratio of 0.25% and continuing with drift ratios of (0.5%, 1%, 1.5%, 2%, 2.5%, 3%… 8%). As reported from literature, the drift ratio is defined as the quotient of deflection measured at the free end of the beam to the length of the beam (Bedirhanoglu et al., 2010; S. J. Hwang et al., 2005; Lee & Yu, 2009; Parra-Montesinos & Wight, 2000). The failure might occur at a ratio less

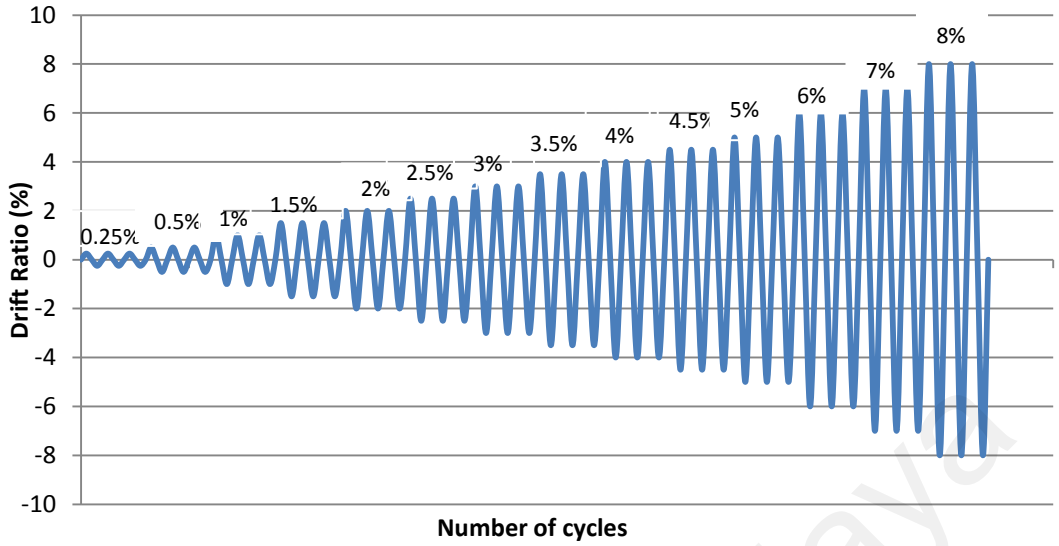

Figure 3.18: Loading history

than 8% or continue to the mentioned value based on the presence of ECC and the type of polymer fibers incorporated in ECC. At each value of drift ratio, the cyclic loading was repeated three times. The rate of actuator motion was 22mm/min.

3.4.7 Parameters of beam-column specimens

14 Beam-column joint specimens were cast and prepared for testing under reversed cyclic loading. The main parameters considered in this program are the inclusion of polymer fibers in ECC, type of polymer fibers, fiber content, reinforcing index and the inclusion of lateral steel hoops within the joint zone. Table 3.6 presents an integrated schedule for the preparation of beam-column joint specimens which includes all the parameters mentioned above. The schedule is divided into three zones and this is based on the type of concrete in the joint zone. The first zone was specified for normal concrete (NC) with two beam-column specimens are NC_1 and NC_2 prepared without and with the inclusion of lateral steel hoops respectively. NC_2 was designed seismically according to the design method detailed in ACI 352R-02 (352R-02, 2002). The second zone was specified for ECC with PVA fibers. Four beam-column specimens are PVA_1

to PVA_4 prepared with different reinforcing indices of PVA fibers without lateral steel hoops. PVA_5 and PVA_6 were prepared with the inclusion of one hoop and two hoops respectively. Similarly, the third zone was specified for ECC with PE fibers. Four beam-column specimens are PE_1 to PE_4 prepared with different reinforcing indices without lateral steel hoops. Furthermore, PE_5 and PE_6 were prepared with the inclusion of one hoop and two hoops respectively.

Table 3.6: Parameters of beam-column specimens

Type of fibers	Symbol of group	Grade of fibers	S	Symbol of specimen	No. of hoops	Aspect ratio (l/d)	Volume of fiber content (V_f%)	Reinforcing index
Normal concrete	NC	–	1	NC_1	–	–	–	–
		–	2	NC_2	4 (Fully seismically reinforced)	–	–	–
Hydraulic poly vinyl alcohol (PVA) fibers	PVA	RECS15-8mm*	3	PVA_1	–	(8/0.038) = 210	2.5	525
		RECS15-12mm*	4	PVA_2	–	(12/0.038) = 316	2.0	632
			5	PVA_3	–		2.5	790
			6	PVA_4	–		3.0	948
			7	PVA_5	1		2.0	632
			8	PVA_6	2		2.0	632
Polyethylene fibers (PE)	PE	4800D*	9	PE_1	–	(12/0.038) = 316	1.5	474
			10	PE_2	–		2.0	632
			11	PE_3	–		2.5	790
		1600D*	12	PE_4	–	(12/0.024) = 500	2.0	1000
		4800D*	13	PE_5	1	(12/0.038) = 316	2.0	632
			14	PE_6	2		2.0	632

*Refer to Table 3.2

3.4.8 Envelope load-deflection (or moment-rotation) relationship

The envelope relationship for load-deflection or moment-rotation is the plotted curve for the tip points of load-deflection (or moment-rotation) hysteresis loops in upper and lower direction of loading. Figure 3.19 indicates this relationship.

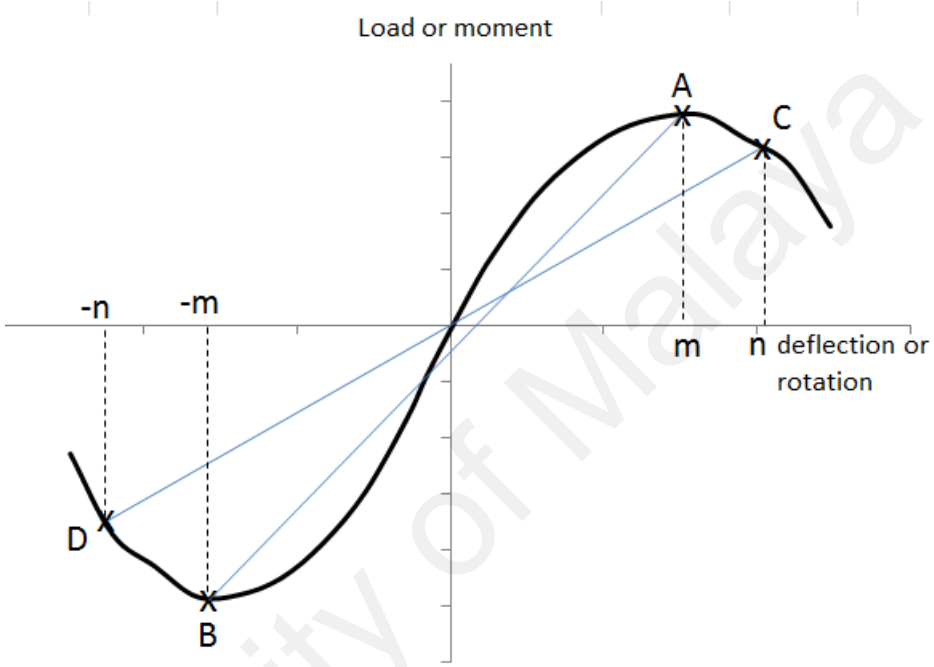

Figure 3.19: Envelope load-deflection (or moment-rotation) relationship

3.4.9 Ultimate shear capacity of the joint

Figure 3.20 shows the free body diagram for the force equilibrium of the exterior beam-column joint frame. From the equilibrium of forces, an equation was formulated to estimate the shear capacity in the joint zone:

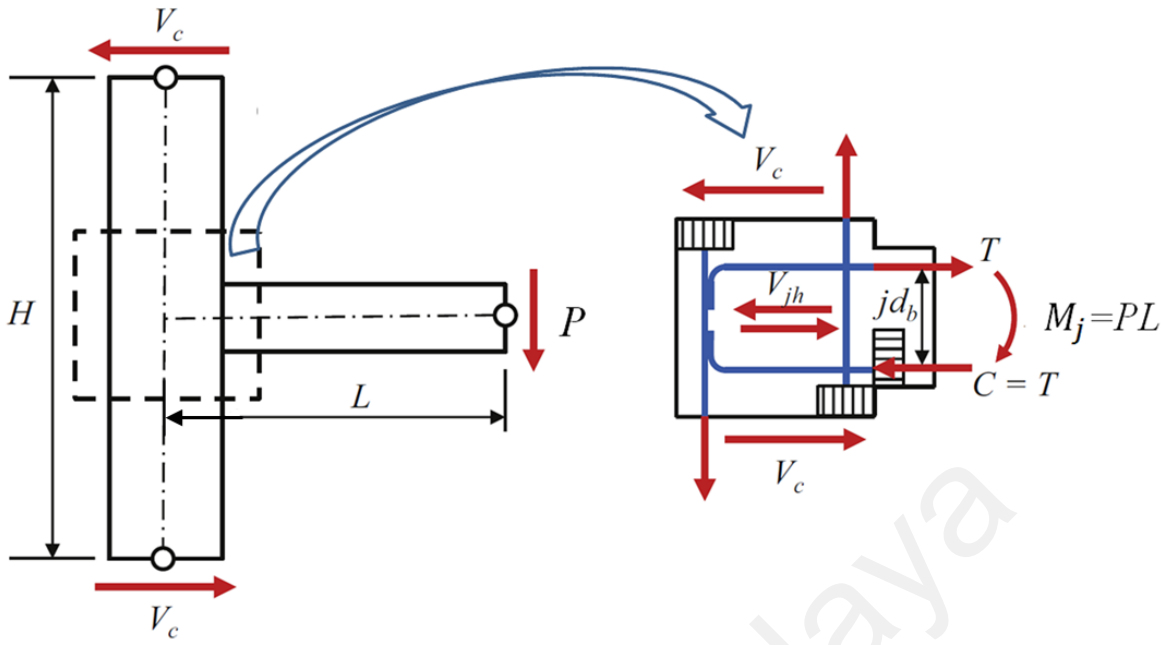

Figure 3.20: Free body diagram of the forces acting on the exterior beam-column joint

$$V_{jh} = T - V_c \quad \text{(Equation 3.3)}$$

$$M_j = PL \quad \text{(Equation 3.4)}$$

$$T = C = \frac{M_j}{jd_b} \quad \text{(Equation 3.5)}$$

$$V_{jh} = \frac{M_j}{jd_b} - V_c \quad \text{(Equation 3.6)}$$

where:

V_{jh} = Ultimate shear force in the joint zone
T = Tension force resultant
C = Internal compression force
V_c = Lateral shear force developed at the tip of the column
M_j = Ultimate moment capacity of the joint
P = Applied ultimate load at the acting point of the beam
L = The distance between the acting point of applied load and the center of the joint
jd_b = The distance between the internal compression and tension force resultants in the beam. j is assumed to be taken 0.9 (Park & Mosalam, 2012; Zhang et al., 2015).
d_b= The effective depth of the beam

3.4.10 Calculation of principal strain values

By referring to Figure 3.11, it is demonstrated that five RSGs were installed on the surface of the joint zone to examine the tensile strain values developed in joint zone. Due to the sensitivity of the strain gauges, it is hard to record the strain values at higher drift levels due to the crack widening and subsequently the damage to these strain gauges. The maximum principal tensile strains calculated from the obtained data from the RSGs installed on the joint zone are considered for the comparison with the other specimens.

After collecting the data observed from the RSGs, some equations were applied to calculate the principal strains (Case & Chilver, 1971) as indicated below:

Referring to Figure 3.21, for $\propto = \beta = 45$, it is found that the following quadratic equation is applicable for principal strains ϵ_1 and ϵ_2 (refer to appendix D):

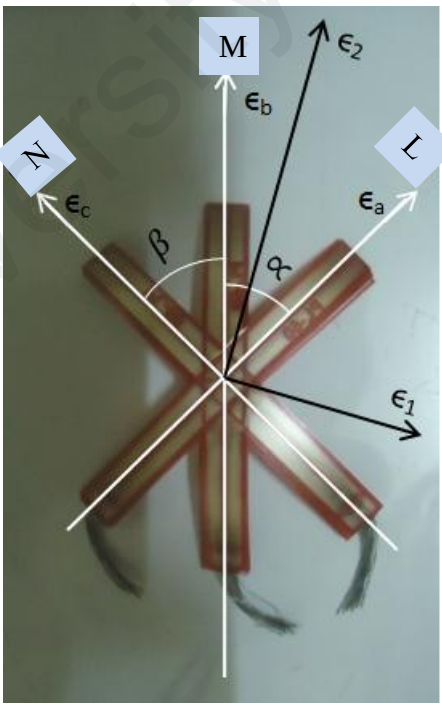

Figure 3.21: Evaluation of principal strains

$$\epsilon^2 - (\epsilon_a + \epsilon_c)\,\epsilon + [\epsilon_a\epsilon_c - \frac{1}{4}(2\epsilon_b - \epsilon_a - \epsilon_c)^2] = 0 \qquad \text{(Equation 3.7)}$$

The solution for the previous equation is:

$$\epsilon_1 \text{ and } \epsilon_2 = 0.5\,(\epsilon_a + \epsilon_c) \pm \sqrt{(\frac{\epsilon_a + \epsilon_c}{2})^2 - [\epsilon_a\epsilon_c - \frac{1}{4}(2\epsilon_b - \epsilon_a - \epsilon_c)^2]} \qquad \text{(Equation 3.8)}$$

3.4.11 Shear deformation analysis in the joint zone

The angular rotation at the joint was measured by a tilt meter to characterize the flexural deformation behavior at the center of joint zone. Thus, and due to the high shear force developed at the joint zone, it is necessary to estimate the amount of shear deformation within the joint zone. From Figure 3.22, the shear deformation analysis needs to measure the elongation and the shortness on the diagonals (ac) and (bd) on the joint (Yuan et al., 2013). Equations 3.10, 3.11 and 3.12 calculate the joint shear deformation angle γ_{sh} as follows:

$$\epsilon_{ac} = \frac{|\Delta_1 + \Delta_1'|}{(ac)}, \qquad \epsilon_{bd} = \frac{|\Delta_2 + \Delta_2'|}{(bd)} \qquad \text{(Equation 3.9)}$$

$$\gamma_{sh} = \psi_1 + \psi_2 \qquad \text{(Equation 3.10)}$$

By applying the small angle theory approach, Equation 3.10 was solved to the following formula (refer to Appendix D):

$$\gamma_{sh} = \psi_1 + \psi_2 = \frac{(ab)^2 + (bc)^2}{2(ab)(bc)}(\epsilon_{ac} + \epsilon_{bd}) \qquad \text{(Equation 3.11)}$$

In this study, the joint is equilateral i.e. ab = bc. By simplifying Equation 3, it becomes as follows:

$$\gamma_{sh} = \psi_1 + \psi_2 = \epsilon_{ac} + \epsilon_{bd} \qquad \text{(Equation 3.12)}$$

It is possible to calculate the shear deformation angle from the RSG readings on the diagonal lines L and N, as shown in Figure 3.21. By referring to Figure 3.11, the sequence of the RSGs within the joint zone is shown. Subsequently, the resultant formula to estimate the shear rotation angle $\gamma_{sh}$is as follows:

$\gamma_{sh} = \psi_1 + \psi_2 =$|Average strain readings on L direction in points 1, 3 and 5 of the joint|+| average strain readings

on N direction in points 2, 3 and 4 of the joint| (Equation 3.13)

Due to RSGs damage at early stage of loading, it was not possible to collect the data for more than 4% of drift ratio.

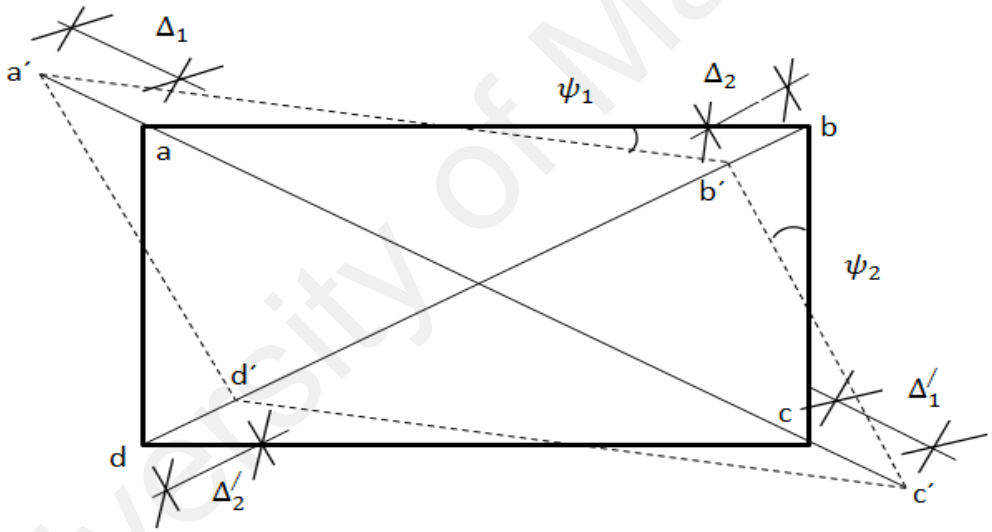

Figure 3.22: Shear deformation analysis in the joint zone

3.4.12 Cumulative energy absorption in beam-column joints

At post-cracking and near to failure stages, the energy generated from the redistribution of loading causes damage to the structure without any warning. Thus, the energy absorption capacity is the highest amount of energy at which the structure is capable of absorbing and leads to a gradual or sudden failure of the structure. As reported in the literature, the amount of cumulative absorbed energy is defined as the sum of the areas encompassed by each hysteresis loop of load–deflection relationship, which is the whole

energy absorbed by the structure. In This section, the cumulative absorbed energy was evaluated for the joint zone only and exclusively from the moment–rotation loops.

Referring to the Figure 3.23, the estimated amount of energy absorption for the hysteresis loop ABCDEA = the shaded area encompassed by the same loop.

The cumulative absorbed energy of a beam-column joint at any drift ratio = sum of the areas encompassed by each loop from the onset of loading until the certain drift ratio (Yuan et al., 2013; Zhang et al., 2015)

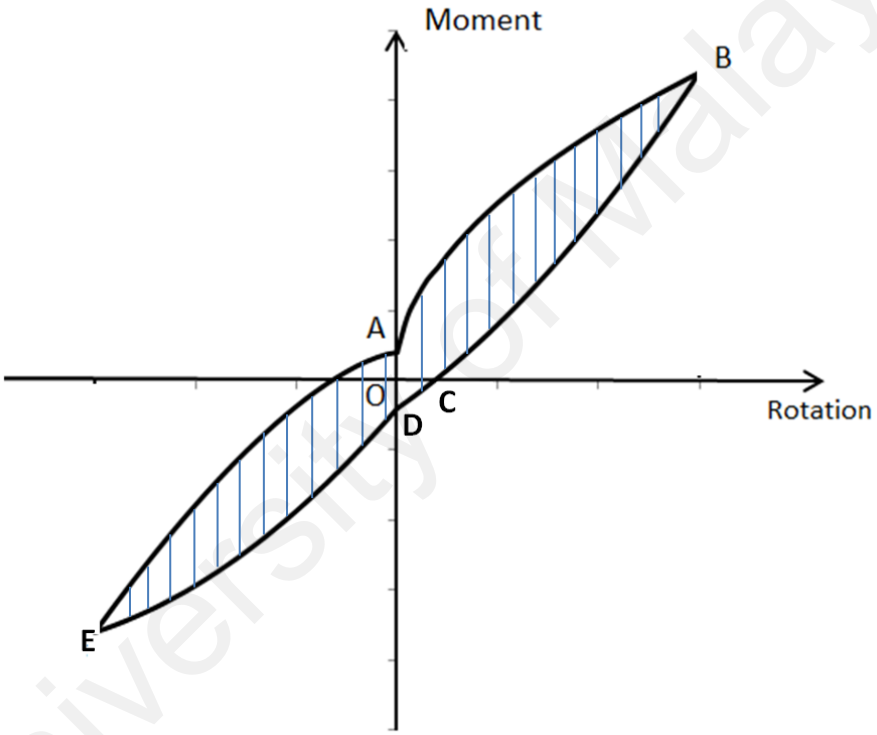

Figure 3.23: Estimation of energy absorption for one hysteresis loop

The cumulative energy absorption is a major function of the ductility and a direct method to evaluate the performance of beam-column joints.

3.4.13 Degradation of stiffness in beam-column specimens

The degradation of stiffness is simply evaluated from the secant stiffness of each loading cycle by calculating the slope of the line connecting each point plotted on the

positive part of the envelope load-deflection curve, i.e. at m or n deflection value of pulling load (point A or C) with the analogous point plotted on the negative part of the envelop curve, i.e. at -m or -n deflection value of pushing load (point B or D), respectively, as shown in Figure 3.19 (Shannag and Alhassan, 2005). the slope of the line AB or CD represents the secant stiffness at certain cycle of drift ratio, is calculated by dividing the total of the pulling and pushing loads on the total of the pulling and pushing displacement (double of m value for line AB). By fitting suitable line for the slope values for each beam-column specimen it is deduced that the absolute value for the slope of the fit line is a function for the rate of stiffness degradation of specimen. Furthermore, this is another method used to estimate the performance of specimens, and it is a good approach for comparison between the specimens.

3.4.14 Hysteresis loops

After conducting the test on each beam-column joint specimen, a part of the obtained results will be plotted for the load-deflection or moment-rotation relationship. The curves for the mentioned results appear as loops so-called “hysteresis loops”.

The term “hysteresis” is defined as, a retardation of an effect when the forces acting upon a body are changed in the direction (Merriam, Merriam, & Webster, 2015)

3.4.15 Pinching effect

The term “pinching” called on the shape of hysteresis loops of load-deflection or moment-rotation relationship of the beam-column joint that appear to be pinched in the middle part (Sutoyo, 2009) (i.e. the middle part of hysteretic loops relatively becomes narrow) due to the vulnerability of joint, as well as the brittle and premature mode of failure

3.4.16 Evaluation of shear strength factor λ for exterior beam-column joints

According to ACI 352R-02 (352R-02, 2002) the allowable shear resistance force for beam-column joints is determined from the following equation:

$V_{jh} = 0.083\gamma\sqrt{f_c'}b_j h_c$ (Equation 3.14)

where γ is constant depends on the type of beam-column joint.

The above equation will be slightly modified to consider a shear factor in SI units:

$V_{jh} = \lambda\sqrt{f_c'}b_j h_c$ where $\lambda = 0.083\gamma$ (Equation 3.15)

$v_{jh} = \lambda\sqrt{f_c'}$ (Equation 3.16)

Based on the type of beam-column joint in this thesis, $\gamma = 12$ (based on the values in the Table shown in ACI 352R-02)

$\lambda = 0.083\gamma = 0.083*12 = 1$

λ is the shear strength factor in SI units proposed by ACI 352R-02

As per ACI 352 R-02, the maximum nominal shear stress in exterior beam-column joints should be:

$v_{jh} \leq \lambda\sqrt{f_c'}$ (Equation 3.17)

From the literature, the ultimate shear strength developed in the joint zone is calculated from the following equation:

$$v_{jh} = \frac{\left(M_j / jd_b\right) - V_c}{b_j h_c}$$ (Equation 3.18)

jd_b is the distance between the internal compression and tension force resultant in the beam which was taken as $0.9d_b$ (Park & Mosalam, 2012; Zhang et al., 2015).

In this section, the shear strength factor (λ) will be evaluated based on the experimental results of exterior beam-column joints. New values of λ will be proposed for ECC joints based on the type of fibers, reinforcing index and the existence of lateral steel hoops in the joint zone. Furthermore, the λ value will be evaluated for joints with normal concrete and compared to the values in ECC joints.

CHAPTER 4: RESULTS AND DISCUSSION

4.1 Introduction

This chapter discusses the results of the experimental programme of three different stages in this project. The first stage presents results in two main lines. The first line is the results on strength and deformation characteristics of engineered cementitious composite (ECC) slabs with different polymer fibers. Results showed for both ECC PVA and ECC PE slabs, that the usage of PVA and PE fibers indicated an increase in flexural strength. The ECC PP slabs behaved like plane concrete due to the zero value of flexural strength. The second line focuses on the standard test method of ASTM C1018 (C1018, 1997) to evaluate the ductility and the amount of energy absorption of ECC slabs. Results presented a new definition for each of ECC PVA and ECC PE materials extending the ASTM C1018 definition of fibrous concrete.

The second stage of experimental programme presents results on the direct tensile behavior of I-shaped ECC specimens under uniaxial tensile loading for evaluating stress-strain relationship and the cut-off point of strain-hardening. Generally, results have shown that the ECC PE specimens showed significant results better than ECC PVA specimens in ultimate tensile stress, strain capacity, bridging of fibers and crack propagation, and ductility.

The third stage of the experimental programme was considered as the most significant stage in this project. This stage presents results on the performance of reinforced concrete ECC exterior beam–column joints under reversed cyclic loading. The ECC joint showed significant improvement in the ultimate shear and moment capacities, as well as in ductility and damage tolerance compared with the normal concrete (NC) specimen at ultimate and failure stages. In addition, the PE specimens showed better results than the PVA specimens in the same aspects mentioned above.

4.2 ECC slabs

4.2.1 First crack load.

As displayed in Figure 4.1 and Table 4.1, the first crack load results for different kinds of polymers in ECC slabs gradually decreased as the reinforcing index increased. Generally, the PVA slabs showed an improvement in the first crack load value compared to the PE slabs by an average of 13.4% based on reinforcing index value of less than 1000. For the ECC PVA slabs, the increase in the reinforcing index from 421 to 474, 527, 632 and 790 led to a reduction in first crack load of about 1.63, 14.2, 22.8, and 35.3%, respectively. For the ECC PP slabs, by increasing the reinforcing index from 375 to 500 and 625, there was a significant reduction in the first crack load of about 32% and 63%, respectively. The same trend as mentioned above was observed in the ECC PE slabs, the increase in reinforcing index from 474 to 632, 750, and 790 reduced the first crack load by about 10.6, 24.2, and 56.5%, respectively.

Consequently, it is concluded that by increasing the reinforcing index, the fibers did not improve the first crack load. However, an increase in the reinforcing index from 1000 to 1250 caused an increase in the first crack load of about 58%. It is inferred that, as the reinforcing index in PE slabs exceeded 1000, the PE fibers began to improve the first crack load.

4.2.2 Peak load at post cracking

After testing the ECC PVA slabs, it can be observed from Figures 4.2 to 4.4 and Table 4.1 that the peak load at post cracking was enhanced by about 30, 29, 31, 32.5 and 24.9%, by increasing the reinforcing index from 316 to 421, 474, 527, 632 and 790, respectively. The increase in the peak load corresponding to the reinforcing index of 790 dropped to 24.9% due to inadequate workability of the composite and the irregular dispersion of the PVA fibers.

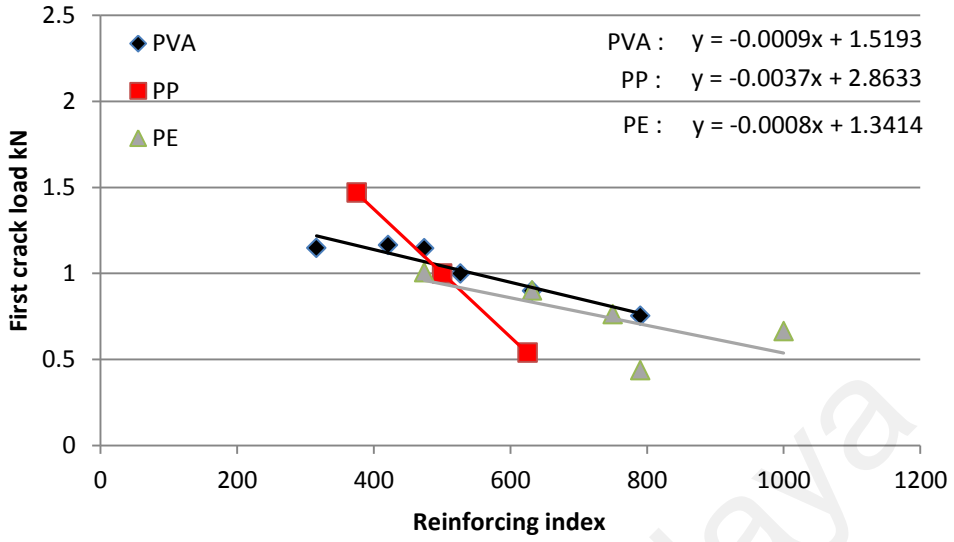

Figure 4.1: Variation of first crack load with reinforcing indices for different polymer fibers

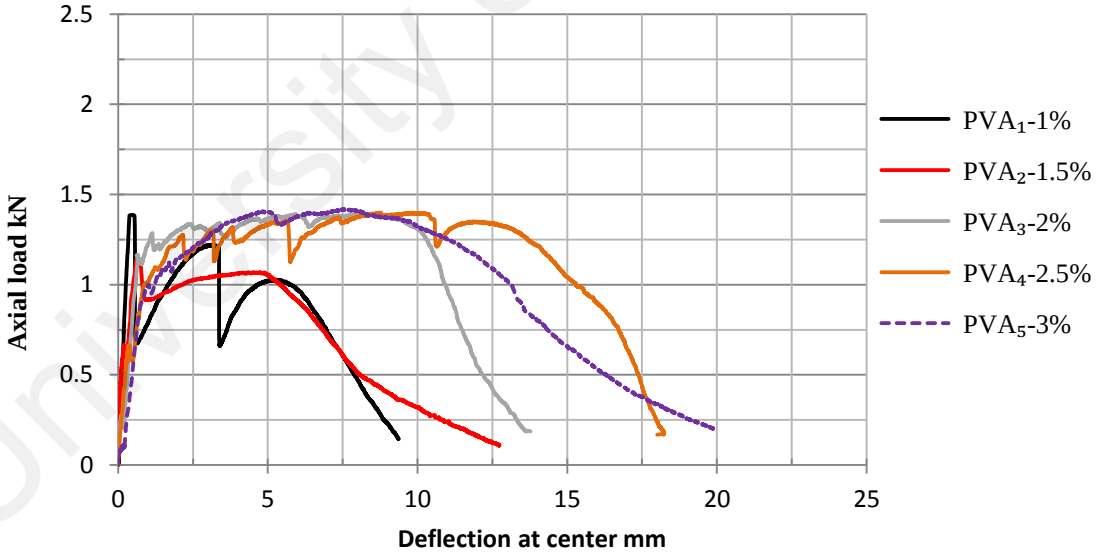

Figure 4.2: Load-deflection relationship for slabs reinforced with PVA RECS15 8mm, A.R=210

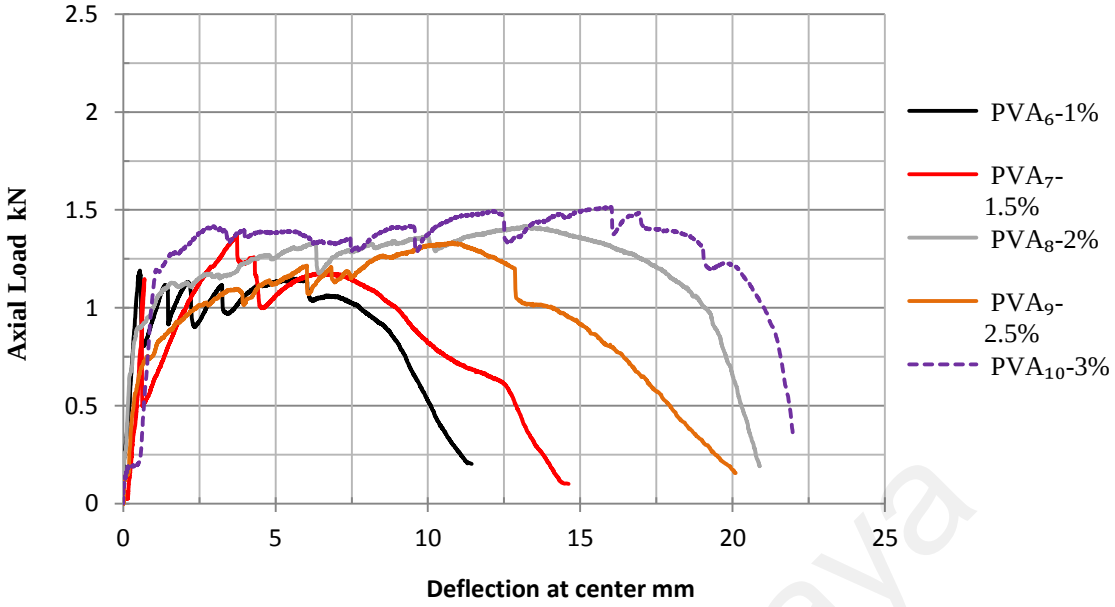

Figure 4.3: Load-deflection relationship for slabs reinforced with PVA-RECS15-12mm, A.R=316

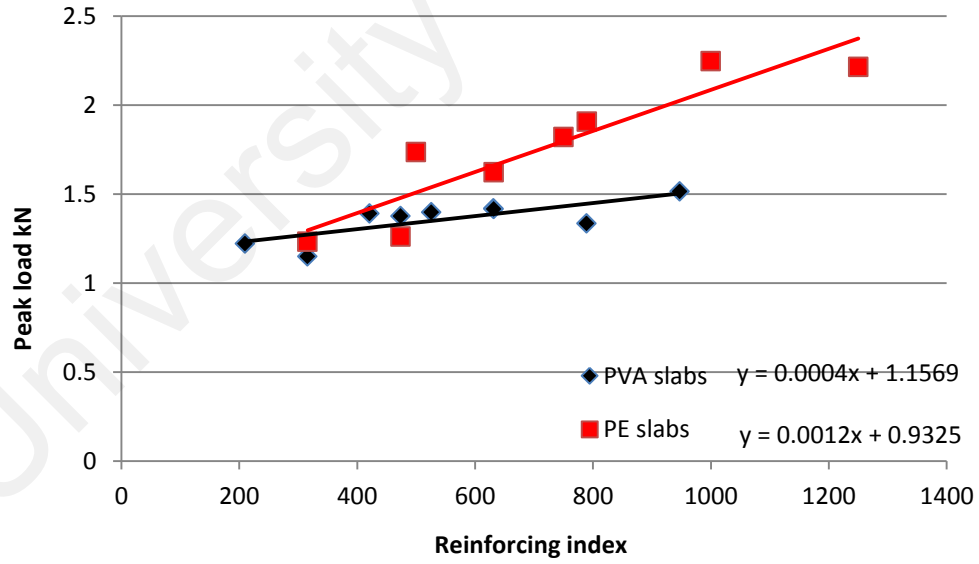

Figure 4.4: Variation of peak load at post cracking with reinforcing index for different polymer fibers

Table 4.1: Flexural testing values obtained for ECC slabs

Symbol of specimen	Reinf -orcing index V_f*(l/d)	Average compre -ssive Strength Mpa	Max. axial load at first cracking KN	Peak load at post cracking KN	Deflection At first crack mm	Ultimate load deflection mm	Deflection at failure mm
PVA_1	210	62.98	1.384	1.222	0.387	3.15	8.67
PVA_6	316	58.49	1.190	1.150	0.550	5.59	10.60
PVA_2	316	54.56	1.148	1.068	0.637	4.89	10.58
PVA_3	421	51.44	1.166	1.391	0.662	7.96	12.56
PVA_7	474	50.94	1.147	1.377	0.698	3.70	13.35
PVA_4	527	50.50	1.000	1.398	0.867	10.20	17.70
PVA_5	631	50.20	0.974	1.420	0.950	8.50	18.50
PVA_8	632	50.12	0.900	1.415	0.506	13.93	20.62
PVA_9	790	48.03	0.754	1.334	0.850	11.00	18.90
PVA_{10}	948	47.31	1.166	1.514	1.050	15.96	21.70
PP_1	375	42.9	1.47	0	-	1.4	1.4
PP_2	500	40.26	1.0	0	-	0.7	0.7
PP_3	625	38.4	0.54	0	-	0.3	0.3
PE_1	316	65.72	1.404	1.232	0.473	6.07	22.28
PE_2	474	60.52	1.008	1.262	0.562	22.50	36.50
PE_5	500	53.44	1.084	1.735	0.625	23.85	43.60
PE_3	632	47.53	0.901	1.623	0.741	27.08	49.95
PE_6	750	45.69	0.764	1.820	0.822	34.43	51.68
PE_4	790	43.74	0.438	1.907	0.989	47.22	69.30
PE_7	1000	41.17	0.665	2.247	1.153	49.66	82.80
PE_8	1250	38.36	1.594	2.215	0.826	13.14	55.89

As displayed in Figure 4.5 and Table 4.1 for the ECC PP slabs, for the three values of reinforcing index, 375, 500, and 625, the peak loads at post cracking reduced to zero after exceeding the first crack stage due to the reduced bonding of the PP fibers with the cement matrix, which was attributed to the smoothness of the surface, (Balaguru et al., 1992) low tensile strength and the E modulus of PP fibers. They could not sustain any loading adequately after the first crack.

As indicated in Figures 4.4, 4.6 and 4.7 and Table 4.1 for the ECC PE slabs, as the reinforcing index increased, the peak load value at post cracking gradually increased. Moreover, by enhancing the reinforcing index value from 474 to 1000 and 1250, there

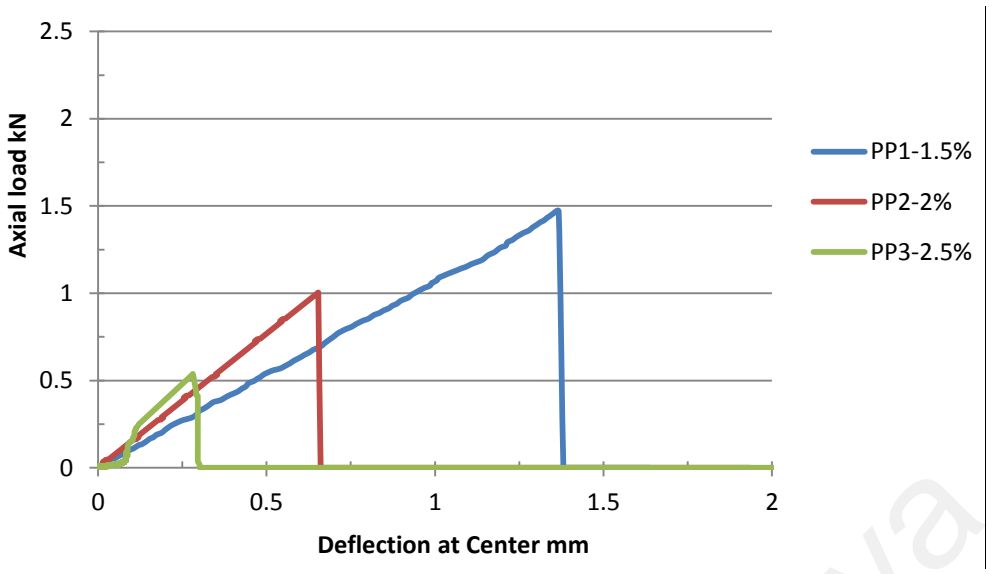

Figure 4.5: Load-deflection relationship for slabs reinforced with PP-Mono Tuf, A.R=250

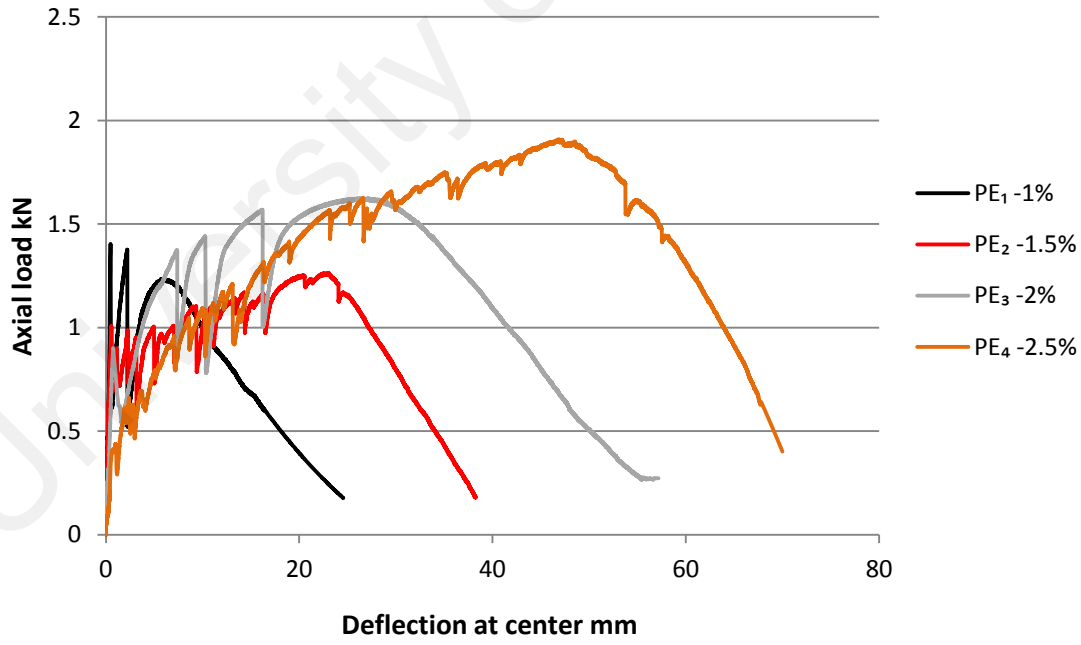

Figure 4.6: Load-deflection relationship for slabs reinforced with PE-4800D, A.R=316

was a substantial enhancement in peak load at post cracking of 78 and 75.5%, respectively, due to the higher reinforcing index, as well as the higher tensile strength and E modulus of the PE 1600D fibers. The reduced value of 75.5% for the peak load increment was due to the non-uniform dispersion of the fibers in the composite. The PE slabs showed a significant improvement in the peak load value at post cracking compared to the PVA slabs of about 14.7% for the same reinforcing index of 632 for PVA_8 and PE_3 slabs. Furthermore, the improvement in the peak load value at post cracking For ECC PE slabs was about 43% based on the same reinforcing index of 790 for PVA_9 and PE_4. This may be attributed to the expected mode of failure of PE fibers, which is bond-slip, rather than the rupture of fibers, for PVA fibers. In addition, the high bond strength generated in the interfacial surfaces of the cementitious matrix and PE fibers is associated with the increased tensile strength for the PE fibers compared to the PVA fibers in sustaining higher loads.

4.2.3 First crack deflection

From Figure 4.8, according to the linear fit of first crack deflection results, it can be recognized that by increasing the reinforcing index value, there is a slight increase in first crack deflection values of ECC PVA slabs, and the increment rate is about 0.08 mm per 100 of reinforcing index. This result indicates that the ECC PVA material tends to be more elastic with a slight decrease in modulus of elasticity as the reinforcing index increases. Moreover, the linear fit for first crack deflection results seems to be more suitable despite the low correlation coefficient.

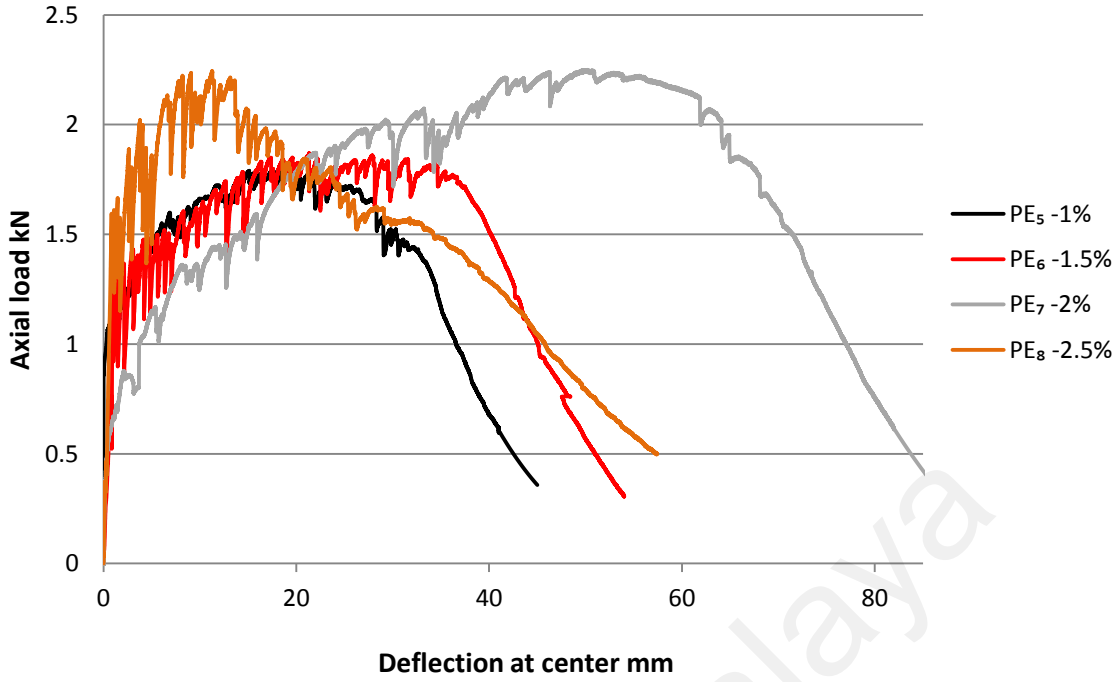

Figure 4.7: Load-deflection relationship for slabs reinforced with PE-1600D, A.R=500

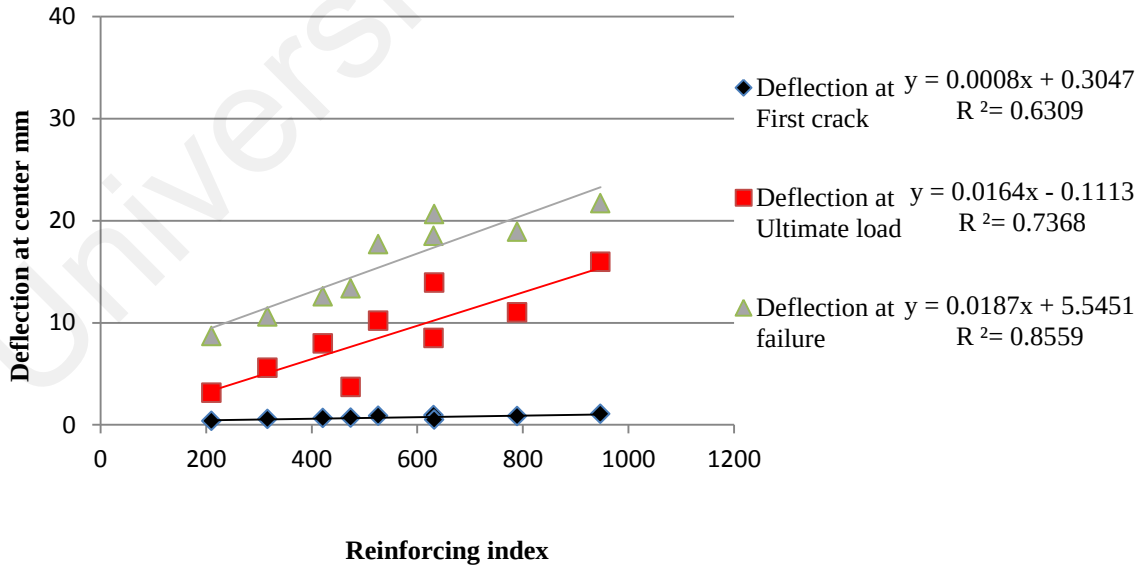

Figure 4.8: Effect of reinforcing index on deflection values of ECC-PVA slabs

The linear fit of first crack deflection results for PE slabs is displayed in Figure 4.9. Accordingly, the results specify that, by increasing the reinforcing index value, the first crack deflection values for ECC PE slabs slightly increased. The increment rate was equal to 0.14 mm per 100 of the reinforcing index. These findings suggest that the ECC PE slabs tend to be more elastic with a slight decrease in the modulus of elasticity when the reinforcing index increases, and the linear fit for first crack deflection results is deemed more suitable. A high correlation coefficient value was observed for ECC PE slabs.

4.2.4 Ultimate load deflection

According to Table 4.1, Figures 4.8 and 4.9, the PE slabs showed a significant improvement in the ultimate load deflection value at post cracking compared to the PVA slabs of about five times the value for the ECC PVA slabs based on the same reinforcing index of 474 for PVA_7 and PE_2. In addition, an improvement in the ultimate load deflection value at post cracking was about 3.3 times the value in the ECC PVA slabs based on the same reinforcing index of 790 for PVA_9 and PE_4. Moreover, the highest values for ultimate load deflection were recorded for the ECC PE slabs. As the reinforcing index increased from 474 to 632, 750, 790, and 1000, a gradual increase in ultimate load deflection was exhibited from 22.5mm to 27.08, 34.43, 47.22, and 49.66 mm, respectively. Thus, the ECC PE slabs showed the highest ductility among the different types of ECC slab. A series of multiple cracks was noticed in the middle region of PE slabs. The observed value for the reinforcing index of 1250 reduced to a lower value of 13.144mm due to the high fiber content and high aspect ratio, which led to a non-homogeneous matrix forming. The regression analysis of deflection results at ultimate load for ECC PE slabs was set a linear fit. From this regression analysis for ECC PE slabs, the high correlation coefficient with a significant increment value of 6.33

mm per 100 of reinforcing index was obtained, as shown in Figure 4.9, indicating that the ductility in ECC PE slabs was significantly improved to higher limits.

For the ECC PVA slabs, as the reinforcing index increased, the ultimate load deflection value increased (except for PVA_7). In other words, increasing the reinforcing index provides better ductility as well as improves the ability of the ECC slabs to bend more freely. The highest value recorded for the PVA slabs was 13.93 mm, which was considerably lower than the PE slab values. The regression analysis of deflection results at ultimate load for ECC PVA slabs is set to be linear fit with a medium correlation coefficient and increment rate of 1.64 mm for each 100 of reinforcing index which is able to improve the ductility of ECC slabs to acceptable limits, as shown in Figure 4.8.

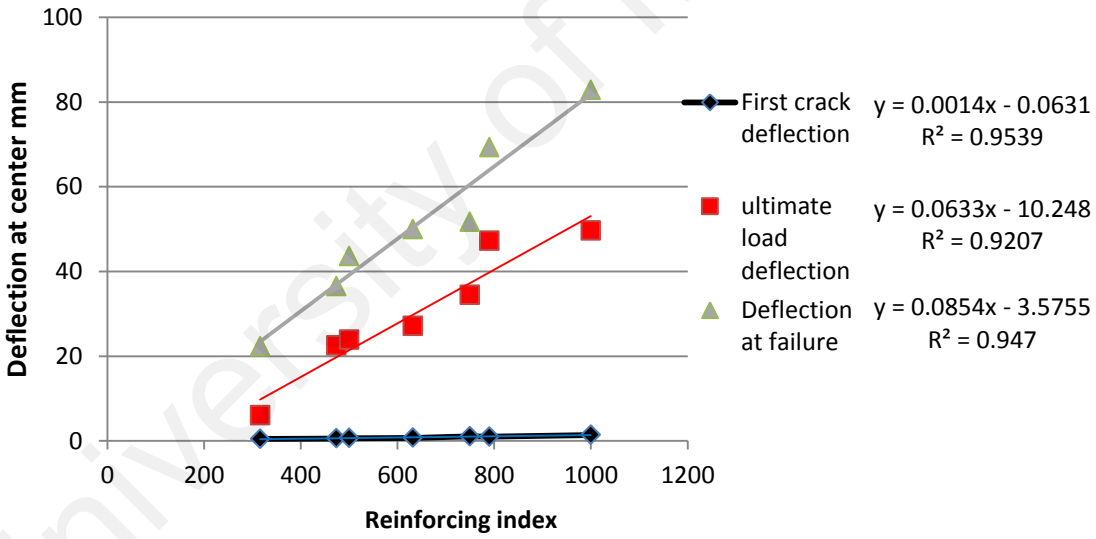

Figure 4.9: Effect of reinforcing index on deflection values of ECC-PE slabs

For the ECC PP slabs, no improvement in ductility was observed. The ECC PP slabs behave like a plain concrete, as the PP fibers are incapable of producing bendable concrete due to the small interfacial bonding as well as the low tensile strength of the PP fibers.

4.2.5 Deflection at failure

The deflection at the failure value for each ECC slab was measured according to the corresponding deflection value of 25% of the peak load at post cracking specified at the descending part of the load–deflection curve. The results from Table 4.1 show that the PE slabs presented a significant improvement in the deflection values at failure compared to the PVA slabs of about 173% based on the same reinforcing index of 474 PVA_7 and PE_2. Furthermore, the improvement in the deflection values at failure was about 267% based on the same reinforcing index of 790 for PVA_9 and PE_4. Consequently, the ECC PE slabs presented the highest deflection values at failure among the various types of ECC slab. The highest value of 82.8mm for PE was recorded, which indicates the highest ductility and ability to bend without any sudden failure. The reduced value of deflection at failure for the higher reinforcing index of 1250 of 55.89mm was due to poor dispersion of the fibers, which led to less ductility of the slabs. Multiple cracking behavior was observed with many cracks extending at the middle part of the PE slab. Besides, the linear fit analysis for the results of PE slabs, as shown in Figure 4.9, was determined more suitable. The increment rate determined from the fit analysis for ECC PE slabs was identified to be 8.54 mm per 100 of reinforcing index. This particular rate is highly distinctive.

In general, for the ECC PVA or PE slabs, the results showed a gradual increase in the deflection at the failure value by increasing the reinforcing index. However, the values obtained for the PVA slabs confirmed that the highest value recorded was 20.62 mm, which was considerably less than the highest value for the PE slabs. The lower value for the deflection at failure indicated the limited ductility of the PVA slabs and their inability to bend more compared to the PE slabs. This behavior could be attributed to the high interfacial frictional and chemical bond established between the PVA fiber surfaces and the cement matrix,(Balaguru et al., 1992; Banthia & Trottier, 1995) which

led to the rupture of the fibers, which in turn limited the flexural performance and deformation of the ECC slabs. Finally, the linear fit analysis for the PVA slabs results is found more suitable. The increment rate determined from fit analysis is 1.87 mm per 100 of reinforcing index which is slightly more than the increment rate of deflection at ultimate load, with better correlation coefficient value, as shown in Figure 4.8.

4.2.6 Load–deflection relationship and crack patterns

For slabs PVA_1 and PVA_2, the strain-hardening behavior could not be observed due to the lower reinforcing index (see Figure 4.2). Therefore, the peak load capacity at post cracking was less than the first crack load. The combined effect of poor fiber content and low aspect ratio resulted in lower flexural performance and ductility compared to the other ECC slabs. Furthermore, a small number of bridging cracks were observed in the middle part of the slab at failure. After the formation of the first crack, the curve dropped gradually and softened due to the localization of the major crack. As for the rest of the ECC PVA slabs starting with PVA_3, for the reinforcing index of 421 until 790, the strain hardening effect and multi-cracking behavior was apparent. Numerous and successive bridging of the cracks as apparent from the trend on the load–deflection curve at the post cracking stage within the region starting from the first crack until the onset of softening of the load–deflection curve. In addition, the bridging mechanism of the PVA fibers enhanced the ultimate strength of the slab over the first crack strength. Nevertheless, the softening part of the load– deflection curve exhibited a sharp slope until failure. Notwithstanding the discernible behavior of the ECC PVA slabs, the required values of deflection were not achieved. Consequently, the ECC PVA slabs did not attain the required ductility due to the rupture of the fibers at failure. To clarify this behavior, it is important to know that the PVA fibers create a high chemical bond with the cement hydrates. At failure, the PVA fibers will rupture rather than fail through

bond-slip (that is, pulling out of the fibers from the main positions in the cement matrix) (Banthia & Trottier, 1995; Pan et al., 2012).

The results for the ECC PP slabs showed that the PP fibers did not have any bridging action and did not improve the ductility due to poor interfacial bonding of the PP fibers, as well as the low tensile strength and E modulus.

For the ECC PE slabs, the results in Figures 4.6 and 4.7 reveal many points of crack bridging within a wide field of deformation. The slabs with PE fibers developed many extensive cracks and multiple sub-cracks within the middle third of the span and achieved a remarkable amount of deflection due to the superb ductility of the PE slabs. The softening part of the load–deflection curve descended in a steady gradual manner and gained a lot of deformation up to failure. The load–deflection curve for the PE slabs created a large area under the curve, which represented the higher energy absorption compared to the small area under the load–deflection curve for the PVA slabs. The prominent behavior of the ECC PE slabs was attributed to the desired mode of failure at which the bond-slip failure of the fibers occurred, as well as to the higher tensile strength and elastic modulus of the fibers. Figure 4.10 shows the slab deformation under the load process and the crack patterns for some of the tested slabs.

4.2.7 Toughness indices

As mentioned earlier, the toughness indices are relative indicators to estimate the flexural performance and toughness characteristics of beam or slab. These values represent the amount of ductility as well as the size of energy absorbed by the beam or slab. To estimate the toughness indices, the ASTM C1018 (C1018, 1997) method needs to locate the first crack point which is not easy to obtain accurately. The method stated in the ASTM C1018 can only determine the toughness indices I_5, I_{10} and I_{20}.

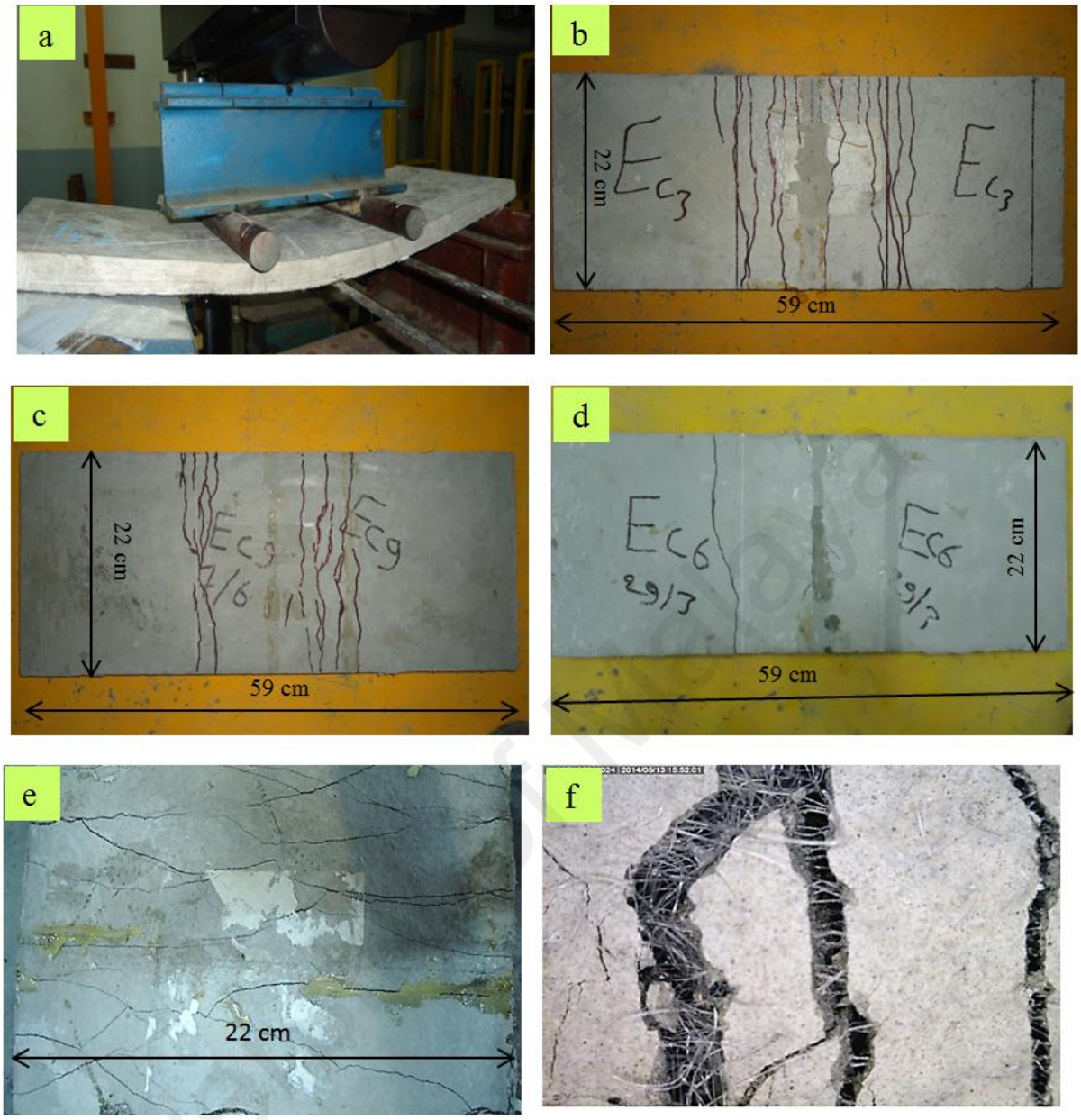

Figure 4.10: (a) ECC slab under testing. Crack pattern for; (b) PVA_3 (RECS15-8mm); (c) PVA_8 (RECS-12mm); (d) PP_1 (Mono Tuf); (e) PE_6 (1600D); and (f) Magnified image for the bridging of cracks in ECC.

4.2.7.1 ECC PVA slabs

From load-deflection relationship for slabs, there is a possibility of determining I_5, I_{10}, I_{20}, I_{30} and I_{40} due to high deflection results in ECC PVA slabs. The ASTM C1018 (C1018, 1997) allows for determination of indices higher than I_{20}. It needs to calculate the area under the load-deflection curve up to 3δ, 5.5δ, 10.5δ and 20.5δ respectively (δ is the deflection value at first crack).

The toughness indices are determined for all ECC PVA test slabs and the results are plotted with the values of reinforcing indices as shown in Figure 4.11. Regarding this relation, all kinds of toughness indices from I_5 to I_{40} were analyzed. As shown in Figure 4.12, increasing the reinforcing indices resulted in increased toughness indices where the most appropriate fit for values of indices was found to be linear. The slope values of the fit lines increase gradually through the values 0.38, 0.84, 1.79, 2.91 and 4.11 per 100 of reinforcing index through the indices I_5, I_{10}, I_{20}, I_{30} and I_{40} respectively. For instance, as the reinforcing index for I_5 increases, the rate of increment for this index is very low which is almost a parallel line to x-axis. The physical interpretation for this phenomenon is that at the onset of post-cracking stage, at 3δ, the mechanism of fiber action has not been significantly activated and the cracks have not been extensively propagated. Moreover, the flexural toughness has not been performed and the desired ductility has not been obtained. By proceeding with the loading stages with higher values of deflection, the cracks begin to propagate and the influence of crack-arrest mechanism of PVA fibers starts to activate, that is, the fibers try to arrest the cracks and bridge them. This phenomenon appears more evidently in the slabs characterized with higher reinforcing indices especially in the advanced stages of loading. At $I_{10,}$ the flexural toughness characteristics and the energy absorption ability of ECC PVA slabs are somewhat evident and would be more evident at higher indices (I_{20} and higher) especially at higher value of reinforcing indices due to the higher slope value of linear fits of toughness indices.

As displayed in Figure 4.11, the toughness indices determined for ECC PVA slabs with reinforcing indices higher than 632 exceed the limitations which they are particularly assigned for ideal elastic-perfectly plastic materials. However, the values determined satisfy the definition stated in ASTM C 1018 of observed range of toughness indices for

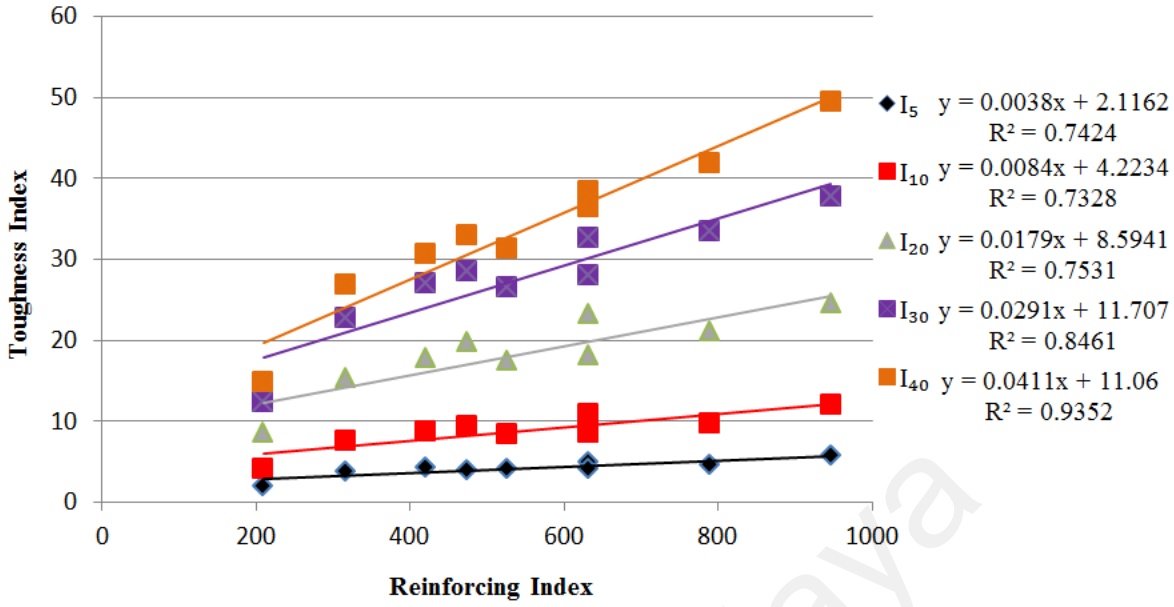

Figure 4.11: Effect of reinforcing index on toughness indices in ECC-PVA slabs

fibrous concrete of indices I_5, I_{10} and I_{20}. In this paper, a new definition to the ASTM C1018 definition is stated for ECC PVA material according to the observed results. The new definition is similar to the ASTM C1018 definition except that there are additional observed ranges for I_{30} and I_{40} as shown in Figure 4.12. From the observed values, the unexpectedly high toughness indices exceeding the upper bound values are attributed to the low first crack load recorded at high reinforcing index slabs resulting in reduced area under first-crack load-deflection curve.

4.2.7.2 ECC PE slabs

This study determined the toughness indices for all ECC PE slabs, and the results are plotted with the values of reinforcing indices shown in Figure 4.13a. However, the 3D regression analysis was applied via the Design-Expert software, indicating the relationship between the reinforcing index, type of toughness, and toughness indices, as displayed in Figure 4.13b. The analysis generated a graph of surface mesh with correlation coefficient equals to 0.967. All the kinds of toughness indices specified in Figures 4.13a and 4.13b employed to estimate the behavior of ECC PE slabs were

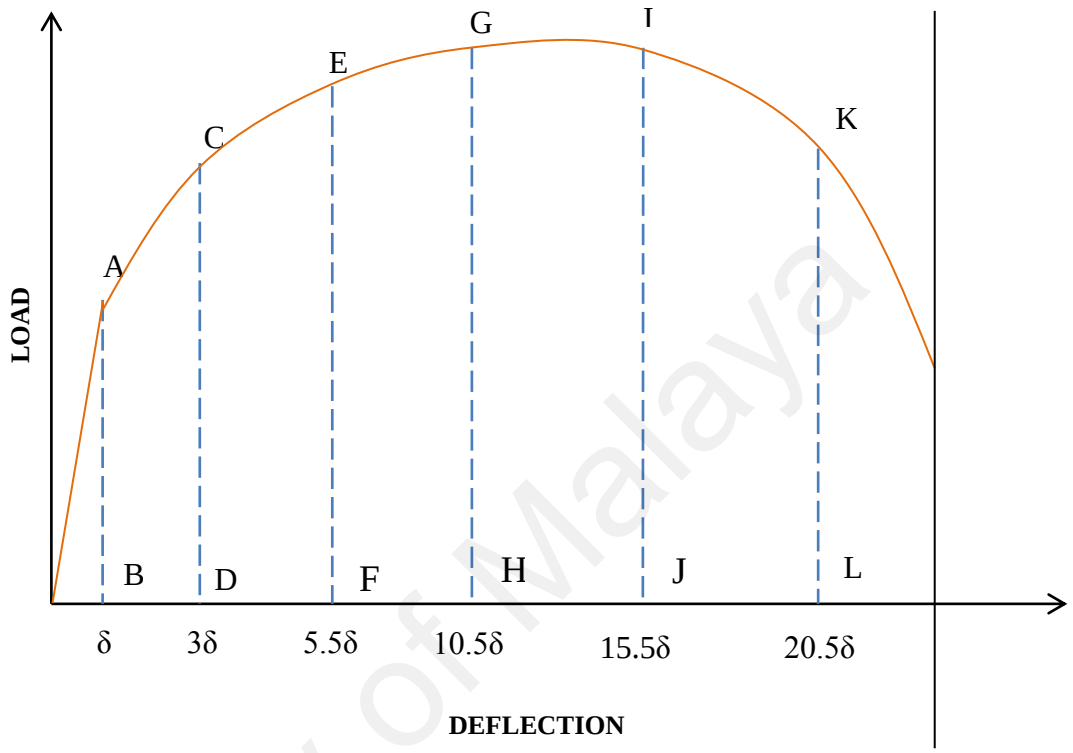

Area basis	Index designation	Deflection criterion	Values of toughness indices		
			Plain concrete	Elastic-perfectly plastic material	Observed range for ECC
OACD	I_5	3δ	1.0	5.0	1 to 6
OACEF	I_{10}	5.5δ	1.0	10.0	1 to 12
OACEGH	I_{20}	10.5δ	1.0	20.0	1 to 25
OACEGIJ	I_{30}	15.5δ	1.0	30.0	1 to 38
OACEGIKL	I_{40}	20.5δ	1.0	40.0	1 to 50

Figure 4.12: Definition of toughness indices in ECC slabs in terms of first-crack deflection based on tests observations

analyzed. As shown in Figures 4.13a and 4.13b, increasing the reinforcing indices resulted in increased toughness indices, in which the most appropriate fit for toughness indices in Figure 4.14a was identified linear. Moreover, when the type of index varied through the indices I_5, I_{10}, I_{20}, I_{30}, I_{40}, I_{50}, until I_{100}, the slope values of the fit lines for PE slabs gradually increased through the values 0.29, 0.7, 1.91, 3.09, 4.27, 5.39, 6.52, 7.64, 8.52, 9.52, and 10.21 per 100 of reinforcing index, respectively. For instance, when the reinforcing index increased, the rate of increment for index I_5 was exceedingly low. The physical interpretation for this phenomenon is that, at the onset of post-cracking stage (at 3δ), the mechanism of fiber action has not been intrinsically stimulated, the cracks have not been excessively propagated, the flexural toughness has not been attained, and the desirable ductility has not been motivated yet. For higher loading stages with the increased values of deflection, the cracks began to propagate, and the effect of crack-arresting mechanism of PE fibers began to be activated (i.e., the fibers tried to restrain and bridge the initiating cracks).

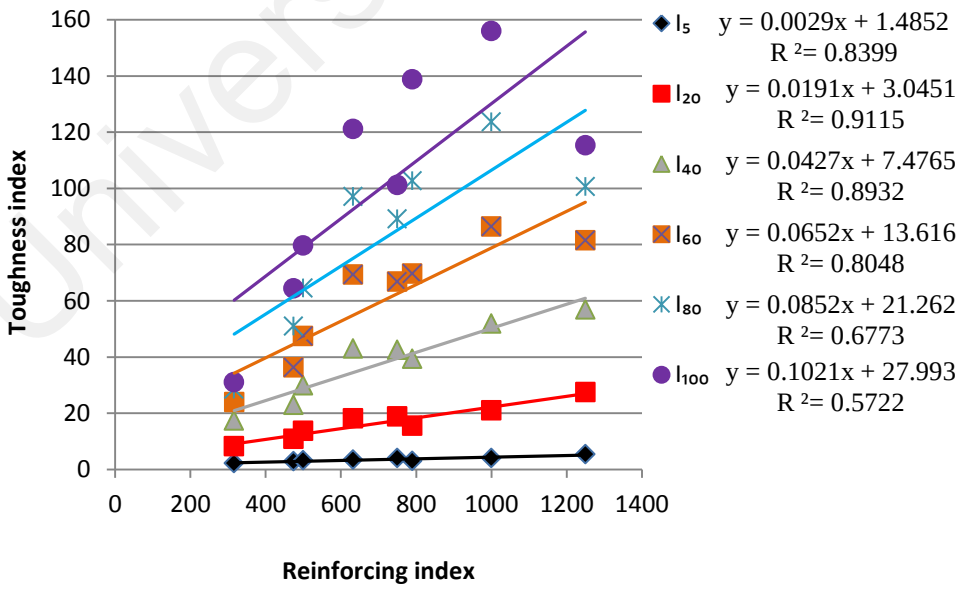

Figure 4.13a: Effect of reinforcing index on toughness indices in ECC-PE slabs

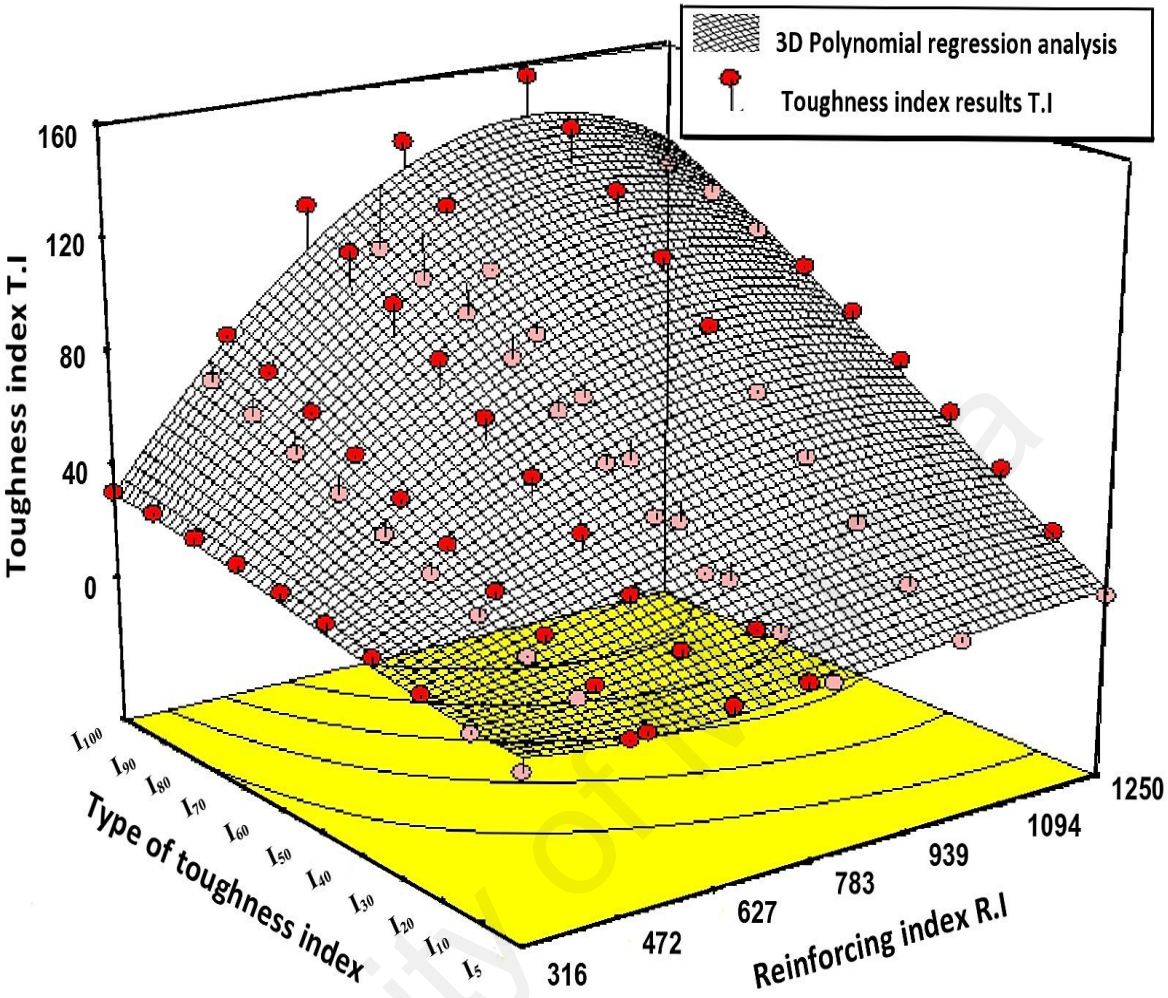

$$Z = 68 + 32.6\,A + 65.17\,B - 22.51\,AB - 22.53\,A^2 - 0.65\,B^2 - 27.82\,A^2\,B - 1.86\,A\,B^2 + 5.92\,A^3 - 4.24\,B^3$$

$R^2 = 0.9744$

where A is Reinforcing index R.I, B is Type of toughness index, and Z is the Toughness index

Figure 4.13b: Effect of reinforcing index on toughness indices in PE ECC slabs, 3D shape illustration

Such an effect was more evident in the slabs with higher reinforcing indices, particularly in the progressive stages of loading. At $I_{10,}$ the flexural toughness features and the energy dispersion capability of PE slabs were comparatively apparent and would be more clear at the progressive indices (I_{20}, I_{30}, and higher), particularly at the increasing value of reinforcing indices. This certainly explains the increased slope value of linear fits of progressive toughness indices. Figure 13b also indicates a decrease in

toughness indices at a reinforcing index of 1250 because of the insufficient fiber dispersion in the ECC mix.

As displayed in Figures 4.13a and 4.13b, the toughness indices evaluated for ECC PE slabs with reinforcing indices higher than 632 exceeded the limitations, which are particularly specified for ideal elastic-perfectly plastic materials.

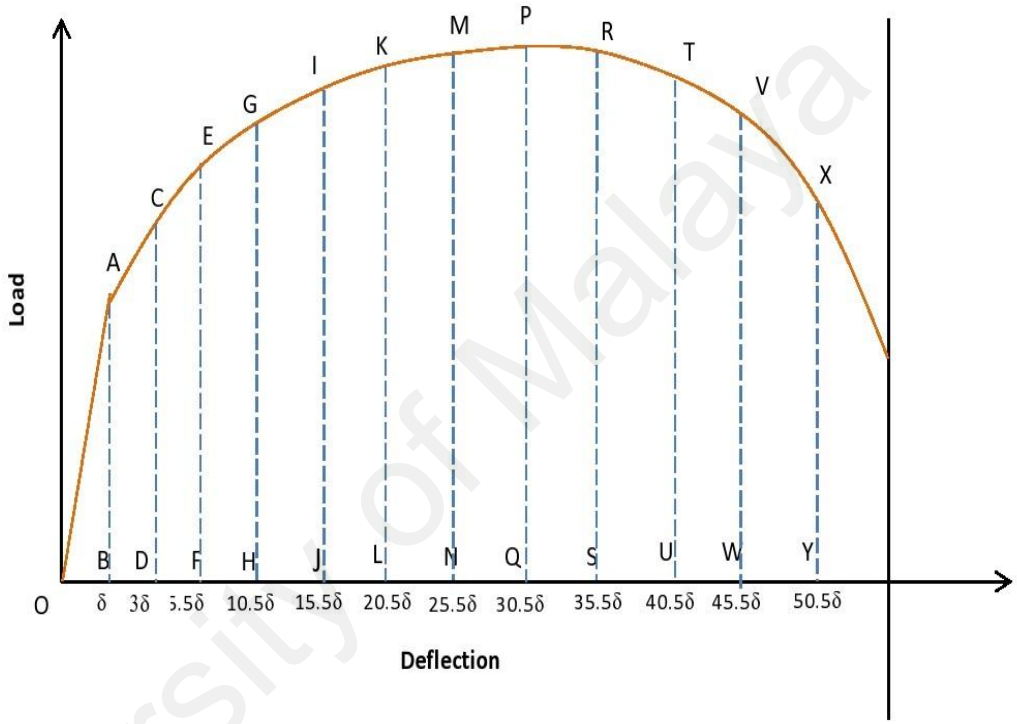

Area basis	Index designation	Deflection criterion	Values of toughness indices		
			Plain concrete	Elastic-perfectly plastic material	Observed range for ECC
OACD	I_5	3δ	1.0	5.0	1 to 6
OACEF	I_{10}	5.5δ	1.0	10.0	1 to 12
OACEGH	I_{20}	10.5δ	1.0	20.0	1 to 27
OACEGIJ	I_{30}	15.5δ	1.0	30.0	1 to 45
OACEGIKL	I_{40}	20.5δ	1.0	40.0	1 to 60
OACEGIKMN	I_{50}	25.5δ	1.0	50.0	1 to 75
OACEGIKMPQ	I_{60}	30.5δ	1.0	60.0	1 to 90
OACEGIKMPRS	I_{70}	35.5δ	1.0	70.0	1 to 105
OACEGIKMPRTU	I_{80}	40.5δ	1.0	80.0	1 to 128
OACEGIKMPRTVW	I_{90}	45.5δ	1.0	90.0	1 to 144
OACEGIKMPRTVXY	I_{100}	50.5δ	1.0	100.0	1 to 160

Figure 4.14: Definition of toughness indices in ECC slabs in terms of first-crack deflection based on tests observations

The toughness indices calculated for the ECC PE slabs satisfied the definition stipulated in ASTM C1018 of the observed range of toughness indices for fibrous concrete of indices I_5, I_{10}, and I_{20}. In this study, a new definition of ASTM C1018 was stipulated for ECC PE material according to the observed results. The new definition is similar to that of the ASTM C1018, except that additional observed ranges of I_{30}, I_{40}, I_{50}, until I_{100} for PE slabs were incorporated into the former, as presented in Figure 4.14. From the observed values, the unforeseen high toughness indices overriding the upper bound values were due to the low first crack load observed at the high reinforcing index of slabs, resulting in reduced area under the first crack load-deflection curve.

4.2.8 Residual strength factor

As mentioned earlier, the residual strength factor is the amount of strength retained in the beam or slab within a specific stage of loading. The ASTM C1018 defines the residual strength factors $R_{5,10}$ and $R_{10,20}$ between the toughness indices I_5 and I_{10}, $I_{10}$and I_{20} respectively. The residual strength factor is not a cumulative number for its predecessor, as it is in toughness index; it presents a situation of retained strength within the particular stage of loading.

4.2.8.1 ECC PVA slabs

For ECC PVA slabs, this study reports the residual strengths $R_{5,10}$, $R_{10,20}$, $R_{20,30}$ and $R_{30,40}$ between the toughness indices I_5 and I_{10}, $I_{10}$and I_{20}, I_{20} and I_{30}, and finally $I_{30}$and I_{40} respectively. As can be shown in Fig. 4.15, the residual strength results determined are highly scattered. The points of $R_{5,10}$, $R_{10,20}$ and $R_{20,30}$ are clustered within a small specific region whereas the points of $R_{30,40}$ are clustered in a lower region. In general, all the residual strength factors increase as the reinforcing index increases which denotes a higher amount of strength retained with increasing of reinforcing index. The regression analysis for all kinds of residual factors is found to be linear with medium values of correlation coefficient. The fit lines for $R_{5,10}$, $R_{10,20}$ and $R_{20,30}$ are mostly to be

identical, the $R_{30,40}$ values are less than the other previous ones of residual factors and the trend of fit line within a lower region. The physical interpretation for this phenomenon is that the values of residual strength factor $R_{30,40}$ represent the retained strengths within the final, or semi-final, region of loading process before failure at which the slab has lost its strength and going to fail.

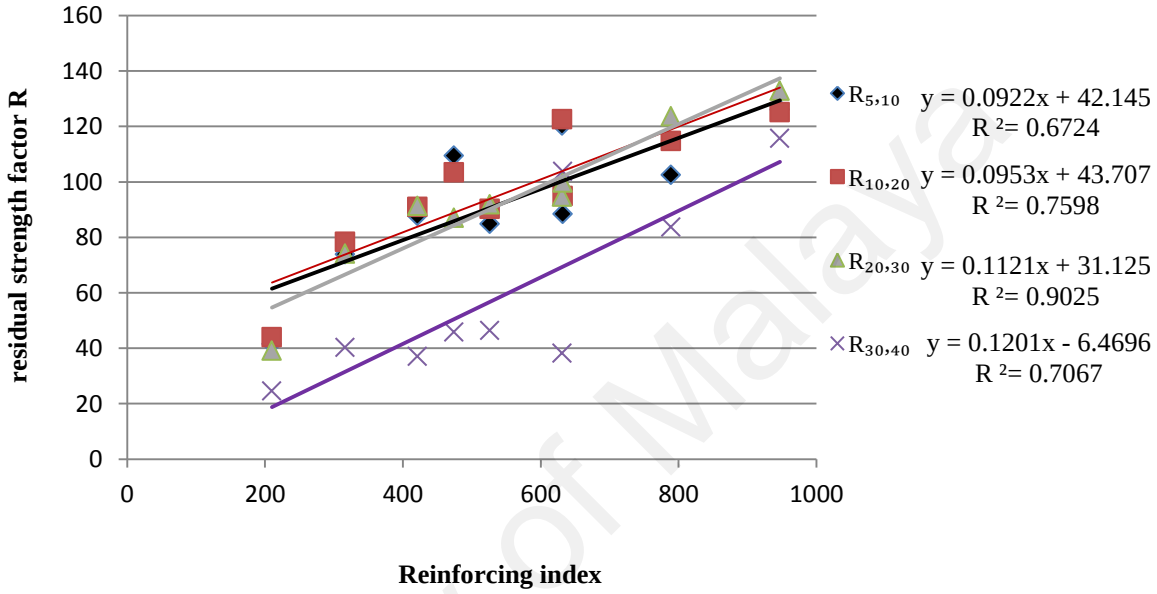

Figure 4.15: Effect of reinforcing index on residual strength factor in ECC PVA slabs

The residual strength factors for ECC PVA slabs with reinforcing indices more than 632 have attained values more than 100. As mentioned previously, the toughness indices for reinforcing indices more than 632 have recorded values higher than their limitations. The differences between toughness indices within this range have attained higher levels which resulted in a residual strength factor more than their limitation.

4.2.8.2 ECC PE slabs

This component provides a situation of stored strength within the limited stage of loading. In this case, the Design-Expert software was again employed to conduct the 3D regression analysis to fit the relation among three parameters (i.e., residual strength factor, type of residual strength factor, and reinforcing index), as exhibited in Figure 4.16.

Accordingly, the analysis produced a surface mesh with correlation coefficient equals to 0.86. Figure 4.16 indicates that all the residual strength factors generally increased when the reinforcing index increased, denoting a higher amount of strength retained with the increase of reinforcing index. However, the observed results in Figure 4.16 for ECC PE slabs showed reduced values of residual strengths at the reinforcing index of 1250 because of inhomogeneous dispersion of fibers into ECC material. Figure 4.16 also reveals that the 3D shape gradually increased in the residual strength factor when it varied from $R_{5,10}$ to $R_{50,60}$. Accordingly, the amount of retained residual strengths for all reinforcing index values gradually increased, implying a higher amount of strength retained by proceeding in the loading process. Moreover, beginning from $R_{50,60}$ through $R_{60,70}$, $R_{70,80}$, $R_{80,90}$ until $R_{90,100}$, the PE slabs gradually began to lose their stored residual strengths. Figure 4.16 further shows that the residual strength values reduced by moving from $R_{50,60}$ toward $R_{90,100}$, verifying that the PE slabs continued to the final stage of post-cracking, which was the failure stage. The failure stage in PE slabs includes five different levels of residual strength values and occurs in a steady-gradual manner, which explains the failure stage of the varying levels of residual strength factors, expressing better flexural performance, higher rates of ductility, and greater energy absorption capacity.

The residual strength factors for ECC PE slabs with reinforcing indices of more than 632 achieved values of more than 100. As previously cited, the toughness indices for reinforcing indices of more than 632 were moved for values higher than their limitations. The variations between toughness indices within this range attained higher levels, incurring a residual strength factors more than their limitation.

4.3 Direct tension I-shaped ECC samples

4.3.1 First crack stress

As displayed in Figure 4.17 and Table 4.2, the first crack stress results of ECC I-shaped samples for PVA and PE fibers. The first crack stress gradually decreased as the reinforcing index increased. On average, the both kinds of samples showed an even estimation of the first crack stress with a slight increase for the PVA samples. For the ECC PVA samples, the increase in the reinforcing index from 316 to 422, 527, 633 and

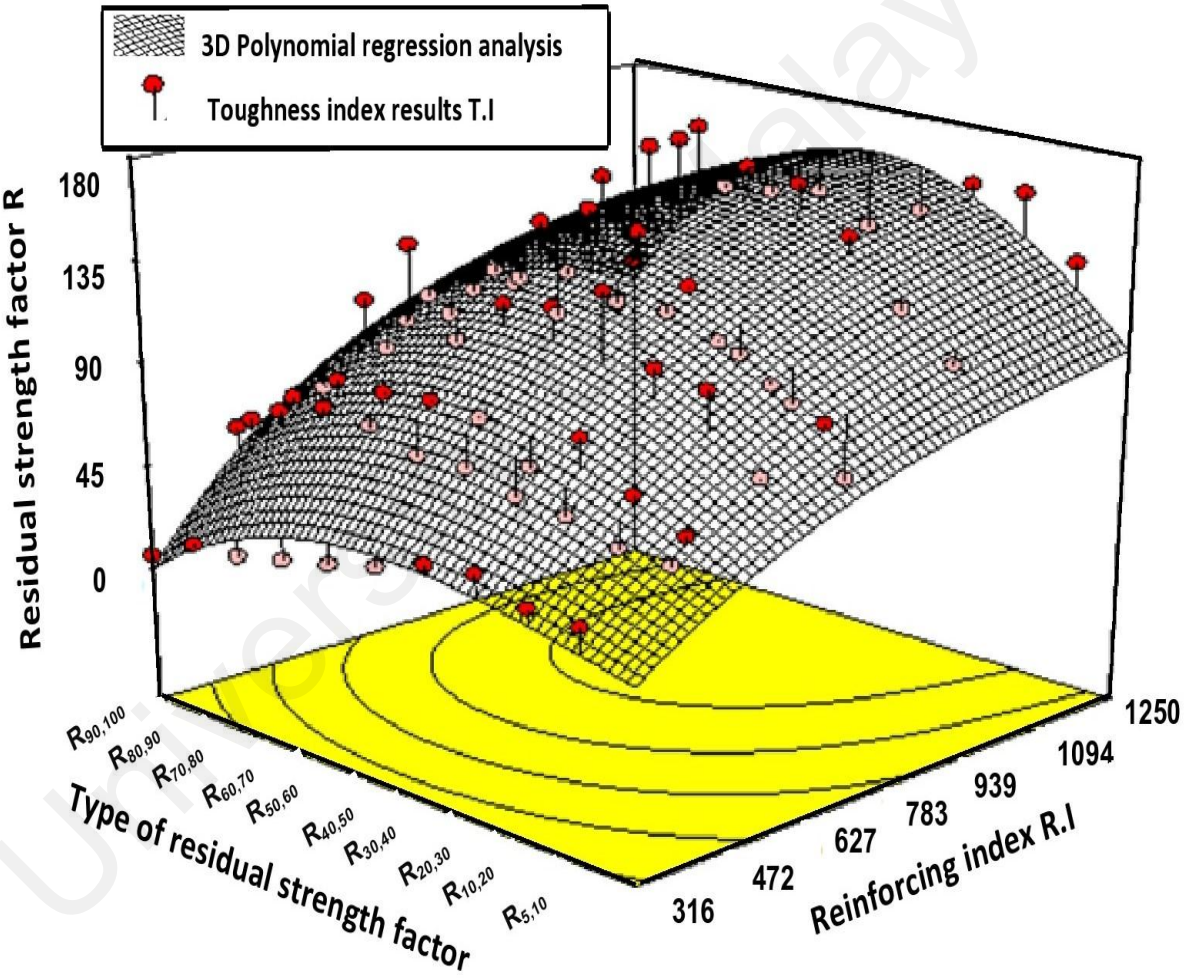

$$Z = 135.17 + 54.48\,A + 5.82\,B - 3.47AB - 34.85\,A^2 - 43.75\,B^2 - 15.63\,A^2\,B - 17.86\,A\,B^2 + 5.28\,A^3 - 7.46\,B^3$$

$R^2 = 0.8776$

where A is the reinforcing index R.I, B is the type of residual strength factor, and Z is the residual strength factor R

Figure 4.16: Effect of reinforcing index on residual strength factor in ECC PE slabs: 3D shape illustration

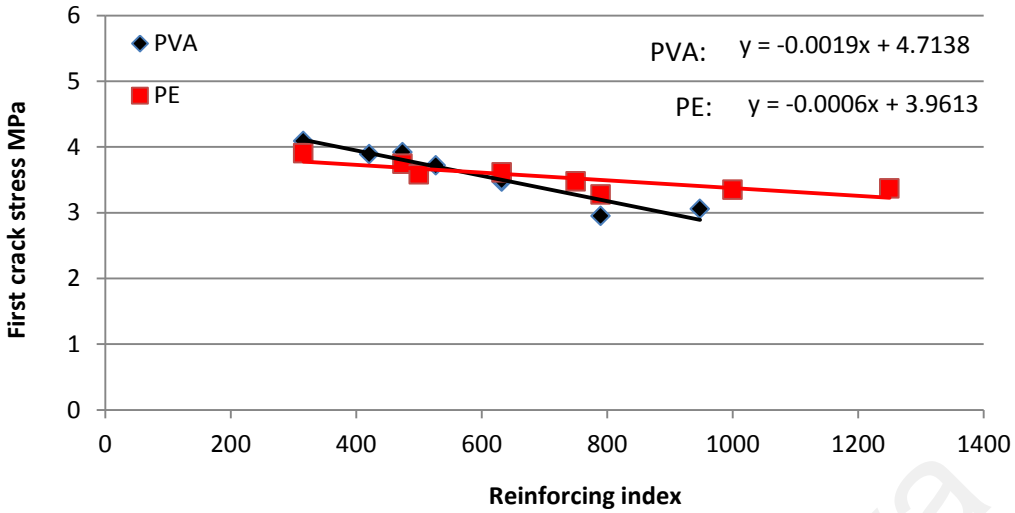

Figure 4.17: Variation of first crack stress with reinforcing indices for ECC I-shaped samples

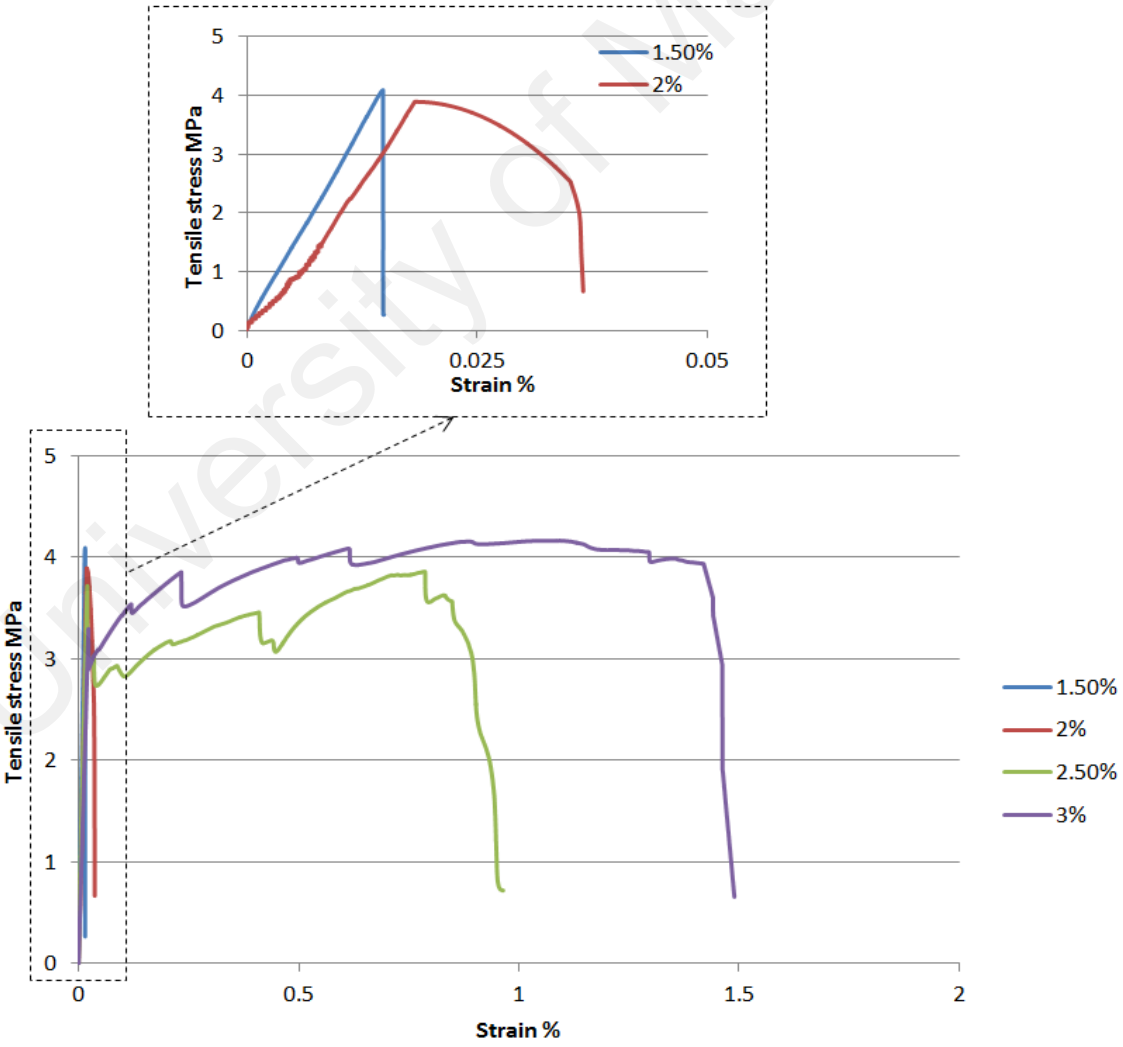

Figure 4.18: Direct tensile stress-strain relationship for ECC I-shaped samples reinforced with PVA RECS15-8mm, A.R=210

790 led to a reduction in first crack load of about 4.9, 9.1, 14.6, and 27.9%, respectively. Similarly, for ECC PE samples, the increase in reinforcing index from 316 to 474, 500, 750, and 790 reduced the first crack load of about 4.1, 8.2, 10.9, and 16%, respectively. Eventually, it is deduced that by increasing the reinforcing index, the fibers did not

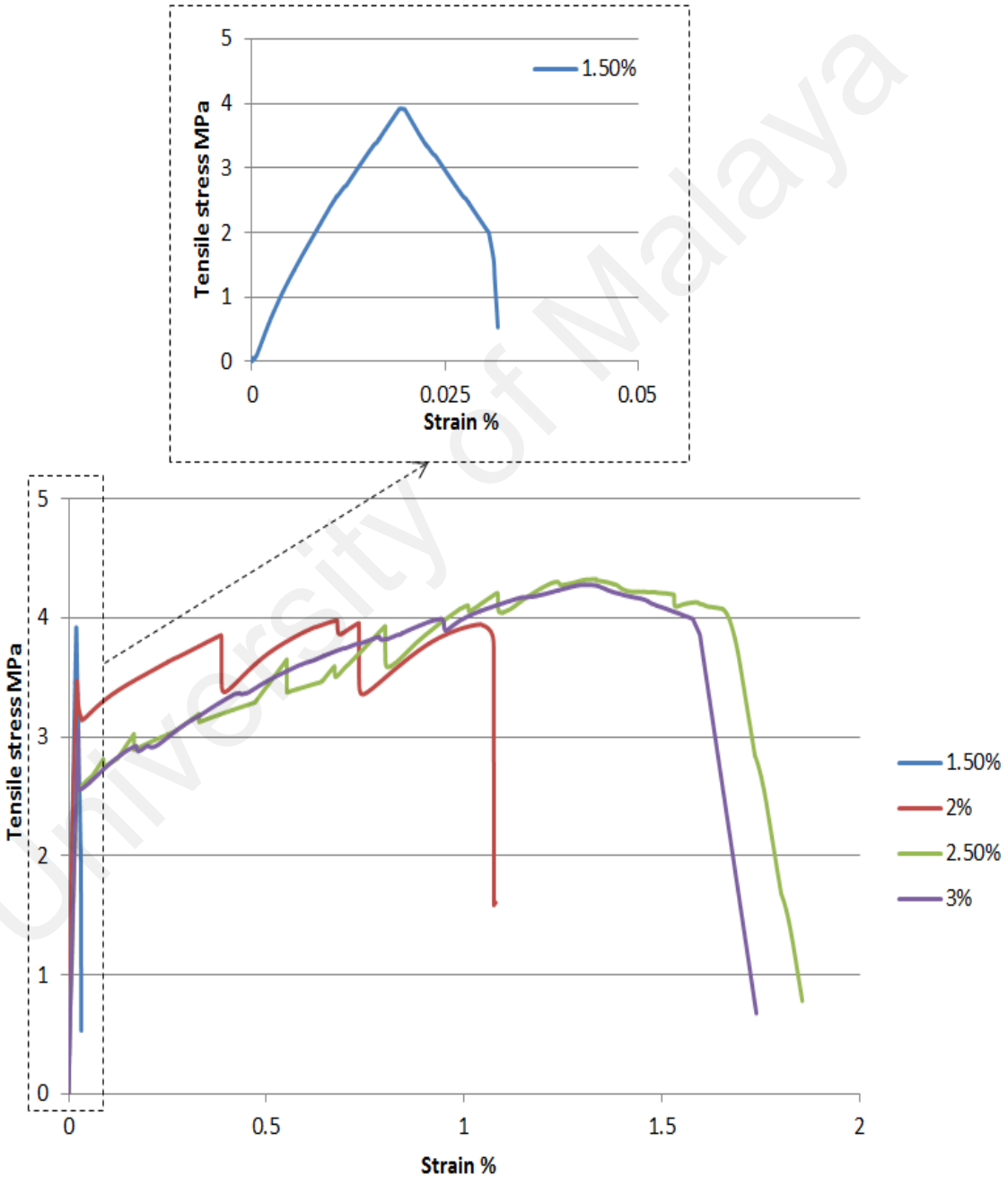

Figure 4.19: Direct tensile stress-strain relationship for ECC I-shaped samples reinforced with PVA RECS15-12mm, A.R=316

improve the first crack load. On the other hand, it was observed that any increase in the reinforcing index exceeding 790 remains the first crack stress without any noticeable change for both kinds of ECC samples.

4.3.2 Ultimate stress capacity at post cracking

After testing the ECC PVA I-shaped samples, it is observed from Figures 4.18 to 4.20 and Table 4.2 that the ultimate stress capacity at post cracking was enhanced of about 51.2, 56, 63.2, 69.2 and 67.7%, by increasing the reinforcing index from 422 to 527, 632, 633, 790 and 948, respectively. The increase in the ultimate stress corresponding to

Table 4.2: Direct tensile testing values obtained from ECC I-shaped specimens

Type of ECC	Symbol of specimen	Reinforcing index	First crack stress MPa	Ultimate stress capacity MPa	First crack strain %	Strain at ultimate stress %	Strain at failure %
ECC-PVA	$TPVA_1$	316	4.093	0.267	0.0148	0.0148	0.0148
	$TPVA_2$	422	3.893	2.552	0.0182	0.0350	0.0366
	$TPVA_5$	474	3.921	2.000	0.0192	0.0307	0.0317
	$TPVA_3$	527	3.720	3.860	0.0199	0.7857	0.9500
	$TPVA_4$	631	3.473	3.981	0.0209	0.6788	1.0802
	$TPVA_6$	632	3.496	4.165	0.0224	1.0943	1.6043
	$TPVA_7$	790	2.95	4.328	0.0235	1.3343	1.8410
	$TPVA_8$	948	3.06	4.280	0.0240	1.2964	1.7250
ECC-PE	TPE_1	316	3.907	3.834	0.0191	0.0600	0.2178
	TPE_2	474	3.747	3.947	0.0208	2.3571	3.3214
	TPE_5	500	3.587	4.160	0.0231	2.7857	3.8571
	TPE_3	632	3.613	4.441	0.0245	2.6786	5.0714
	TPE_6	750	3.481	4.680	0.0256	3.1500	4.8571
	TPE_4	790	3.280	5.147	0.0254	3.5357	5.8929
	TPE_7	1000	3.350	5.361	0.0265	3.8571	6.4286
	TPE_8	1250	3.370	4.853	0.0271	3.4286	5.4643

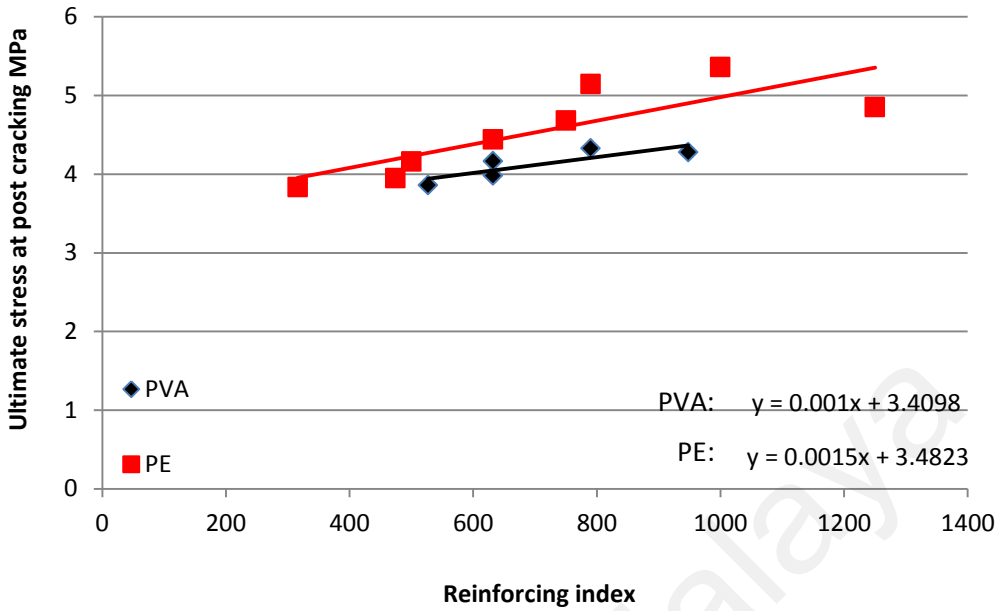

Figure 4.20: Variation of ultimate stress at post cracking with reinforcing index for ECC I-shaped samples

the reinforcing index of 948 dropped to 67.7% is attributed to the high amount of PVA fibers incorporated in fresh ECC led to the irregular dispersion of the PVA fibers.

As indicated in Figures 4.20 to 4.22 and Table 4.2 for the ECC PE I-shaped samples, as the reinforcing index increased from 474 to 632, 750, 790, 1000 and 1250, the ultimate stress value at post cracking gradually increased about 12.5, 18.6, 30.4, 35.8 and 23%. The drop in value of ultimate stress corresponding to reinforcing index 1250 attributed to the high amount of PE fibers led to lack in homogeneity and non-uniform dispersion of fibers in fresh ECC.

On average, the PE samples showed remarkable improvement in the ultimate stress value compared to the PVA samples of 26.6%. In addition, the PE samples showed an improvement in the ultimate stress value at post cracking compared to the PVA samples of about 11.5% for the same reinforcing index of 632 for $TPVA_4$ and TPE_3 samples. Furthermore, an improvement in the ultimate stress value at post cracking was observed

for TPE_4 sample about 18.9% over the corresponding stress value for $TPVA_7$ based on the same reinforcing index of 790. This may be attributed to the expected mode of failure of PE fibers, which is bond-slip, rather than the rupture of fibers for PVA fibers. In addition, the high bond strength generated in the interfacial surfaces of the cementitious composite and PE fibers is associated with the increased tensile strength of the PE fibers compared to the PVA fibers in sustaining higher stresses.

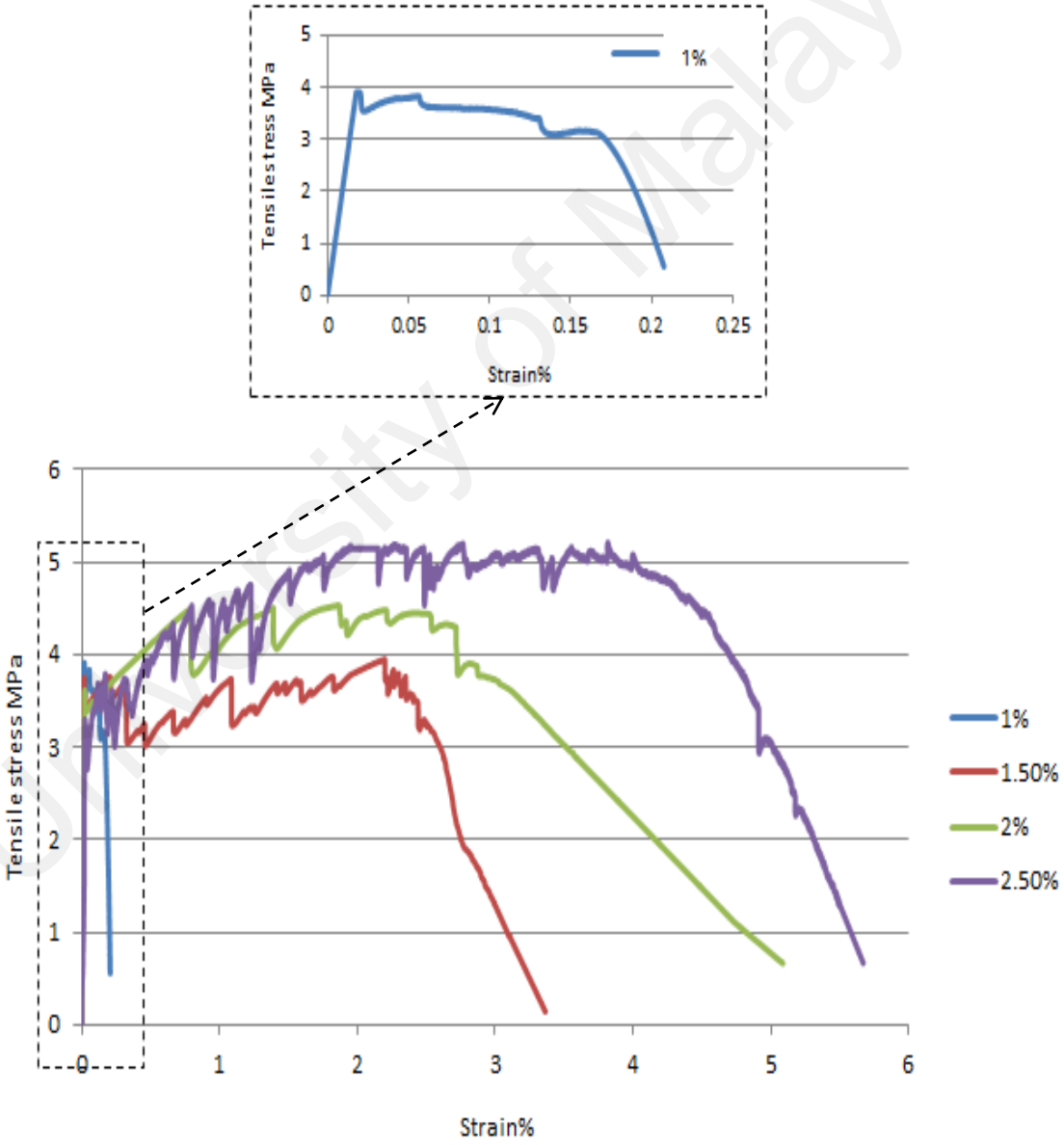

Figure 4.21: Direct tensile stress-strain relationship for ECC I-shaped samples reinforced with PE-4800D, A.R=316

4.3.3 First crack strain

The linear fit of first crack strain results for PVA and PE I-shaped samples is displayed in Figures 4.23 and 4.24. Accordingly, the results for both kinds of ECC samples showed that the increase in the reinforcing index value resulted in a slight increase in the first crack strain. Generally, the increment rate is about 0.001% per 100 of the reinforcing index. These findings suggest that the ECC samples tend to be more elastic with a slight decrease in the modulus of elasticity when the reinforcing index increases. Finally, the linear fit for first crack strain results is deemed more suitable.

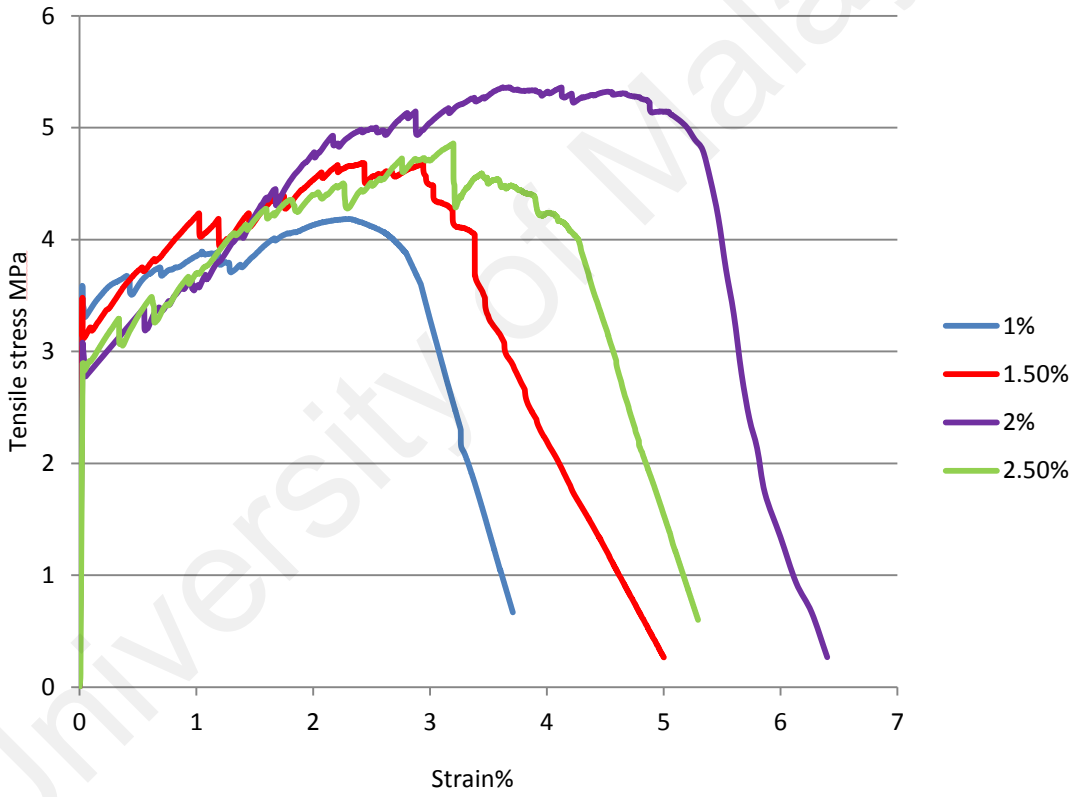

Figure 4.22: Direct tensile stress-strain relationship for ECC I-shaped samples reinforced with PE-1600D, A.R=500

4.3.4 Strain at post cracking

As shown in Figures 4.23, 4.24 and Table 4.2, the strain value at post cracking is directly proportional to the reinforcing index of PVA or PE fibers. According to Table 4.2, the PE I-shaped samples showed a remarkable improvement in the strain value at

post cracking of about four times the value in the ECC PVA samples based on the same reinforcing index of 632 for $TPVA_4$ and TPE_3. In addition, the PE samples showed an improvement in the strain value at post cracking about 2.7 times the value in the ECC PVA samples based on the same reinforcing index of 790 for $TPVA_7$ and TPE_4 samples. Moreover, the highest values for strain value at post cracking were recorded for the ECC PE samples. For PE samples, as the reinforcing index increased from 474 to 632, 750, 790, and 1000, a gradual increase in strain value at post cracking varied from 2.36% to 2.68, 3.15, 3.54, and 3.86%, respectively. A series of multiple cracks was noticed in the middle region of PE samples. The observed strain value at R.I equals to 1250 reduced to a lower value by 3.43% due to the high fiber content and high aspect ratio, which led to a non-homogeneous matrix.

For the ECC PVA samples, as the reinforcing index increased, the strain value at post cracking also increased. For instance, as the reinforcing index increased from 527 to 633, 790 and 948, the strain value at post cracking also increased from 0.786% to 1.094, 1.335 and 1.296, respectively. The highest value recorded for the PVA samples was 1.335%, which is considerably lower than the highest value for PE samples. The drop in strain value at R.I equals to 948 is due to the non-uniform dispersion of fibers in the ECC matrix. Based on the previous analysis, the ECC PE samples showed considerably higher ductility than the ECC PVA samples. The regression analysis of strain results at post cracking for each of PVA and PE samples is set to be linear fit with an increment rate of 0.14 and 0.15% per 100 of reinforcing index, respectively, which is able to improve the ductility of ECC samples to acceptable limits.

4.3.5 Strain at failure

The strain value at failure for each ECC I-shaped sample was evaluated according to the corresponding stress value of 25% of the ultimate stress at post cracking specified at the descending part of the stress-strain curve. It is noticed from Figures 4.23 and 4.24 that

the trend of strain values at failure, is likely to be similar to the trend of strain values at post cracking with higher values. The results in the PE samples reveal that the increase in reinforcing index from 474 to 500, 632, 790, and 1000 led to a significant increase in the strain value at failure from 3.32% to 3.85, 5.07, 5.89 and 6.42%, respectively. Similarly, the increase in the reinforcing index for PVA samples from 527 to 632, 790 and 948 caused an increase in the strain value at failure from 0.95% to 1.6, 1.84 and 1.73, respectively. The result from the Table 4.2 showed that the PE samples presented a significant improvement in the strain values at failure compared to the PVA samples of about 4.7 times the value for the ECC PVA samples based on the same reinforcing index of 632 for $TPVA_4$ and TPE_3. Furthermore, the improvement in the strain values at failure for PE samples was about 267% based on the same reinforcing index of 790 for PVA_7 and PE_4. Consequently, the ECC PE samples presented significantly higher strain values at failure than the corresponding values for ECC PVA samples. The highest value of 6.43% for PE sample was recorded, which indicates the highest ductility and ability to deform without any sudden failure. Multiple cracking behavior was observed with many cracks extending at the middle part of the PE sample. As shown in Figures 4.23 and 4.24, the linear fit analysis for both results is found more suitable. For ECC PVA samples, the increment rate determined from fit analysis is 0.19% per 100 of reinforcing index. Besides, the increment rate determined from the fit analysis for ECC PE samples was identified to be 0.3% per 100 of reinforcing index. This particular rate is highly distinctive.

In general, for the ECC PVA or PE samples, the results showed a gradual increase in the strain value at failure by increasing the reinforcing index. However, the values obtained for the PVA samples confirmed that the highest value recorded was 1.84%, which was considerably less than the highest value for the PE slabs. The lower value for the strain at failure indicated the limited ductility of the PVA samples and their inability to deform

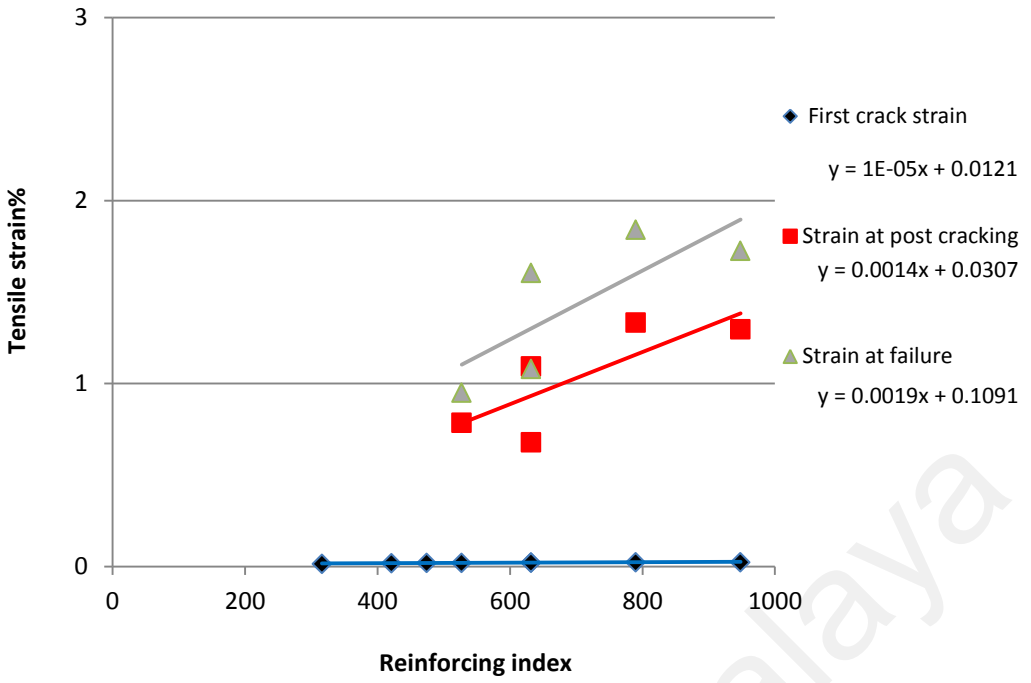

Figure 4.23: Effect of reinforcing index on strain values for PVA I-shaped samples

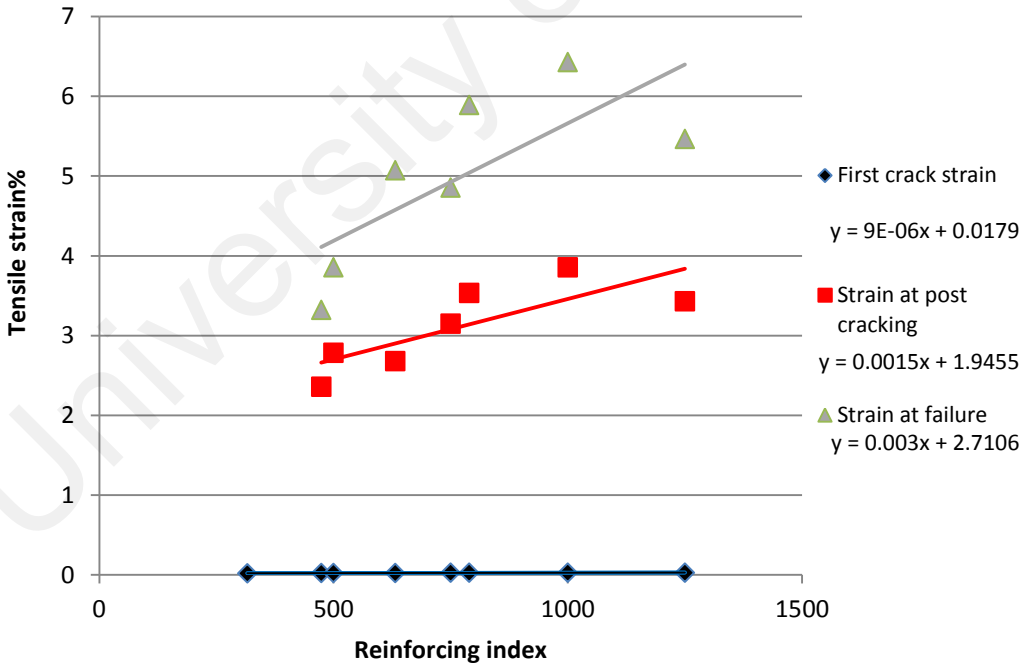

Figure 4.24: Effect of reinforcing index on strain values for PE I-shaped samples

more compared to the PE samples. This behavior could be attributed to the high interfacial frictional and chemical bond established between the PVA fiber surfaces and the cement matrix (Balaguru et al., 1992) which led to the rupture of the fibers, which in turn limited the tensile performance and deformation of the ECC samples.

4.3.6 Stress-strain relationship and crack patterns

Referring to Figures 4.18, 4.19 and 4.21, the $TPVA_1$, $TPVA_2$, $TPVA_5$ and TPE_1 samples characterized with softening behavior of the stress-strain relationship (i.e. the ultimate tensile stress is lower than the first crack stress) due to the insufficient fiber content and/or lower aspect ratio. Regarding the tensile performance and ductility, the results obtained were unpromising compared to the other ECC tensile samples. In addition, after the first crack appearance, the crack localized and widened leading to a sudden drop in the curve and causing the failure. Starting from the reinforcing index of 527 until 948, the ECC PVA samples characterized with strain-hardening and multi-cracking behavior. Moreover, the trend of the stress-strain curve at the post cracking stage within the region starting from the first crack until the onset of softening of the stress-strain curve reveals abundant and sequent bridging of the cracks. The ultimate strength of the I-shaped PVA samples was enhanced over the first crack strength due to the crack-arresting mechanism of PVA fibers. Furthermore, the undesirable mode of failure of PVA fiber (i.e. fiber rupture) resulted in less tensile strain values and poor ductility despite the discernible behavior of PVA samples.

Referring to the Figures 4.21 and 4.22, The ECC PE I-shaped samples exhibited perfect tensile performance. Multiple bridging of cracks and sub-cracks observed within an extensive range of deformation. Moreover, the perfect ductility of PE samples resulted in a noticeable amount of tensile strain. Furthermore, the desirable mode of failure of PE fiber (i.e. bond-slip failure of the fibers) resulted in a significant behavior of strain-

hardening and higher deformation. Figure 4.25 shows the I-shaped sample deformation under the tensile load process and the crack patterns for some of the tested samples.

4.3.7 Strain hardening behavior and cut-off point

The strain hardening behavior is simply defined as the bridging mechanism ability of the PVA or PE fibers to enhance the ultimate strength of the I-shaped sample over its first crack strength. For ECC-PVA I-shaped samples, Figures 4.26 shows the behavior of PVA mixtures with different reinforcing indices under flexure and direct tension. Direct tensile tests of PVA samples specify the cut-off point of ECC based on the basic definition of ECC by evaluating the strain hardening behavior of PVA samples using different reinforcing indices. It was shown from results of the tensile samples that the cut-off point for ECC PVA is set at reinforcing index equals to 527. As indicated in Figure 4.26, the effect of reinforcing index in both direct tension I-shaped PVA specimens and flexural PVA slabs has shown different behavior of strain-hardening. Unlike the cut-off point in direct tension, the cut-off point in flexure slabs is set at reinforcing index equals to 421.

The results of direct tensile tests of PE I-shaped samples and flexural PE slabs gave the cut-off point of the reinforcing index for strain hardening behavior in ECC. In addition, the findings reveal identical behavior in strain hardening. The cut-off point for ECC PE direct tension I-shaped samples is apparent at the reinforcing index of 474 similar to that of flexural slabs (Figure 4.27).

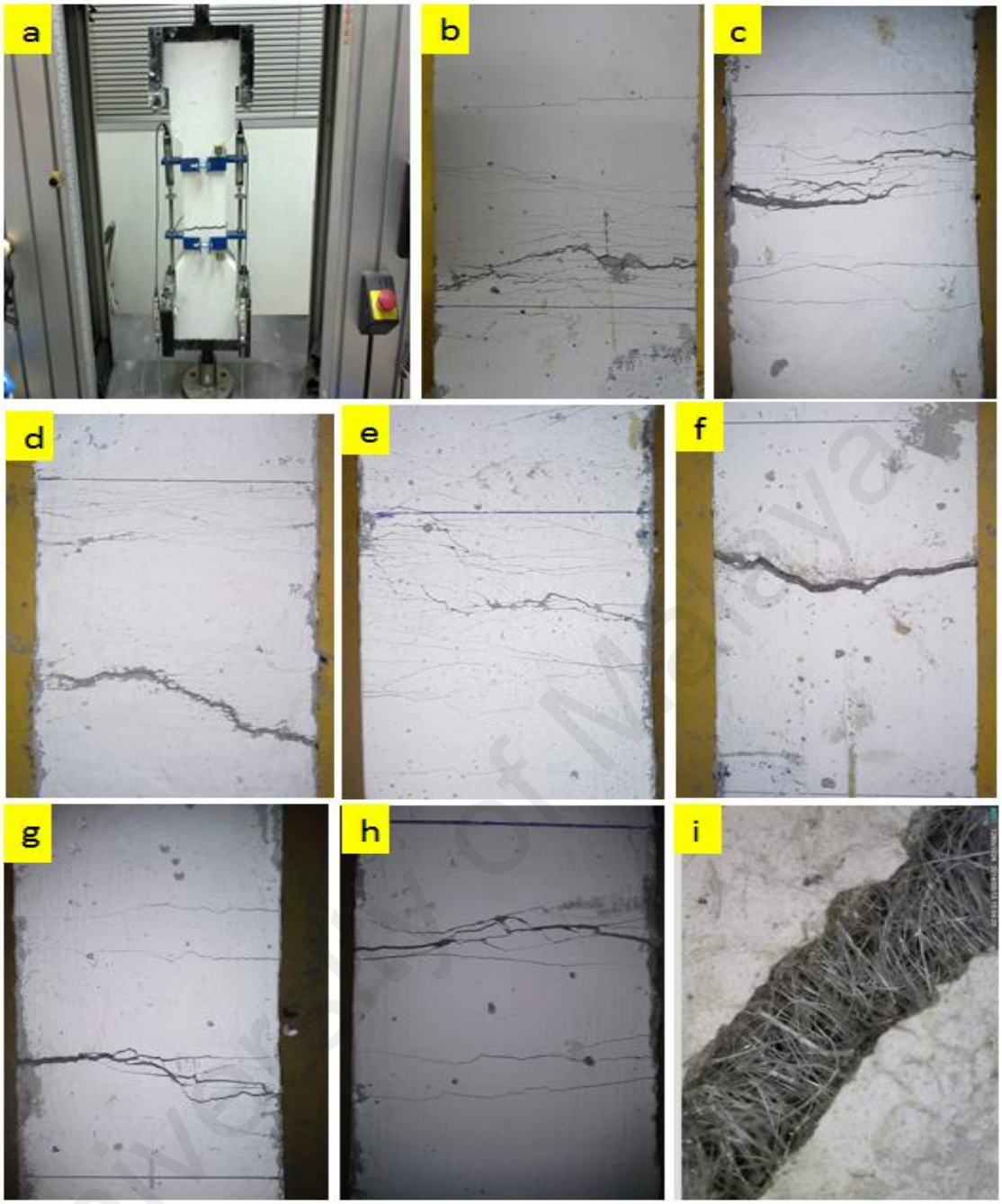

Figure 4.25: (a) I-shaped sample under tensile loading. Crack propagation in: (b) TPE_2 (c) TPE_4 (d) TPE_5 (e) TPE_7 (f) $TPVA_2$ (g) $TPVA_7$ (h) $TPVA_8$ (i) Crack bridging in I-shaped sample

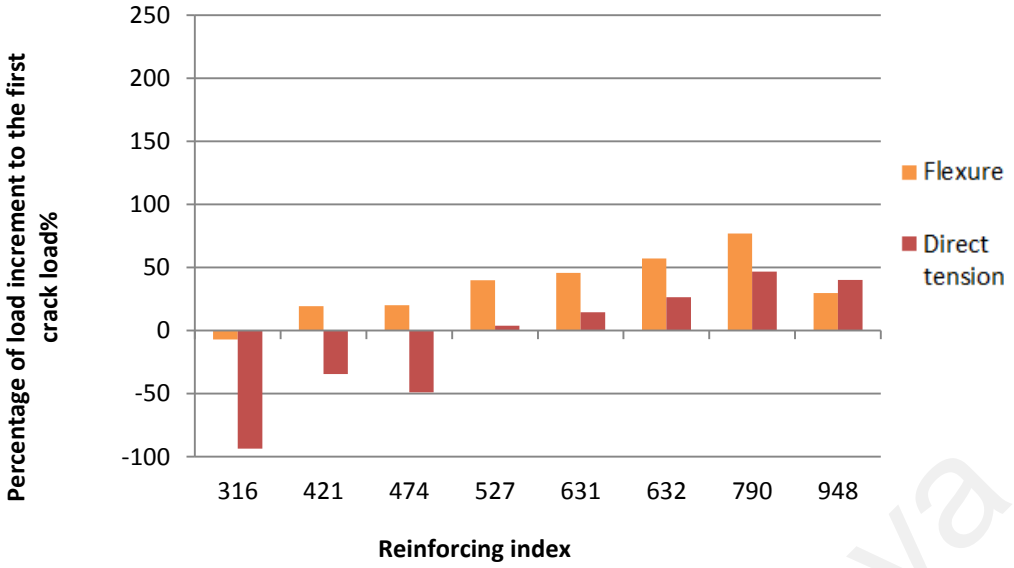

Figure 4.26: Increment of ultimate load over the first crack load in flexural and direct tension tests for ECC-PVA

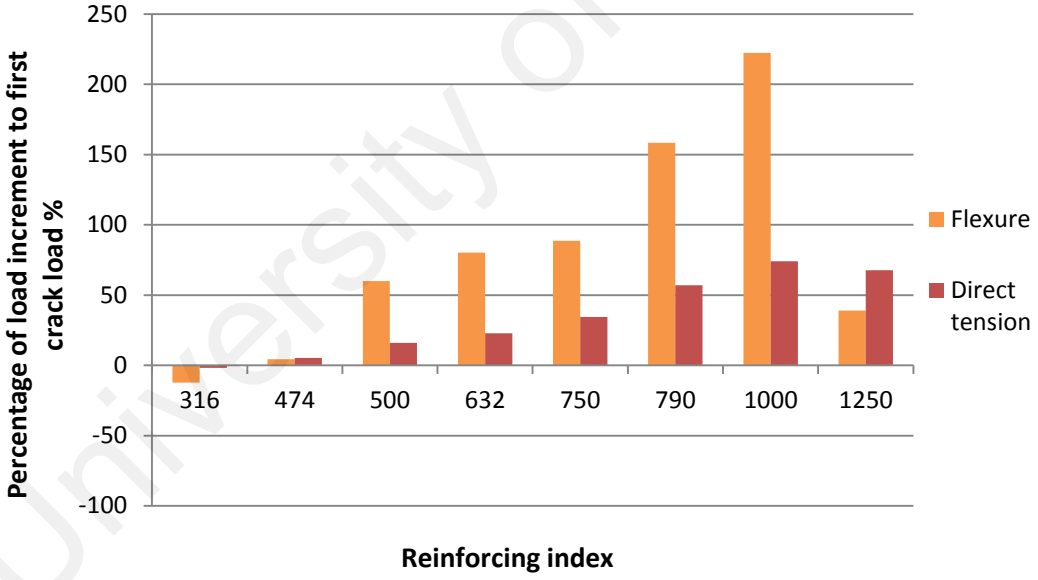

Figure 4.27: Increment of ultimate load over the first crack load in flexural and direct tension tests for ECC-PE

4.4 Reinforced concrete exterior beam-column joints

In this section, results and discussion of 14 beam-column specimens are presented. The investigation of results is displayed in three main trajectories. The first trajectory is the investigation of results for the normal concrete (NC) specimens which are represented in the NC_1 (with no inclusion of lateral steel hoops in the joint zone) and NC_2 (with inclusion of lateral steel hoops designed according to the ACI 352R-02 provisions) (352R-02, 2002). The second trajectory is the results of the PVA specimens, are represented by the specimens PVA_1 to PVA_6. The third trajectory is the results of PE specimens, are represented by the specimens PE_1 to PE_6 (refer to Table 3.6).

The investigation is based on some parameters which are, the effect of steel hoops in the NC and ECC joint, effect of ECC inclusion in the joint zone, effect of type of fibers (PVA or PE) in the ECC and effect of fiber reinforcing index.

4.4.1 Mode of failure and crack propagation

4.4.1.1 Normal concrete (NC) specimens

For the first specimen cast with NC and without lateral steel hoops, the first crack appeared at a load equals to 14 kN and deflection equals to 5.5 mm (at drift ratio of 0.5%) in the beam about 65 mm away from the face of the column, as shown in Figure 4.28a. When the testing proceeded, the cracks in the beam appeared within a distance of 450 mm from the face of the joint with a 100 mm average spacing of cracks. The overall length of the crack propagation from the upper and lower faces of the beam was about 110 mm to 125mm along the beam depth. No significant width of cracks was observed.

The last crack in the beam appeared with a load of 46 kN and the deflection of 22 mm (at drift ratio of 2%) and the onset of yielding of longitudinal bars occurred at load of 40 kN with the deflection of 22 mm (drift ratio 2%). The cracks in the joint zone initiated at load of 33kN and the deflection of 16.5 mm (drift ratio 1.5%) and propagated in a

diagonal form. The average of the crack spacing in the joint zone was about 35 to 50 mm with visible width of cracks.

The average ultimate load capacity of the specimen is 49 kN at deflection of 33 mm (drift ratio 3%) and an average ultimate moment and shear capacity of the joint of 60

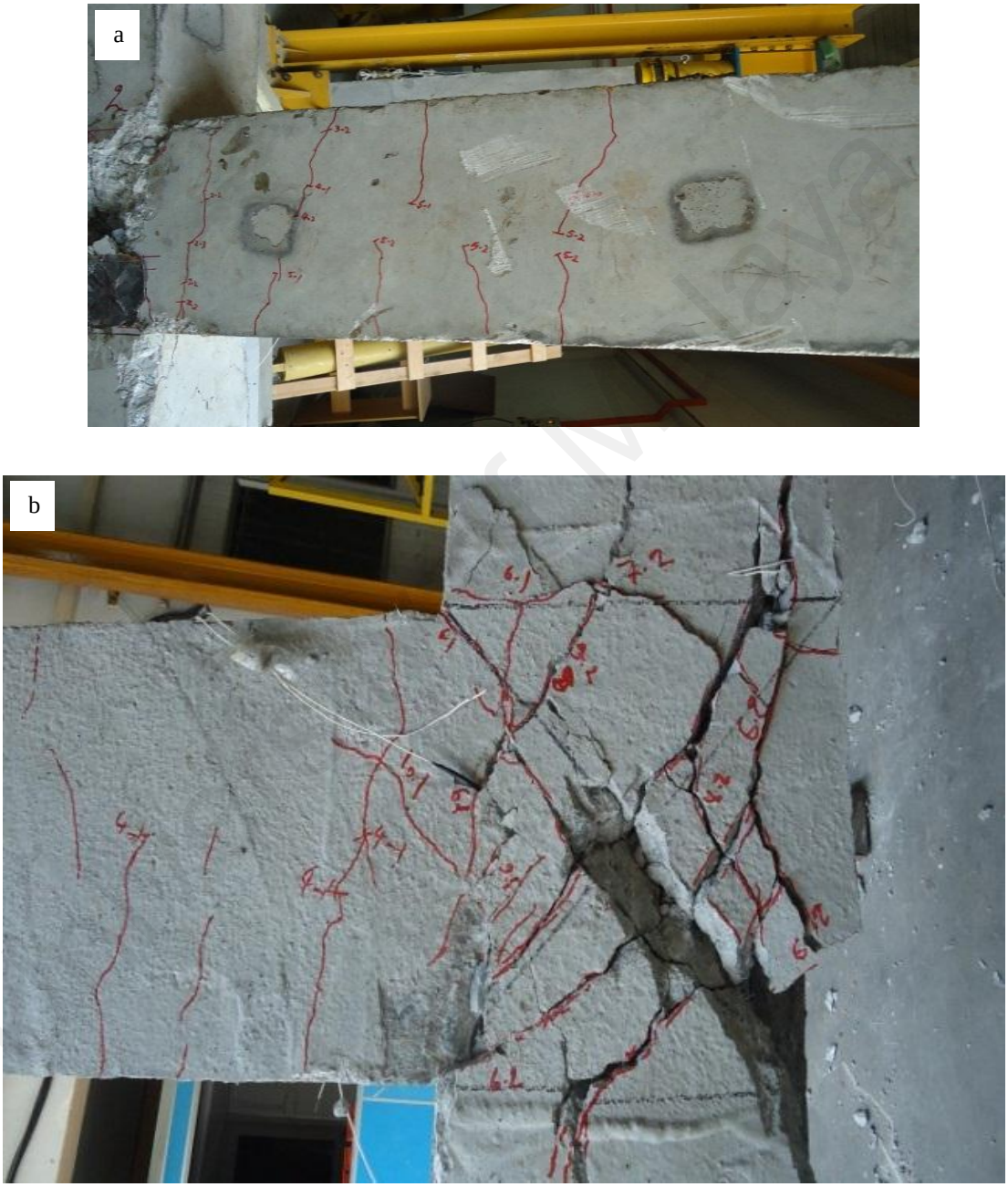

Figure 4.28: Crack propagation in (a) beam (b) joint zone of the NC_1 beam–column specimen

kN.m and 287 kN, respectively. After exceeding the cycles of 3% drift ratio, a drop in the load started and the cracks continued to propagate and widen severely within the joint zone.

As shown in Figure 4.28b, splitting of the concrete was monitored apparently in the joint zone and finally a part of the concrete was crushed into several pieces indicating a brittle shear failure in the joint. Load amount at failure stage shows a decrease of about 52% of the ultimate load capacity at 49.5 mm (4.5% drift ratio). In other words, the drop rate was about 34.7% for each 11 mm increase in deflection (1% drift ratio). Table 4.3 shows the summary of testing results for NC_1 specimen.

For the second specimen (NC_2) cast with NC and designed according to ACI-ASCE Committee 352R-02 (352R-02, 2002) , the first crack appeared at a load equals to 13 kN and deflection equals to 5.5 mm (at drift ratio of 0.5%) in the beam about 83 mm away from the face of the column, as shown in Figure 4.29a. When the testing proceeded, the cracks in the beam appeared within a distance of 610 mm from the face of the joint with crack spacing ranging 55 and 85 mm. The overall length of the crack propagation from the upper and lower faces of the beam was about 100 mm to 140mm along the beam depth. No significant width of cracks was observed.

The last crack in the beam appeared with a load of 56.6 kN and the deflection of 44 mm (at drift ratio of 4%) and the onset of yielding of longitudinal bars occurred at load of 52.5 kN with the deflection of 38.5 mm (drift ratio 3.5%). The cracks in the joint zone initiated at load of 36 kN and the deflection of 22 mm (drift ratio 2%) and propagated in a diagonal form. The average of the crack spacing in the joint zone was about 10 to 35 mm with reduced width of cracks compared to NC_1 specimen.

The average ultimate load capacity of the specimen is 59 kN at deflection of 44 mm (drift ratio 4%) and an ultimate moment and shear capacity of the joint of 72 kN.m and 346 kN, respectively. After exceeding the cycles of 4% drift ratio, a drop in the load

started and a main crack localized near the outer face of the column continued to propagate and widen severely within the joint zone.

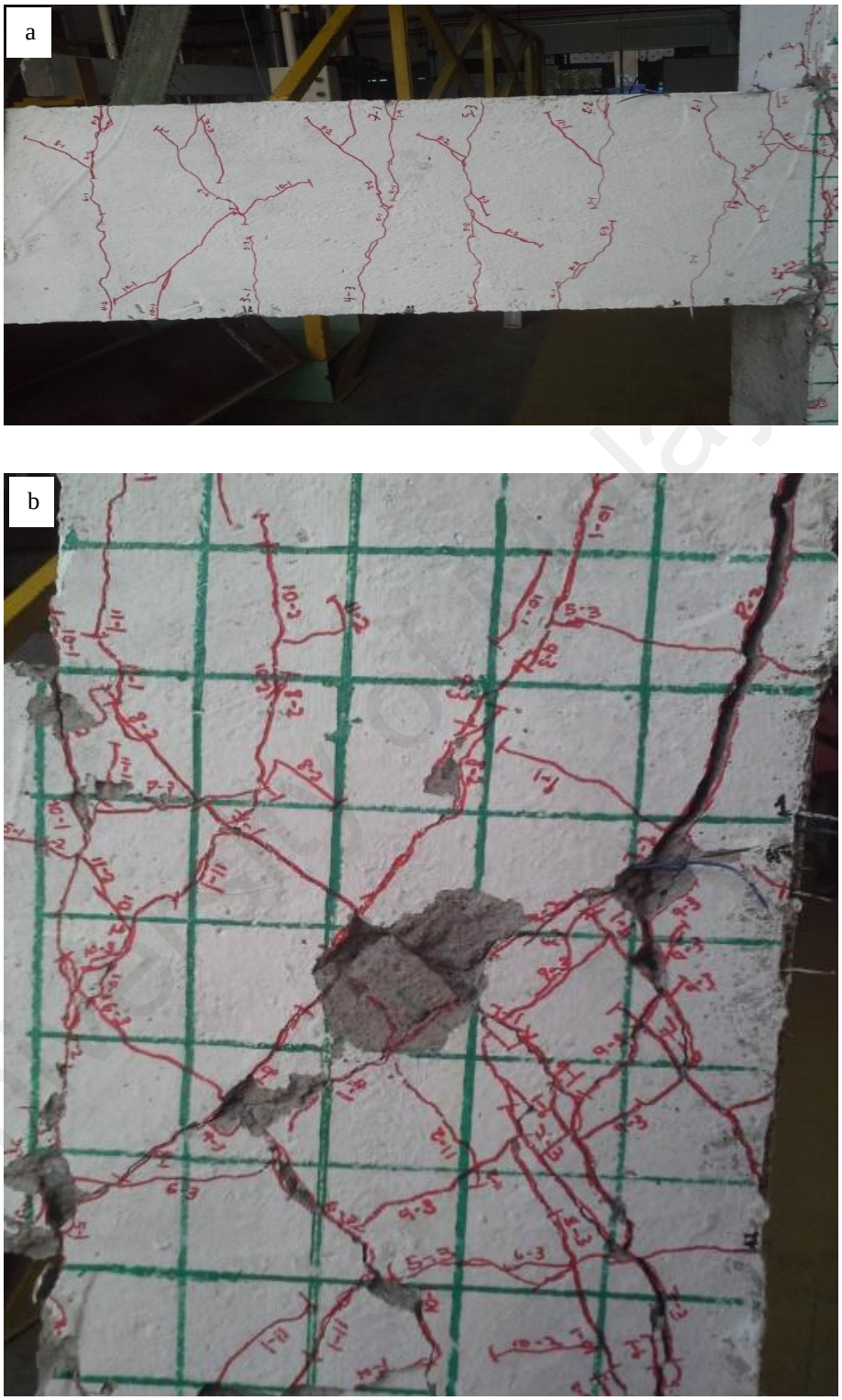

Figure 4.29: Crack propagation in (a) beam (b) joint zone of the NC_2 beam–column specimen

As shown in Figure 4.29b, simple splitting of the concrete was monitored at the center of the joint and small areas in the joint zone. However, the joint zone was almost intact and the concrete wasn't crushed into pieces as observed in NC_1 indicating a shear failure with moderate ductility in the joint. Load amount at failure stage shows a decrease of about 20% of the ultimate load capacity at 55 mm (5% drift ratio). In other words, the drop rate was about 20% for each 11 mm increase in deflection (1% drift ratio). Table 4.3 shows the summary of testing results for NC_2 specimen.

4.4.1.2 ECC-PVA specimens

Commonly, for all ECC-PVA specimens at failure stage, the ECC condition in joint zone was observed intact. No splitting or crushing in the ECC-PVA joint was observed. The beam–column joint failed owing to the high shear forces generated in the joint zone associated with a ductile mode of failure caused by the ECC characteristics of high ductility and high shear strength.

For PVA_1 specimen cast with ECC–PVA mix with V_f =2.5% and A.R = 210 (R.I = 525), the first crack was observed in the beam at a 12 kN load and deflection of 5.5 mm (drift ratio 0.5%) about 25 mm away from the face of the column. As shown in Figure 4.30a, all the cracks observed in the beam appeared within a distance, about 640 mm measured from the face of the column with crack spacing ranging 18 and 90 mm and crack length between 40 and 165 mm.

The last crack in the beam appeared with a load of 56 kN and the deflection of 49.5 mm (at drift ratio of 4.5%) and the onset of yielding of longitudinal bars occurred at load of 47 kN with the deflection of 33 mm (drift ratio 3%). Meanwhile, the first visible crack commenced in the joint zone at 27 kN load and deflection of 16.5 mm (drift ratio 1.5%) in the direction parallel to the diagonals of the joint.

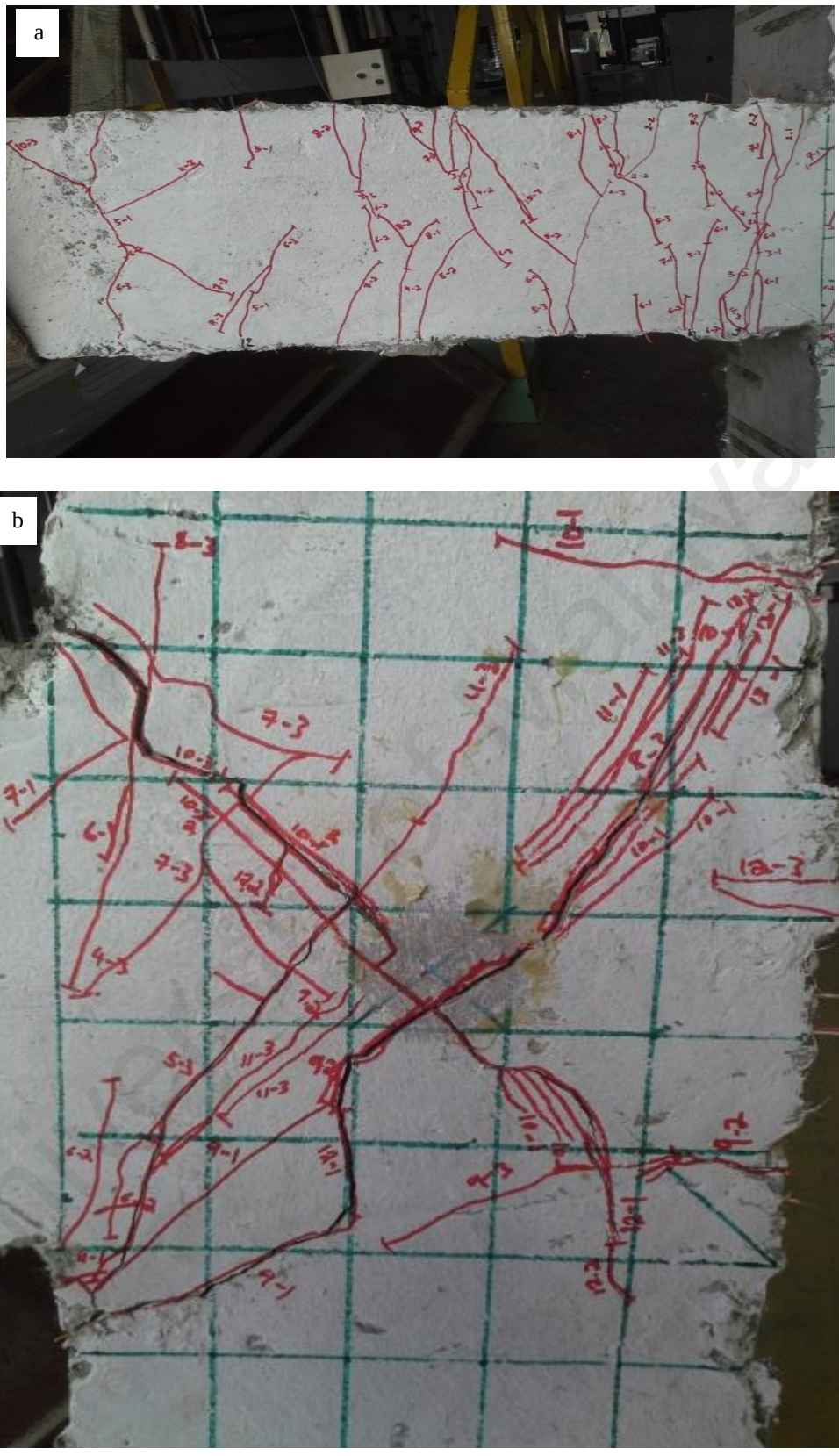

Figure 4.30: Crack propagation in (a) beam (b) joint zone of PVA_1 beam–column specimen

As shown in Figure 4.30b, the main cracks developed in the joint zone and subdivided into smaller branches forming a moderate density of tiny cracks with reduced crack

spacing and width. The estimated spacing of cracks was 4 mm to 70 mm with almost invisible width of cracks.

The specimen sustained an average ultimate load of 57 kN at deflection of 49.5 mm (drift ratio 4.5%) with a moment at the joint of 70 kN.m and shear force capacity of 335 kN. The drop in the load initiated after 4.5% drift ratio and the load value decreased about 15.7% of the ultimate load capacity at deflection of 66 mm (6% drift ratio). In other words, the drop rate was 10.5% for each 11 mm increase in deflection (1% drift ratio).

Finally, failure occurred in the joint zone because of localization of two main cracks on both diagonals commencing from the meeting points of beam boundaries and inner column boundary. Table 4.3 shows the summary of testing results for PVA_1 specimen.

For PVA_2 specimen cast with ECC–PVA mix with V_f =2% and A.R = 316 (R.I= 632), the first crack was observed in the beam at a 10 kN load and deflection of 5.5 mm (drift ratio 0.5%) about 60 mm away from the face of the column. As shown in Figure 4.31a, all the cracks observed in the beam appeared within a distance, about 625 mm measured from the face of the column with crack spacing ranging 43 and 58 mm and crack length between 55 and 164 mm.

The last crack in the beam and the onset of longitudinal bars yielding were observed at a 48 kN load and deflection of 33 mm (drift ratio 3%). Meanwhile, the first visible crack commenced in the joint zone at 38 kN load and deflection of 22 mm (drift ratio 2%) in the direction parallel to the diagonals of the joint. As shown in Figure 4.31b, the main cracks developed in the joint zone and subdivided into smaller branches forming a dense network of tiny cracks with reduced crack spacing and width. The estimated spacing of cracks was 3 mm to 9 mm with almost invisible width of cracks.

This specimen sustained an average ultimate load of 61 kN at deflection of 38.5 mm (drift ratio 3.5%) with a moment at the joint of 75 kN.m and shear force capacity of 358 kN. The drop in the load initiated after 3.5% drift ratio and the load value decreased about 31% of the ultimate load capacity at deflection of 66 mm (6% drift ratio). In other words, the drop rate was 12% for each 11 mm increase in deflection (1% drift ratio).

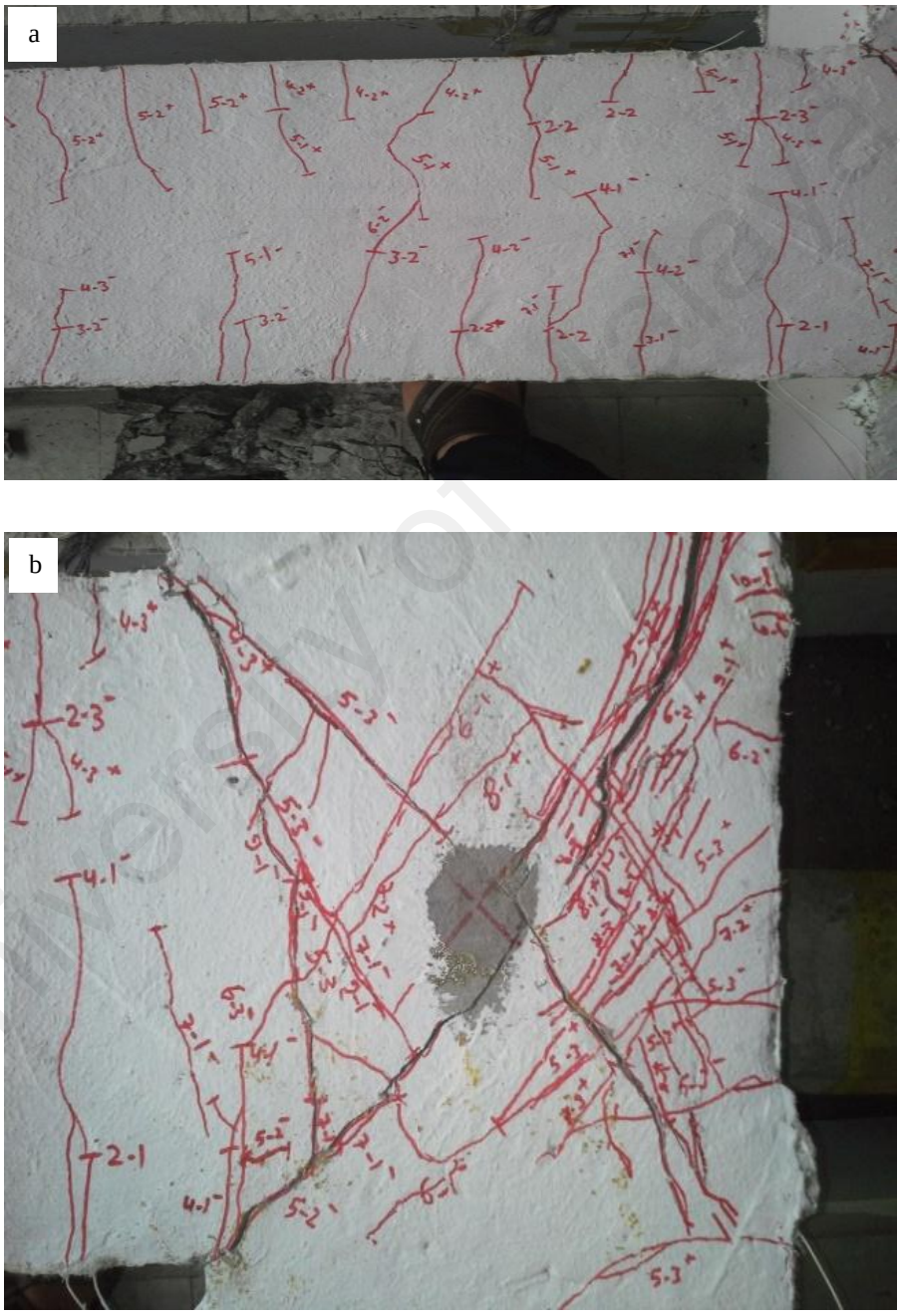

Figure 4.31 Crack propagation in (a) beam (b) joint zone of PVA_2 beam–column specimen

Finally, failure occurred in the joint zone because of the localization of the two main cracks on both diagonals of the joint. Table 4.3 shows the summary of testing results for PVA_2 specimen.

For PVA_3 specimen cast with ECC–PVA mix with V_f =2.5% and A.R = 316 (R.I= 790), the first crack was observed in the beam at a 7 kN load and deflection of 2.75 mm (drift ratio 0.25%) about 100 mm away from the face of the column. As shown in Figure 4.32a, all the cracks observed in the beam appeared within a distance, about 650 mm measured from the face of the column with crack spacing ranging 35 and 75 mm and crack length between 65 and 150 mm.

The last crack in the beam appeared with a load of 75 kN and the deflection of 49.5 mm (at drift ratio of 4.5%) and the onset of yielding of longitudinal bars occurred at load of 58 kN with the deflection of 33 mm (drift ratio 3%). Meanwhile, the first visible crack commenced in the joint zone at 40.6 kN load and deflection of 22 mm (drift ratio 2%) in the direction parallel to the diagonals of the joint. As shown in Figure 4.32b, the main cracks developed in the joint zone and subdivided into smaller branches forming a dense network of tiny cracks with reduced crack spacing and width. The estimated spacing of cracks was 3 mm to 12 mm with almost invisible width of cracks.

The specimen sustained an average ultimate load of 72.5 kN at deflection of 49.5 mm (drift ratio 4.5%) with a moment at the joint of 89 kN.m and shear force capacity of 425 kN. The drop in the load initiated after 4.5% drift ratio and the load value decreased about 12% of the ultimate load capacity at deflection of 77 mm (7% drift ratio). In other words, the drop rate was 4.8% for each 11 mm increase in deflection (1% drift ratio). Finally, failure occurred in the joint zone because of the localization of the two main cracks on both diagonals of the joint. Table 4.3 shows the summary of testing results for PVA_3 specimen.

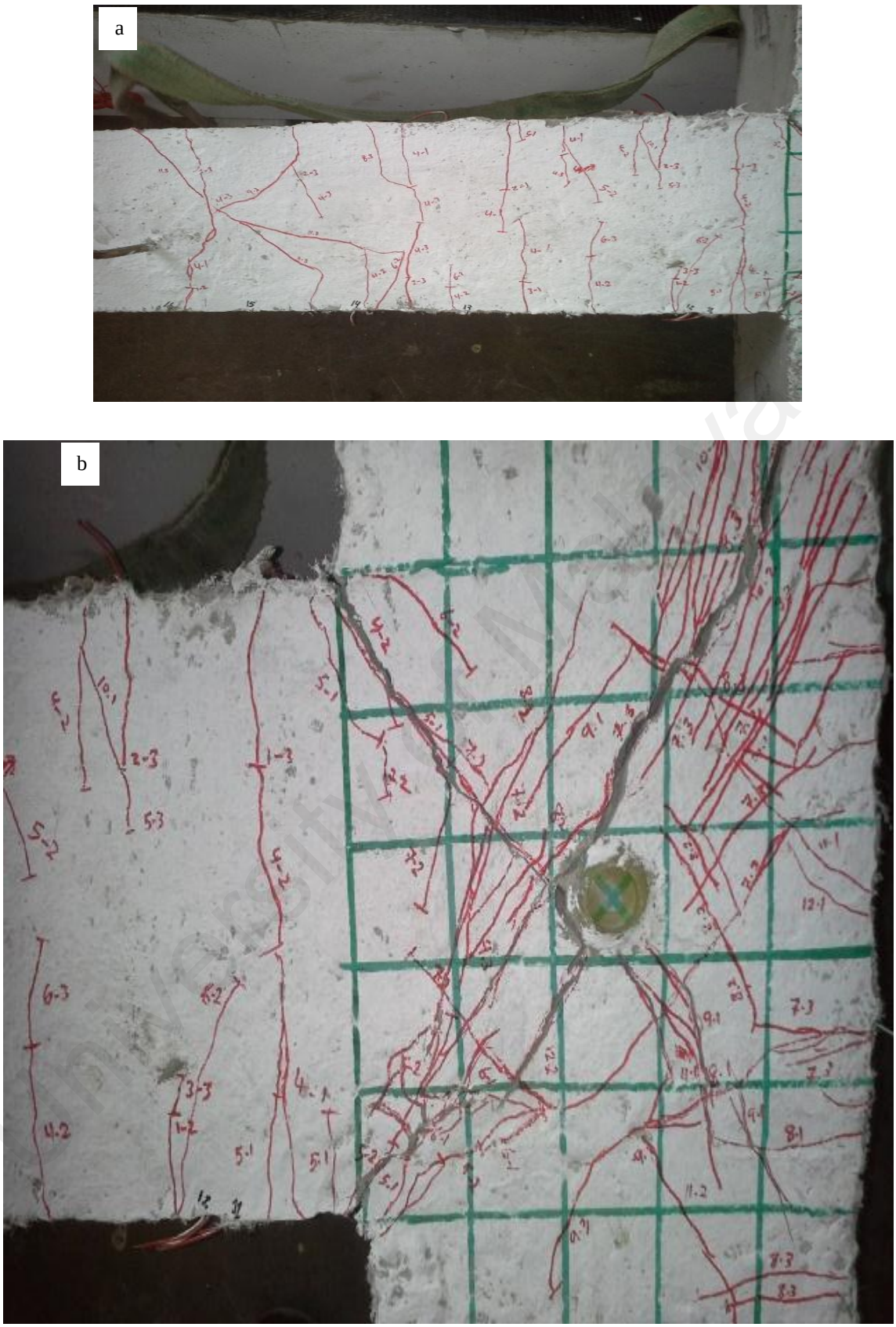

Figure 4.32: Crack propagation in (a) beam (b) joint zone of PVA_3 beam–column specimen

For PVA_4 specimen cast with ECC–PVA mix with V_f =3% and A.R = 316 (R.I= 948), the first crack was observed in the beam at a 11 kN load and deflection of 5.5 mm (drift ratio 0.5%) about 55 mm away from the face of the column. As shown in Figure 4.33a, all the cracks observed in the beam appeared within a distance, about 660 mm measured from the face of the column with crack spacing ranging 18 and 60 mm and crack length between 55 and 190 mm.

The last crack in the beam appeared with a load of 62.4 kN and the deflection of 49.5 mm (at drift ratio of 4.5%) and the onset of yielding of longitudinal bars occurred at load of 58 kN with the deflection of 33 mm (drift ratio 3%). Meanwhile, the first visible crack commenced in the joint zone at 30 kN load and deflection of 16.5 mm (drift ratio 1.5%) in the direction parallel to the diagonals of the joint. As shown in Figure 4.33b, the main cracks developed in the joint zone and subdivided into smaller branches forming a dense network of tiny cracks with reduced crack spacing and width. The estimated spacing of cracks was 3 mm to 80 mm with almost invisible width of cracks.

The specimen sustained an average ultimate load of 65.5 kN at deflection of 49.5 mm (drift ratio 4.5%) with a moment at the joint of 80 kN.m and shear force capacity of 384 kN. The drop in the load initiated after 4.5% drift ratio and the load value decreased about 16.5% of the ultimate load capacity at deflection of 77 mm (7% drift ratio). In other words, the drop rate was 6.6% for each 11 mm increase in deflection (1% drift ratio).

Finally, failure occurred in the joint zone because of the localization of the two main cracks on both diagonals commencing from the meeting points of beam boundaries and inner column boundary. Table 4.3 shows the summary of testing results for PVA_4 specimen.

For PVA_5 specimen, one lateral steel hoop was installed in the joint zone and cast with ECC–PVA mix with V_f =2% and A.R = 316 (R.I= 632). The first crack was observed in

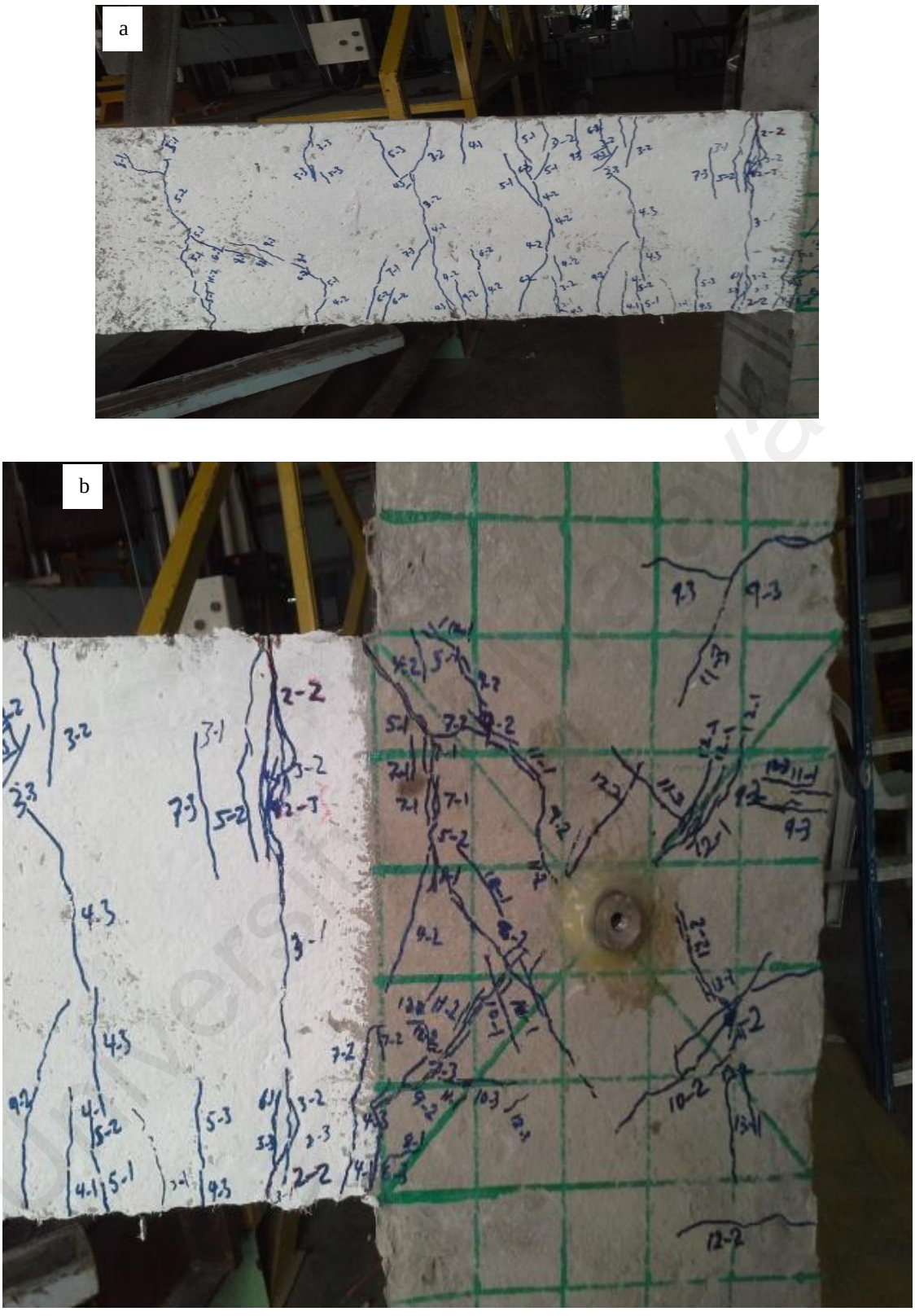

Figure 4.33: Crack propagation in (a) beam (b) joint zone of PVA_4 beam–column specimen

the beam at a 12.4 kN load and deflection of 5.5 mm (drift ratio 0.5%) about 50 mm away from the face of the column. As shown in Figure 4.34a, all the cracks observed in

the beam appeared within a distance, about 730 mm measured from the face of the column with crack spacing ranging 20 and 105 mm and crack length between 70 and 175 mm.

The last crack in the beam appeared with a load of 55.6 kN and the deflection of 77 mm (at drift ratio of 7%) and the onset of yielding of longitudinal bars occurred at load of 51.6 kN with the deflection of 27.5 mm (drift ratio 2.5%). Meanwhile, the first visible crack commenced in the joint zone at 51.6 kN load and deflection of 27.5 mm (drift ratio 2.5%) on the diagonals of the joint. As shown in Figure 4.34b, the main cracks developed in the joint zone and subdivided into smaller branches forming a dense network of tiny cracks with reduced crack spacing and width. The estimated spacing of cracks was 5 mm to 30 mm with almost invisible width of cracks.

The specimen sustained an average ultimate load of 73.5 kN at deflection of 49.5 mm (drift ratio 4.5%) with a moment at the joint of 90.1 kN.m and shear force capacity of 432 kN. The drop in the load initiated after 4.5% drift ratio and the load value decreased about 22.1% of the ultimate load capacity at a deflection of 77 mm (7% drift ratio). In other words, the drop rate was 8.84% for each 11 mm increase in deflection (1% drift ratio). At the failure stage, the joint zone was observed intact. No splitting, crushing, or damage in the ECC-PVA joint was observed except that a small piece of ECC broke away from the upper-outer edge of joint zone, as shown in Figure 4.34b.

The beam–column joint failed owing to the high shear forces generated in the joint zone associated with a ductile mode of failure caused by the ECC characteristics of high ductility and high shear strength combined with the effect of steel hoop inclusion.

Finally, failure occurred in the joint zone because of the localization of a main crack propagated from the upper-outer edge of joint zone in the direction of joint diagonal. Table 4.3 shows the summary of testing results for PVA_5 specimen.

Figure 4.34: Crack propagation in (a) beam (b) joint zone of PVA_5 beam–column specimen

For PVA_6 specimen, two lateral steel hoops were installed in the joint zone and cast with ECC–PVA mix with V_f =2% and A.R = 316 (R.I= 632). The first crack was observed in the beam at 11.2 kN load and deflection of 5.5 mm (drift ratio 0.5%) about 65 mm away from the face of the column. As shown in Figure 4.35a, all the cracks observed in the beam appeared within a distance, about 660 mm measured from the face of the column with crack spacing ranging 15 and 70 mm and crack length between 40 and 160 mm.

The last crack in the beam appeared with a load of 72.3 kN and the deflection of 66 mm (at drift ratio of 6%) and the onset of yielding of longitudinal bars occurred at load of 56.5 kN with the deflection of 27.5 mm (drift ratio 2.5%). Meanwhile, the first visible crack commenced in the joint zone at 31.7 kN load and a deflection of 16.5 mm (drift ratio 1.5%) in the direction parallel to the diagonals of the joint. As shown in Figure 4.35b, the main cracks developed in the joint zone and subdivided into smaller branches forming a dense network of tiny cracks with reduced crack spacing and width. The estimated spacing of cracks was 3 mm to 35 mm with almost invisible width of cracks.

The specimen sustained an average ultimate load of 77.7 kN at deflection of 49.5 mm (drift ratio 4.5%) with a moment at the joint of 95.2 kN.m and shear force capacity of 456 kN. The drop in the load initiated after 4.5% drift ratio and the load value decreased about 8.22% of the ultimate load capacity at deflection of 77 mm (7% drift ratio). In other words, the drop rate was 3.29% for each 11 mm increase in deflection (1% drift ratio. The beam–column joint failed owing to the high shear forces generated in the joint zone associated with a ductile mode of failure caused by the ECC characteristics of high ductility and high shear strength combined with the effect of steel hoops inclusion.

Finally, failure occurred in the joint zone because of the localization of a main crack propagated and widened from the upper-outer edge of joint zone in the direction of joint diagonal. Table 4.3 shows the summary of testing results for PVA_6 specimen.

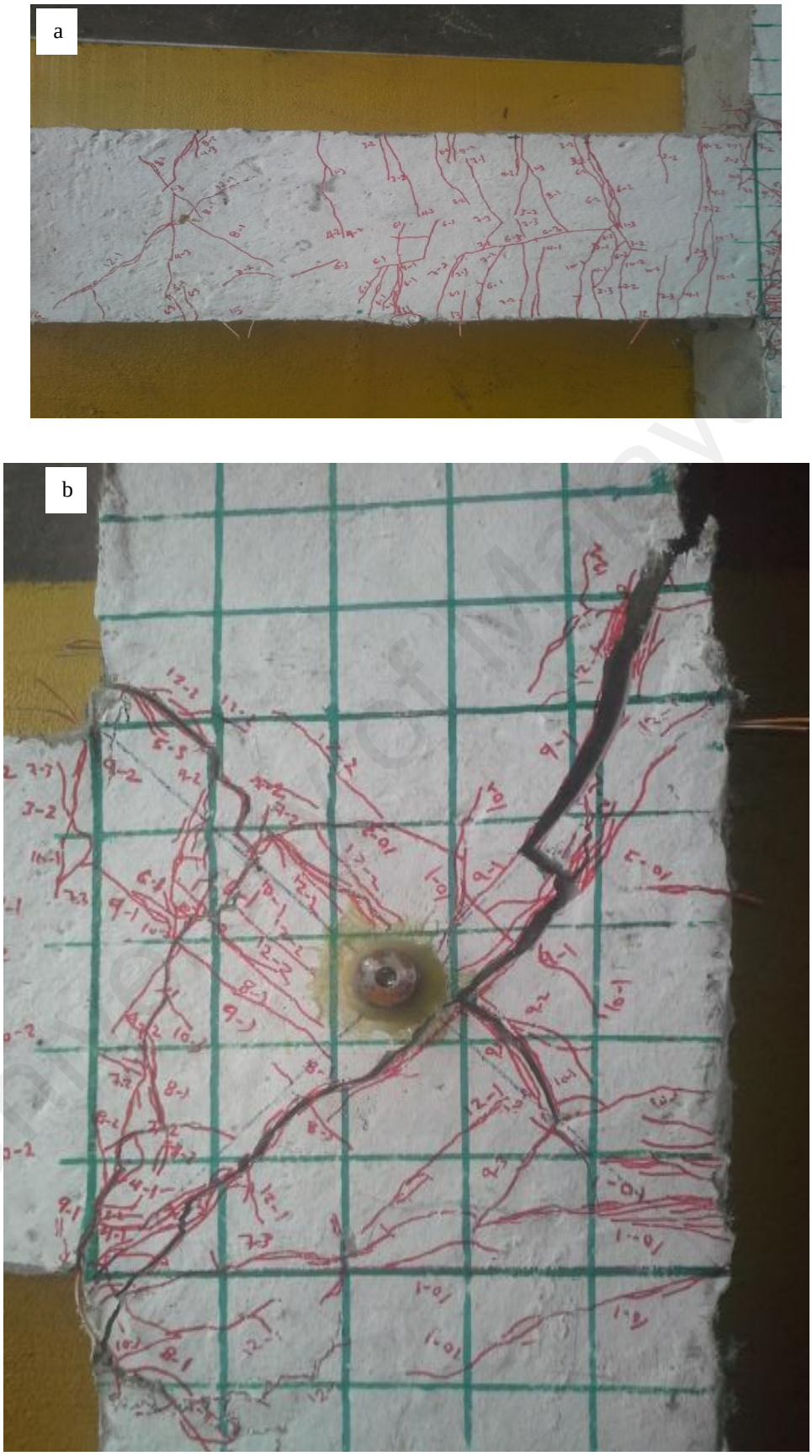

Figure 4.35: Crack propagation in (a) beam (b) joint zone of PVA_6 beam–column specimen

4.4.1.3 ECC-PE specimens

Commonly, for all ECC-PE joints at failure stage, the ECC material condition within the joint region was observed entirely intact. No splitting or crushing for the ECC material was occurred. The beam–column joint failed due to the high shear forces generated in the joint region associated with a ductile mode of failure caused by the ECC characteristics of high ductility and high shear strength.

For the specimen (PE_1) cast with ECC–PE mix, with V_f = 1.5% and A.R = 316 (R.I = 474), the first crack was observed in the beam at 9.2 kN load and deflection of 5.5 mm (0.5% drift ratio) about 80 mm away from the face of the column. As shown in Figure 4.36a, all the cracks observed in the beam appeared within a distance, about 660 mm measured from the face of the column with crack spacing ranging 9 and 54 mm and crack length between 38 and 130 mm.

The last crack in the beam was observed at a 55 kN load and deflection of 55 mm (5% drift ratio). Further, the onset of beam longitudinal bars yielding was observed at a 50 kN load and deflection of 33 mm (3% drift ratio). Meanwhile, the first visible crack commenced in the joint zone at 39 kN load and deflection of 27.5 mm (2.5% drift ratio) in the direction parallel to the depth of the column. As shown in Figure 4.36b, many cracks developed in the joint region and subdivided into smaller branches forming highly dense network of tiny cracks on diagonals and inner part of the joint towards the beam with infinitesimal crack spacing and width. The estimated spacing of cracks was 2 mm to 5 mm with almost invisible width of cracks.

The specimen resisted an average ultimate load of 61 kN at deflection of 66 mm (drift ratio 6%) with a moment at the joint of 74.7 kN.m and shear force capacity of 358 kN. The drop in the load initiated after 5% drift ratio and the load value decreased about an average of 14.2% of the ultimate load capacity at deflection of 88 mm (8% drift ratio).

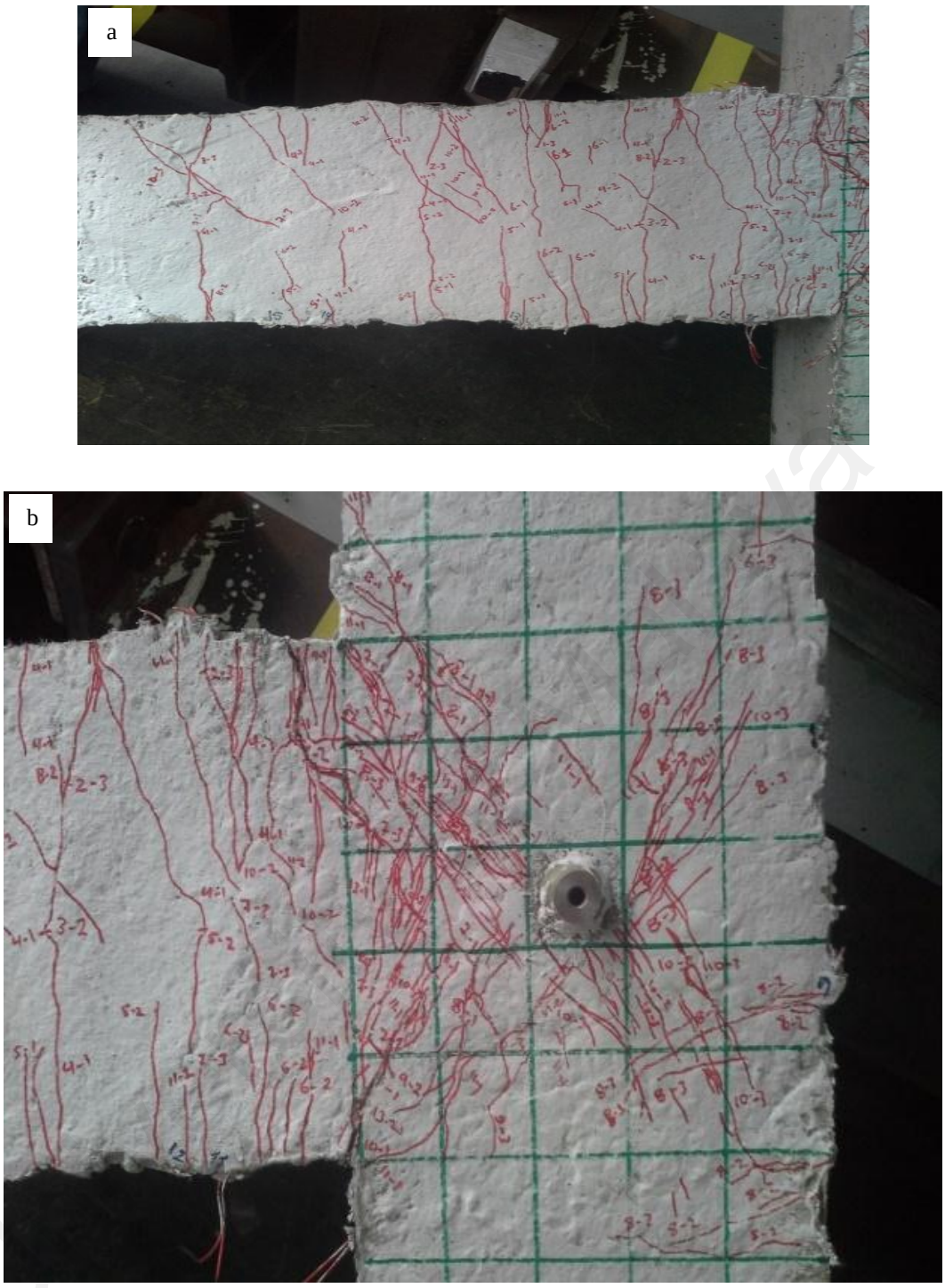

Figure 4.36 Crack propagation in (a) beam (b) joint zone of PE_1 beam–column specimen

In other words, the drop rate was 7.1% for each 11 mm increase in deflection (1% drift ratio).

Finally, the failure occurred in the joint region due to a main flexural crack initiated from the upper face of the beam about 25 mm away from the face of the column and

propagated diagonally inside the joint zone. At failure stage, the crack localized within the joint zone indicating mix mode of flexural-shear failure. Table 4.3 shows the summary of testing results for PE_1 specimens.

For the PE_2 specimen cast with ECC–PE mix, with V_f = 2% and A.R = 316 (R.I = 632), the first crack was observed in the beam at an 8.7 kN load and deflection of 5.5 mm (0.5% drift ratio) about 38 mm away from the face of the column. As shown in Figure 4.37a, all the cracks observed in the beam appeared within a distance, about 670 mm measured from the face of the column with crack spacing ranging 7 and 60 mm and crack length between 43 and 172 mm.

The last crack in the beam was observed at a 71 kN load and deflection of 66 mm (6% drift ratio) and the onset of beam longitudinal bars yielding was observed at a 61 kN load and deflection of 38.5 mm (3.5% drift ratio). Meanwhile, the first visible crack commenced in the joint region at 30 kN load and deflection of 16.5 mm (1.5% drift ratio) in the direction parallel to the diagonals of the joint. As shown in Figure 4.37b, many cracks developed in the joint region and subdivided into smaller branches forming highly dense network of tiny cracks on diagonals and the majority of the joint zone with infinitesimal crack spacing and width. The estimated spacing of cracks was 2 mm to 5 mm with almost invisible width of cracks.

This specimen resisted an average ultimate load of 67.4 kN at deflection of 66 mm (drift ratio 6%) with a moment at the joint of 82.5 kN.m and shear force capacity of 395 kN. The drop in the load initiated after 6% drift ratio and the load value decreased about an average of 15.8% of the ultimate load capacity at deflection of 88 mm (8% drift ratio). In other words, the drop rate was 7.9% for each 11 mm increase in deflection (1% drift ratio).

Finally, failure occurred in the joint zone because of the localization of the two main cracks on both diagonals commencing from the meeting points of beam boundaries and

inner column boundary. Table 4.3 shows the summary of testing results for PE_2 specimen.

Figure 4.37 Crack propagation in (a) beam (b) joint zone of PE_2 beam–column specimen

For specimen PE_3 cast with ECC–PE mix, with V_f = 2.5% and A.R = 316 (R.I = 790), the first crack was observed in the beam at 9.2 kN load and deflection of 5.5 mm (0.5% drift ratio) about 54 mm away from the face of the column. As shown in Figure 4.38a, all the cracks observed in the beam appeared within a distance, about 510 mm measured from the face of the column with crack spacing ranging 23 and 75 mm and crack length between 19 and 163 mm.

The last crack in the beam was observed at a 72 kN load and deflection of 66 mm (6% drift ratio) and the onset of beam longitudinal bars yielding was observed at a 54 kN load and deflection of 33 mm (3% drift ratio). Meanwhile, the first visible crack commenced in the joint zone at 34.6 kN load and deflection of 22 mm (2% drift ratio) propagated in horizontal direction. As shown in Figure 4.38b, many cracks developed in the joint region and subdivided into smaller branches forming highly dense network of tiny cracks on diagonals and on the majority of the joint zone with infinitesimal crack spacing and width. The estimated spacing of cracks was 2 mm to 5 mm with almost invisible width of cracks.

The specimen resisted an average ultimate load of 77.7 kN at deflection of 66 mm (drift ratio 6%) with a moment at the joint of 95.2 kN.m and shear force capacity of 456 kN. The drop in the load initiated after 6% drift ratio and the load value decreased about an average of 7.2% of the ultimate load capacity at deflection of 88 mm (8% drift ratio). In other words, the drop rate was 3.6% for each 11 mm increase in deflection (1% drift ratio).

Finally, failure occurred in the joint zone because of the localization of the two main cracks on both diagonals commencing from the meeting points of beam boundaries and inner column boundary. Table 4.3 shows the summary of testing results for PE_3 specimen.

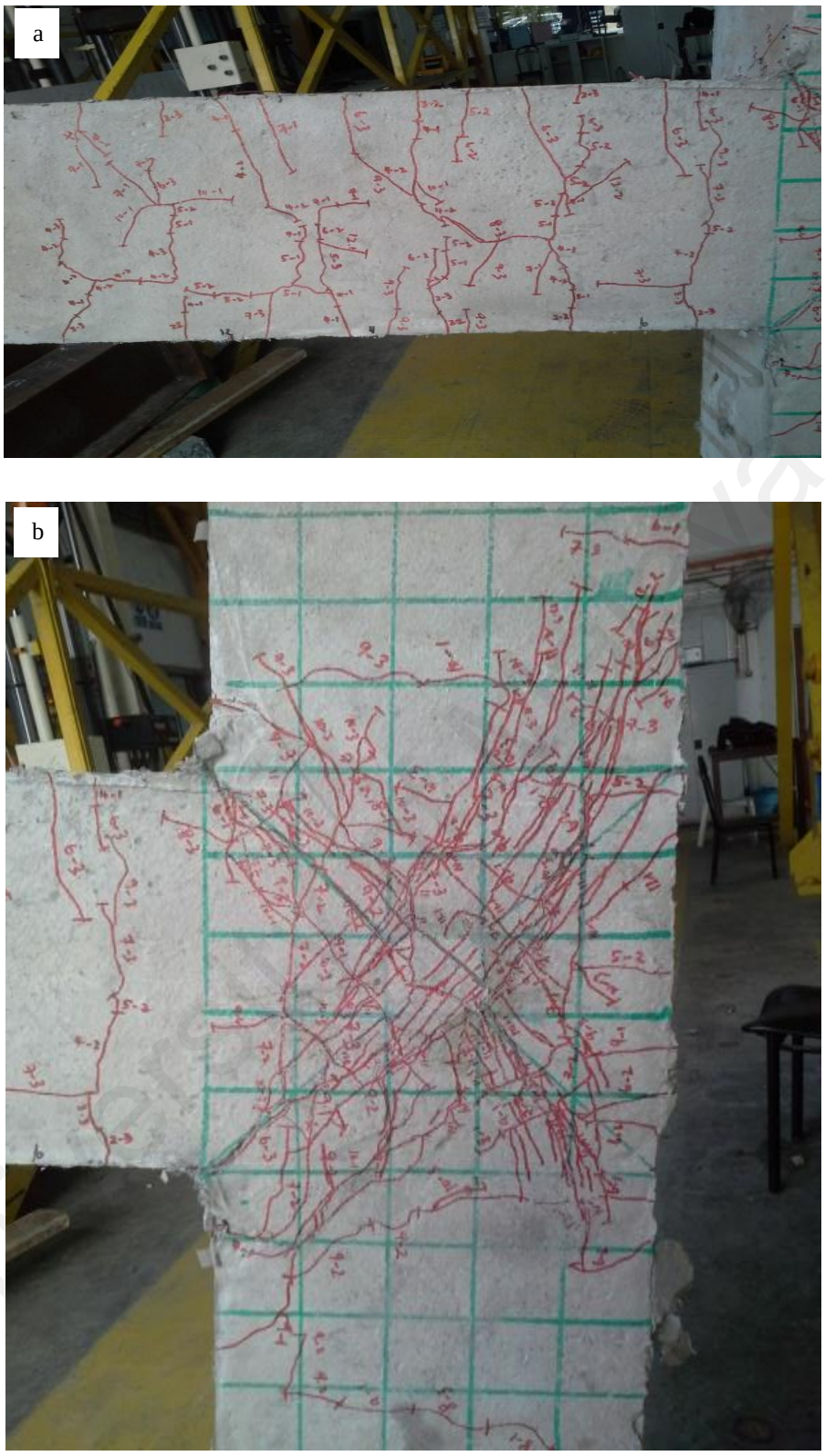

Figure 4.38 Crack propagation in (a) beam (b) joint zone of PE_3 beam–column specimen

For specimen PE_4 cast with ECC–PE mix, with V_f = 2% and A.R = 500 (R.I = 1000), the first crack was observed in the beam at 9.5 kN load and deflection of 5.5 mm (0.5%

drift ratio) about 45 mm away from the face of the column. As shown in Figure 4.39a, all the cracks observed in the beam appeared within a distance, about 600 mm measured from the face of the column with crack spacing ranging 14 and 65 mm and crack length between 38 and 150 mm.

The last crack in the beam was observed at a 76.5 kN load and deflection of 66 mm (6% drift ratio) and the onset of beam longitudinal bars yielding was observed at a 68 kN load and deflection of 33 mm (3% drift ratio). Meanwhile, the first visible crack commenced in the joint zone at 55.5 kN load and deflection of 27.5 mm (2.5% drift ratio) propagated in the direction parallel to joint diagonals. As shown in Figure 4.39b, many cracks developed in the joint region and subdivided into smaller branches forming highly dense network of tiny cracks on diagonals and on the majority of the joint zone with infinitesimal crack spacing and width. The estimated spacing of cracks was 1 mm to 5 mm with almost invisible width of cracks.

The specimen resisted an average ultimate load of 80 kN at deflection of 49.5 mm (drift ratio 4.5%) with a moment at the joint of 98 kN.m and shear force capacity of 470 kN. The drop in the load initiated after 4.5% drift ratio and the load value decreased about an average of 15% of the ultimate load capacity at deflection of 88 mm (8% drift ratio). In other words, the drop rate was 4.3% for each 11 mm increase in deflection (1% drift ratio).

Finally, failure occurred in the joint zone because of the localization of the two main cracks on both diagonals commencing from the meeting points of beam boundaries and inner column boundary. Table 4.3 shows the summary of testing results for PE_4 specimen.

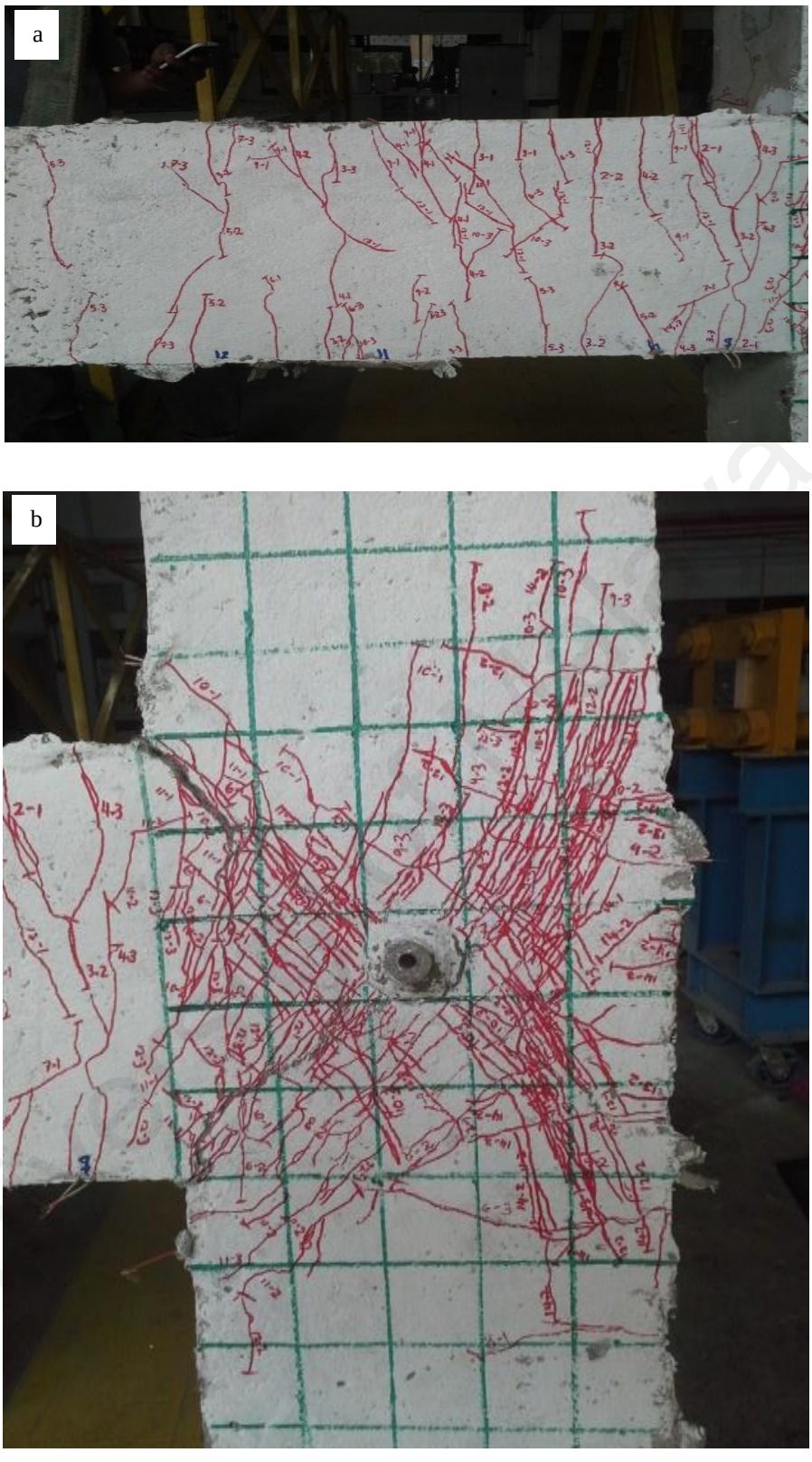

Figure 4.39 Crack propagation in (a) beam (b) joint region of PE_4 beam–column specimen

For specimen PE_5, one lateral steel hoop was installed in the joint zone and cast with ECC–PE mix with V_f =2% and A.R = 316 (R.I= 632). The first crack was observed in

the beam at 11.6 kN load and deflection of 5.5 mm (0.5% drift ratio) about 65 mm away from the face of the column. As shown in Figure 4.40a, all the cracks observed in the beam appeared within a distance, about 600 mm measured from the face of the column with crack spacing ranging 15 and 70 mm and crack length between 40 and 170 mm.

The last crack in the beam was observed at a 81.5 kN load and deflection of 49.5 mm (4.5% drift ratio) and the onset of beam longitudinal bars yielding was observed at a 57 kN load and deflection of 27.5 mm (2.5% drift ratio). Meanwhile, the first visible crack commenced in the joint zone at 34.5 kN load and deflection of 16.5 mm (1.5% drift ratio) propagated on the joint diagonal. As shown in Figure 4.40b, many cracks developed in the joint zone and subdivided into smaller branches forming highly dense network of tiny cracks on the diagonals and on the majority of the joint zone with infinitesimal crack spacing and width. The estimated spacing of cracks was 1 mm to 5 mm with almost invisible width of cracks.

The specimen resisted an average ultimate load of 87.3 kN at deflection of 66 mm (drift ratio 6%) with a moment at the joint of 107 kN.m and shear force capacity of 512 kN. The drop in the load initiated after 6% drift ratio and the load value decreased about an average of 13.6% of the ultimate load capacity at deflection of 88 mm (8% drift ratio). In other words, the drop rate was 6.57% for each 11 mm increase in deflection (1% drift ratio).

The beam–column joint failed due to the high shear forces generated in the joint zone associated with a ductile mode of failure caused by the ECC characteristics of high ductility and high shear strength combined with the effect of steel hoop inclusion.

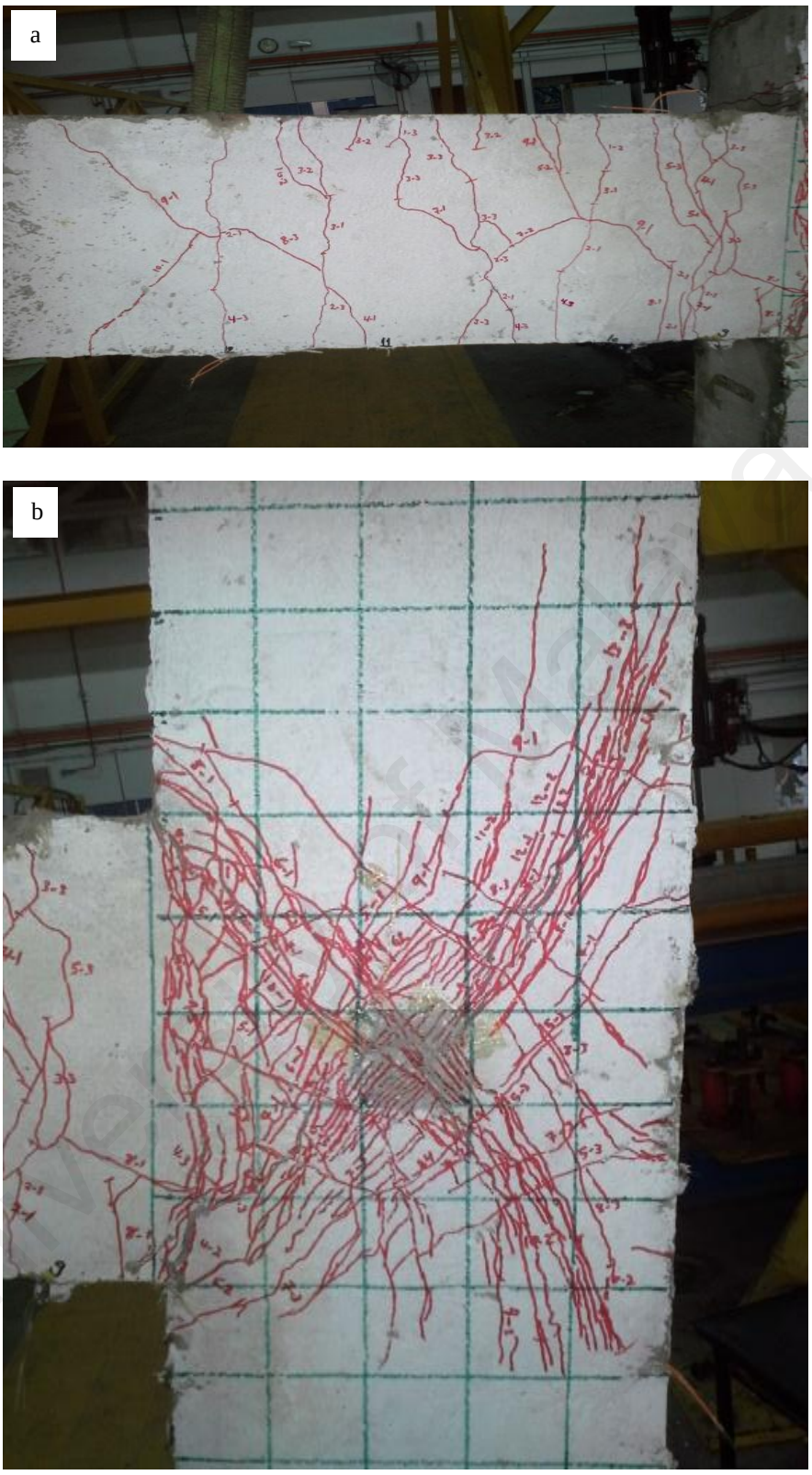

Figure 4.40 Crack propagation in (a) beam (b) joint region of PE_5 beam–column specimen

Finally, failure occurred in the joint zone because of the localization of the two main cracks on both diagonals commencing from the meeting points of beam boundaries and

inner column boundary. Table 4.3 shows the summary of testing results for PE_5 specimen.

For PE_6 specimen, two lateral steel hoops were installed in the joint zone and cast with ECC–PE mix with V_f =2% and A.R = 316 (R.I= 632). The first crack was observed in the beam at 14 kN load and deflection of 5.5 mm (0.5% drift ratio) about 70 mm away from the face of the column. As shown in Figure 4.41a, all the cracks observed in the beam appeared within a distance, about 640 mm measured from the face of the column with crack spacing ranging 15 and 60 mm and crack length between 35 and 160 mm.

The last crack in the beam was observed at a 89 kN load and deflection of 77 mm (7% drift ratio) and the onset of beam longitudinal bars yielding was observed at a 56 kN load and deflection of 27.5 mm (2.5% drift ratio). Meanwhile, the first visible crack commenced in the joint zone at 18.5 kN load and deflection of 11 mm (1% drift ratio) propagated on the joint diagonal. As shown in Figure 4.41b, many cracks developed in the joint zone and subdivided into smaller branches forming highly dense network of tiny cracks on the diagonals and in the majority of the joint zone with infinitesimal crack spacing and width. The estimated spacing of cracks was 1 mm to 5 mm with almost invisible width of cracks.

The specimen resisted an average ultimate load of 92.7 kN at deflection of 66 mm (drift ratio 6%) with a moment at the joint of 114 kN.m and shear force capacity of 544 kN. The drop in the load initiated after 6% drift ratio and the load value decreased about an average of 13.85% of the ultimate load capacity at deflection of 88 mm (8% drift ratio). In other words, the drop rate was 6.93% for each 11 mm increase in deflection (1% drift ratio). The beam–column joint failed due to the high shear forces generated in the joint

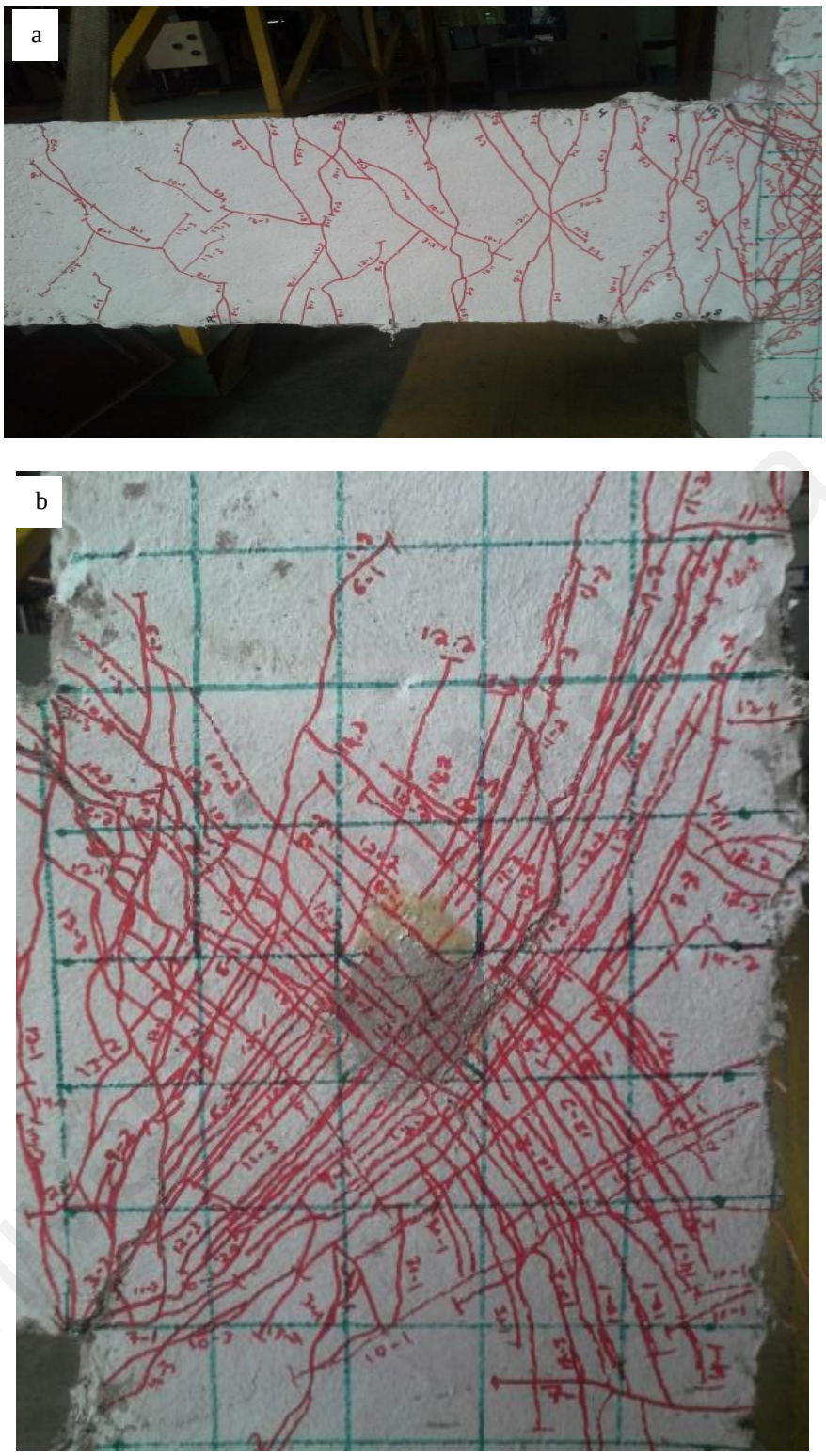

Figure 4.41 Crack propagation in (a) beam (b) joint region of PE_6 beam–column specimen

zone associated with a ductile mode of failure caused by the ECC characteristics of high ductility and high shear strength combined with the effect of steel hoops inclusion.

Finally, the failure occurred in the joint region due to a main flexural crack initiated from the upper face of the beam about 35 mm away from the face of the column and propagated diagonally inside the joint zone. At failure stage, the crack localized within the joint zone indicating mix mode of flexural-shear failure. Table 4.3 shows the summary of testing results for PE_6 specimen.

4.4.2 Load–deflection relationship

The load-deflection relationship was plotted for all beam-column specimens. Figures 4.42 to 4.55 appeared as hysteresis loops in different shapes. Some of them appeared in pinched shape and the others appeared in widened shape will be discussed in this section.

a) Effect of lateral steel hoops in normal concrete (NC) joints

The pinching effect for the NC_1 specimen was clear owing to the smaller area of loops (as shown in Figure 4.42) because of the brittle mode of failure. In contrast, for the NC_2 specimen (designed according to ACI-ASCE Commettee352R-02) (352R-02, 2002), the hysteresis loops area was wider and more regular than the loops corresponding to NC_1 specimen with a moderate pinching effect due to the mode of failure which is characterized with moderate ductility, (as shown in Figure 4.43).

b) Effect of the ECC inclusion in the joint zone

As shown in Figures 4.43 and 4.44, the hysteresis loops area for the PVA_1 specimen, of low reinforcing index, is slightly wider than the corresponding loops for NC_2 with moderate ductility owing to the better behavior of hysteresis loops despite the reduced load capacity of the joint. In addition, by comparing the other ECC-PVA specimens of higher reinforcing indices (PVA_2 or PVA_3) with NC_2, the loops behavior is much better than the corresponding loops behavior for NC_2 with reduced pinching effect and better

Table 4.3: Summary for testing progress results of beam–column specimens

Specimen	First crack features in the beam zone			Distance of cracks appearance in the beam measured from the face of column. mm	Crack spacing in:		First crack appearance in the joint zone		Onset of yielding in the beam longitudinal bars		Ultimate load capacity kN	Ultimate moment at the joint kN.m	Ultimate shear capacity at the joint kN	Drift ratio corresponds to ultimate load capacity%	Drift ratio corresponds to failure stage%	Rate of drop in load capacity%
	Load kN	Drift ratio %	Location measured from the face of column mm		Beam mm	Joint zone mm	Load kN	Drift ratio %	Load kN	Drift ratio %						
NC_1	14	0.5	65	450	100	35-50	33	1.5	40	2	49	60	289	3	4.5	35
NC_2	13	0.5	83	610	85	10-35	36	2	52	3.5	59	72.3	346	4	5	20
PVA_1	12	0.5	25	640	18-90	3-70	27	1.5	47	3	57	70	372	4.5	6	10.5
PVA_2	10	0.5	60	625	43-58	3-9	38	2	48	3	61	74.7	398	3.5	6	12
PVA_3	7	0.25	100	650	35-75	3-12	41	2	58	3	72.5	88.8	478	4.5	7	4.8
PVA_4	11	0.5	55	660	18-60	3-80	30	1.5	58	3	65.5	80.2	433	4.5	7	6.6
PVA_5	12.4	0.5	50	730	20-105	5-30	52	2.5	52	2.5	73.5	90.1	482	4.5	7	8.8
PVA_6	11.2	0.5	65	660	15-70	3-35	32	1.5	56	2.5	77.7	95.2	506	4.5	7	8.2
PE_1	8.8	0.5	80	660	9-54	2-5	39	2.5	50	3	61	74.7	396	6	8	7.1
PE_2	8.7	0.5	38	670	7-60	2-5	30	1.5	61	3.5	67.4	82.5	442	6	8	7.9
PE_3	9.2	0.5	54	510	23-75	2-5	35	2	54	3	77.7	95.2	522	6	8	3.6
PE_4	9.5	0.5	45	600	14-65	1-5	55	2.5	68	3	80	98	537	4.5	8	4.3
PE_5	11.6	0.5	65	600	15-70	1-5	35	1.5	57	2.5	87.3	106.9	574	6	8	6.6
PE_6	14	0.5	70	640	15-60	1-5	19	18	56	2.5	92.7	113.6	613	6	8	6.9

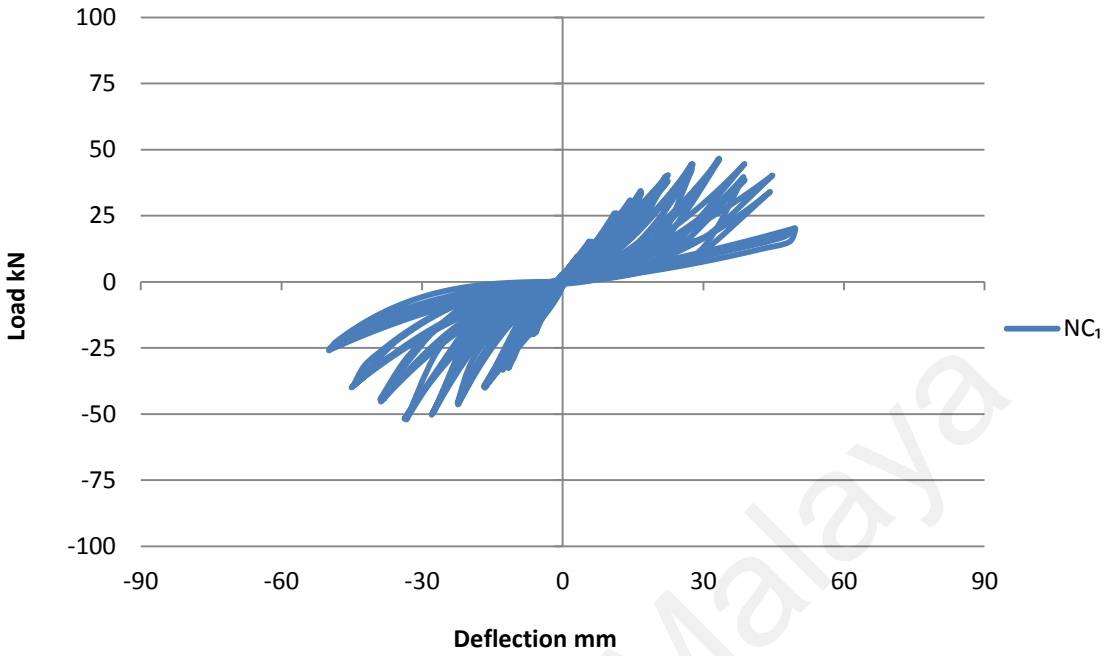

Figure 4.42: Cyclic load versus deflection relationship for beam–column joint NC_1

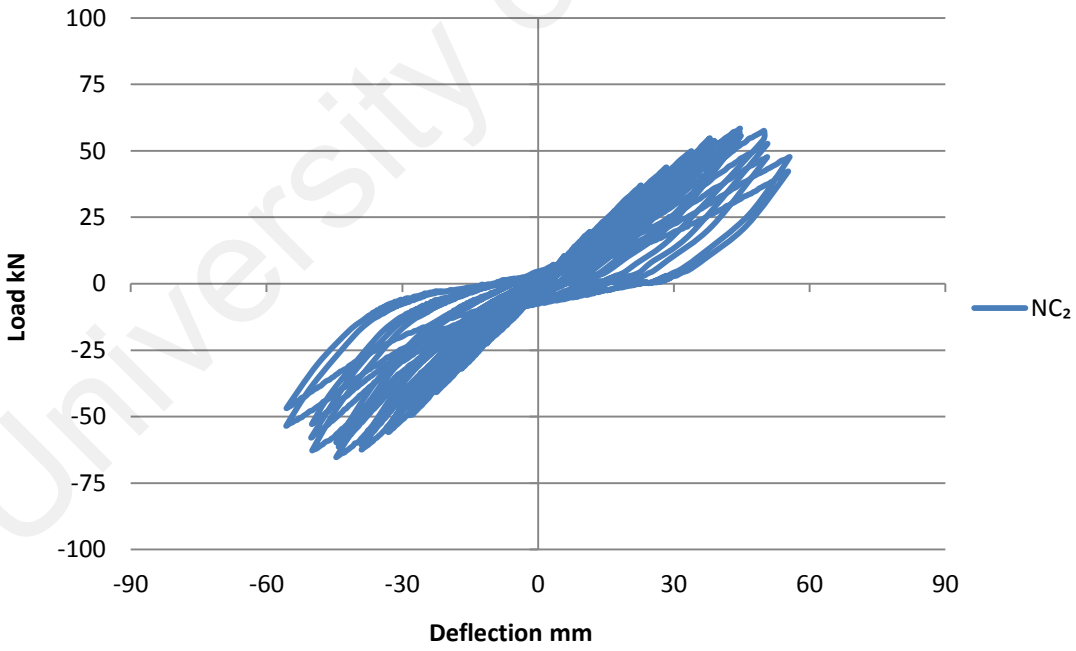

Figure 4.43: Cyclic load versus deflection relationship for beam–column joint NC_2

ductility. However, for PE_1 specimen, the hysteresis loops behavior is much better than the corresponding loops behavior for NC_2 with wider and more regular loops (as shown

in Figure 4.50) owing to the perfect ductility and damage tolerance of the ECC-PE with the ductile mode of failure.

c) Effect of type of ECC in the joint zone

As shown in Figures 4.45 and 4.51, the hysteresis loops behavior for PE_2 is much better than the corresponding loops behavior for PVA_2 with wider and more full and regular loops despite the same reinforcing index value indicating better ductility, better damage tolerance and reduced pinching effect. The perfect behavior of PE specimen is attributed to the desired mode of bond-slip failure of PE fibers (i.e. pulling out the fibers from the original positions). In contrast, the failure in the PVA specimens is due to the fiber rupture which leads to less ductility. As shown in Figures 4.46 and 4.52, an improved cyclic performance was observed for the PVA_3 and it is rather similar to the cyclic performance of PE_3 specimen in the ultimate load capacity, ductility, and damage tolerance.

d) Effect of polymer fibers reinforcing index

Generally, as for the ECC specimens, the hysteresis loops behavior was improved as the reinforcing index increased. For the ECC-PVA group of specimen, the hysteresis loops behavior for PVA_2 specimen (of R.I= 632) is slightly better than the corresponding loops behavior for PVA_1 specimen (of R.I= 525), as shown in Figures 4.44 and 4.45, with better spread in the loops area associated with better ductility and damage tolerance. Moreover, for PVA_3 and PVA_4 specimens (of R.I= 790 and 948 respectively), the hysteresis loops behavior is almost the same for both specimens, as shown in Figures 4.46 and 4.47, with reduced pinching effect and improved hysteresis loops behavior compared to the cyclic performance of PVA_1 and PVA_2 specimens.

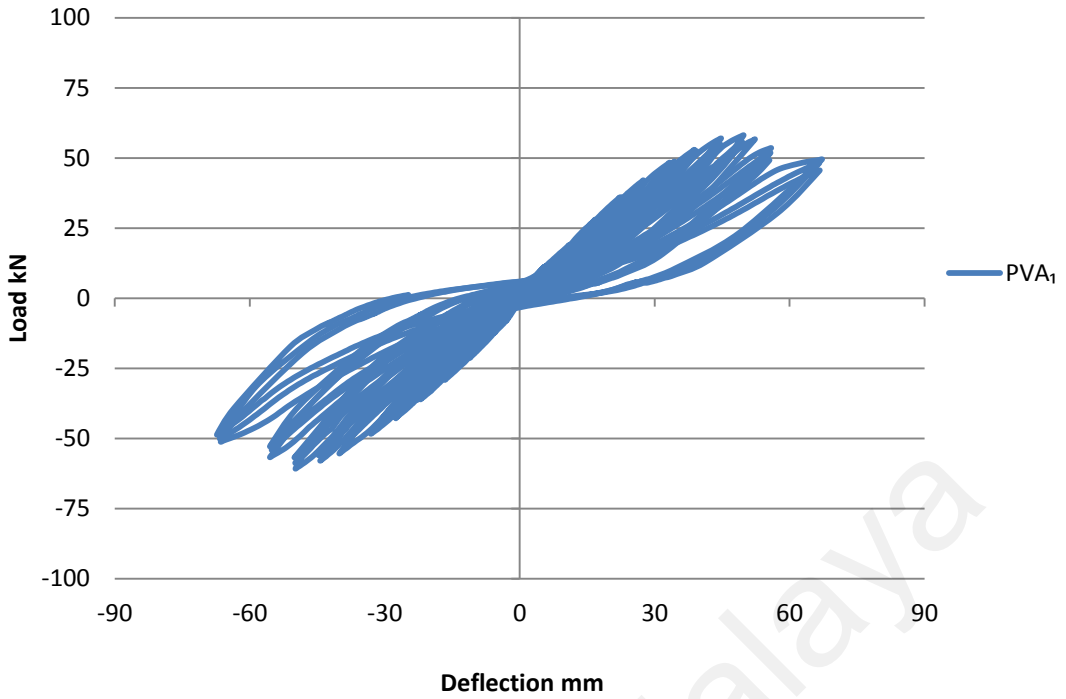

Figure 4.44: Cyclic load versus deflection relationship for beam–column joint PVA_1

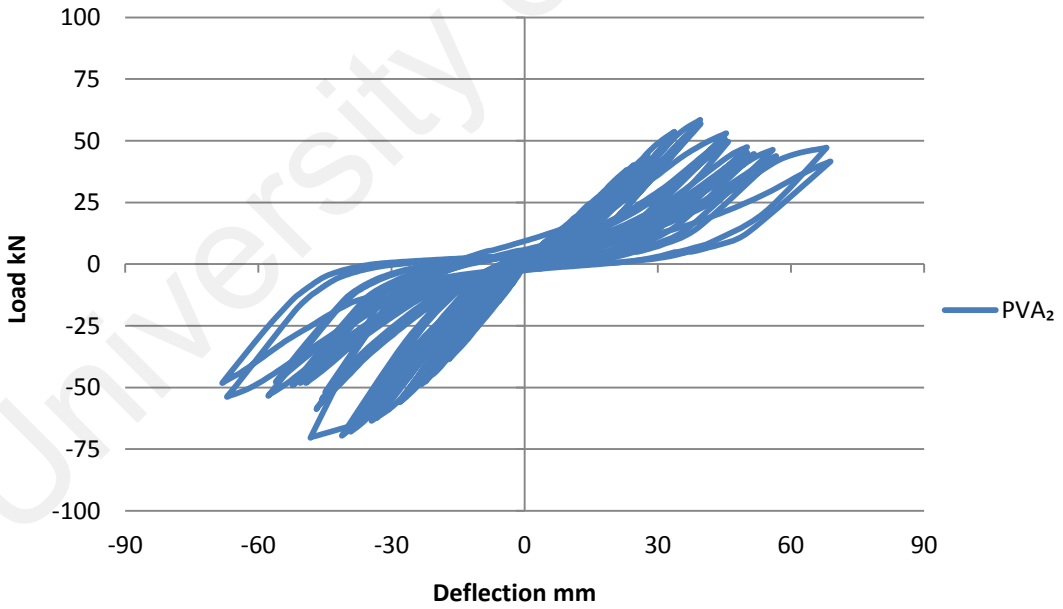

Figure 4.45: Cyclic load versus deflection relationship for beam–column joint PVA_2

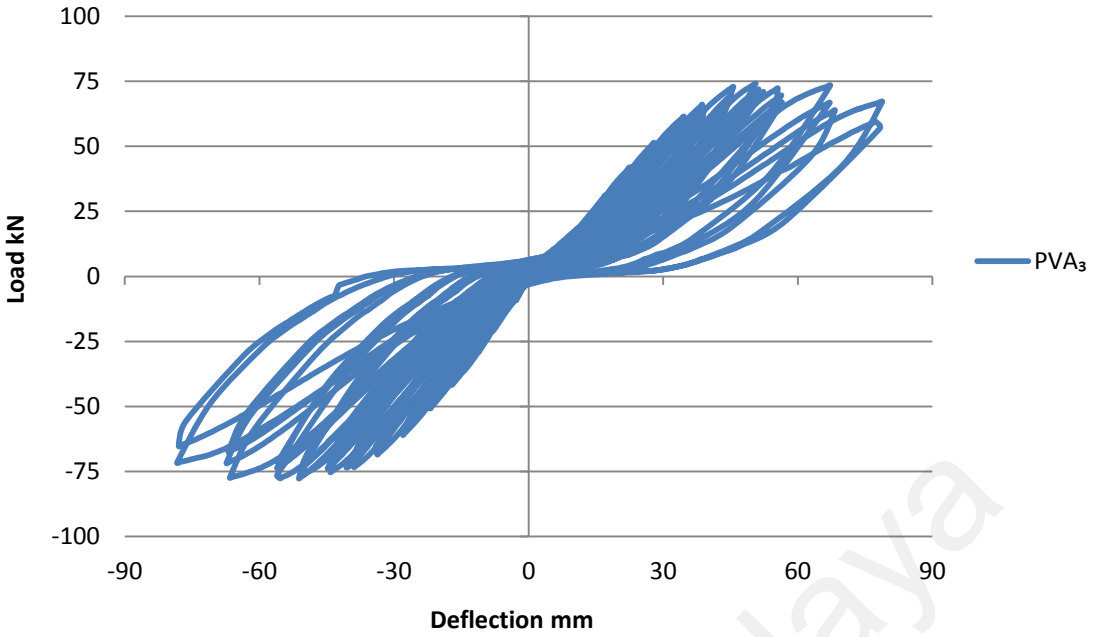

Figure 4.46: Cyclic load versus deflection relationship for beam–column joint PVA_3

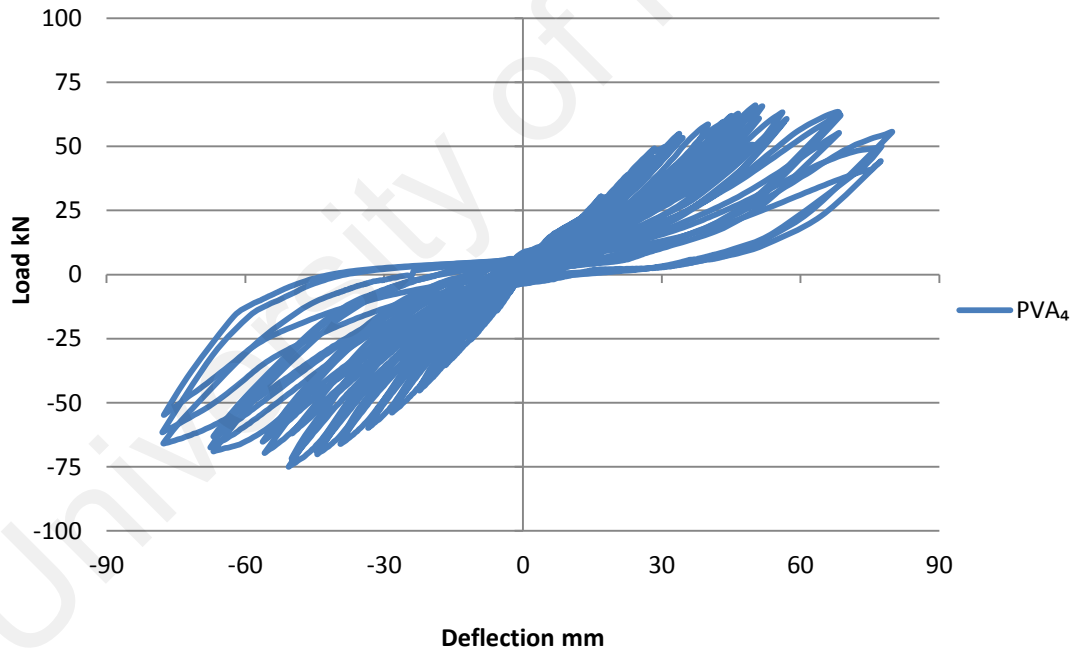

Figure 4.47: Cyclic load versus deflection relationship for beam–column joint PVA_4

For the ECC-PE group of specimens, the hysteresis loops behavior of PE_2 (of R.I= 790 is clearly better than the corresponding loops behavior for PE_1 (of R.I= 632), as shown in Figures 4.50 and 4.51. It shows better spread with wider loops area compared to PE_1 specimen. In addition, for the PE_3 and PE_4 specimens, the hysteresis loops behavior is much better than the corresponding loops behavior for PE_2 specimen with full and wider loops area. As shown in Figures 4.52 and 4.53, the both PE_3 and PE_4 specimens showed almost the same hysteresis loops performance with a slight improvement for PE_4 compared to PE_3 specimen.

e) Effect of lateral steel hoops inclusion in ECC joints

Owing to the inclusion of steel lateral hoops in the joint zone, the PVA_5 and PVA_6 specimens (including 1 and 2 steel hoops in the joint zone, respectively.) showed clear improvement in the hysteresis loops behavior compared to the corresponding loops behavior for PVA_2 (with no inclusion of steel hoops), as shown in Figures 4.45, 4.48 and 4.49, with an improvement in ductility, damage tolerance and ultimate load capacity. In addition, the hysteresis loops performance of both PVA_5 and PVA_6 specimens is almost the same with a slight increase in load capacity for PVA_6 compared to the PVA_5 specimen.

For the ECC-PE group of specimens, due to the steel hoops inclusion in the joint zone, the PE_5 and PE_6 specimens showed a significant performance in the hysteresis loops behavior with full, stable and wider loops area and better ductility compared to the corresponding loops behavior for PE_2 specimen, as shown in Figures 4.51, 4.54 and 4.55. Moreover, for both PE_5 and PE_6 specimens, same behavior was almost observed with small increase in the load capacity for PE_6 specimen over the corresponding value for PE_5 specimen.

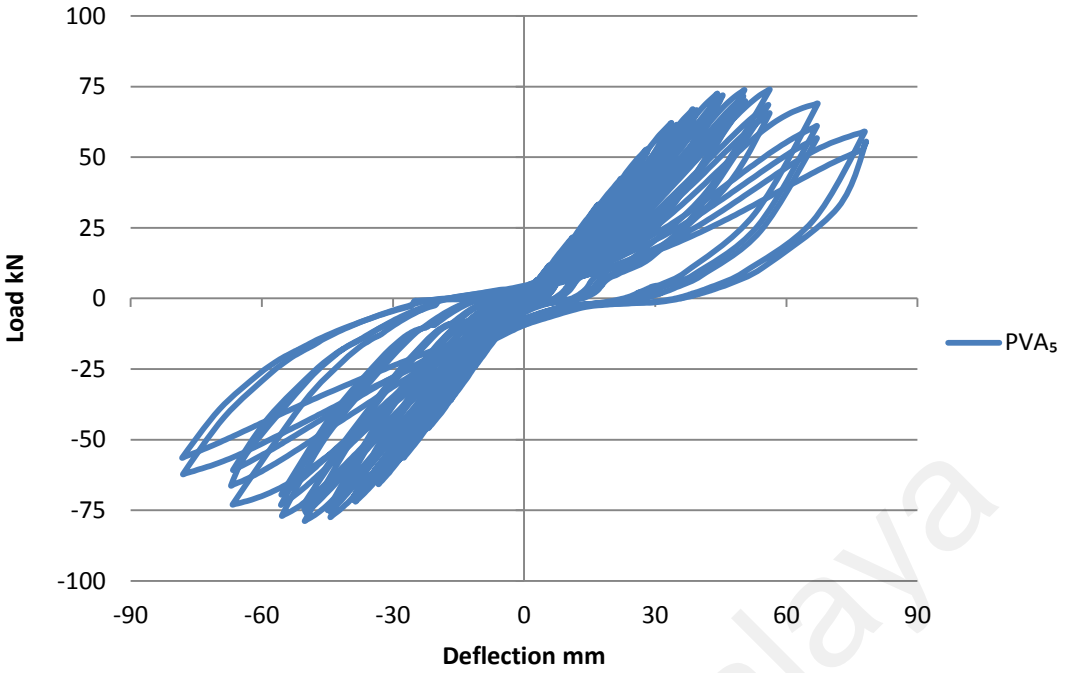

Figure 4.48: Cyclic load versus deflection relationship for beam–column joint PVA_5

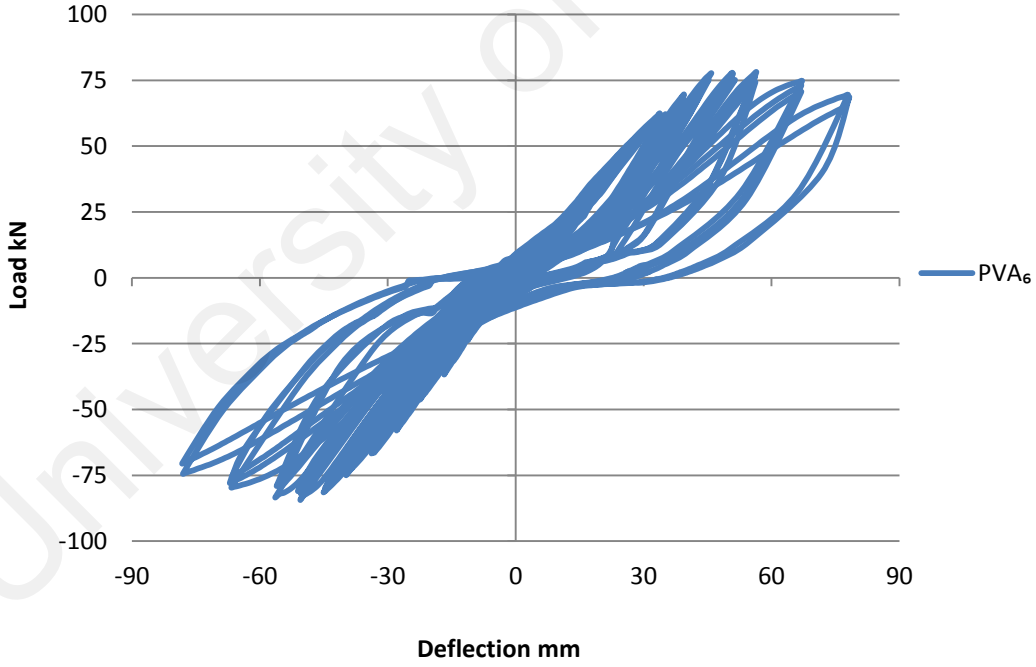

Figure 4.49: Cyclic load versus deflection relationship for beam–column joint PVA_6

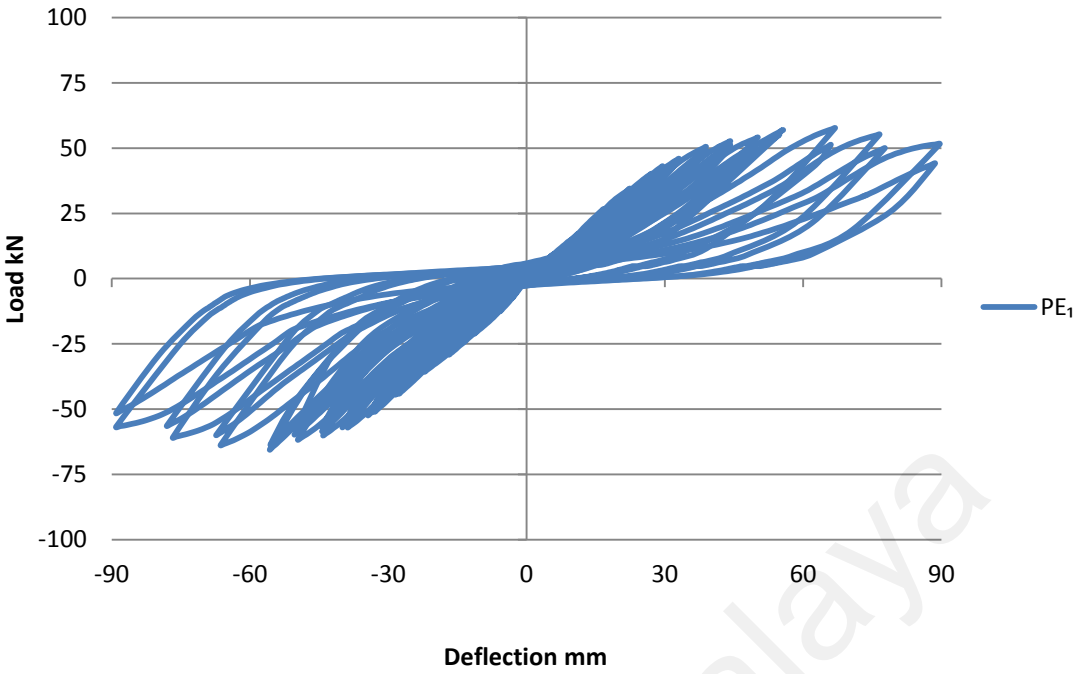

Figure 4.50: Cyclic load versus deflection relationship for beam–column joint PE_1

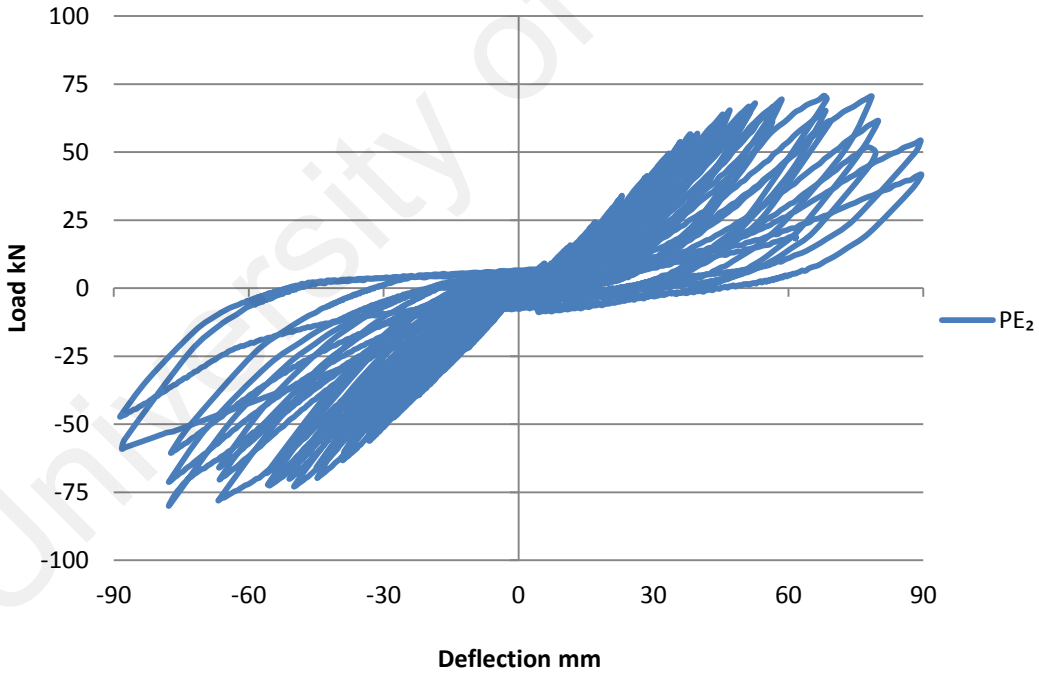

Figure 4.51: Cyclic load versus deflection relationship for beam–column joint PE_2

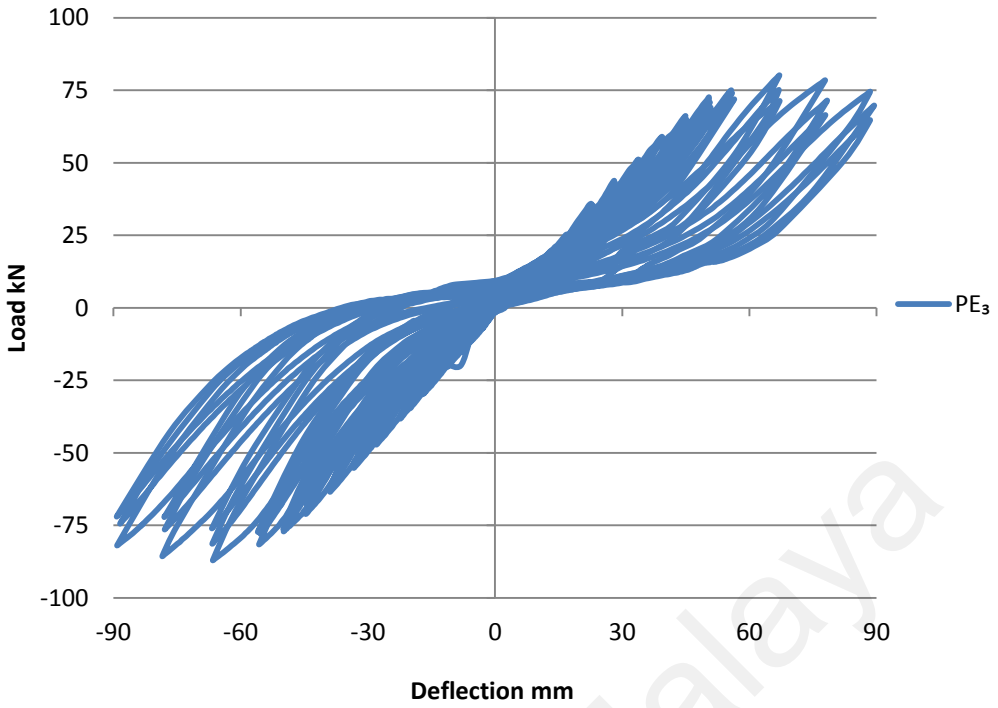

Figure 4.52: Cyclic load versus deflection relationship for beam–column joint PE_3

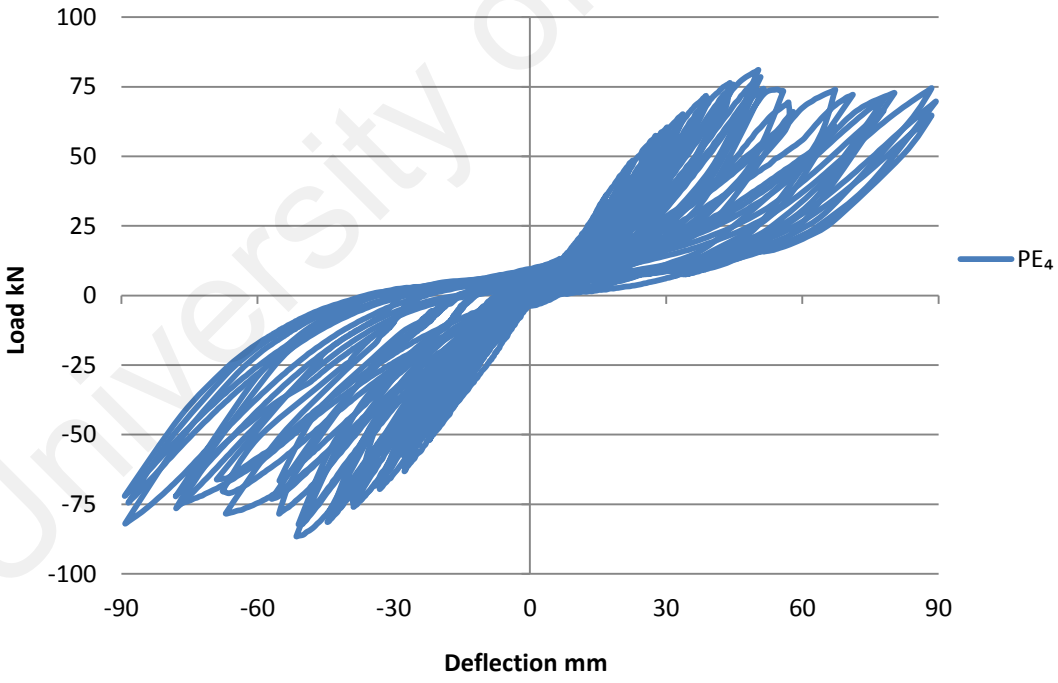

Figure 4.53: Cyclic load versus deflection relationship for beam–column joint PE_4

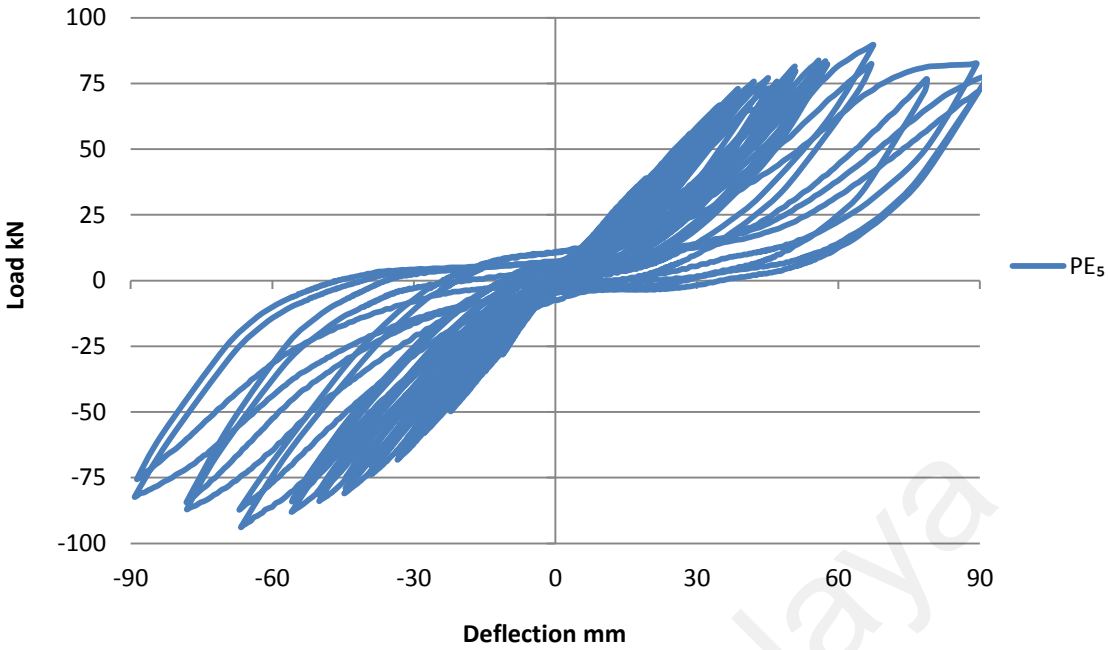

Figure 4.54: Cyclic load versus deflection relationship for beam–column joint PE_5

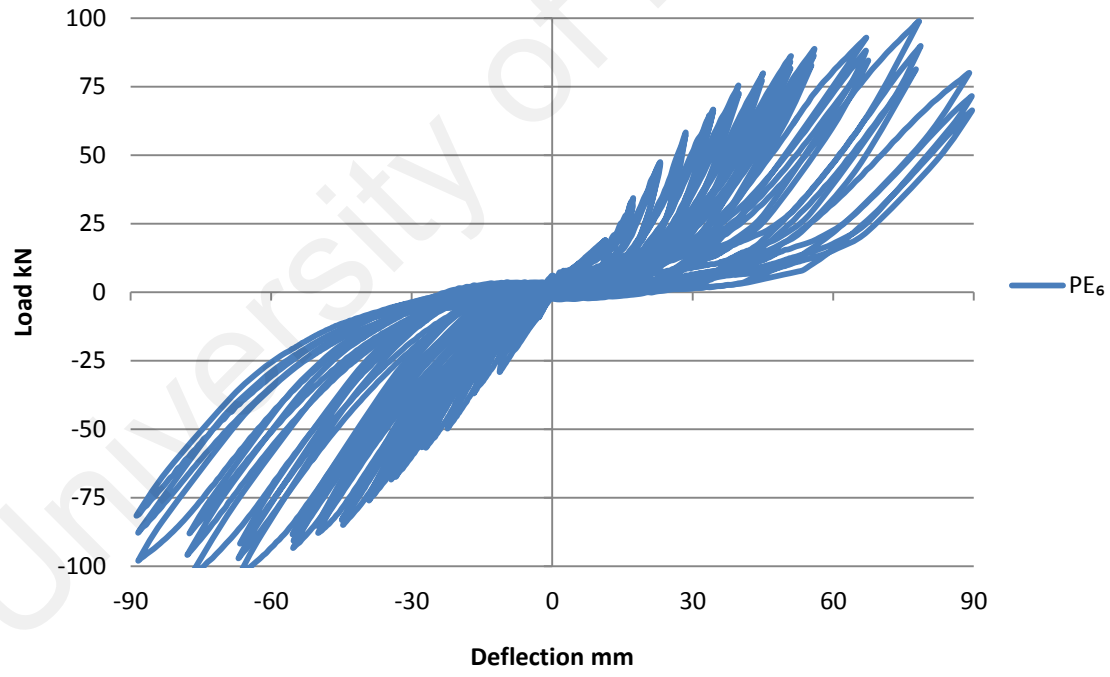

Figure 4.55: Cyclic load versus deflection relationship for beam–column joint PE_6

4.4.3 Load–deflection envelope

Figures 4.56 to 4.67 show the load-deflection envelope relationship and the variation in ultimate load capacity of beam-column joints. Some of the curves tend to descend sharply and the others descend in a steady gradual manner creating large area under the curve that will be discussed below.

a) Effect of lateral steel hoops in NC joints

Figures 4.56 and 4.57 show an increase in the ultimate load capacity for the NC_2 specimen of about 20.4%, over the corresponding load value for the NC_1 specimen due to the inclusion of lateral steel hoops in the joint zone. In addition, the NC_2 envelope curve formed an area under the curve wider than the corresponding area for NC_1 specimen due to better ductility. As indicated in Table 4.3, the descending part of the NC_2 envelope curve gradually decreased and failed at a deflection value higher than the corresponding deflection value for the NC_1 specimen. The failure in NC_1 occurred at 4.5% of drift ratio with a drop rate in ultimate load capacity equals to 35% while for NC_2 specimen the failure occurred at 5% of drift ratio with a drop rate of ultimate load capacity equals to 20% which indicates better performance of NC_2, as shown in Figure 4.58.

b) Effect of the ECC inclusion in the joint zone

Referring to Figures 4.56 and 4.57, the load deflection envelope curve for the PVA_1 specimen (of lowest R.I) shows almost a similar ultimate load capacity compared to the NC_2 specimen. In addition, the area encompassed by the envelope curve for PVA_1 specimen is wider than the corresponding area for the NC_2 specimen due to better ductility.

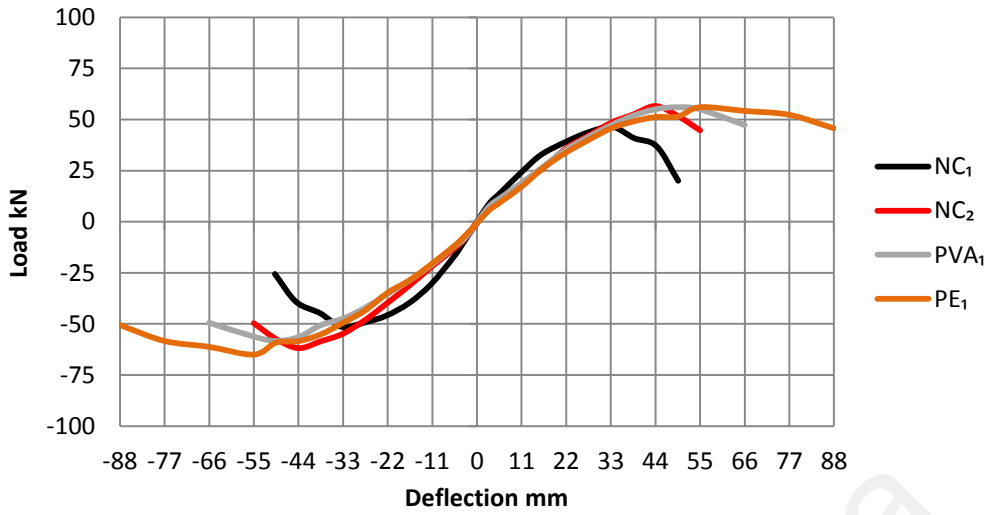

Figure 4.56: Effect of ECC inclusion in the joint zone on the load-deflection envelope curve

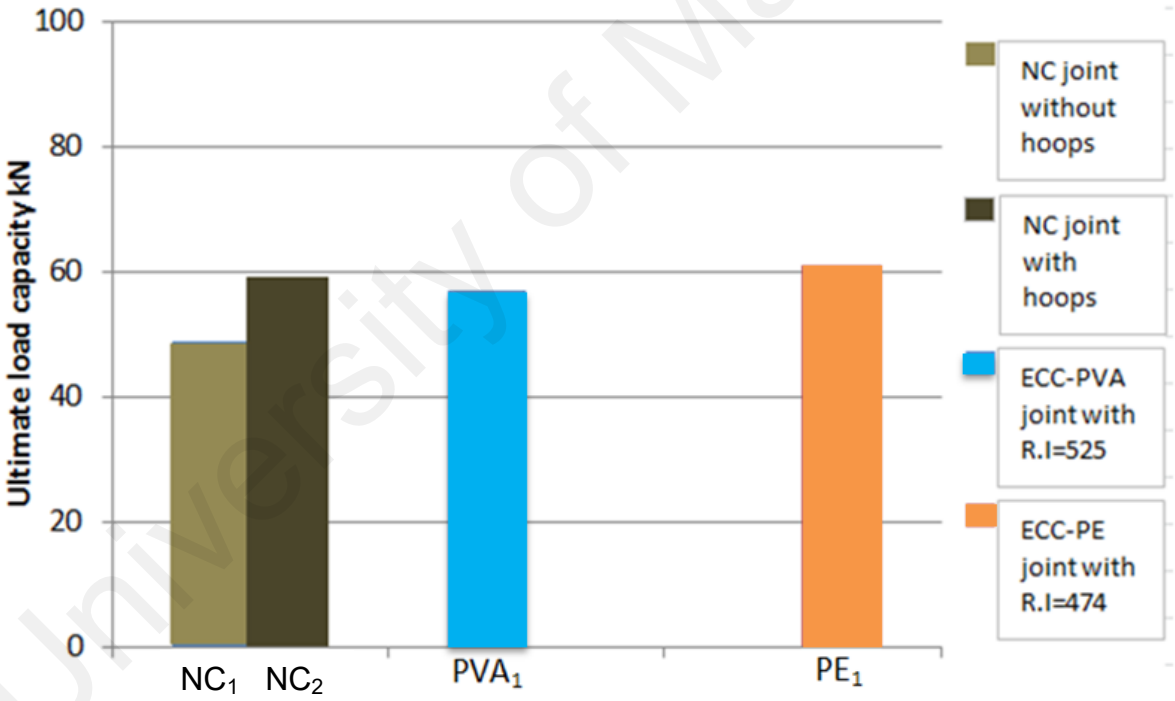

Figure 4.57: Effect of ECC inclusion in the joint zone on the ultimate load capacity

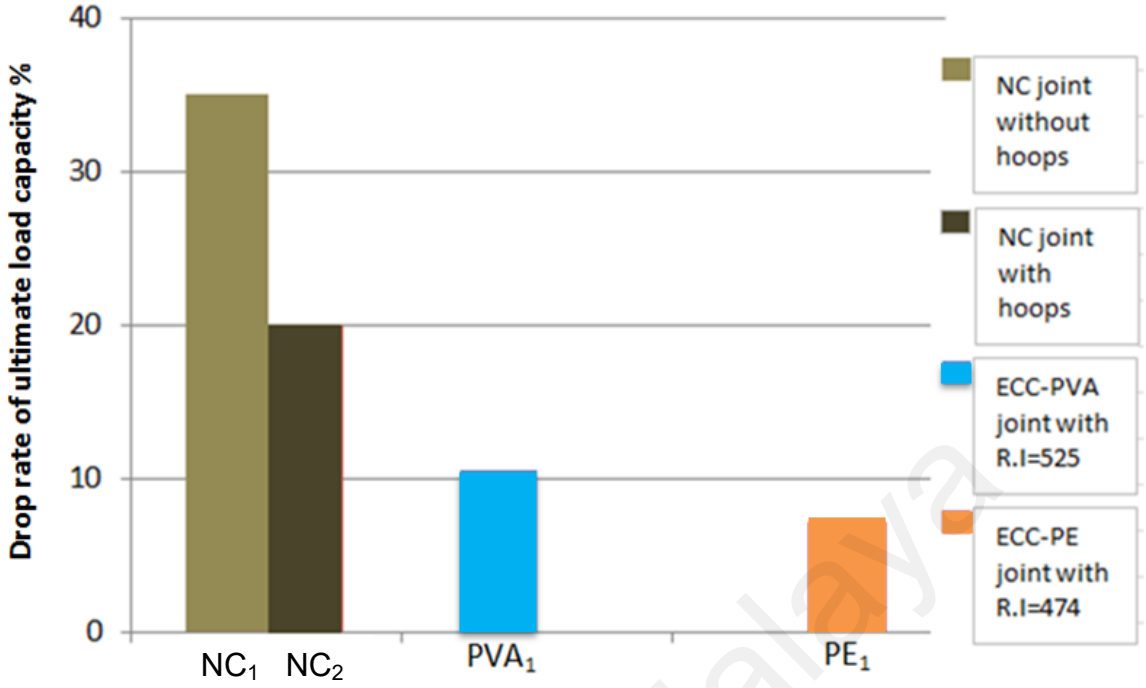

Figure 4.58: Effect of ECC inclusion in the joint zone on the drop rate of ultimate load capacity

Furthermore, the area encompassed by the envelope curve for PE_1 specimen is greatly wider than the corresponding area encompassed by the envelope curve for NC_2 specimen despite almost the similar ultimate load capacity due to the perfect ductility of the PE_1 joint. The descending part of the PVA_1 and PE_1 envelope curve gradually decreased and failed at a deflection value higher than the corresponding deflection value for the NC_2 specimen. As indicated in Table 4.3, the failure for NC_2 specimen occurred at 5% of drift ratio with drop rate in ultimate load capacity equals to 20% while for PVA_1 and PE_1 the failure occurred at 6 and 8% of drift ratio with a drop rate in ultimate load capacity equals to 10.5 and 7.1%, respectively (Figure 4.58), which refers to the remarkable performance of ECC joints.

c) Effect of the type of ECC in the joint zone

As displayed in Figures 4.59 and Figure 4.60, the PE_2 specimen (of R.I= 632) significantly shows an area encompassed by the envelope curve wider than the corresponding area encompassed by the envelope curve for PVA_2 specimen (of equivalent R.I mentioned above) with small increase in ultimate load capacity of 9.8%.

The descending part of the PE_2 envelope curve gradually decreased and failed at a deflection value higher than the corresponding deflection value for PVA_2 specimen. In addition, the area encompassed by the envelope curve for PE_3 specimen (of R.I= 790) is greatly wider than the corresponding area encompassed by the envelope curve for PVA_3 specimen (of equivalent R.I of 790) despite the small increase in ultimate load capacity of 6.5% for PE_3 specimen. The descending part of the PE_3 envelope curve gradually decreased and failed at a deflection higher than the corresponding deflection value for the PVA_3 specimen.

As indicated in Table 4.3, the failure for PE_2 and PE_3 specimens occurred in 8% of drift ratio with a drop rate of ultimate load capacity equals to 7.9% and 3.6%, respectively, while for PVA_2 and PVA_3 specimens, the failure occurred at 6% and 7% of the drift ratio with a drop rate of ultimate load capacity equals to 12% and 4.8%, respectively, indicating remarkable performance of PE joints, as shown in Figure 4.61.

d) Effect of polymer fibers reinforcing index

For both groups of PVA and PE specimens, by increasing the reinforcing index of PVA or PE fibers, the encompassed area by the load-deflection envelope curve of ECC specimen will increase, with the improvement in ultimate load capacity of specimen, as shown in Figures 4.62 and 4.63. For the PVA group of specimens, the area encompassed by the load-deflection envelope curve increased by increasing the reinforcing index value indicating slight increase for PVA_2 specimen and valuable increase for PVA_3

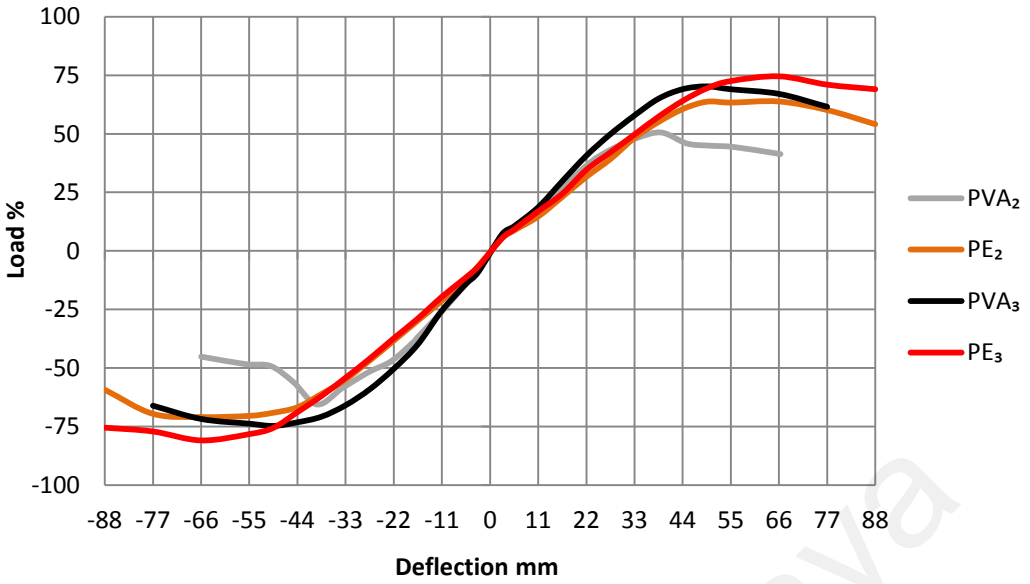

Figure 4.59: load-deflection envelope relationship for PVA_2, PE_2, PVA_3 and PE_3 specimens

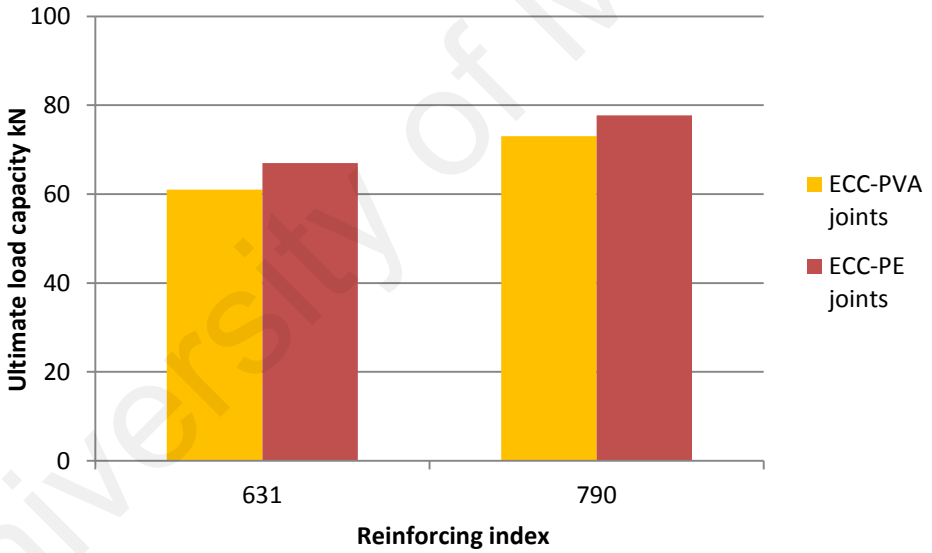

Figure 4.60: Effect of type of ECC inclusion in the joint zone on the ultimate load capacity

specimen compared to the PVA_1(Figures 4.62 and 4.63a). The ultimate load capacity for PVA_2 and PVA_3 specimens also increased over the PVA_1 specimen about 7 and 28%. Regarding the specimen PVA_4 with the highest reinforcing index, the area encompassed

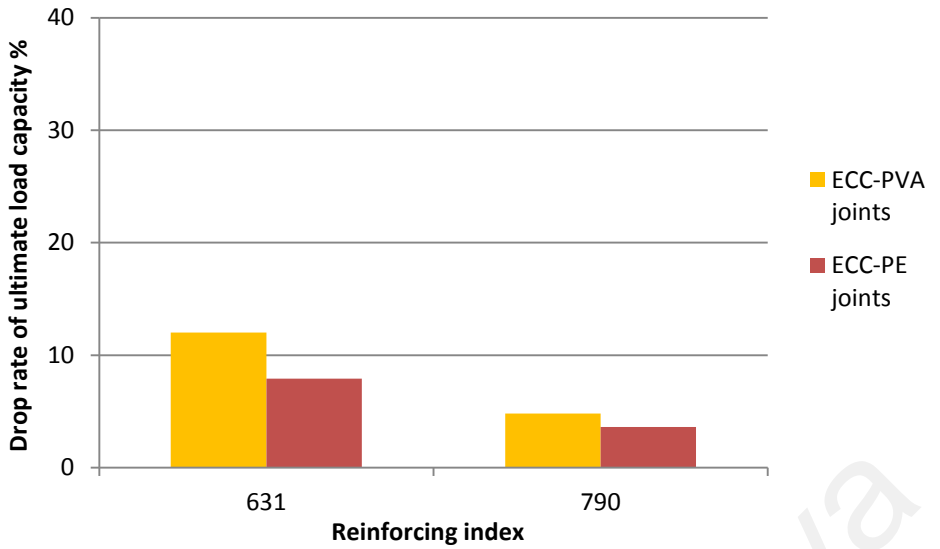

Figure 4.61: Effect of type of ECC inclusion in the joint zone on the rate of drop in ultimate load capacity

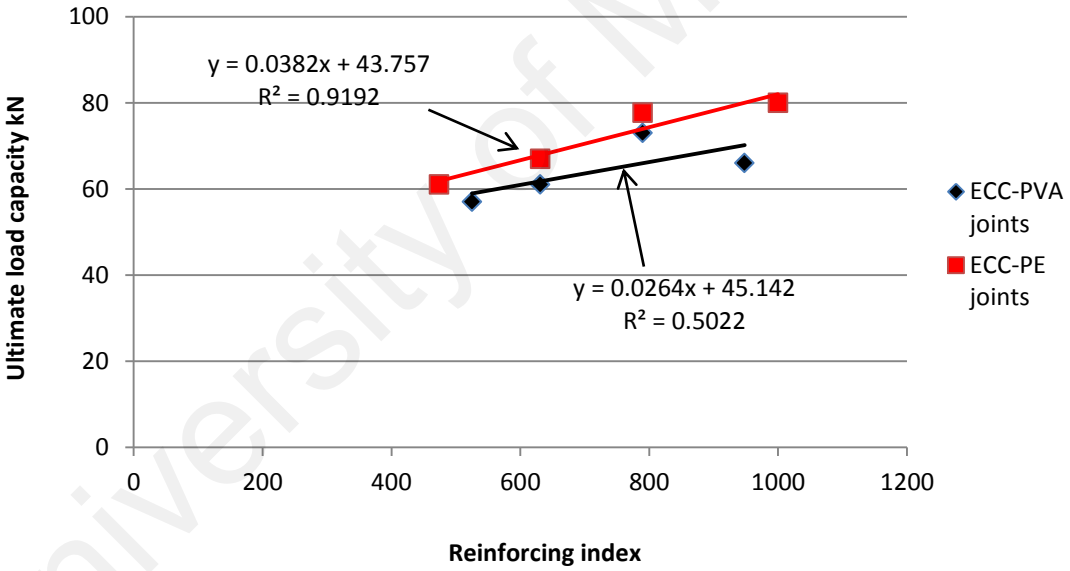

Figure 4.62: Effect of reinforcing index on ultimate load capacity of beam-column joint

by the load-deflection envelope curve is lesser than the corresponding area for PVA_3 specimen with lesser ultimate load capacity of 9.6% due to the higher fiber content in the ECC mix which led to a non-homogenous dispersion of fibers in the fresh ECC.

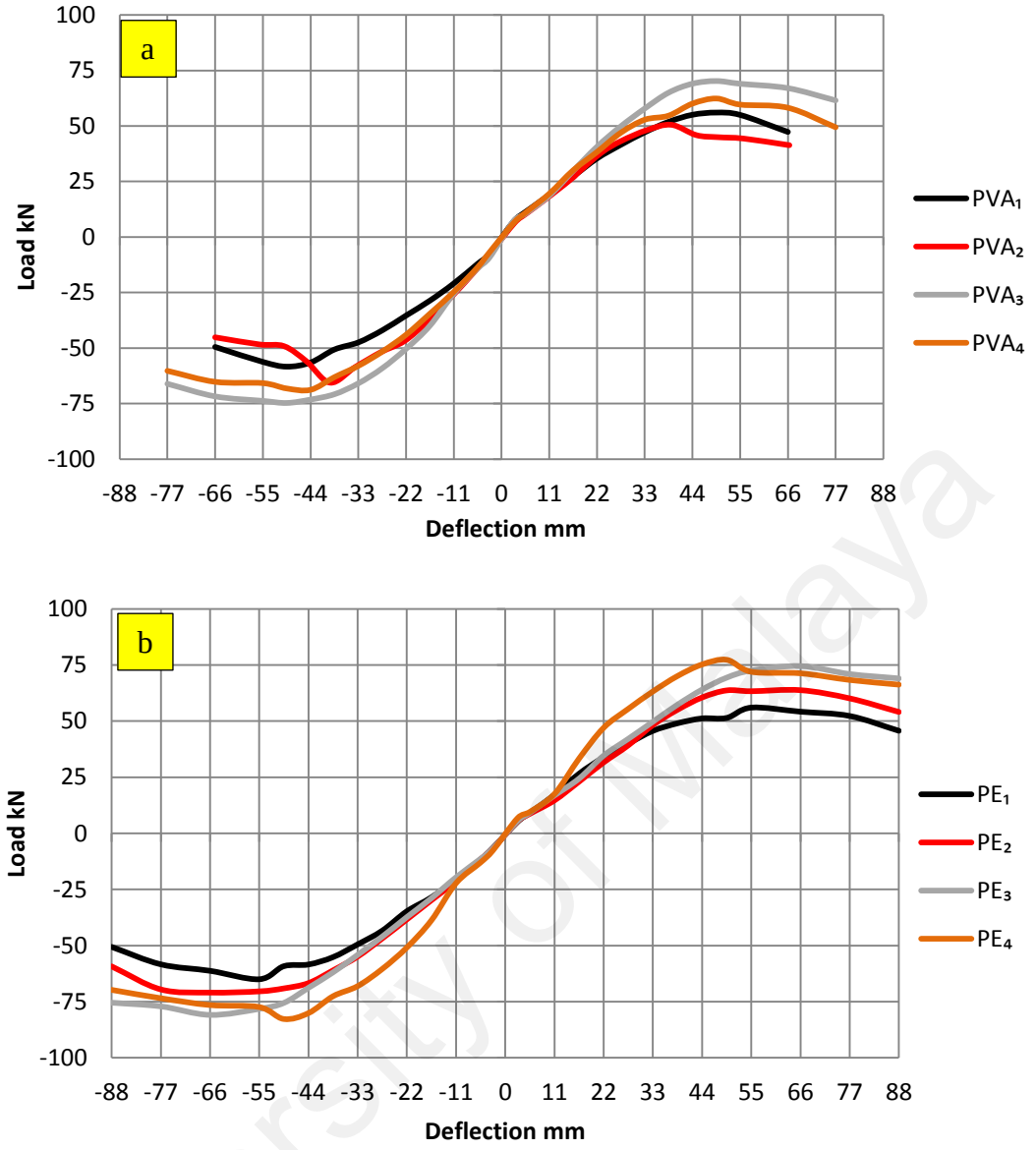

Figure 4.63: Effect of reinforcing index on load-deflection envelope curve for (a) ECC-PVA specimens, and (b) ECC-PE specimens

The descending part of both PVA_3 and PVA_4 envelope curves showed better behavior compared to PVA_1 and PVA_2 specimens, and failed at a deflection value higher than the corresponding deflection value for PVA_1 and PVA_2 specimens.

As indicated in Table 4.3, the failure in PVA_1 and PVA_2 specimens occurred at 6% of the drift ratio with a drop rate of ultimate load capacity equals to 10.5 and 12%, while in PVA_3 and PVA_4 specimens, the failure occurred at 7% of the drift ratio with a drop rate of ultimate load capacity equals to 4.8 and 6.6% respectively, as shown in Figure 4.64.

For the ECC-PE group of specimens, the area encompassed by the load-deflection envelope curve gradually increased by the increase in the reinforcing index. Moreover, a gradual increase in the ultimate load capacity for PE_2, PE_3 and PE_4 specimens over the PE_1 specimen was observed of about 9.8, 27.4 and 31%, respectively (Figures 4.62 and 4.63b).

The descending part of the both PE_3 and PE_4 specimens envelope curves showed better behavior compared to the PE_1 and PE_2 specimens. All the PE group of specimens failed at the same deflection. A linear fit analysis seems to be more suitable for ultimate load capacity results of PVA and PE joints despite the low correlation coefficient for PVA results ,as shown in Figure 4.62. As indicated in the Table 4.3, the failure in all the PE specimens mentioned above occurred at 8% of the drift ratio with a drop rate of ultimate load capacity equals to 7.1, 7.9, 3.6 and 4.3% for PE_1, PE_2, PE_3 and PE_4 specimens, respectively, as shown in Figure 4.64.

e) Effect of lateral steel hoops inclusion in ECC joints

Figures 4.65 and 4.66 show the effect of the lateral steel hoops inclusion in the ECC joint zone on the encompassed area by the load-deflection envelope curve. For the ECC-PVA group of specimens, a noticeable increase in the area encompassed by the envelope load-deflection curve was observed with the inclusion of one steel hoop in the joint zone (PVA_5) compared to the joint without hoops (PVA_2), with an increase in the ultimate load capacity of 17%, as shown in Figures 4.65a and 4.66. The inclusion of two hoops in the joint zone (PVA_6) also showed a significant increase in the area encompassed by the load-deflection envelope curve compared to the specimen without hoops. However, it shows a slight increase in the encompassed area by the load-deflection envelope curve with slight increase in ultimate load capacity of 5.7% compared to the inclusion of one hoop, as shown in Figure 4.66. The descending part of

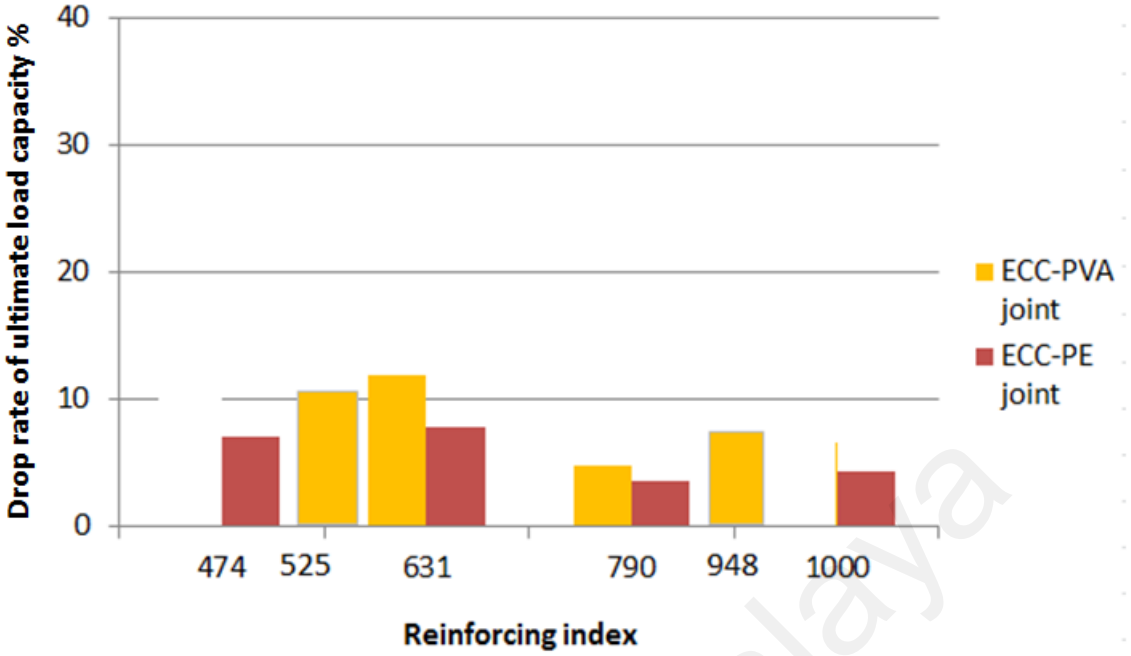

Figure 4.64: Effect of reinforcing index on the drop rate of in ultimate load capacity of beam-column specimens

both PVA_5 and PVA_6 envelope curves showed better envelope curves showed better behavior compared to PVA_2 specimen, and failed at a deflection value higher than the corresponding deflection value for PVA_2 specimens. As indicated in the Table 4.3, the failure in PVA_5 and PVA_6 specimens occurred in 7% of drift ratio with a drop rate of ultimate load capacity equals to 8.8 and 8.2% respectively, while in PVA_2 specimen, the failure occurred in 6% of the drift ratio with a drop rate of ultimate load capacity equals to 12% (Figure 4.67).

For the ECC-PE group of specimens, a noticeable increase in the ultimate load capacity of 30.3% was observed by the inclusion of one steel hoop in the joint zone (PE_5) compared to the joint without steel hoops (PE_2), as shown in Figures 4.65b and 4.66. However, the inclusion of two hoops in the PE joint zone slightly increased the ultimate load capacity of about 6.2% compared to the one hoop inclusion (Figure 4.66). The

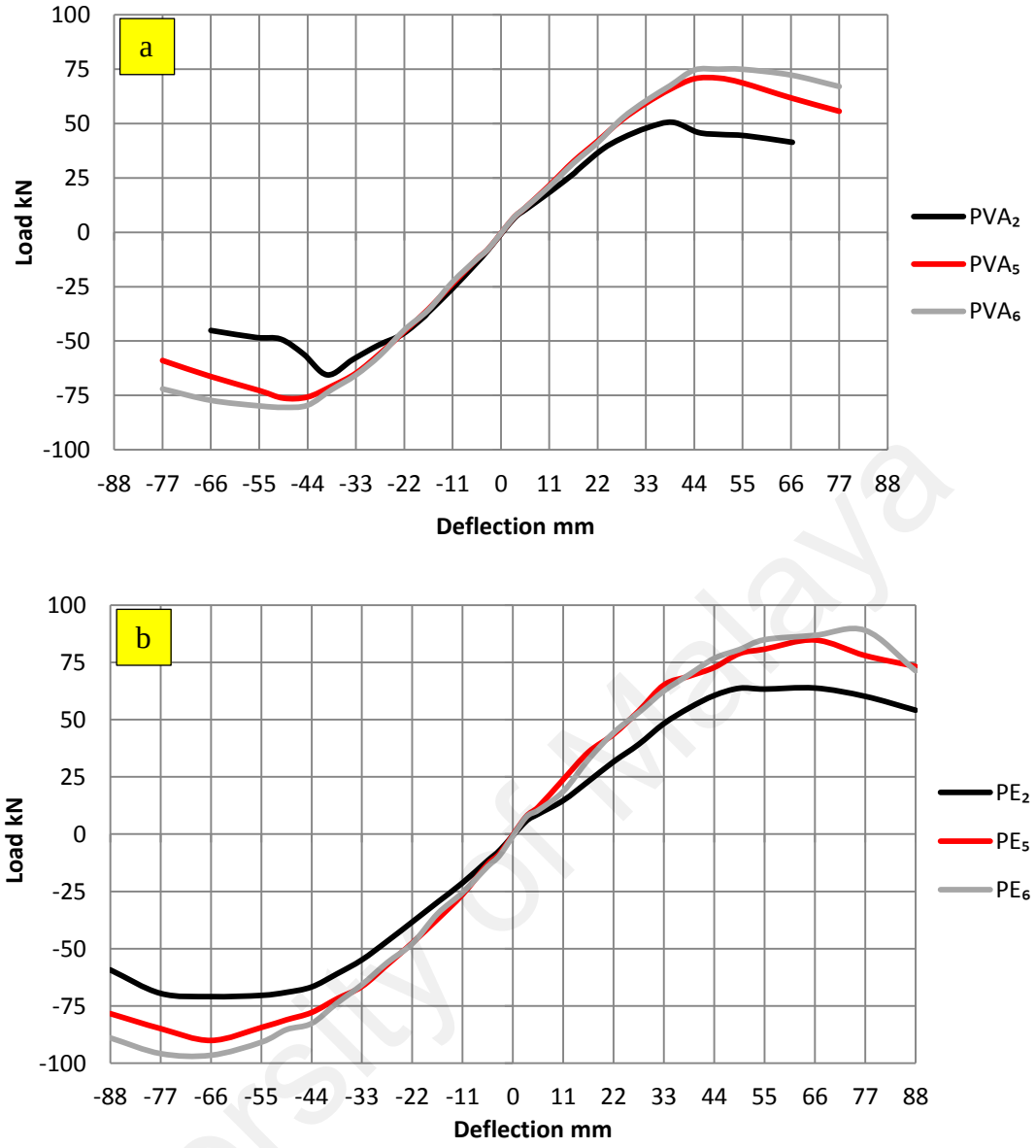

Figure 4.65: Effect of lateral steel hoops inclusion on the load-deflection envelope curve for (a) ECC-PVA specimens, and (b) ECC-PE specimens

descending part of both PE_5 and PE_6 envelope curves showed better behavior compared to PE_2 specimen. All the PE specimens mentioned above failed at the same deflection value. As indicated in the Table 4.3, the failure in all PE specimens mentioned above occurred in 8% of drift ratio with a drop rate of ultimate load capacity equals to 7.9, 6.6 and 6.9% for PE_2, PE_5 and PE_6, respectively (Figure 4.67).

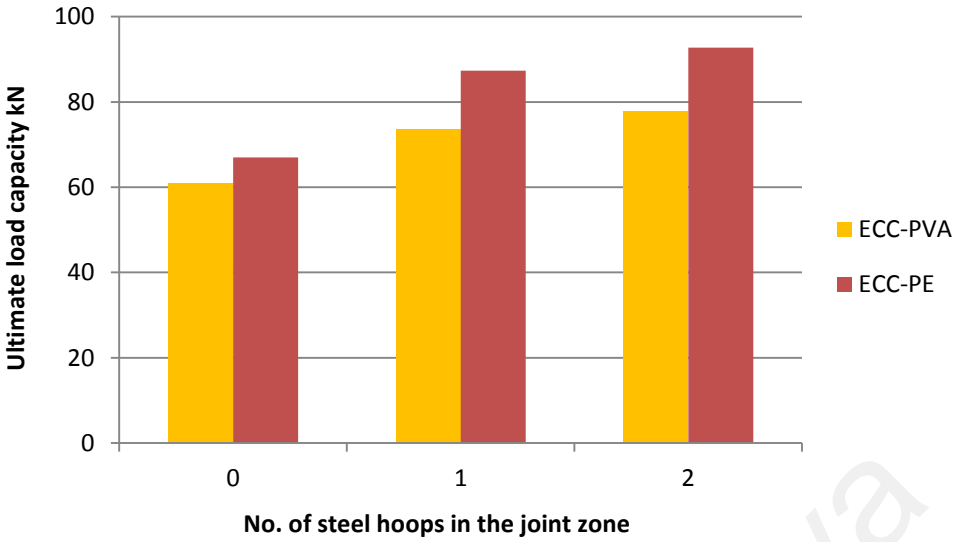

Figure 4.66: Effect of lateral steel hoops inclusion on the ultimate load capacity for ECC-PVA specimens, and ECC-PE specimens

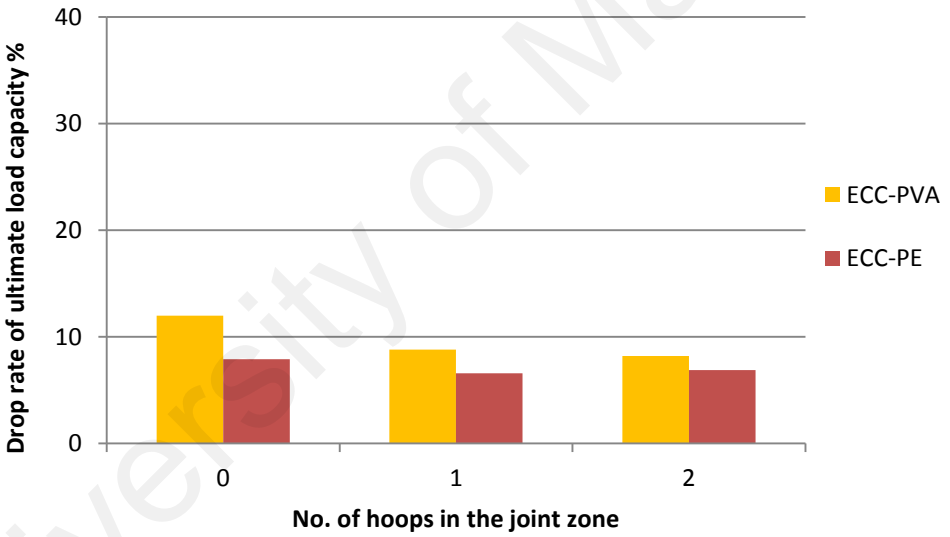

Figure 4.67: Effect of lateral steel hoops inclusion on the drop rate of ultimate load capacity for ECC-PVA specimens, and ECC-PE specimens

4.4.4 Ultimate shear capacity

The ultimate shear capacity of beam-column joint depends on the tensile force in the steel bars (which depends on the bond between concrete and steel bars), tension block resistance of ECC in the tension zone of the beam section and the shear resistance provided due to the confinement of concrete by the lateral steel hoops, the shear resistance provided by the ECC inclusion in the beam-column joint zone and the grade

of concrete. The ultimate shear capacity is evaluated from Figure 4.20 and stated in section 3.4.9. Table 4.3 shows the experimental results of the ultimate shear capacity for the exterior beam-column joints.

a) Effect of the lateral steel hoops in normal concrete (NC) joints

As indicated in Figure 4.68, the inclusion of steel hoops in the NC_2 joint zone significantly increased the ultimate shear capacity by about 20.6% compared to the shear capacity of the NC_1 joint.

b) Effect of the ECC inclusion in the joint zone

Figure 4.68 shows that the replacement of the NC_1 joint (without lateral steel hoops in the joint zone) with the ECC-PVA mix of the lowest value of R.I (PVA_1) improved the ultimate shear capacity of about 16.7%, and reduced of about 3% compared to the designed NC joint (NC_2). In addition, the PVA_2 specimen (with R.I equals to 631) improved the ultimate shear capacity of the joint by about 3.5% compared to the NC_2 joint. Moreover, using the ECC-PE mix of R.I equals to 474 (PE_1) instead of NC_2 joint increased the ultimate shear capacity by about 3.5%. It is concluded that the inclusion of ECC PE in the joint zone is more effective than the inclusion of ECC-PVA in the joint zone, with the lowest reinforcing index.

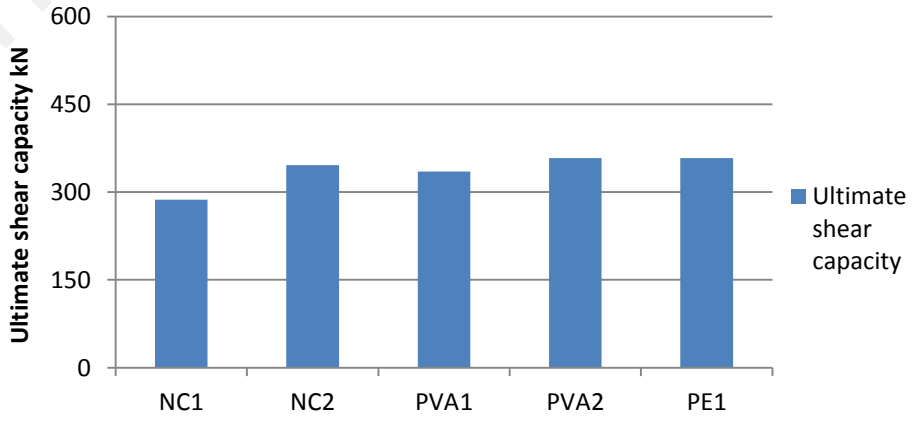

Figure 4.68: Effect of the ECC inclusion in the joint zone on ultimate shear capacity

c) Effect of type of ECC in the joint zone

Figure 4.69 has shown that the replacement of ECC-PVA mix (PVA_2 joint) with ECC-PE mix (PE_2 joint) in the joint zone, with the same R.I of 631, increased the ultimate shear capacity by about 10.3%, Similarly, the replacement of ECC-PVA (PVA_3 joint) with ECC-PE mix (PE_3 joint) in the joint zone, with the same R.I of 790, increased the ultimate shear capacity by about 7.2%. It is inferred that the PE joints shows better performance in ultimate shear and load capacity, ductility and damage tolerance compared to the PVA joints at the same R.I value.

d) Effect of polymer fibers reinforcing index

Generally, the ultimate shear capacity for ECC joints increased with the increase in the reinforcing index of fibers. For the ECC-PVA group of specimens, the ultimate shear capacity for the PVA_2, PVA_3 and PVA_4 joints increased over the PVA_1 joint about 6.9, 26.9 and 14.6%, respectively, as shown in Figure 4.70. The reduced value for PVA_4

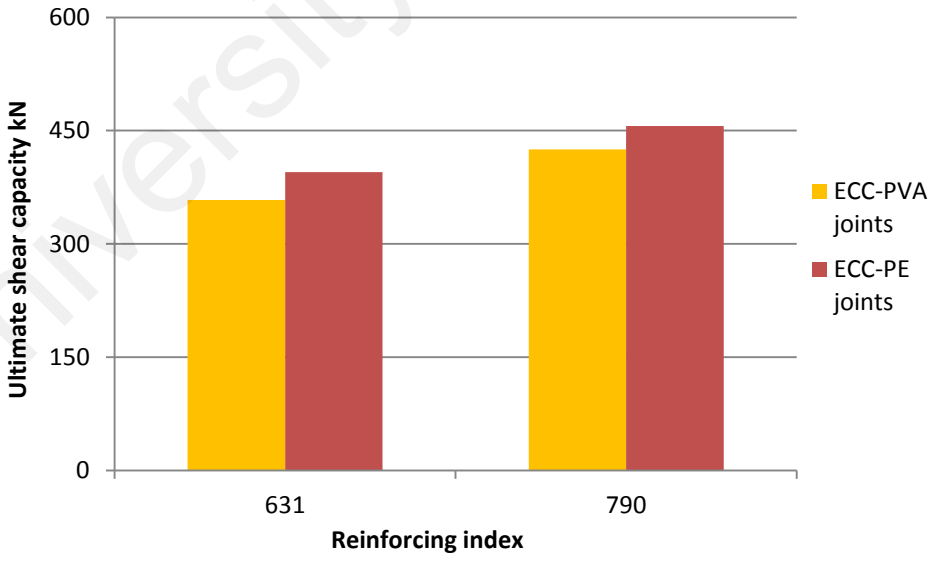

Figure 4.69: Effect of type of ECC in the joint zone on ultimate shear capacity

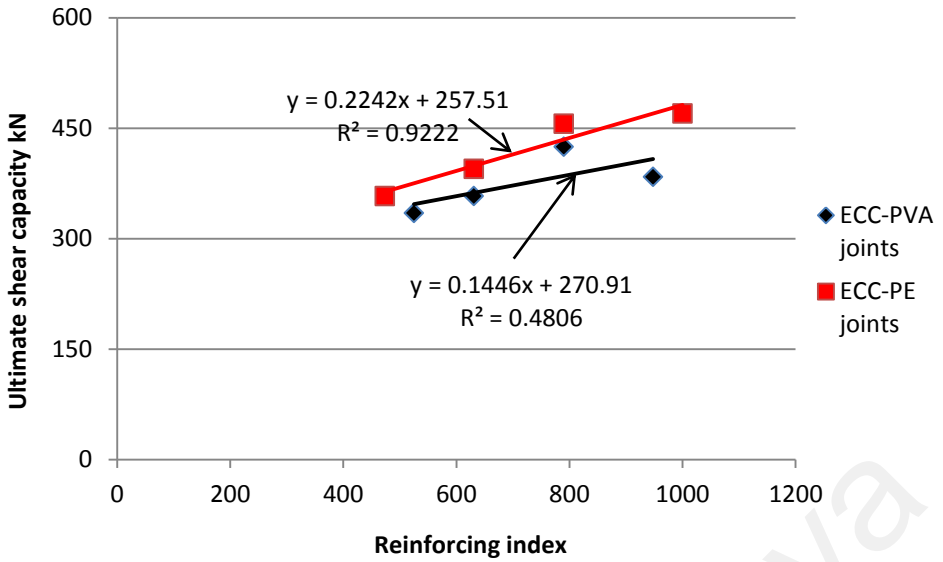

Figure 4.70: Effect of the reinforcing index on ultimate shear capacity of ECC joints

joint is attributed to a lack in workability and poor dispersion of fibers in ECC mix due to the higher amount of fiber content. Similarly, for the ECC-PE group of specimens, the ultimate shear capacity for PE_2, PE_3 and PE_4 joints increased over the PE_1 joint about 10.3, 27.4 and 31.3%, respectively, as shown in Figure 4.70. From the compared results, it is drawn that the increase in the R.I of PE joints is more effective than the increase in the R.I of PVA specimens on the ultimate shear capacity of the joint. A linear fit was suggested to be suitable for the ultimate shear capacity results of ECC joints despite the low correlation for PVA results. The higher slope value for the fit line of PE joints ensures the results obtained above.

e) Effect of lateral steel hoops inclusion in ECC joint zone

Figure 4.71 shows the effect of the lateral steel hoops inclusion in ECC joint zone on the ultimate shear capacity of the ECC joint. For the ECC-PVA group of specimens, the ultimate shear capacity of the PVA_5 and PVA_6 joints increased over the PVA_2 joint by about 20.7 and 27.4%. Small increase in ultimate shear capacity for the PVA_6 joint was observed over the PVA_5 specimen by about 5.6%. Similarly, for the ECC-PE group of

specimens, the ultimate shear capacity for the PE_5 and PE_6 joints increased over the PE_2 joint by about 29.6% and 37.7%. Furthermore, small increase in ultimate shear capacity in the PE_6 joint was observed over the PE_5 joint by about 6.2% (Figure 4.71). Results found that a noticeable increase in the ultimate shear capacity was observed with the inclusion of one steel hoop in the joint zone. However, small increase in ultimate shear capacity was observed with the inclusion of two steel hoops in the joint zone compared to the shear capacity of joints with one steel hoop inclusion.

4.4.5 Moment-rotation relationship

The rotation was measured at the middle point of joint zone by a tilt meter installed for this purpose. Figures 4.72 to 4.85 show the hysteresis loops for the beam-column joint specimens are plotted for the moment versus rotation at the joint.

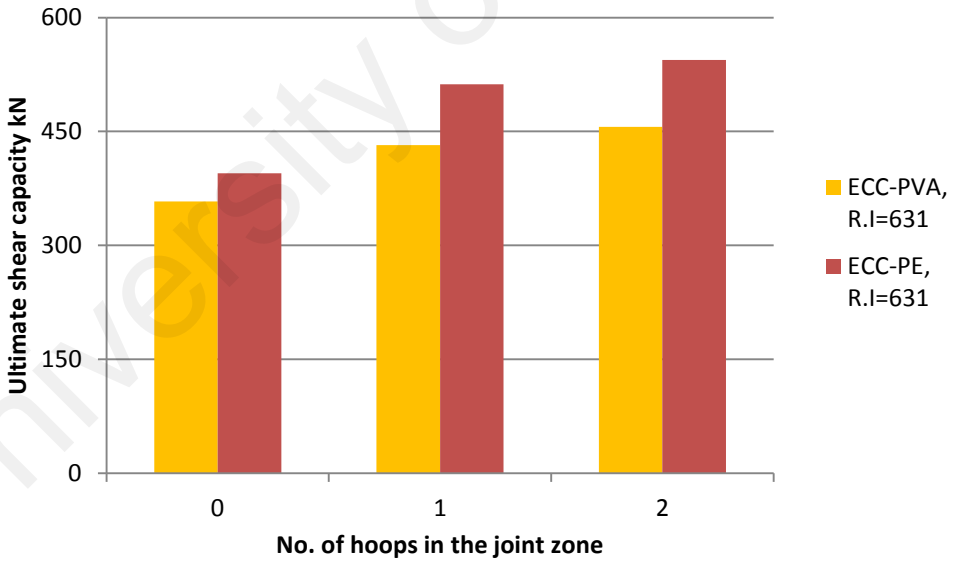

Figure 4.71: Effect of lateral steel hoops inclusion on shear capacity of ECC joint zone

a) Effect of lateral steel hoops in NC joints

Figure 4.72 shows the significant effect of pinching in the NC_1 specimen (without lateral steel hoops in the joint zone) due to the minimized loop area which is attributed

to the brittle failure mode. On the other hand, Figure 4.73 shows wider loop area and better spread of loop was observed for the NC_2 specimen (with lateral steel hoops in the joint zone) especially in the negative part of the hysteresis loops. However, the positive part of the loops for the NC_2 specimen are overlapped and not spread regularly due to the fragmentation of concrete on the surface of joint which impedes the tilt meter from recording correctly.

b) Effect of the ECC inclusion in the joint zone

As shown in Figure 4.74, the hysteresis loops of moment-rotation for the PVA_1 specimen are wider and better spread than the corresponding hysteresis loops for NC_2 specimen (Figure 4.73). However, a pinching effect was rather observed for PVA_1 specimen due to the lower value of reinforcing index. For PE_1 specimen (Figure 4.80), the hysteresis loops area is wider and more spread than the corresponding loops area for NC_2.with reduced pinching effect due to the perfect ductility of ECC-PE and the perfect mechanism of fibers bridging.

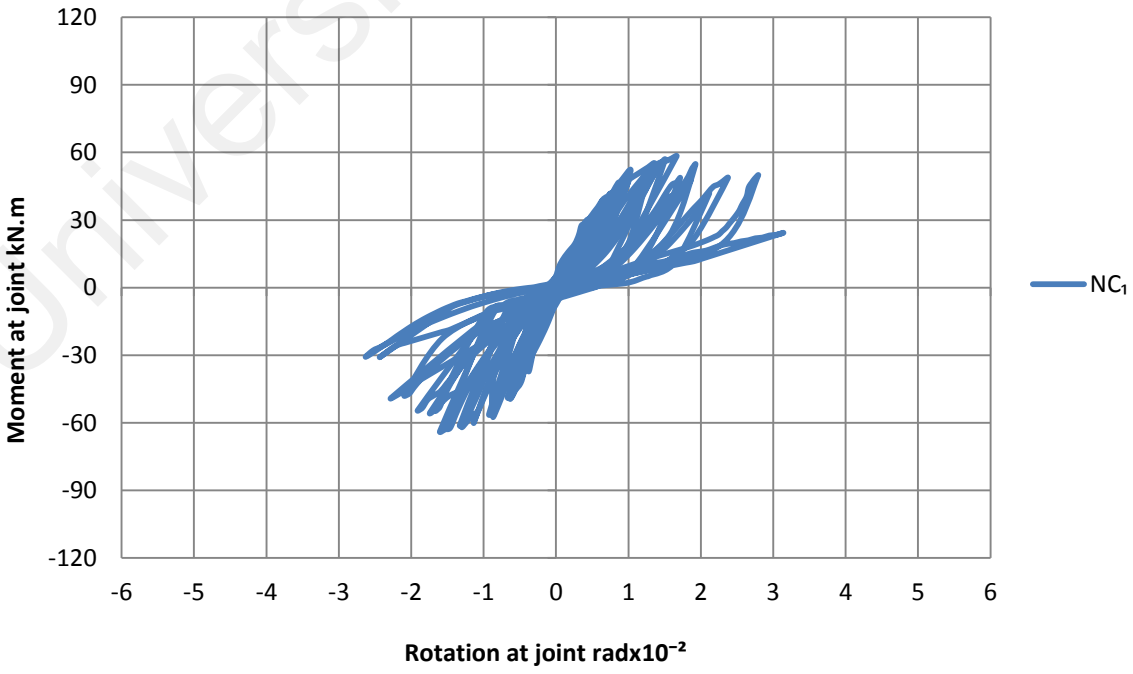

Figure 4.72: Moment–rotation relationship at the joint for NC_1 specimen

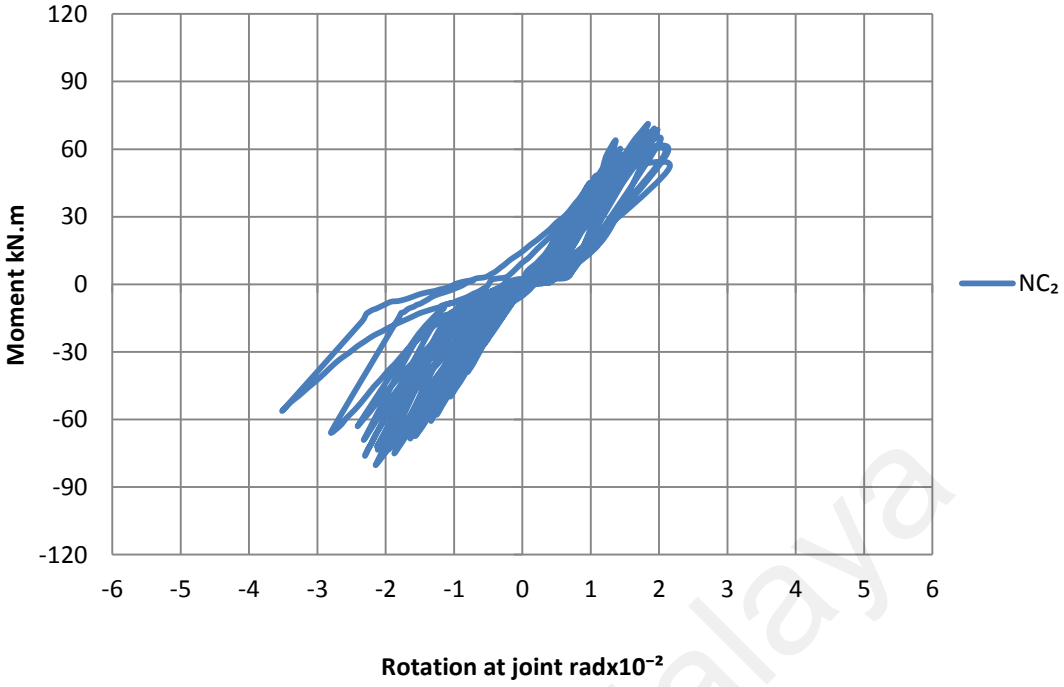

Figure 4.73: Moment–rotation relationship at the joint for NC_2 specimen

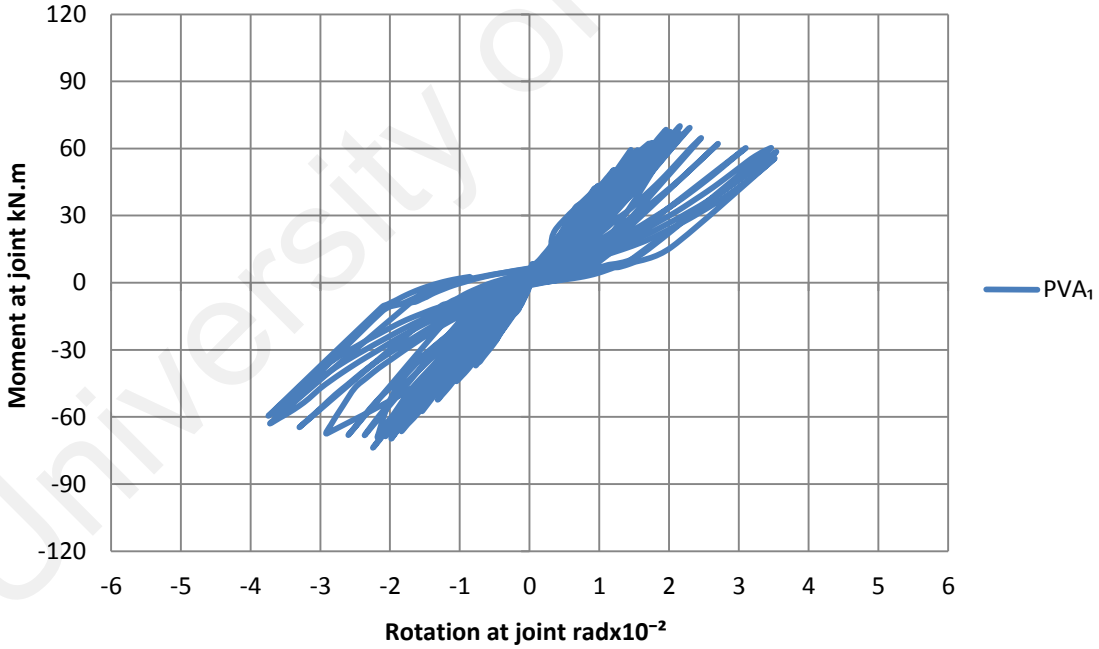

Figure 4.74: Moment–rotation relationship at the joint for PVA_1 specimen

c) Effect of type of ECC in the joint zone

Figure 4.81 shows a significant behavior of loops for PE_2 specimen with wider area and more spread compared to the PVA_2 specimen (Figure 4.75) due to the perfect ductility of ECC-PE. Similarly, Figure 4.82 shows a significant behavior in the hysteresis loops for the PE_3 specimen with more extensive and spread area of loops compared to the corresponding loops for PVA_3 specimen (Figure 4.76).

d) Effect of polymer fibers reinforcing index

Figures 4.74 to 4.77 indicate the positive effect of the reinforcing index increase on the moment-rotation hysteresis loops behavior of the ECC-PVA group of specimens. A gradual improvement in the loops behavior was observed with the increase in the reinforcing index with a gradual decrease of pinching effect. The loops behavior for PVA_3 specimen is somehow better and more regular than the corresponding loops behavior for PVA_4 specimen owing to the insufficient homogeneity of the ECC mix because of higher fiber content. Similarly, Figures 4.80 to 4.83 show a significant effect

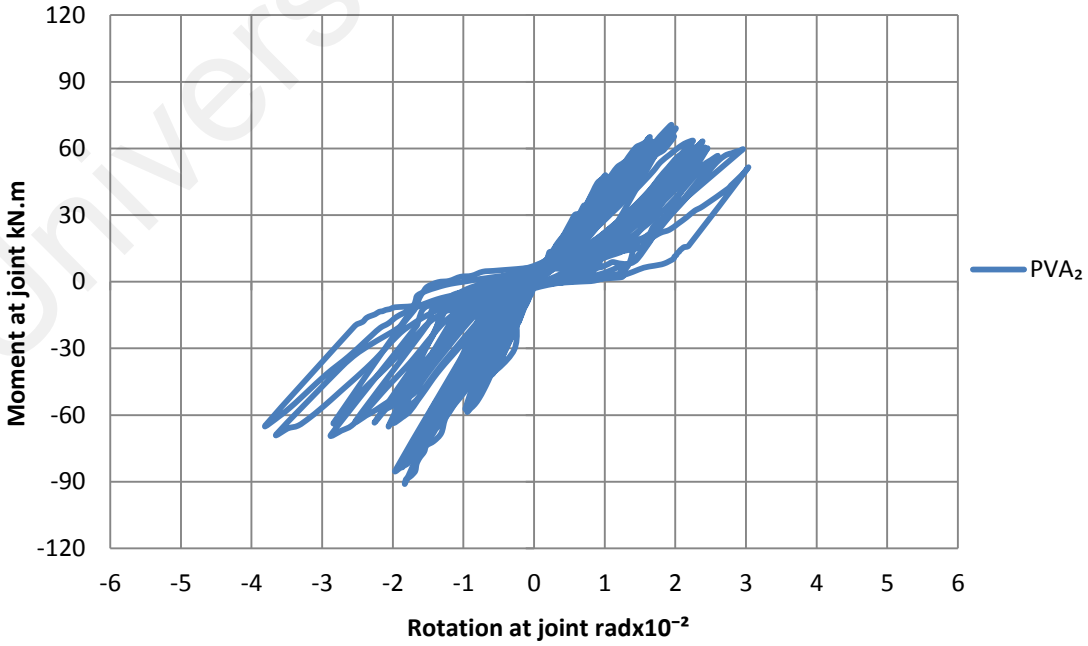

Figure 4.75: Moment–rotation relationship at the joint for PVA_2 specimen

of the reinforcing index increase on the hysteresis loops behavior of the ECC-PE group of specimens. Wider area with more regular and denser of loops with reduced effect of pinching was observed as the increase in the reinforcing index.

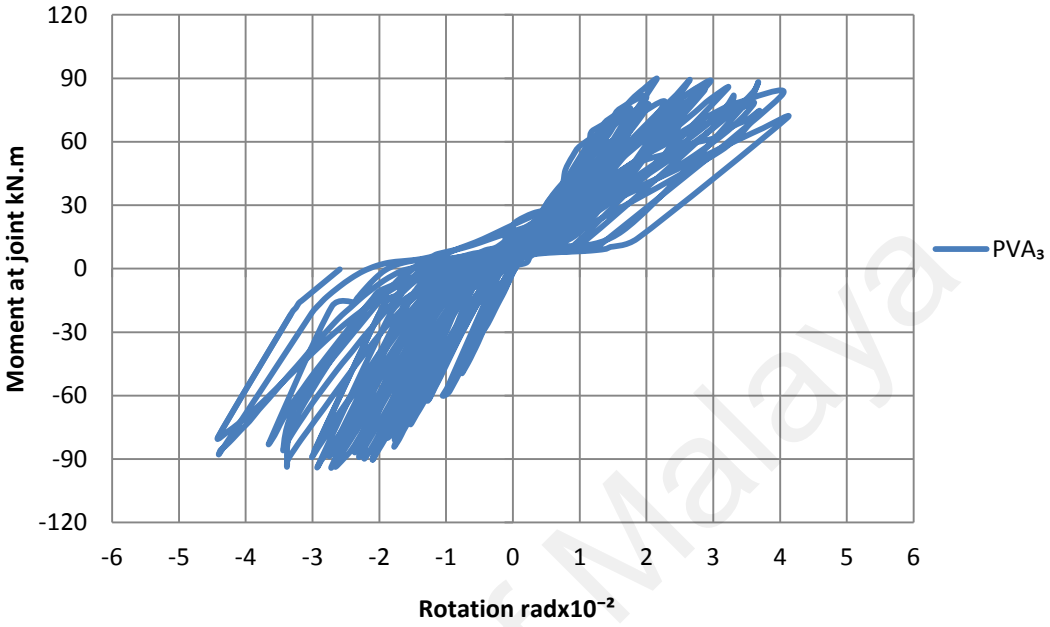

Figure 4.76: Moment–rotation relationship at the joint for PVA_3 specimen

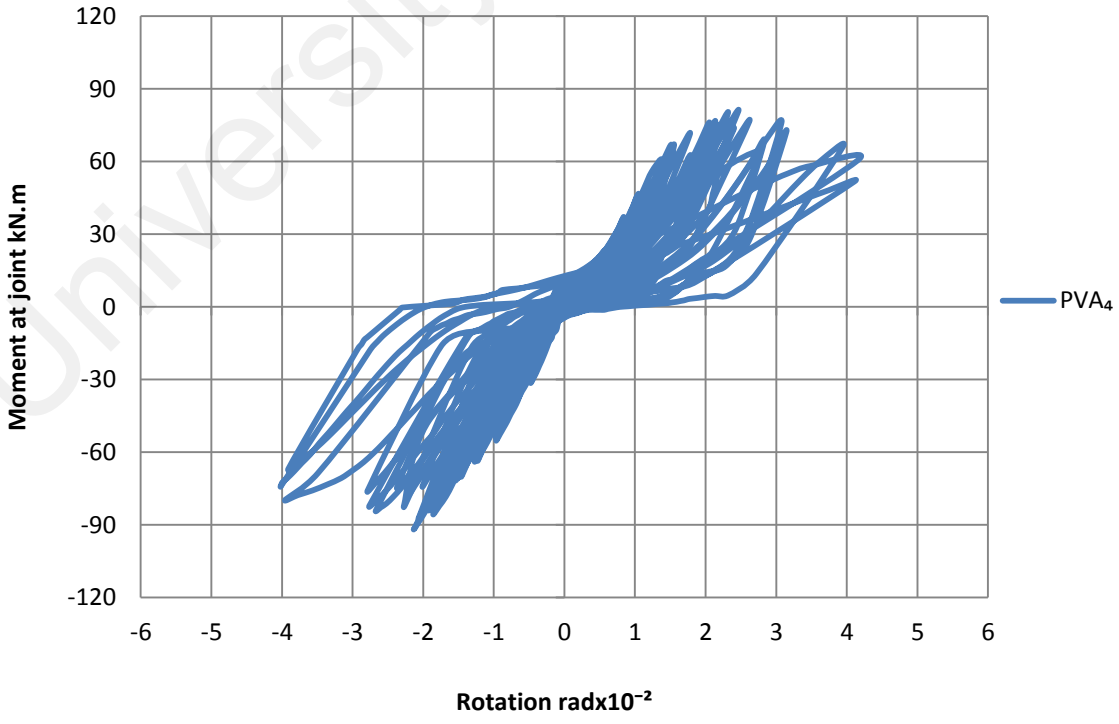

Figure 4.77: Moment–rotation relationship at the joint for PVA_4 specimen

e) Effect of the lateral steel hoops inclusion in ECC joint zone

As indicated in the Figures 4.74, 4.78 and 4.79, the hysteresis loops behavior of PVA_5 and PA_6 specimens (with one and two hoops in the joint hoops, respectively) is much better than the corresponding loops behavior of the PVA_2 specimen (without any hoops in the joint zone) with wider loops area, better regularity and reduced effect of pinching. Similarly, the Figures 4.81, 4.84 and 4.85 indicate the positive effect of lateral steel hoops inclusion in the ECC-PE joints. The PE_5 and PE_6 specimens (with one and two hoops in the joint zone, respectively) showed an improved behavior of hysteresis loops with wider area, denser, more regular and better spread of loops compared to the PE_2 specimen (without any hoops in the joint zone).

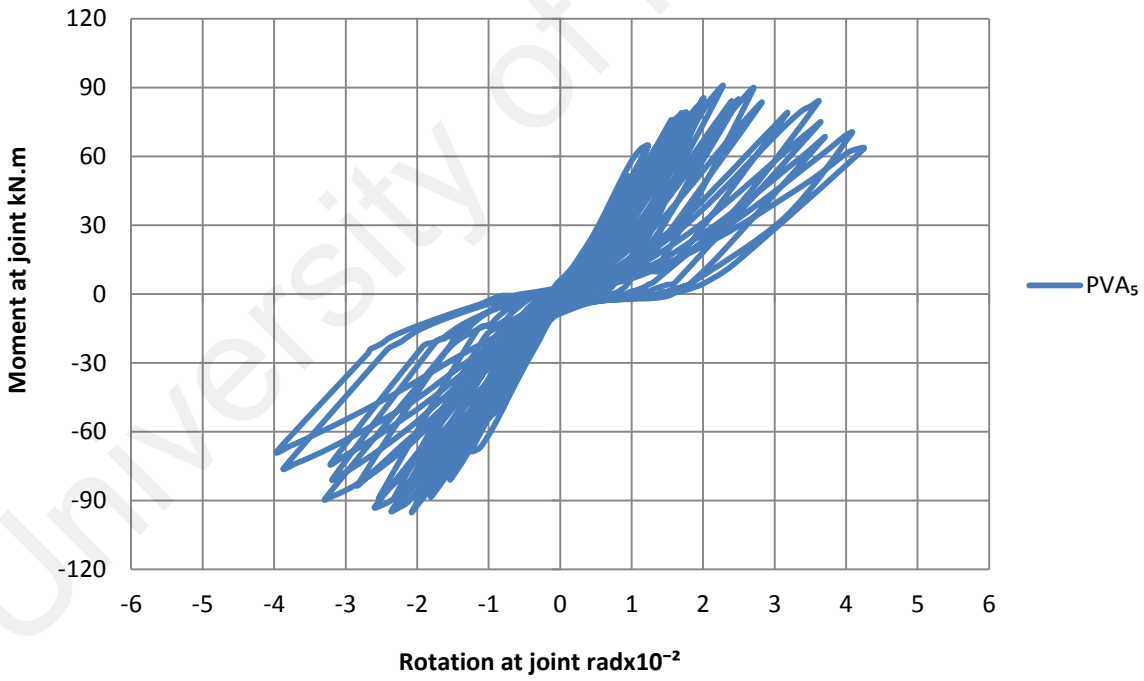

Figure 4.78: Moment–rotation relationship at the joint for PVA_5 specimen

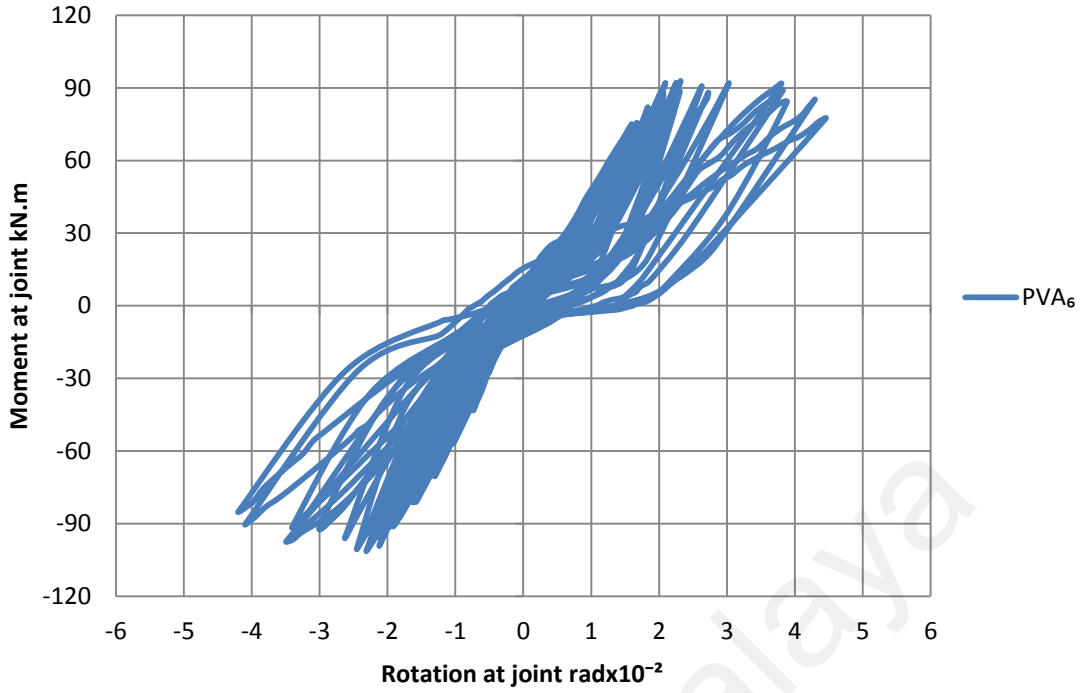

Figure 4.79: Moment–rotation relationship at the joint for PVA_6 specimen

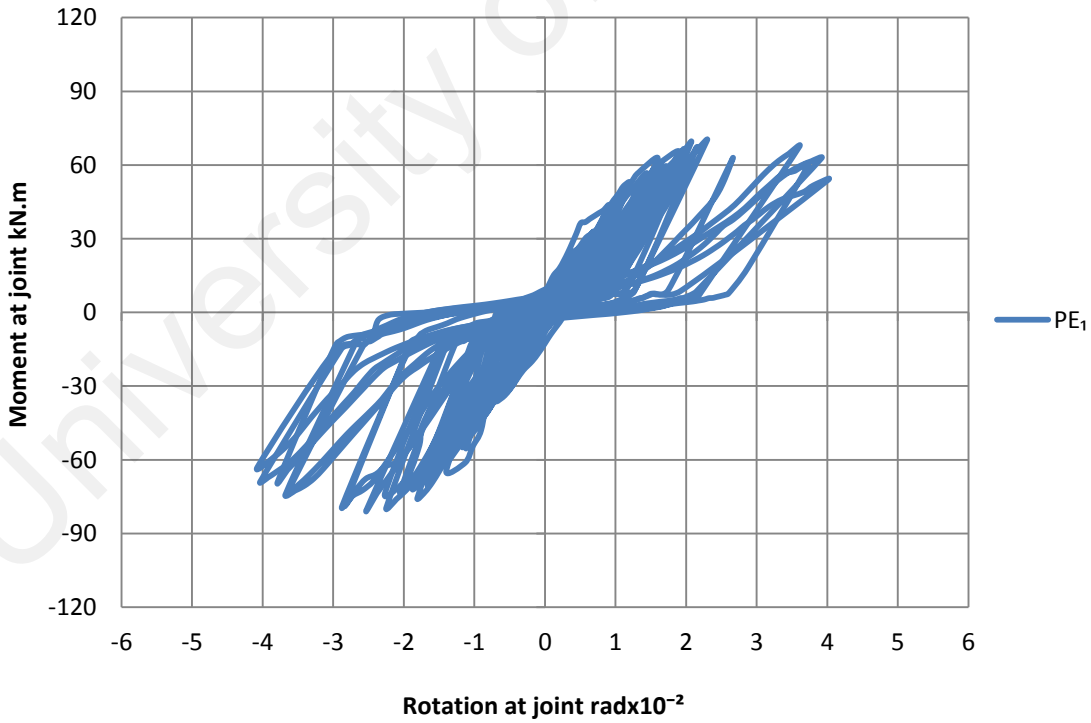

Figure 4.80: Moment–rotation relationship at the joint for PE_1 specimen

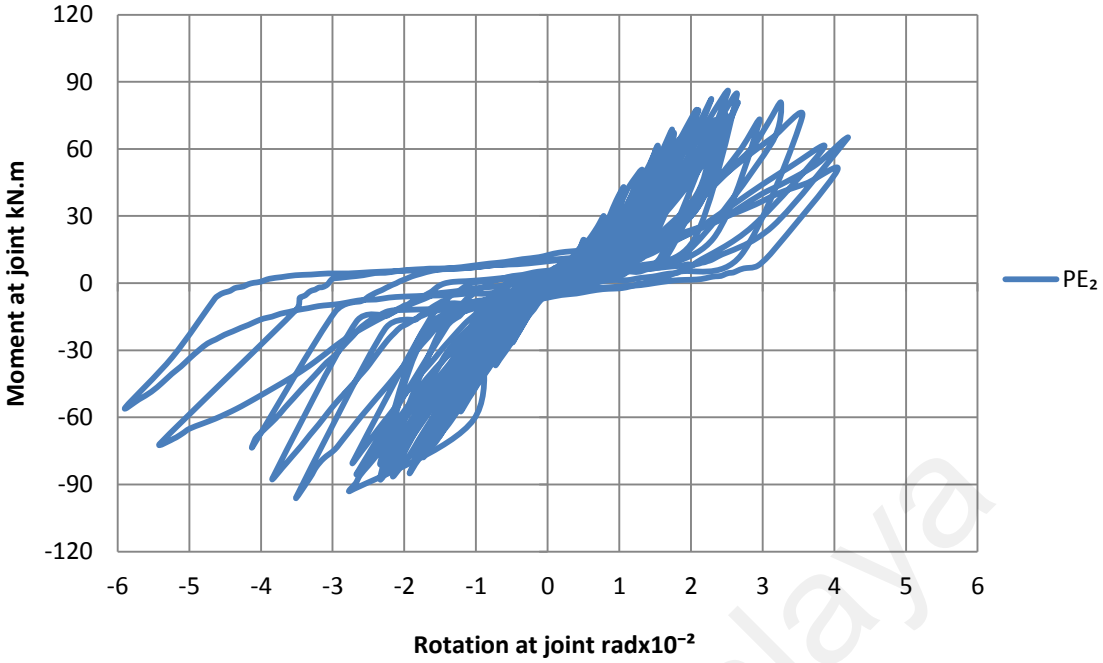

Figure 4.81: Moment–rotation relationship at the joint for PE_2 specimen

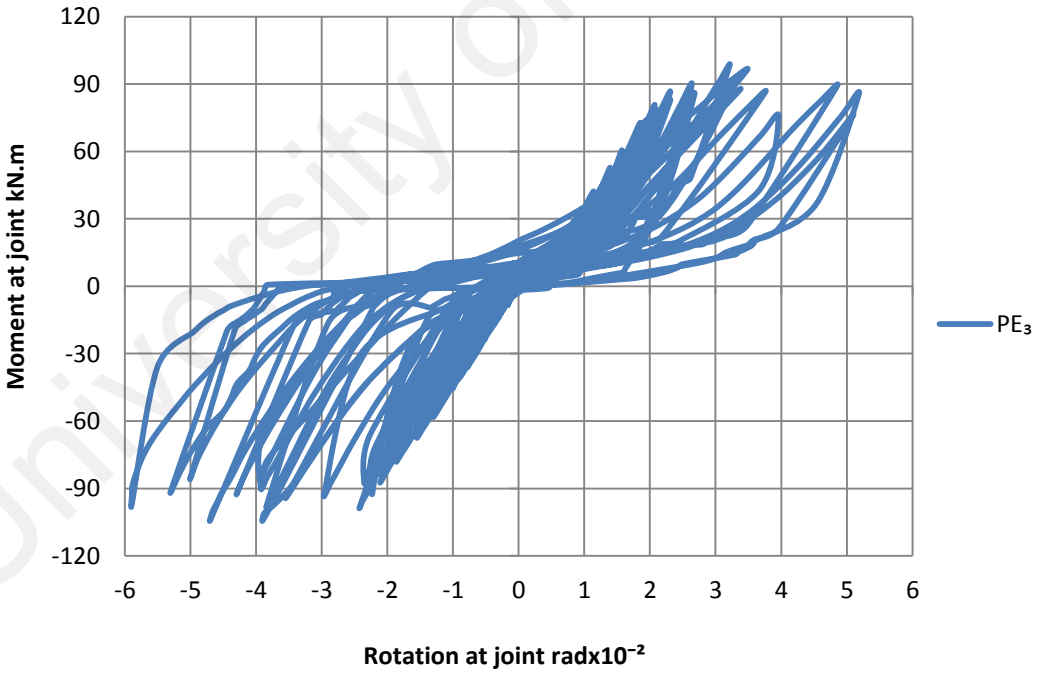

Figure 4.82: Moment–rotation relationship at the joint for PE_3 specimen

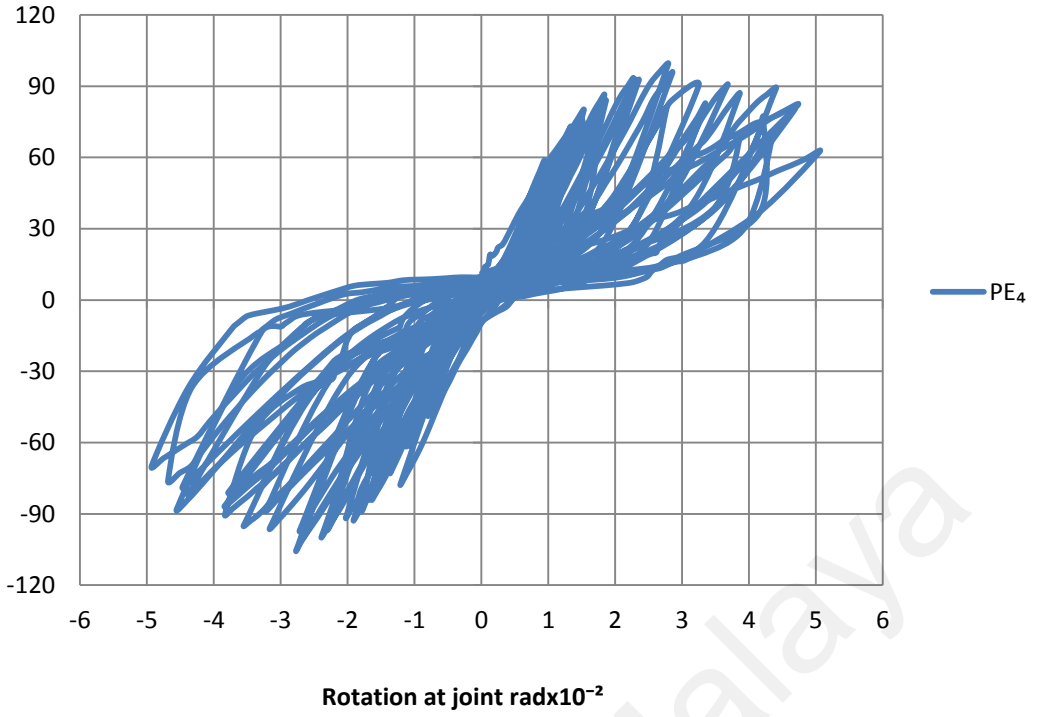

Figure 4.83: Moment–rotation relationship at the joint for PE_4 specimen

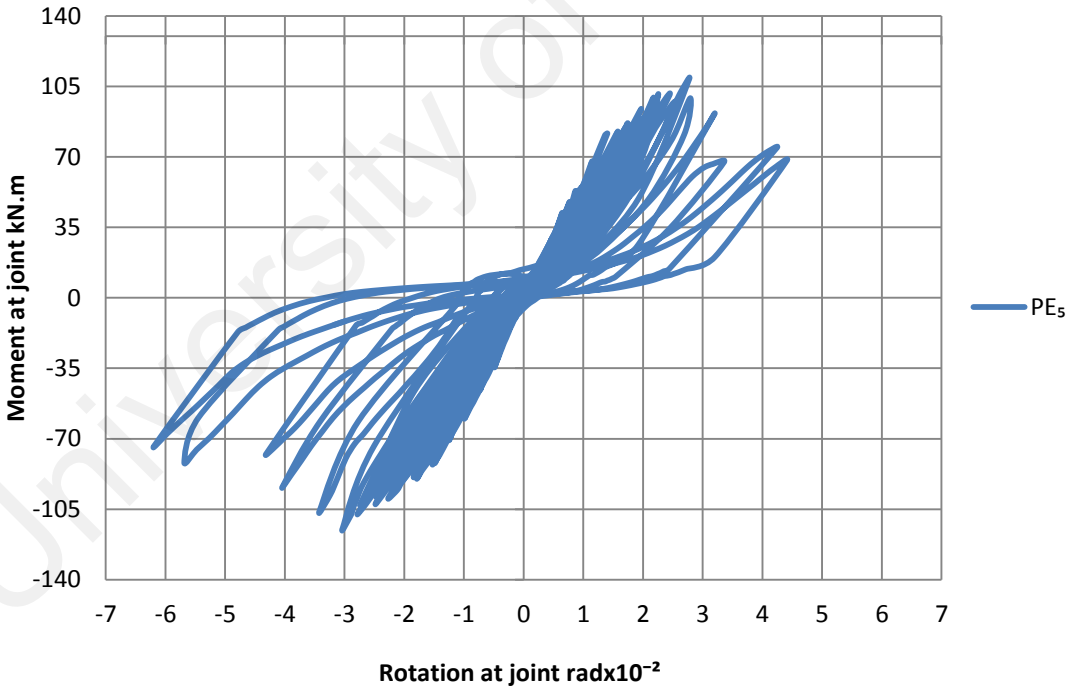

Figure 4.84: Moment–rotation relationship at the joint for PE_5 specimen

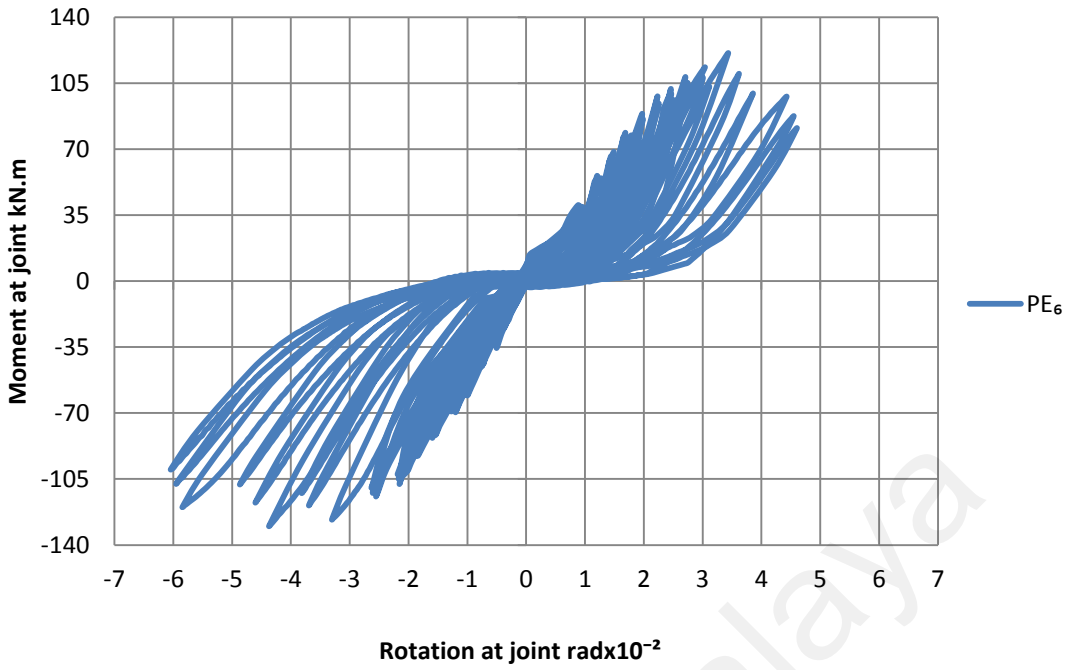

Figure 4.85: Moment–rotation relationship at the joint for PE_6 specimen

4.4.6 Moment-rotation envelope relationship

In this section, moment-rotation envelope curves will be plotted for the beam-column joints and several parameters will be discussed such as the ultimate moment capacity and the rotation value at ultimate and failure stages.

a) Effect of lateral steel hoops in normal concrete (NC) joints

The moment-rotation envelope curve for the NC_1 and NC_2 specimens is indicated in the Figure 4.86. The curve indicated an increase in the ultimate moment value for the NC_2 specimen of about 20% more than the corresponding moment value for the NC_1 specimen. Moreover, Figure 4.87 shows an increase in the rotation value for the NC_2 joint of about 33% and 7% more than the corresponding rotation value for NC_1 specimen at ultimate capacity and failure stage, respectively, which denotes better deformation and ductility for NC_2 specimen.

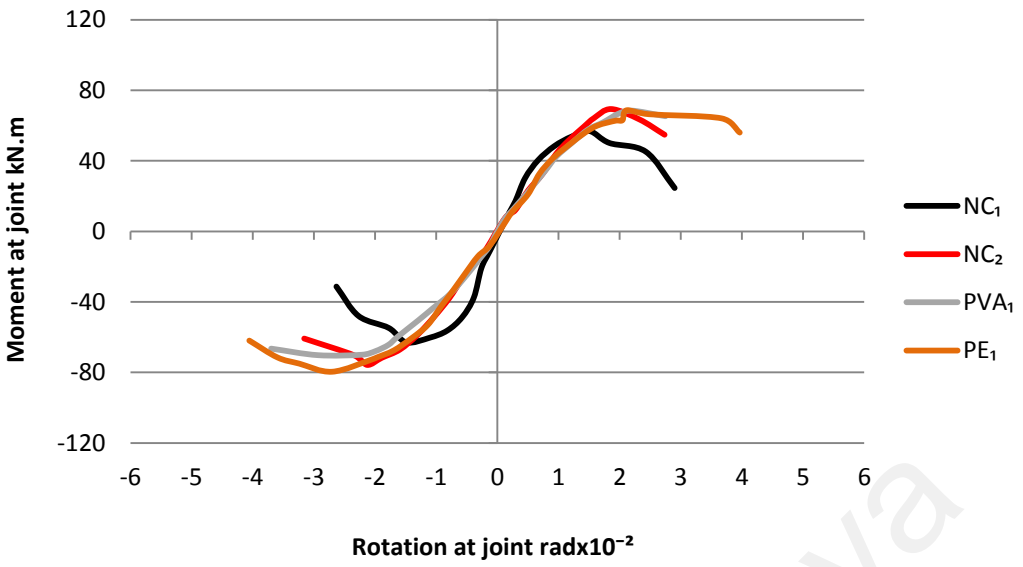

Figure 4.86: Moment-rotation envelope relationship for the NC_1, NC_2, PVA_1, and PE_1 specimens

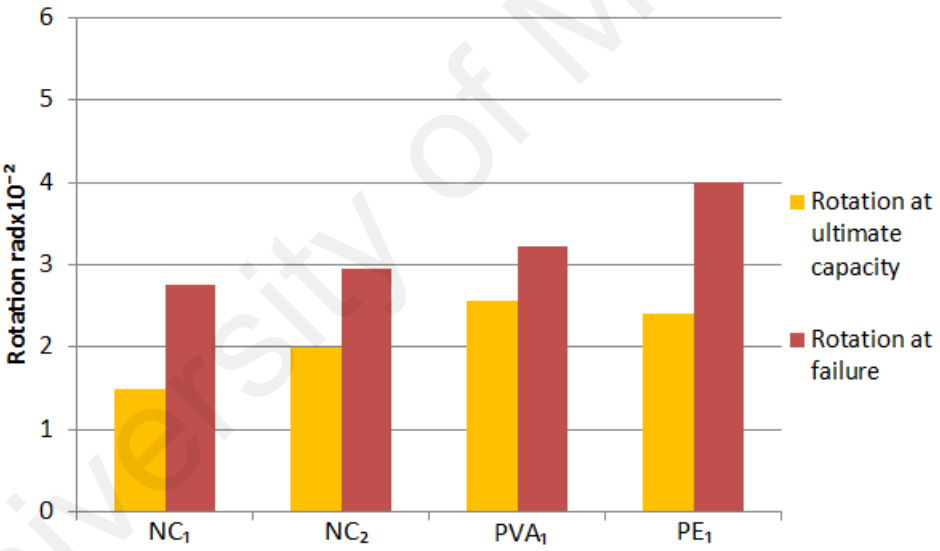

Figure 4.87: Effect of the ECC inclusion in the joint zone on the rotation value

b) Effect of the ECC inclusion in the joint zone

The moment rotation envelope curve for the NC_1, NC_2, PVA_1 and PE_1 specimens is shown in Figure 4.86. The curve indicated an increase in the ultimate moment value for the PVA_1 specimen of about 16.7% more than the corresponding moment value for

the NC_1 specimen and 2.8% less than the corresponding moment value for the NC_2 specimen. In addition, Figure 4.87 shows an increase in the rotation value for the PVA_1 specimen about 28.7% and 9.5% more than the corresponding rotation value for NC_2 specimen at ultimate capacity and failure stage, respectively. Similarly, the envelope curve for the PE_1 specimen indicated an increase in the ultimate moment value of about 4% more than the corresponding moment value for the NC_2 specimen. Moreover, Figure 4.87 shows an increase in the rotation value for the PE_1 specimen about 20.7% and 36.1% more than the corresponding rotation value for NC_2 specimen at ultimate capacity and failure stage respectively, which denotes perfect ductility and damage tolerance for the PE_1 specimen.

c) Effect of type of ECC in the joint zone

Figure 4.88 shows the moment rotation envelope curve for the PVA_2, PE_2, PVA_3 and PE_3 specimens. The envelope curve for the PE_2 specimen indicated an increase in the ultimate moment value of about 9.4% more than the corresponding moment value for the PVA_2 specimen. Moreover, Figure 4.89 shows a significant increase in the rotation value for the PE_2 specimen about 63.6% and 38% more than the corresponding rotation value for the PVA_2 specimen at ultimate capacity and failure stage, respectively. Similarly, the envelope curve for the PE_3 specimen indicated an increase in the ultimate moment value of about 6.7% more than the corresponding moment value for the PVA_3 specimen. Moreover, Figure 4.89 shows an increase in the rotation value for the PE_3 specimen about 31.5% and 12.7% more than the corresponding rotation value for the PVA_3 specimen at ultimate capacity and failure stage, respectively, which denotes better ductility and damage tolerance of the ECC-PE joints compared to the ECC-PVA joints.

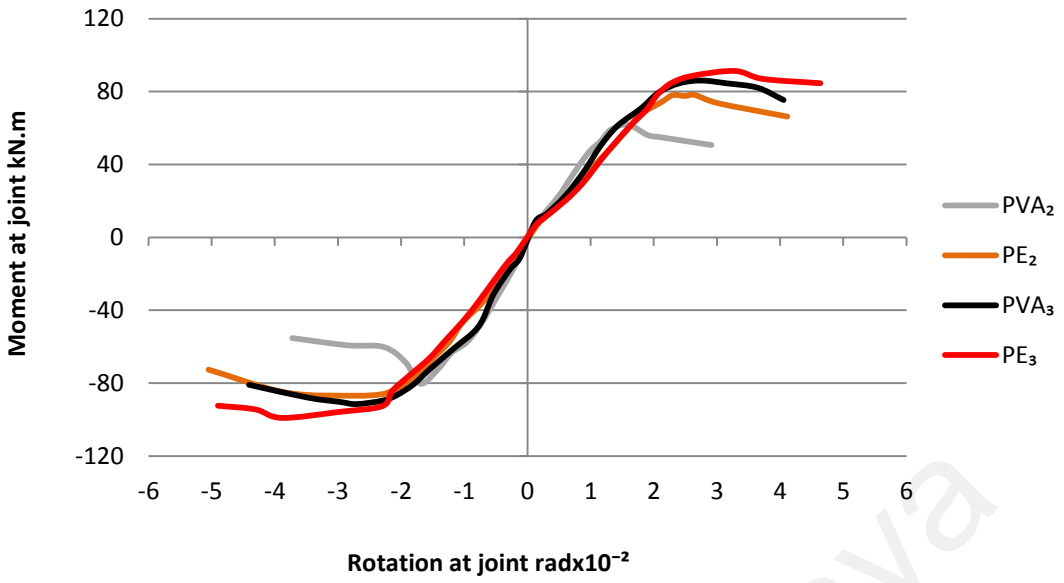

Figure 4.88: Moment-rotation envelope relationship for the PVA_2, PE_2, PVA_3, and PE_3 specimens

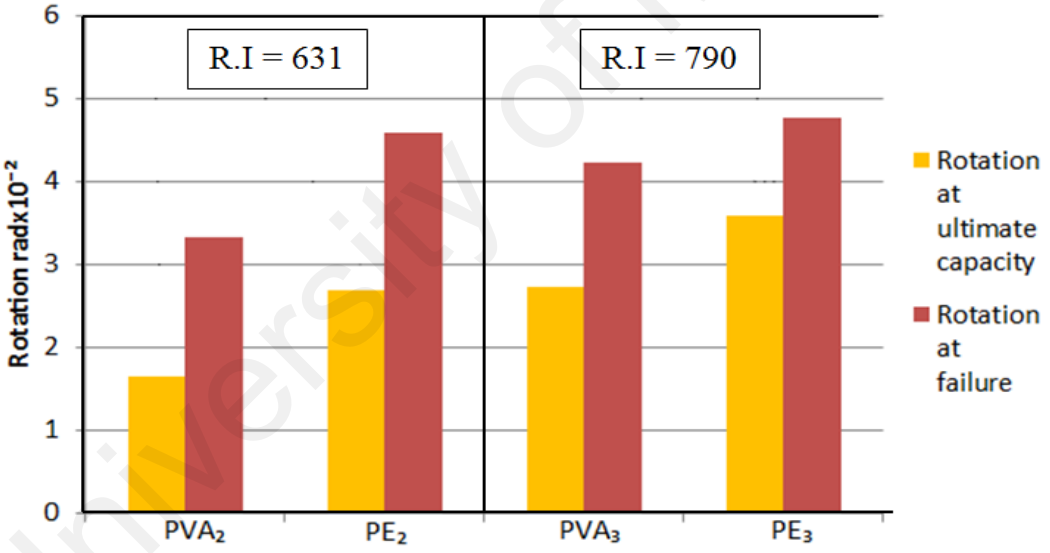

Figure 4.89: Effect of type of ECC in the joint zone on the rotation value

d) Effect of polymer fibers reinforcing index

Figure 4.90a shows the effect of reinforcing index on the moment-rotation envelope curve for the group of PVA specimens. The Figure indicated an increase in the ultimate

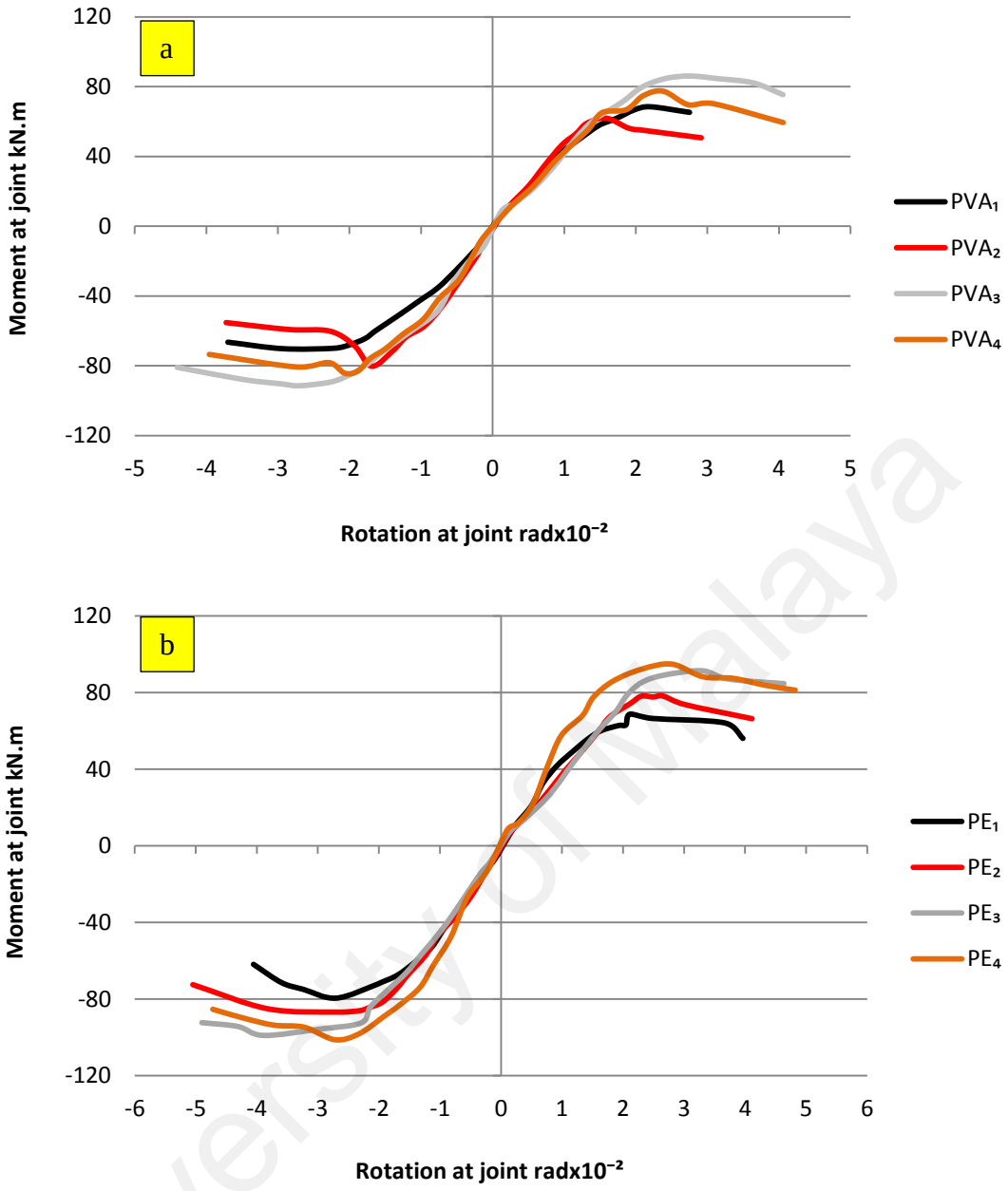

Figure 4.90: Effect of the reinforcing index on the moment-rotation envelope relationship in the (a) ECC-PVA joints (b) ECC-PE joints

moment capacity for the PVA_2, PVA_3 and PVA_4 specimens of 7.1, 27.1 and 14.3% more than the corresponding moment value for the PVA_1 specimen, respectively. Moreover, Figure 4.91a showed an increase in the rotation value for the PVA_2, PVA_3 and PVA_4 specimens of about 2.9, 31.2 and 24.3%, more than the corresponding rotation value for the PVA_1 specimen at the failure stage, respectively. Similarly, the envelope curve in Figure 4.90b showed an increase in the ultimate moment capacity for

the PE_2, PE_3 and PE_4 of about 9.3, 26.7 and 30.7% more than the corresponding moment value for the PE_1 specimen, respectively. Moreover, Figure 4.91b shows an increase in the rotation value for the PE_2, PE_3 and PE_4 specimen of about 14.2, 18.1 and

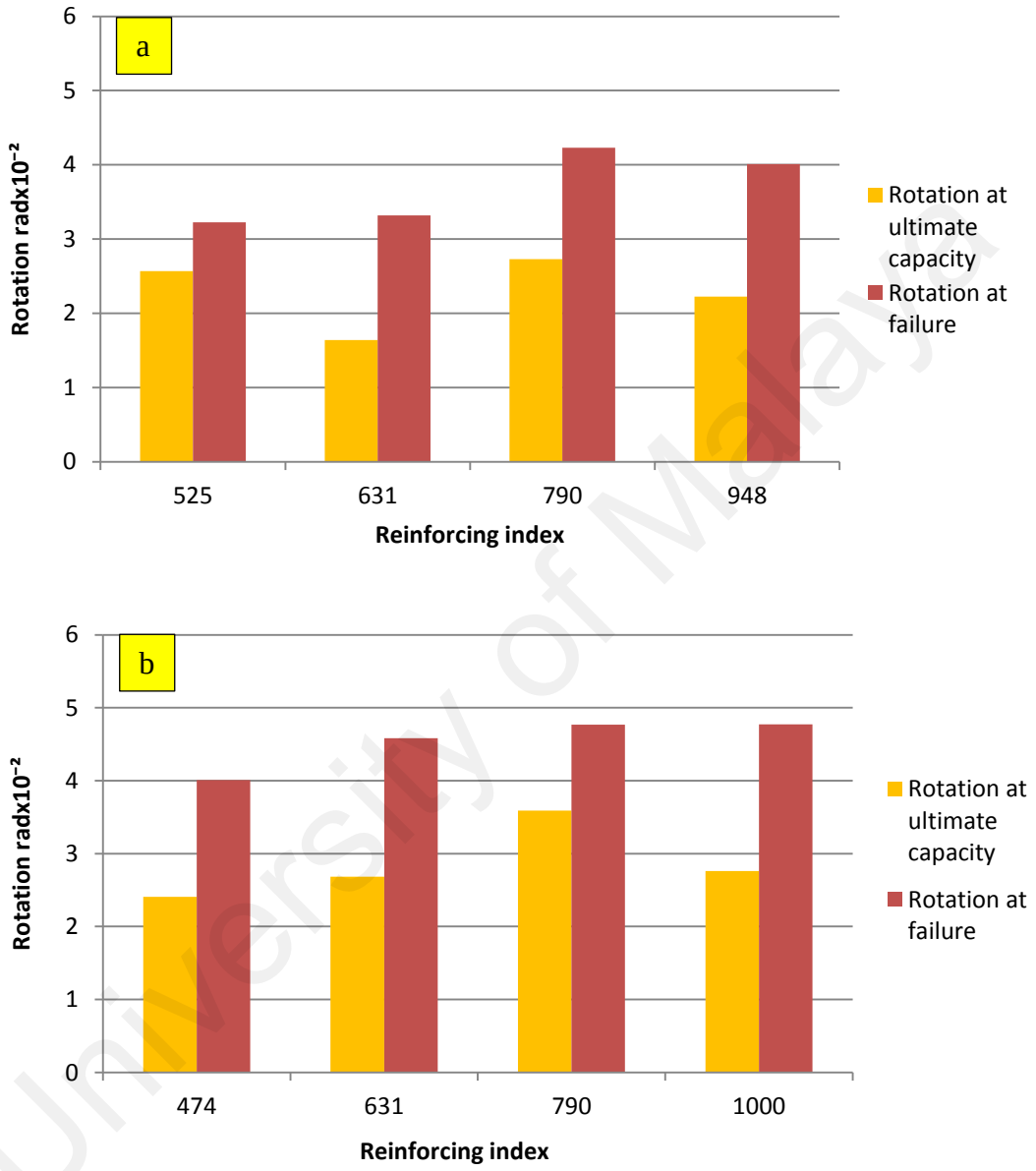

Figure 4.91: Effect of the reinforcing index on the rotation value in the (a) ECC-PVA joints (b) ECC-PE joints

19% more than the corresponding value of the PE_1 specimen at failure stage, respectively. The increase in the rotation value denotes better ductility, higher energy absorption capacity and damage tolerance for the both groups of specimens as the increase in the reinforcing index.

e) Effect of the lateral steel hoops inclusion in ECC joint zone

Figure 4.92a, showed the effect of the lateral steel hoops inclusion in the ECC joint zone on the moment-rotation envelope curve for the group of PVA specimens. The figure showed an increase in the ultimate moment value for PVA_5 and PVA_6 of about 20 and 26.7% more than the corresponding moment value for PVA_2 specimen, respectively. Moreover, Figure 4.93a showed an increase in the rotation value for the PVA_5 and PVA_6 specimens of about 27.5 and 28.3%, more than the corresponding rotation value for the PVA_2 specimen at failure stage, respectively. Similarly, the envelope moment-rotation curve in Figure 4.92b showed an increase in the ultimate moment value for the PE_5 and PE_6 specimens of about 30.5 and 37.8% more than the corresponding moment value for the PE_2 specimen, respectively. Moreover, Figure 4.93b showed an increase in the rotation value for the PE_5 and PE_6 specimen of about 12 and 13.5% more than the corresponding rotation value for the PE_2 specimen at failure stage, respectively. The increase in the rotation value denotes better ductility, higher energy absorption capacity and damage tolerance for the both groups of specimens due to the inclusion of lateral steel hoops in the joint zone. However, small improvement in the ductility was observed with the inclusion of the two hoops compared to the one hoop inclusion in the joint zone for the both groups of ECC.

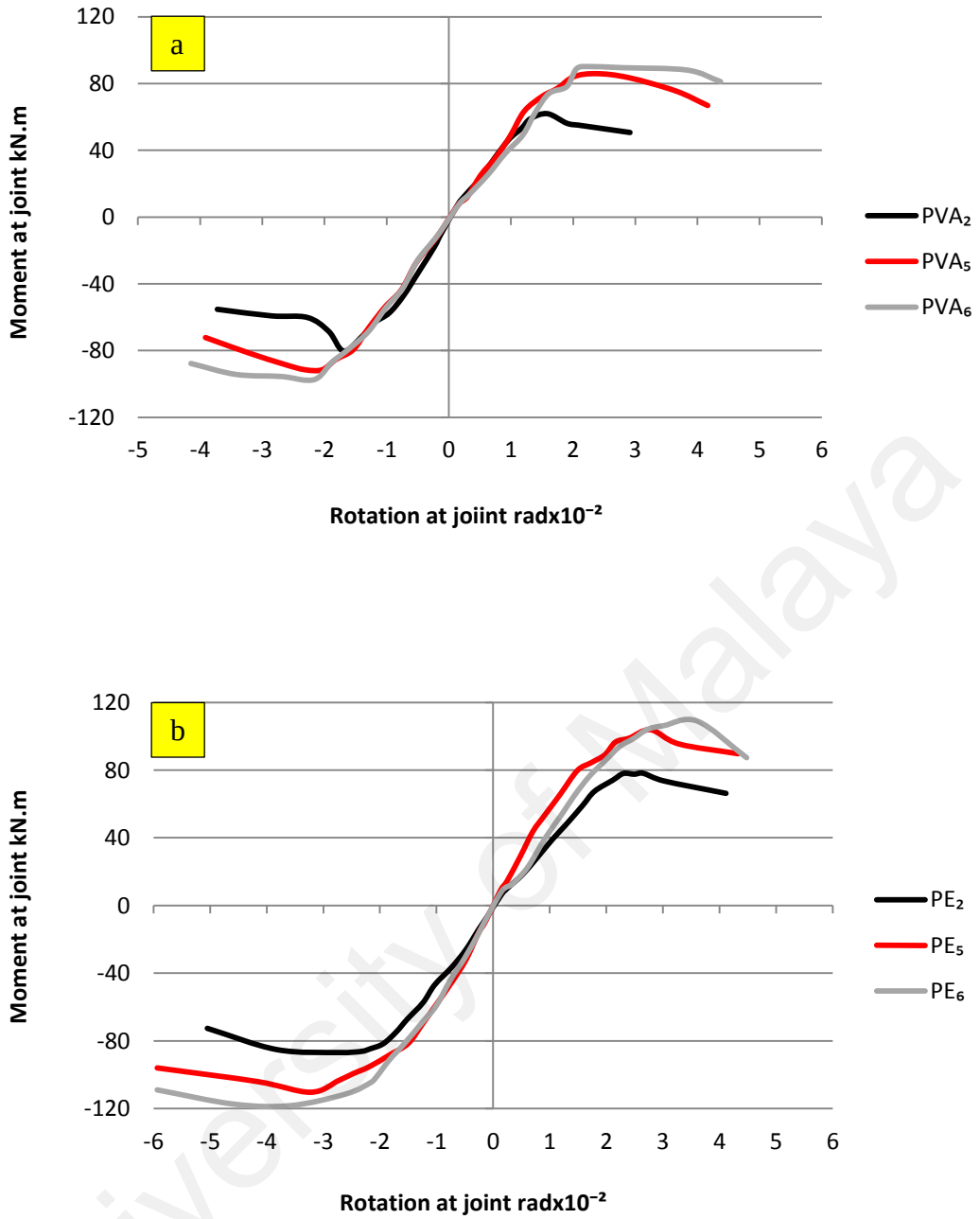

Figure 4.92: Effect of lateral reinforcement inclusion in the joint zone on the moment-rotation envelope relationship in (a) ECC-PVA joints (b) ECC-PE joints

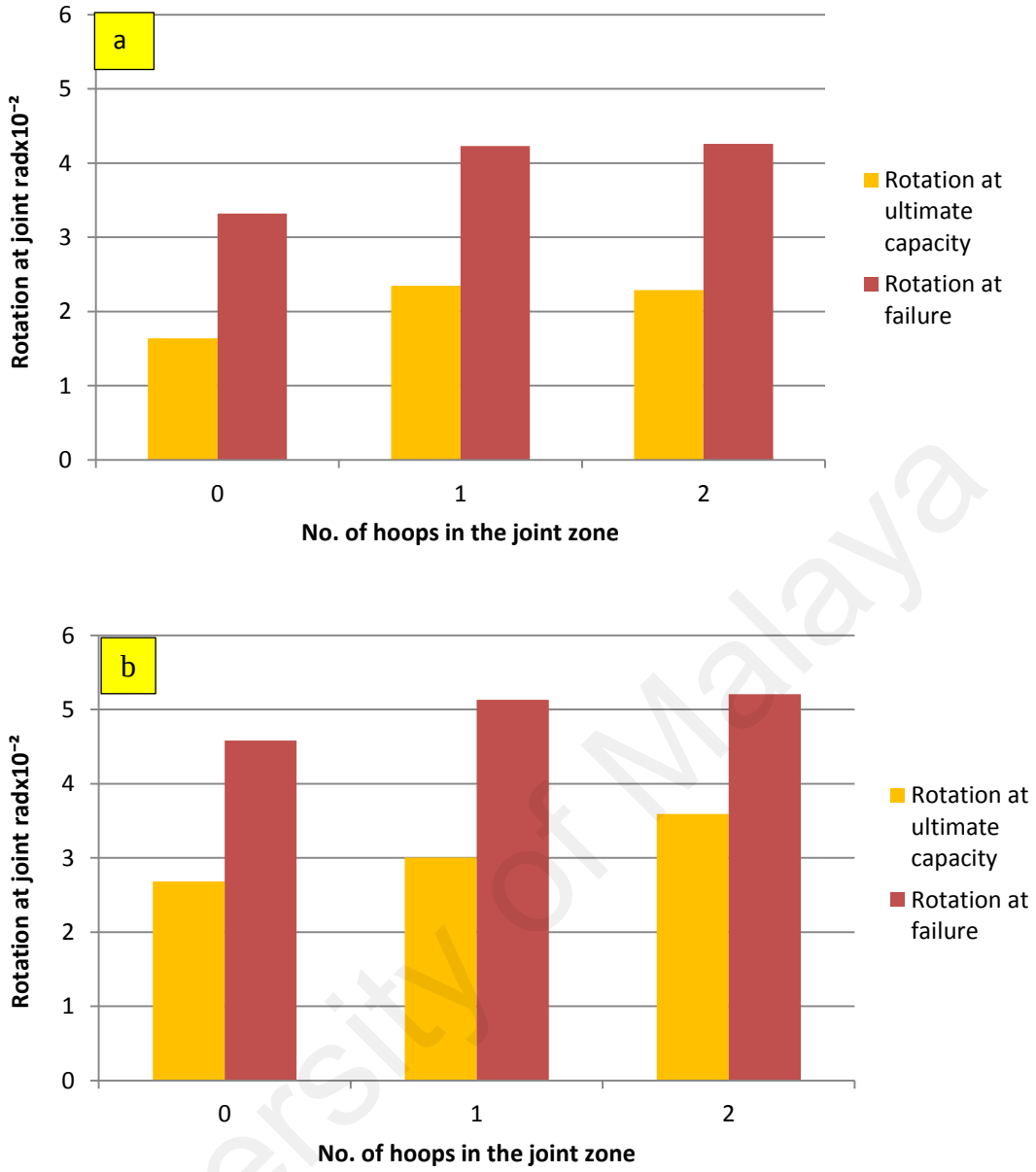

Figure 4.93: Effect of the lateral reinforcement inclusion on the rotation value in the (a) ECC-PVA joints (b) ECC-PE joints

4.4.7 Principal strain

4.4.7.1 Principal strain value in the brittle joints

Principal strain values of the joint are calculated from the maximum values of the data recorded from the RSGs and installed at five different points in the joint zone. The NC_1 is the beam-column joint with the highest brittleness of the joint among the beam-column joints due to the normal concrete inclusion with the absence of the lateral steel hoops in the joint zone. After conducting the test and due to the high brittleness of NC1

joint, a few premature cracks were initiated in the NC_1 joint zone with concrete crushing at the early stage of loading. Thus, it is observed that the RSGs started to record higher values of strains. subsequently, it was found that the highest values of the maximum principal strain results in the joint zone among the beam-column joints was recorded for the NC_1 joint due to the severity of the cracks initiated in the joint zone at the early stages of loading which results in higher principal strain values and early damage of RSGs, as shown in Figure 4.94.

4.4.7.2 Principal strain values in the ductile joints

The beam-column joints (except NC_1) characterized with ductile behavior at different levels. It was observed from the principal strain results that the strain values are related to the density of cracks network propagated in the joint zone. The denser crack network in the joint zone gave the higher values of principal strain. With increase in loading, the RSGs records continue to increase until the onset of crack localization. The RSGs within the localized cracks start to damage while the other RSGs start to release the values of subsequent records. It was found that the RSGs records are acceptable until the drift ratio level of 4% for considering suitable results of principal strains within the joint zone. For example, the normal concrete NC_2 joint with 4 steel hoops installed in the joint zone, showed the least density of cracks network, results in reduced values of principal strains, which denotes minimal ductility. However, the ECC-PE joints showed the highest values of the principal strains due to the highest density network of tiny cracks, homogeneously propagated in the joint zone which denotes the highest ductility. It is inferred that the cracks density level in the joint zone is a function of the ductility.

a) Effect of the ECC inclusion in the joint zone

Figure 4.94 shows the effect of the ECC inclusion in the joint zone on the principal strain results. For the NC_1 joint characterized with brittle mode of failure, higher result

of principal strains was observed due to the severity of cracks in the joint zone (as shown in Figure 4.28) at the early stage of loading. However, for the group of NC_2, PVA_1 and PE_1 joints characterized with ductile mode of failure (as shown in Figures 4.29, 4.30 and 4.36), the lowest result of principal strain values was observed in the NC_2 specimen which denotes the lowest level of ductility. In addition, the highest result of principal strain values was found for the PE_1 joint which denotes the highest level of ductility in this group of joints.

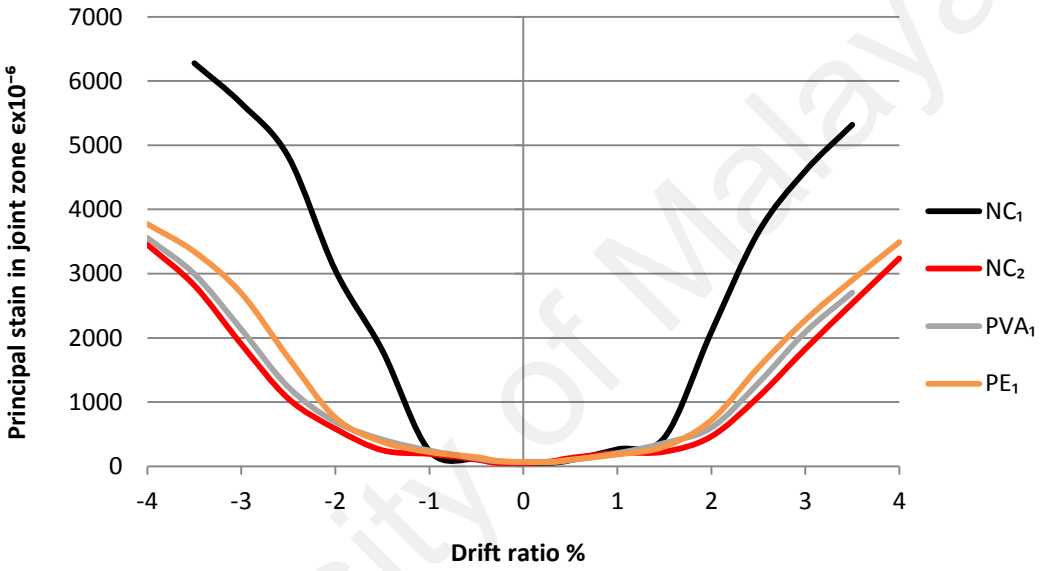

Figure 4.94: Effect of the ECC inclusion in the joint zone on the principal strain values

b) Effect of type of ECC in the joint zone

Figure 4.95 shows the principal strain results for both groups of ECC joints represented in the PVA_2, PE_2, PVA_3 and PE_3 joints. Referring to the Figures 4.31, 4.32, 4.37 and 4.38, all the joints mentioned above failed in a ductile manner. For the same value of R.I, Figure 4.95 showed a significant increase in the principal strain values for the PE_2 and PE_3 specimens compared to the PVA_2 and PVA_3 specimens, respectively, which denotes better ductility, energy absorption capacity and perfect performance for ECC-PE joints.

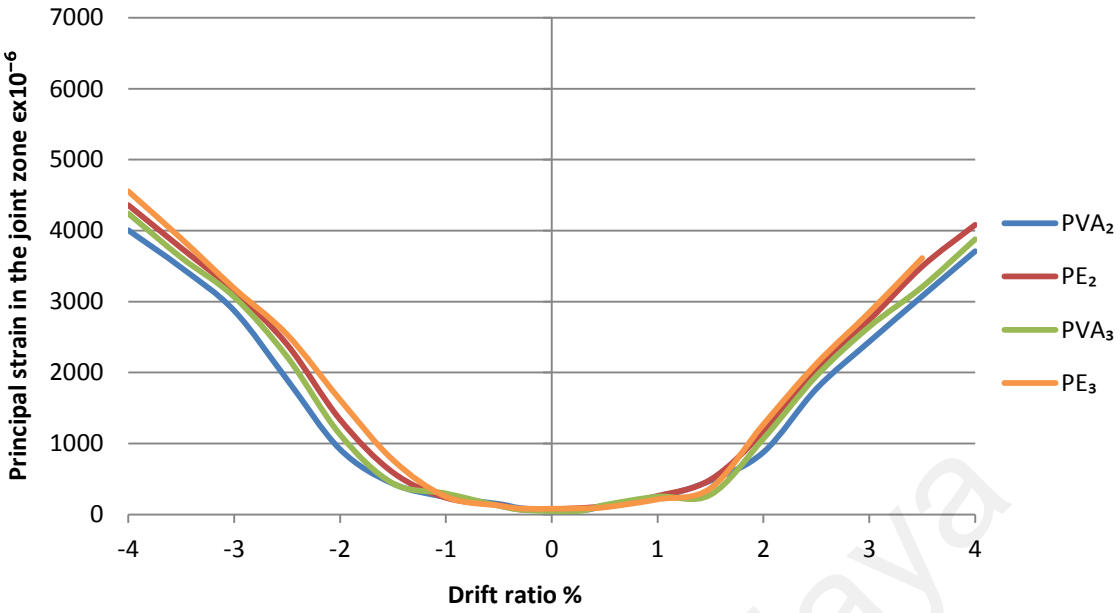

Figure 4.95: Effect of type of ECC in the joint zone on the principal strain values

c) Effect of polymer fibers reinforcing index

Figure 4.96 shows the effect of the reinforcing index on the principal strain results of the both groups of ECC-PVA and ECC-PE joints. Referring to the Figures 4.30 to 4.33 and 4.36 to 4.39, the joints of both groups failed in a ductile manner. For the group of ECC-PVA joints, PVA_1 joint, with lower reinforcing index, showed the lowest result of principal strain values which denotes the lowest level of ductility in the ECC-PVA group. Despite the higher reinforcing index for the PVA_4 joint, the PVA_3 joint showed the highest result of the principal strain values, as shown in Figure 4.96a, which denotes the highest level of ductility due to a poor dispersion of fibers in the ECC mix of PVA_4 joint during casting (as shown in Figure 4.96a). For the group of ECC-PE joints, PE_1 joint, with lower reinforcing index, showed the lowest result of principal strain values which denotes the lowest level of ductility in the ECC-PE group while the PE_4 joint, with higher reinforcing index, showed the highest result of the principal strain values in this group which denotes the highest level of ductility and perfect performance in this group (as shown in Figure 4.96b).

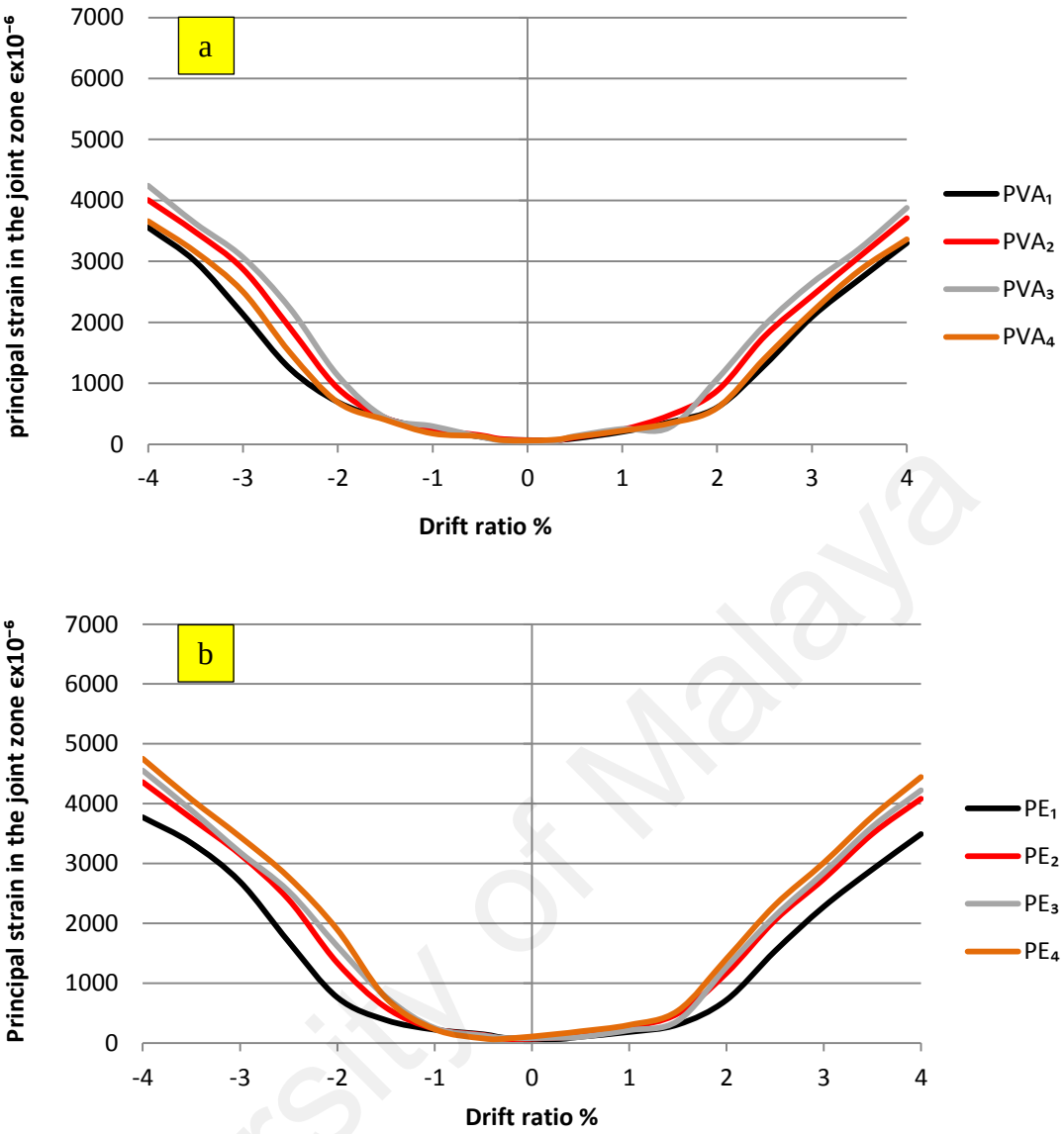

Figure 4.96: Effect of the reinforcing index on the principal strain values in (a) ECC-PVA joints (b) ECC-PE joints

d) Effect of lateral steel hoops inclusion in ECC joint zone

Figure 4.97 shows the effect of the lateral steel hoops inclusion in the joint zone on the principal strain results of the both groups of ECC-PVA and ECC-PE joints. Referring to the Figures 4.31, 4.34, 4.35, 4.37, 4.40 and 4.41, all the joints of both groups failed in a ductile manner. For the ECC-PVA group, PVA_2 showed the lowest result of principal strain values which denotes the lowest level of ductility in the ECC-PVA group (as shown in Figure 4.97a) due to the zero inclusion of steel hoops, while for the PVA_6 joint with two hoops inclusion, showed the highest result of the principal strain values

which denotes the highest level of ductility in the group. For the PE group, PE_2 showed the lowest result of principal strain values which denotes the lowest level of ductility in the ECC-PE group (as shown in Figure 4.97b) due to the zero inclusion of steel hoops, while the PE_6 joint showed the highest result of principal strain values which denotes the highest level of ductility in the PE group due to the inclusion of two hoops. Due to the remarkable performance of the ECC-PE joints, the PE_5 and PE_6 joints in Figure 4.98 showed higher result of principal strain values compared to the corresponding results of PVA_5 and PVA_6 joints, respectively.

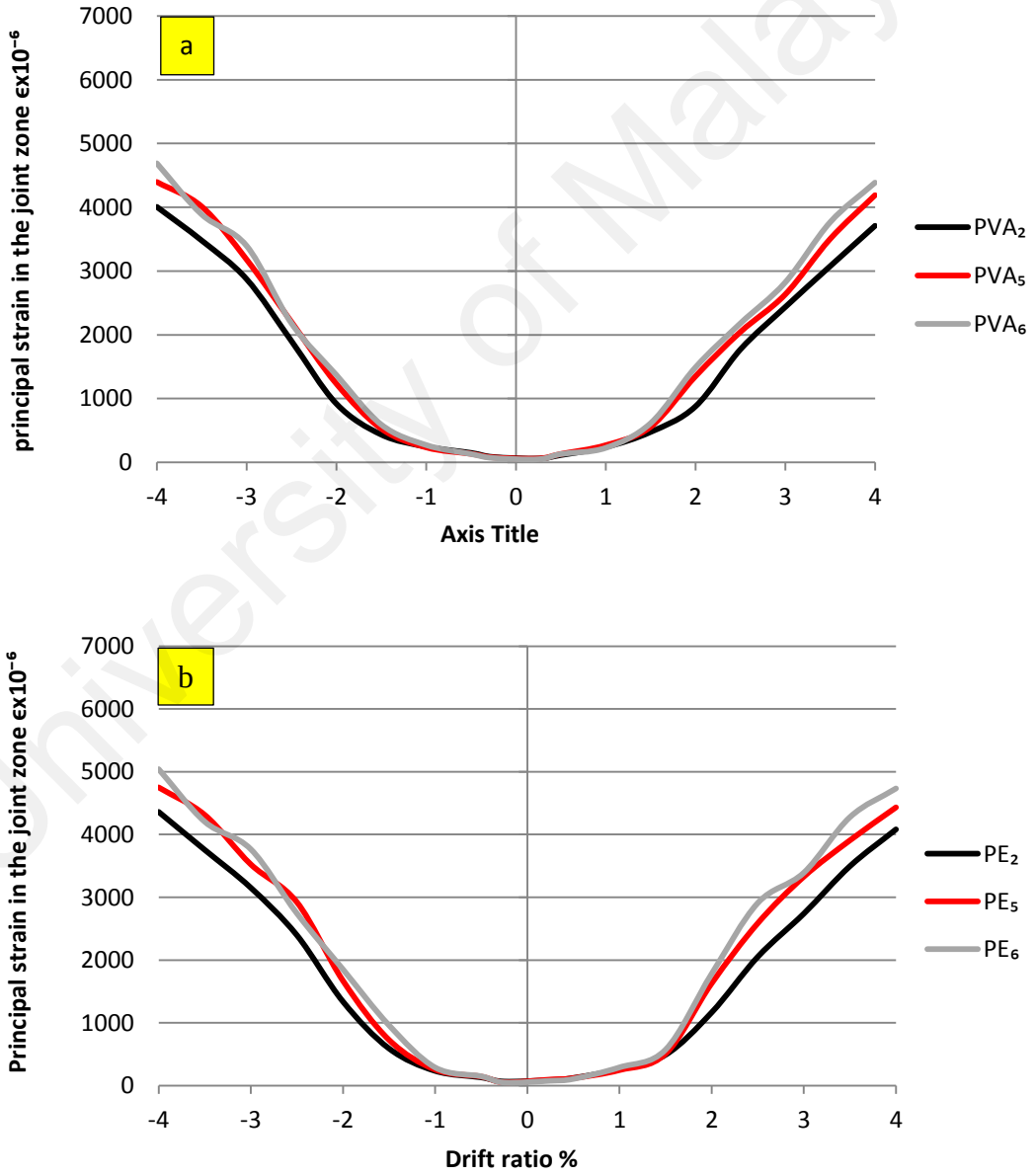

Figure 4.97: Effect of the lateral reinforcement inclusion in the joint zone on the principal strain values in (a) ECC-PVA joints (b) ECC-PE joints

4.4.8 Shear deformation

Shear rotation angle of the joint zone was calculated depending on the strain values on the diagonals of the joint, as shown in the Figure 3.12, and the equations given in Section 3.4.11.

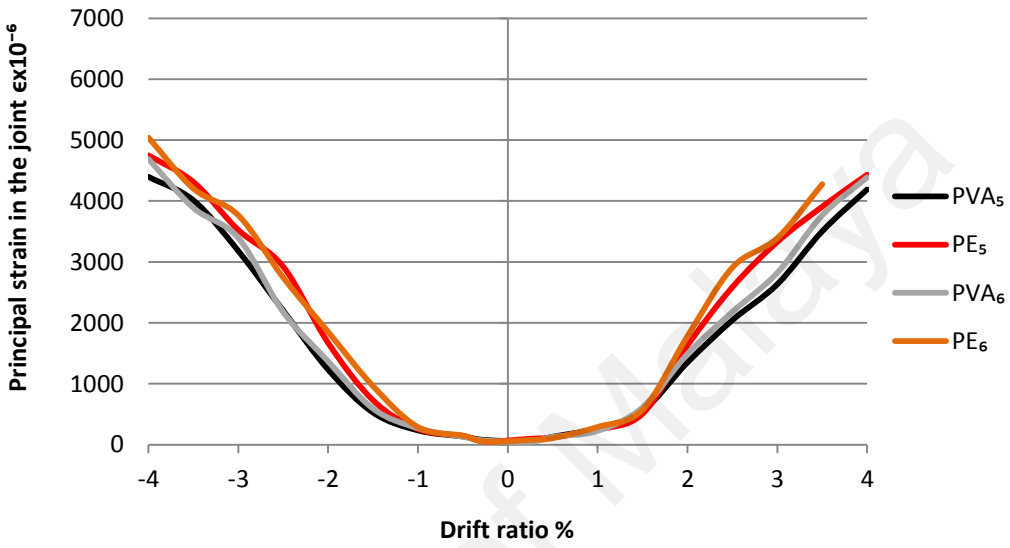

Figure 4.98: Effect of type of ECC with the inclusion of lateral reinforcement in the joint zone on the principal strain results

a) Effect of the ECC inclusion in the joint zone

As shown in Figure 4.99, the brittle mode of failure in the NC_1 joint (without steel hoops in the joint zone) led to an excessive amount of shear rotation angle within the joint zone at the early stage of loading which is the highest value among all the specimens. For the group of NC_2, PVA_1 and PE_1 ductile joints, the denser crack network, the higher shear rotation angle. Figure 4.99 shows higher amount of shear rotation for PE_1 joint (of the lowest R.I) than the corresponding amount of shear rotation for the NC_2 and PVA_1 (of the lowest R.I) due to the higher density of the cracks propagated in the joint zone which denotes perfect ductility and damage tolerance. In contrast, the NC_2 joint shows lower amount of shear rotation due to the lower density of the cracks propagated in the joint zone which denotes lower ductility.

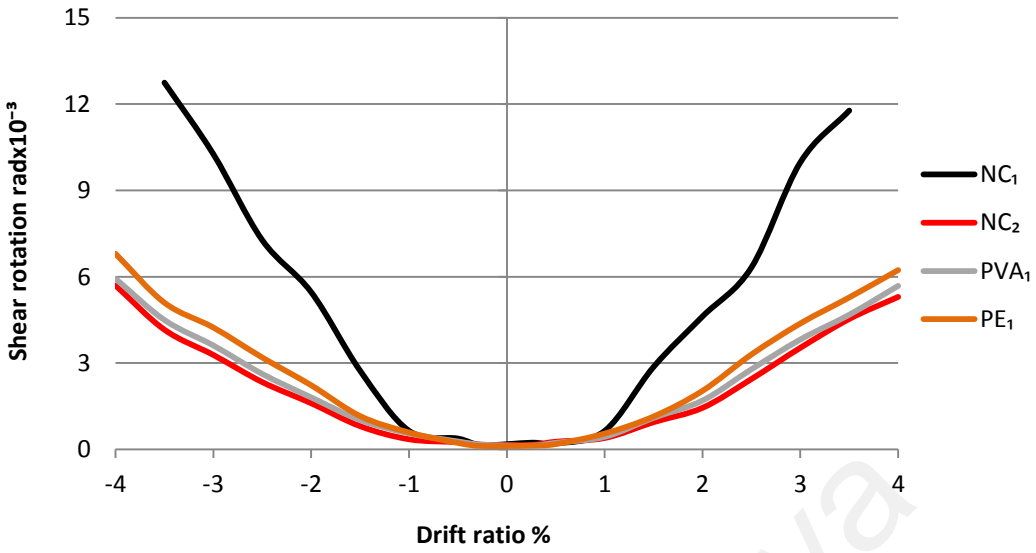

Figure 4.99: Effect of the ECC inclusion in the joint zone on the shear rotation results

b) Effect of type of ECC in the joint zone

Figure 4.100 shows the shear rotation results for the both groups of ECC joints represented in PVA_2, PE_2, PVA_3 and PE_3 joints. For the same R.I value, and due to the higher density of cracks propagated in the ECC-PE joint zone, PE_2 and PE_3 joints showed higher amount of shear rotation compared to the corresponding amount of shear rotation value for PVA_2 and PVA_3 joints, respectively, which showed a reduced amount of shear rotation due to the lower density of the cracks propagated in the joint zone. It is inferred that the ECC-PE joints have higher performance characteristics compared to the ECC-PVA joints.

c) Effect of polymer fibers reinforcing index

Figure 4.101 shows the effect of the reinforcing index on the shear rotation results of the both groups of ECC-PVA and ECC-PE joints. For ECC-PVA group, the PVA_1 joint, with the lowest reinforcing index, showed the lowest values of shear rotation in the group due to the lower crack density propagated in the joint zone, as shown in Figure

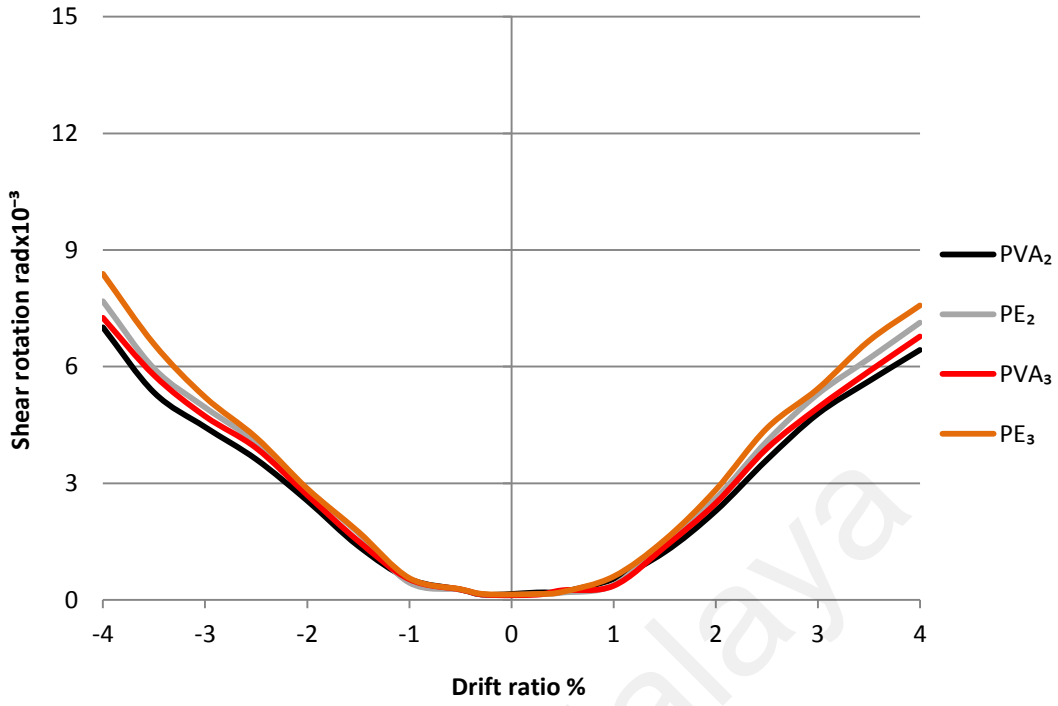

Figure 4.100: Effect of type of ECC in the joint zone on the shear rotation results

4.101a, despite the highest reinforcing index of PVA_4 joint, PVA_3 showed the highest values of shear rotation in the group which denotes the highest crack density in the joint zone due to the high fiber content in the ECC mix of PVA_4 joint led to a non-uniform dispersion. For the ECC-PE group, the PE_1 joint, with the lowest reinforcing index, showed the lowest values of shear rotation in the group while the PE_4 joint, with the highest reinforcing index, showed the highest values of shear rotation in the group, as shown in Figure 4.101b. It is inferred that the increase in the R.I led to an increase in the shear rotation values which improved the ductility and damage tolerance of the joint.

d) Effect of the lateral steel hoops inclusion in ECC joint zone

Figure 4.102 shows the effect of the lateral steel hoops inclusion in the ECC joint zone on the shear rotation results of the both groups of ECC-PVA and ECC-PE joints. For the ECC- PVA group, the PVA_5 and PVA_6 joints (with 1 and 2 hoops in the joint zone)

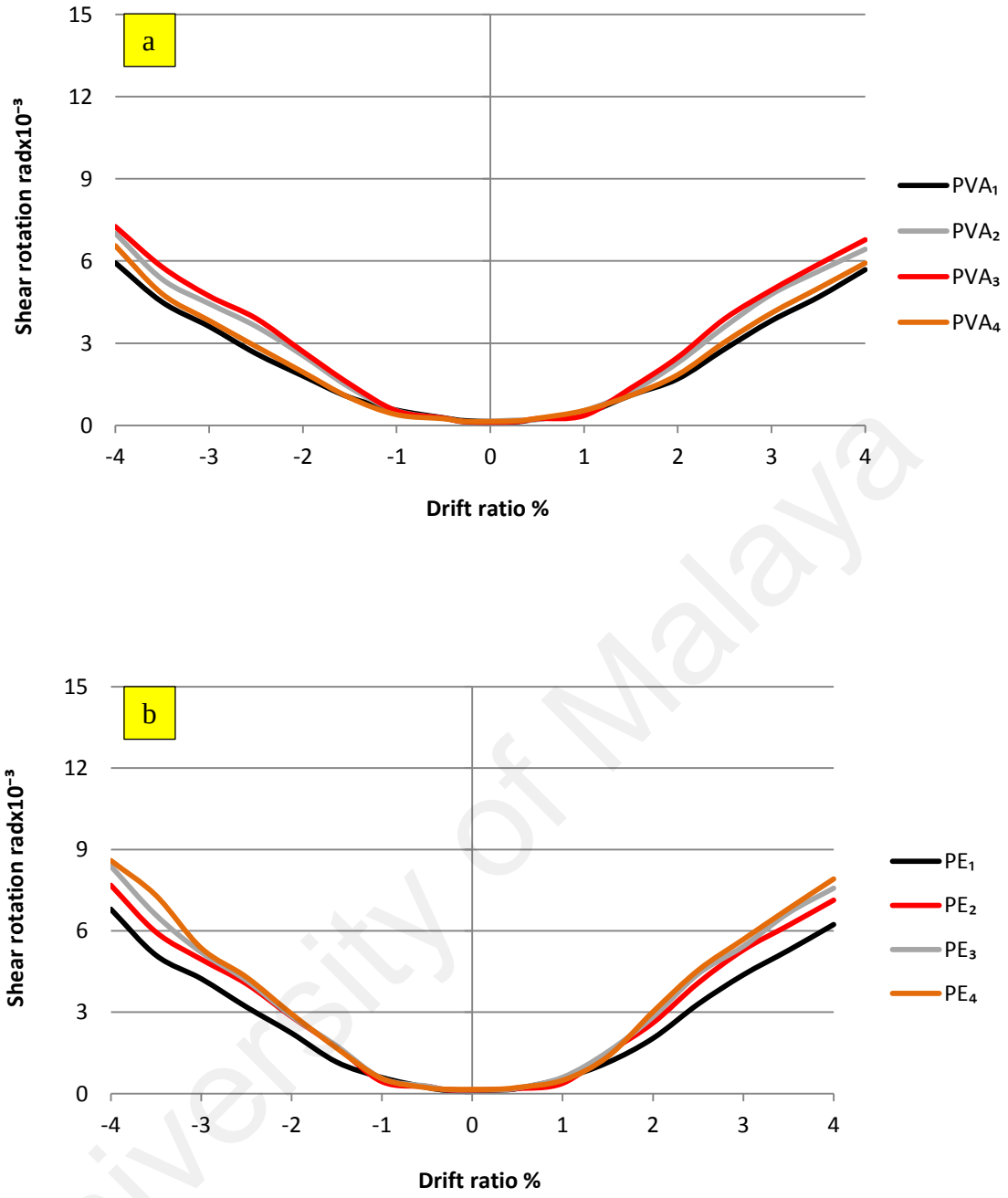

Figure 4.101: Effect of the reinforcing index on the shear rotation results in (a) ECC-PVA joints (b) ECC-PE joints

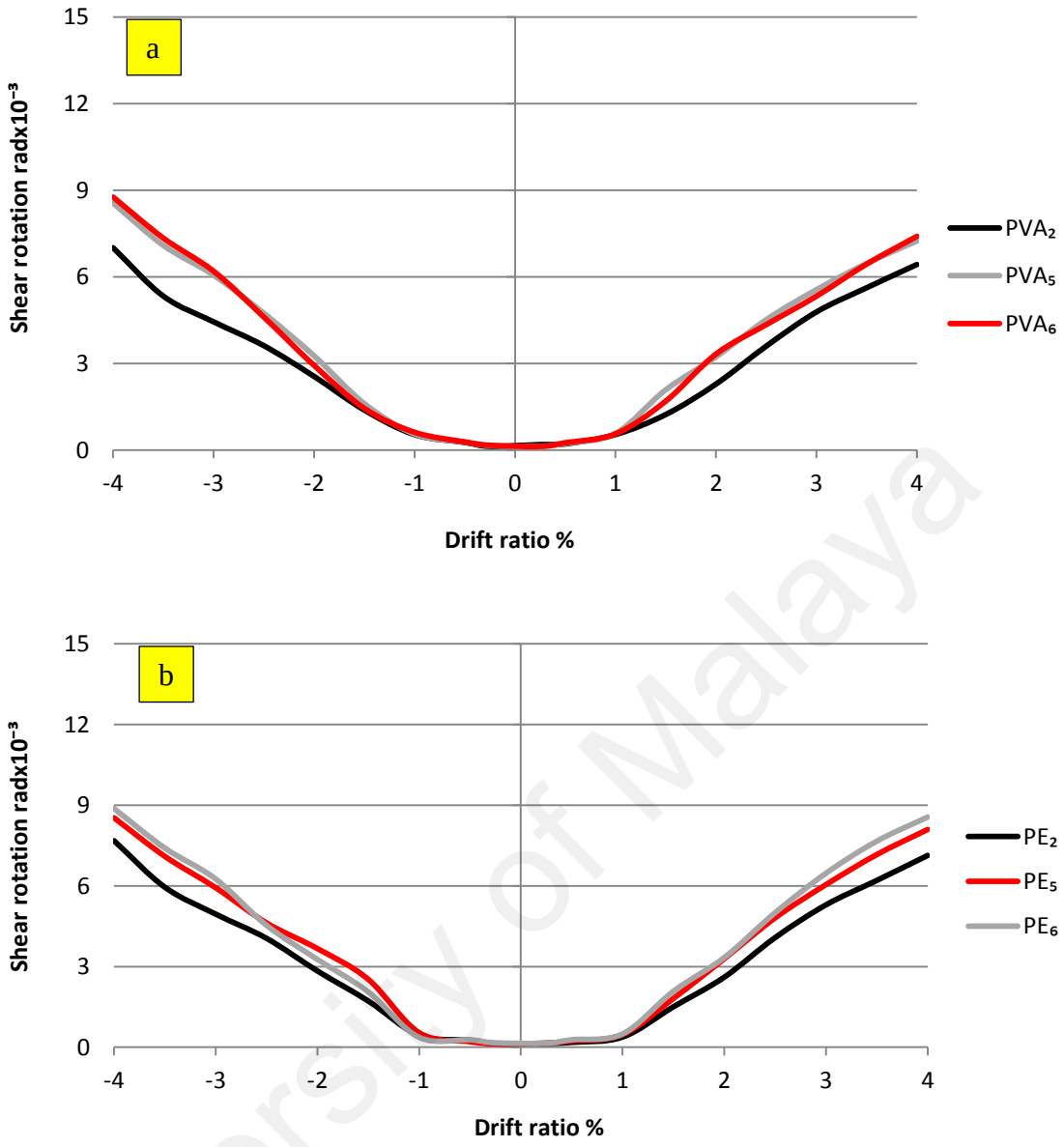

Figure 4.102: Effect of the lateral reinforcement inclusion in the joint zone on the shear rotation results in (a) ECC-PVA joints (b) ECC-PE joints

showed higher results of shear rotation compared to the corresponding results for PVA_2 joint, as shown in Figure 4.102a, due to the lateral steel hoops inclusion in the joint zone. Moreover, PE_5 and PE_6 showed higher results of shear rotation compared to the corresponding results for the PE_2 joint, as shown in Figure 4.102b, due to the steel hoops inclusion in the joint zone. Besides, the first hoop inclusion in the joint zone significantly enhanced the shear rotation amount. However, the second hoop inclusion enhanced the shear rotation to a limited extent. Due to the better performance of ECC-

PE joints, Figure 4.103 shows higher shear rotation results for PE_5 and PE_6 compared to the corresponding results for the PVA_5 and PVA_6 joints especially at the positive part of the drift ratio.

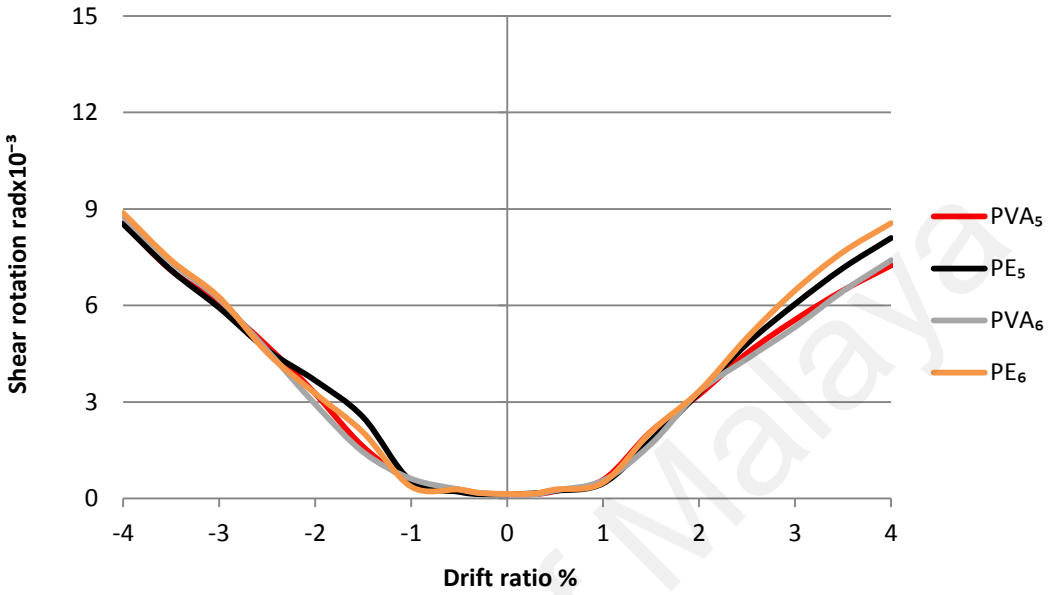

Figure 4.103: Effect of type of ECC with the inclusion of lateral reinforcement in the joint zone on the shear rotation results

4.4.9 Strain distribution

Strain values were recorded from the strain gauges installed on the beam longitudinal steel bars. Due to the sensitivity of the strain gauges, the strain values recorded after 4% of drift ratio are not acceptable when the small cracks start to widen for most of the beam-column specimens. Therefore, the comparison among the beam-column specimens is based on the strain distribution values recorded until the drift ratio of 4%, except for NC_1 specimen, the strain values are acceptable until 3% of drift ratio due to the severity of premature cracks.

4.4.9.1 Normal concrete specimens

Figure 4.104 indicates the strain values for NC_1 specimen along the beam longitudinal steel bars within the beam and the joint zone. It is observed a fluctuation in the strain

distribution along the longitudinal steel bars due to premature cracks developed in the joint zone with widening of the cracks in early stages of loading, as shown in Figure 4.104. In addition, the vulnerability of the joint due to the absence of the lateral steel hoops in the joint zone caused irregular load redistribution in the beam and the joint zone which caused high fluctuation in the strain values. In contrast, the lateral steel hoops inclusion and the confinement of concrete core in the NC_2 joint zone modified the load distribution at the beam and joint zone which led to a better strain distribution along the steel bars, as shown in Figure 4.105. In addition, the yielding of steel bars in NC_1 specimen occurred at 2% of the drift ratio while in NC_2 specimen occurred at 3% of the drift ratio. Table 4.4 shows an average of maximum strain values, in positive and negative direction of loading, of 4451$\mu\epsilon$ was recorded on beam longitudinal steel bars for the NC_1 specimen inside the joint zone at drift ratio of 3% while an average of maximum strain values of 3841$\mu\epsilon$ was recorded on longitudinal steel bars for the NC_2 specimen on the interface surface of the beam and joint at the drift ratio of 4%.

4.4.9.2 ECC specimens

Generally, due to the high performance of ECC and its contribution in enhancing the shear capacity of beam-column joint, the joint is quite robust to redistribute the load in the beam and the joint zone uniformly. In addition, the crack bridging mechanism characteristics and the perfect ductility enabled the ECC specimens to regulate and reduce the strain values in the steel bars and transfer the yielding point of steel bars to the later stage of loading. Figures 4.106 to 4.117 indicate a regular distribution of the strain values along the longitudinal steel bars in ECC specimens at different levels of loading from the early stages until 4% of the drift ratio. The consistent deformation between the steel bars and the surrounding ECC is a function of high homogeneous bond developed at the interfacial surface of steel bars and ECC. Table 4.4 indicates

Table 4.4: Strain values along the beam longitudinal steel bars

Type of specimens	Symbol of specimen	Drift ratio at which the yielding of longitudinal steel bars occurs %	Maximum strain* value at drift ratio of 3% με	Reduction in the strain value at 3% of drift ratio compared to NC_1 %	Maximum strain* value at drift ratio of 4% με	Position of maximum strain value along the beam longitudinal steel bars
NC	NC_1	2	4451	-	-	Inside the joint zone⁺
	NC_2	3	2737	38	3841	Inside the joint zone⁻ Inside the joint zone⁺ Interfacial surface⁻
ECC-PVA specimens	PVA_1	3	3183	28	4236	At the face of column⁺ Interfacial surface⁻
	PVA_2	3	2881	35	3977	At the face of column⁺ Inside the joint zone⁻
	PVA_3	2.5	2876	35	3755	At the face of column⁺ Interfacial surface⁻
	PVA_4	3	2850	36	3862	At the face of column⁺ At the face of column⁻
	PVA_5	2.5	3060	31	4063	Inside the joint zone⁺ Inside the joint zone⁻
	PVA_6	3	2847	36	3782	Inside the joint zone⁺ At the face of column⁻
ECC-PE specimens	PE_1	3	2878	35	3141	Interfacial surface⁺ At the face of column⁻
	PE_2	3	2599	42	3008	Interfacial surface⁺ At the face of column⁻
	PE_3	3	2342	47	3595	Inside the joint zone⁺ Inside the joint zone⁻
	PE_4	3	2615	41	3552	At the face of column⁺ Inside the joint zone⁻
	PE_5	3	2871	35	3845	Inside the joint zone⁺ Interfacial surface⁻
	PE_6	3	2847	36	3573	At the face of column⁺ Interfacial surface⁻

⁺ Positive direction of loading
⁻ Negative direction of loading
*Average value of two directions

the results of the average of maximum strain values along the beam longitudinal steel bars for both drift ratios of 3% and 4%. The results are compared to the normal concrete specimen at 3% of drift ratio and significant reductions in strains are observed in the other specimens. Based on the steel bars strain results, several main points were inferred:

1. For NC_1 specimen, the yielding of beam longitudinal steel bars occurred at the drift ratio of 2% while the yielding in NC_2 specimen occurred at the drift ratio of

3%. A reduction in strain value was observed in NC_2 of about 38% compared to NC_1 due to the confinement of concrete in the joint zone

2. For ECC-PVA specimens, the yielding of beam longitudinal steel bars occurred at the drift ratio of 2.5 or 3%, while the yielding of beam longitudinal steel bars for ECC-PE specimens occurred at the drift ratio of 3%.
3. For ECC-PVA specimens, an average value of strain reduction, compared to NC_1 specimen, was recorded of about 34% while an average of strain reduction value of about 39% for ECC-PE specimens was recorded.
4. For ECC-PVA specimens, Table 4.4 shows an average of maximum strain values of longitudinal steel bars, until 4% of the drift ratio, range from 3800 to 4250 με while the corresponding values of the maximum strain for ECC-PE specimens range from 3000 to 3850.

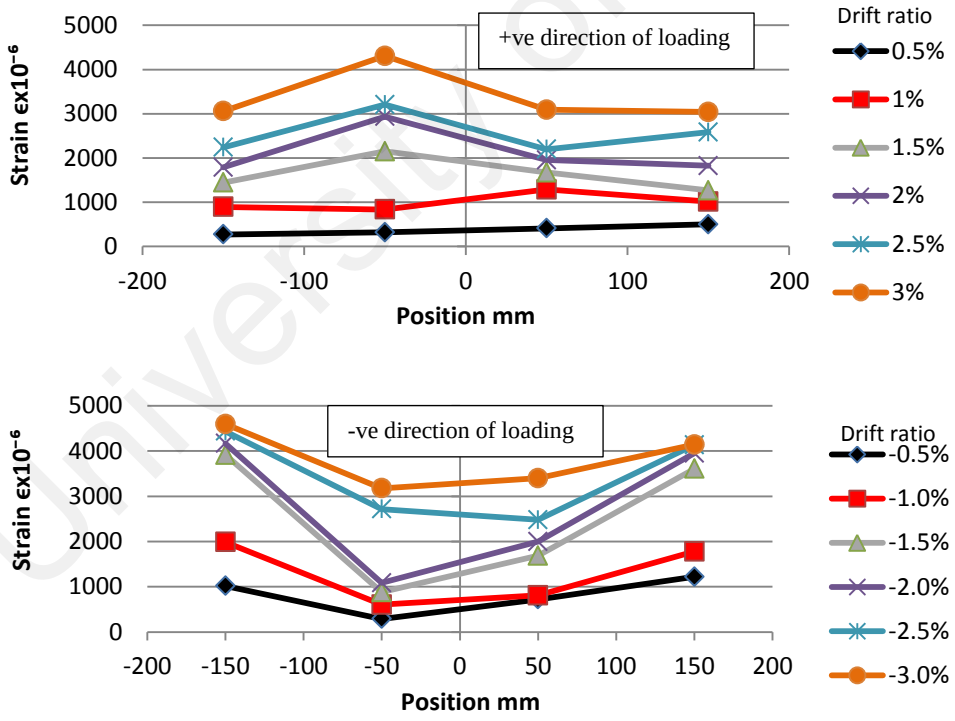

Figure 4.104: Strain distribution along beam longitudinal steel bars for NC_1 specimen

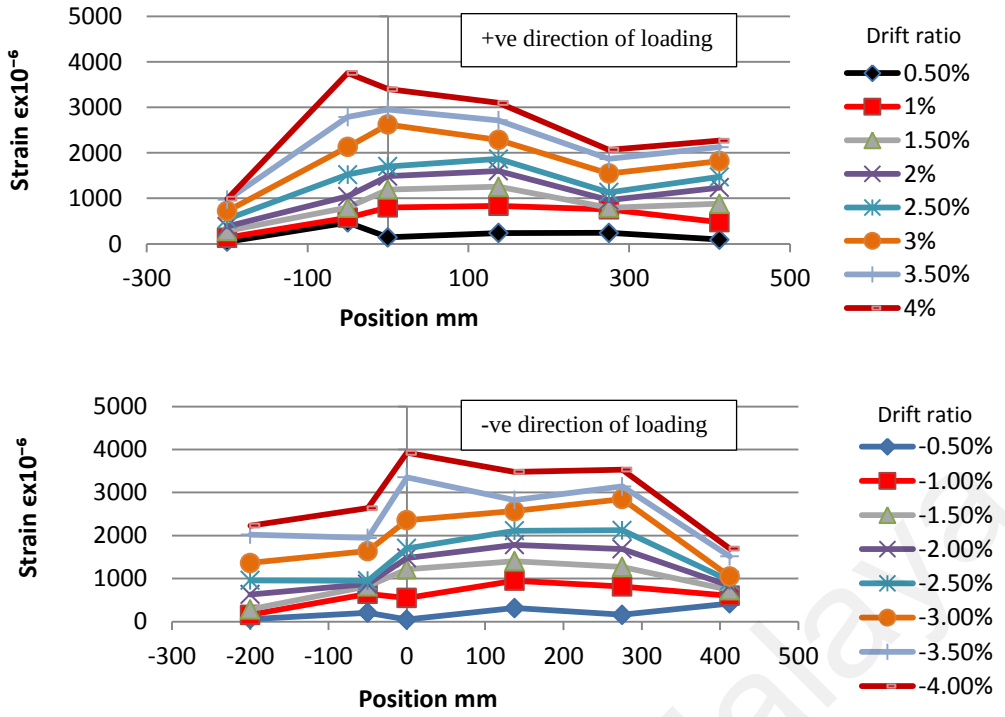

Figure 4.105: Strain distribution along beam longitudinal steel bars for NC_2 specimen

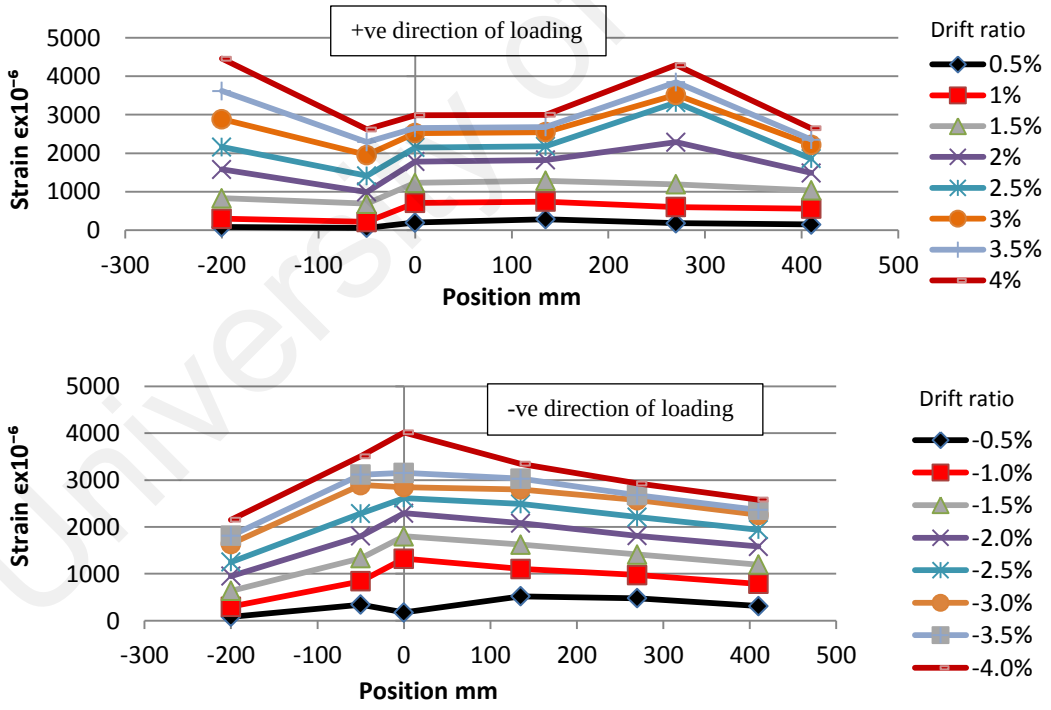

Figure 4.106: Strain distribution along beam longitudinal steel bars for PVA_1 specimen

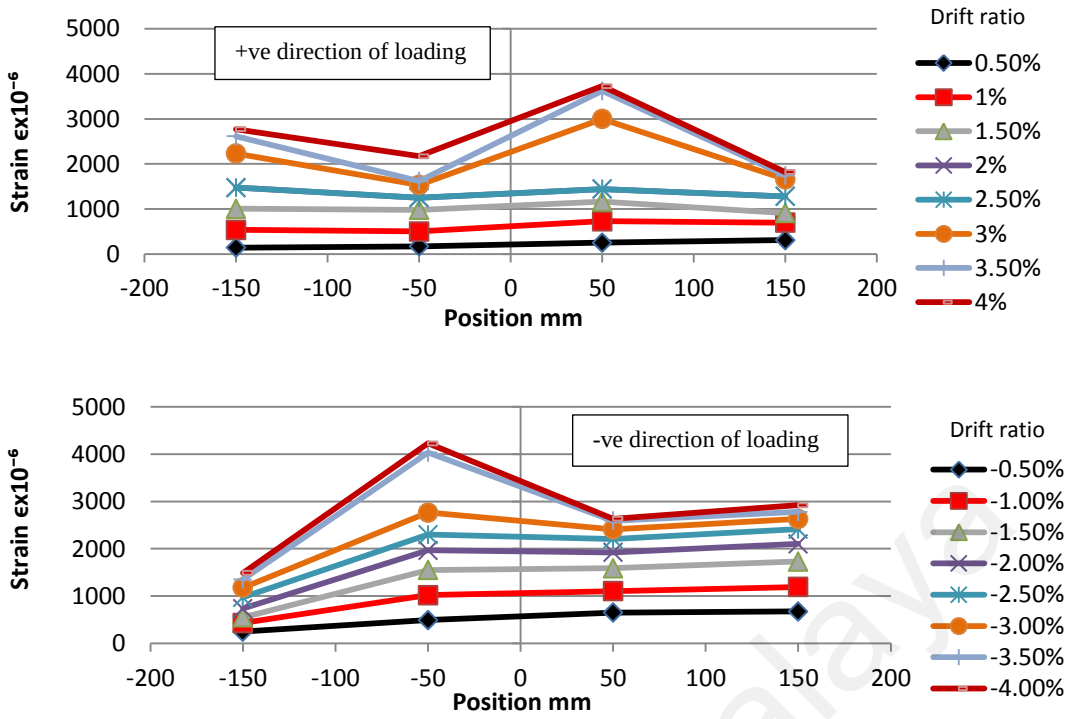

Figure 4.107: Strain distribution along beam longitudinal steel bars for PVA_2 specimen

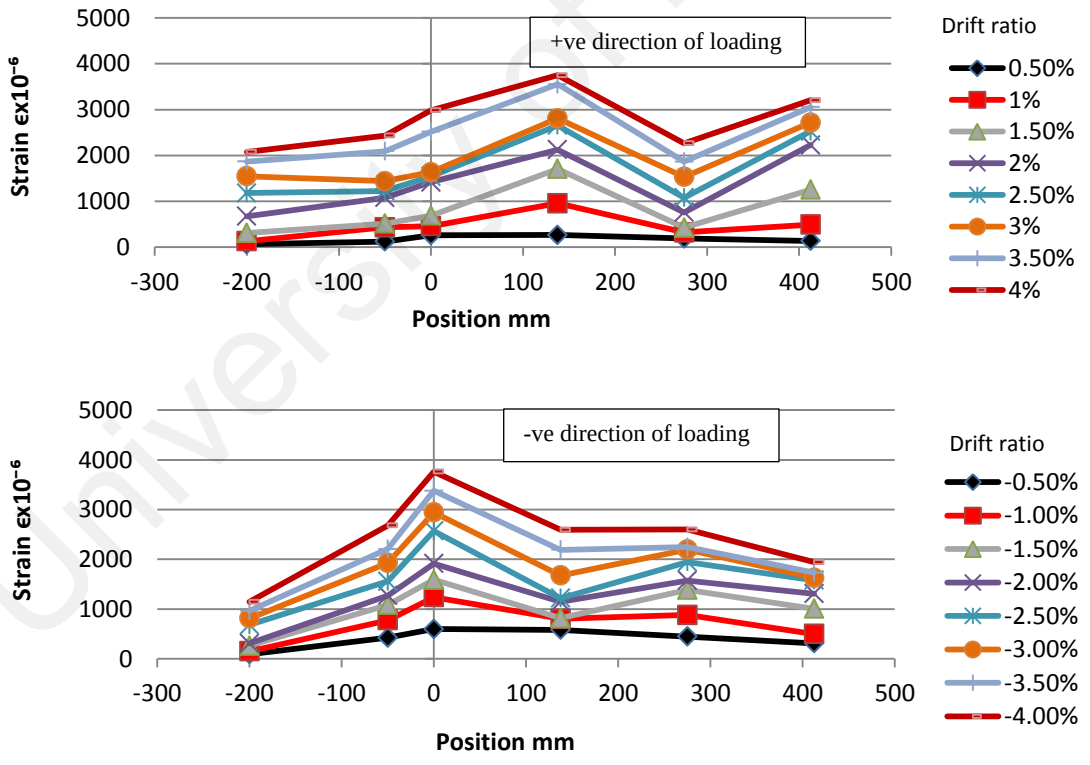

Figure 4.108: Strain distribution along beam longitudinal steel bars for PVA_3 specimen

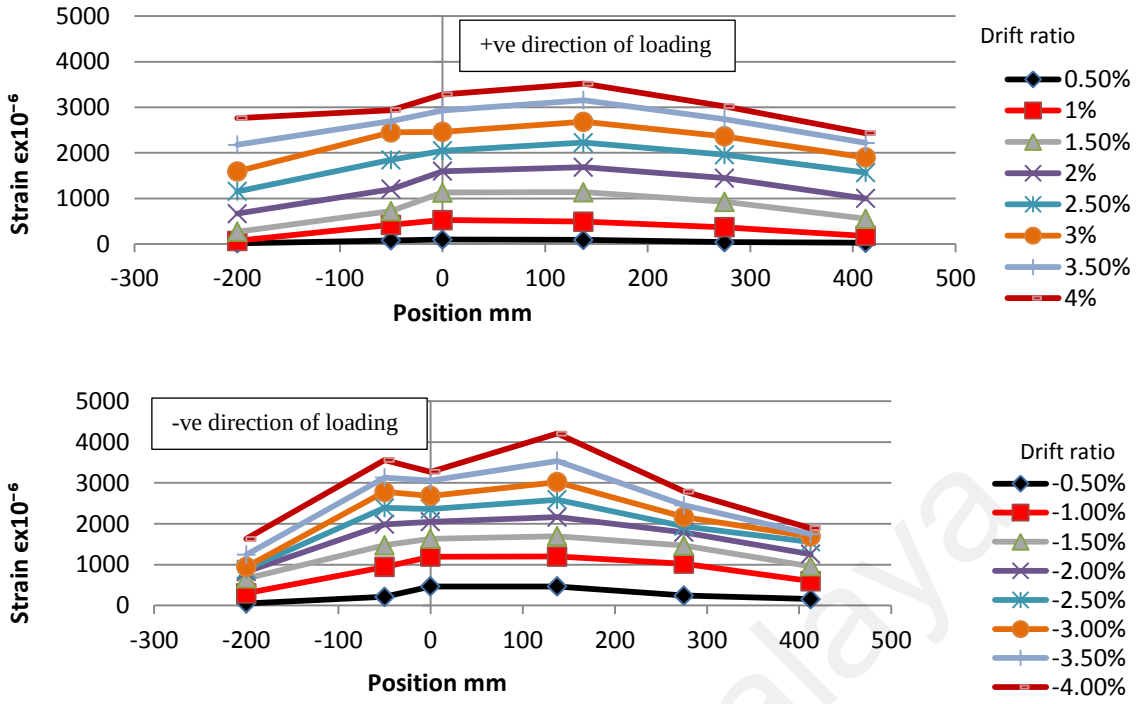

Figure 4.109: Strain distribution along beam longitudinal steel bars for PVA_4 specimen

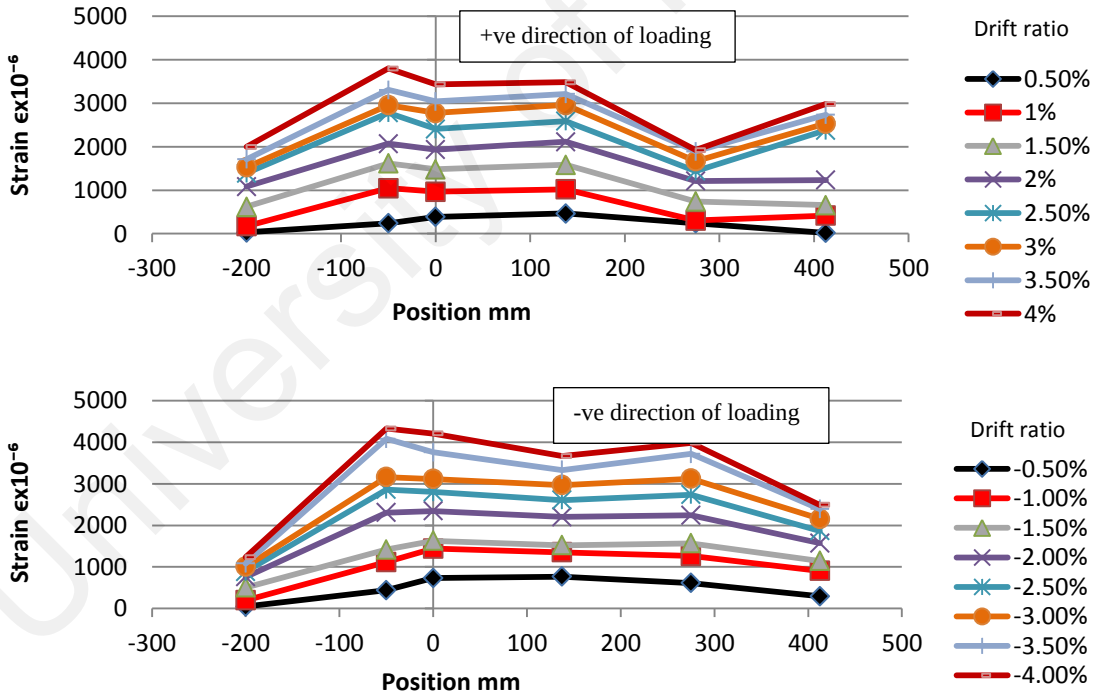

Figure 4.110: Strain distribution along beam longitudinal steel bars for PVA_5 specimen

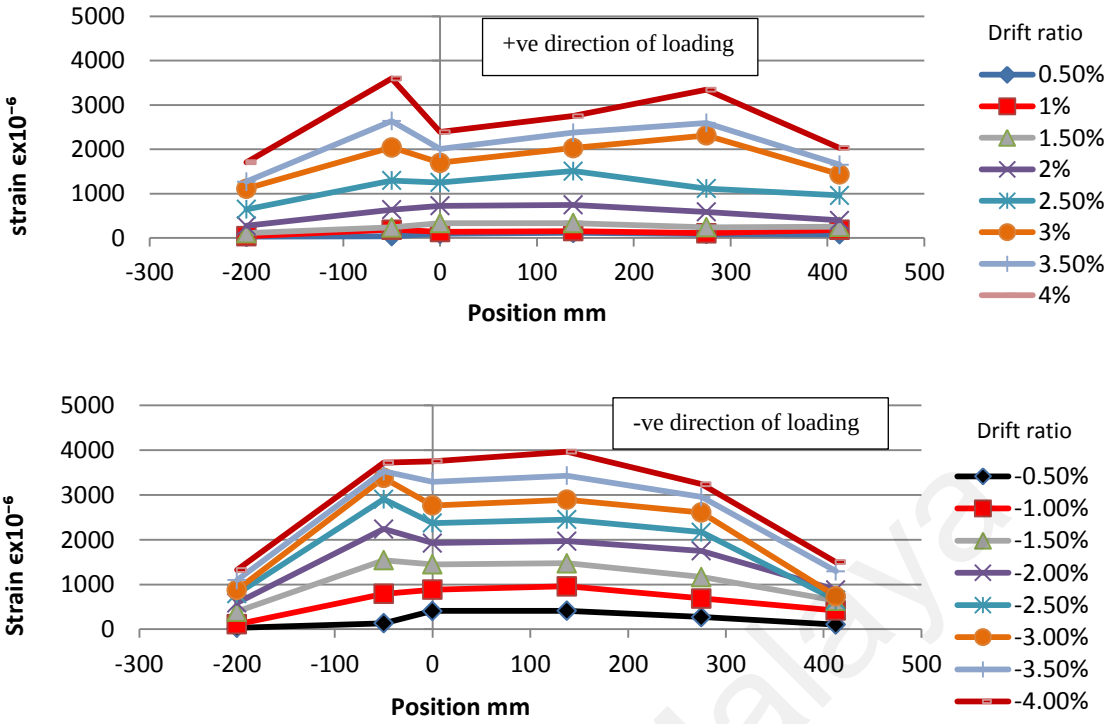

Figure 4.111: Strain distribution along beam longitudinal steel bars for PVA_6 specimen

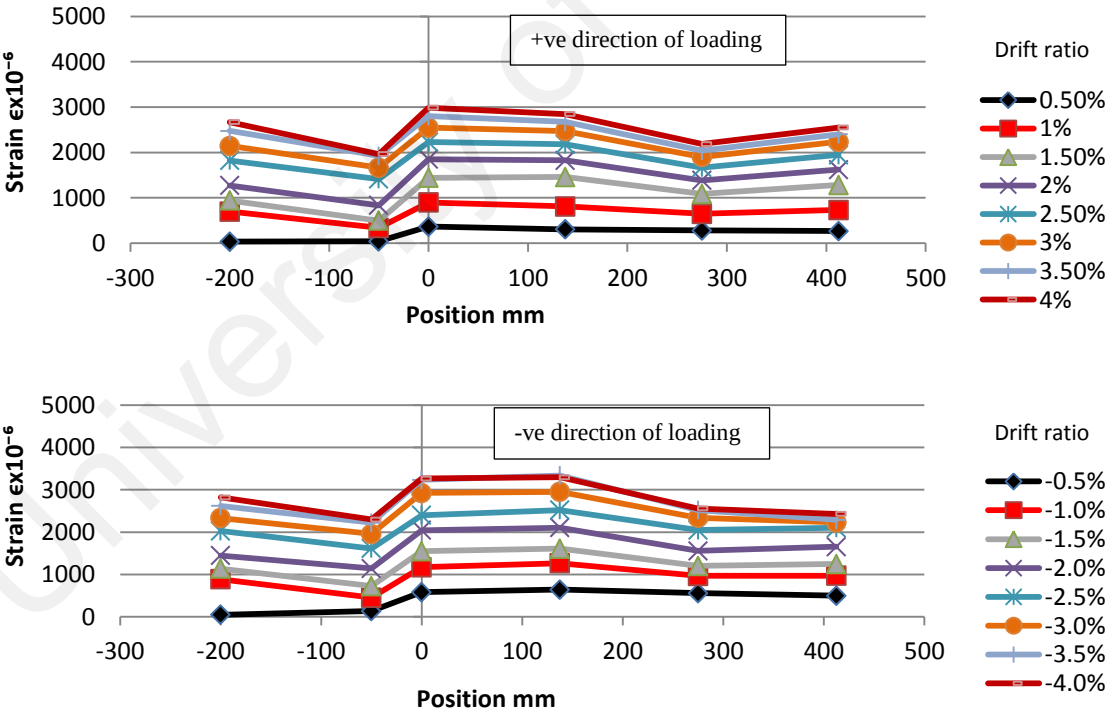

Figure 4.112: Strain distribution along beam longitudinal steel bars for PE_1 specimen

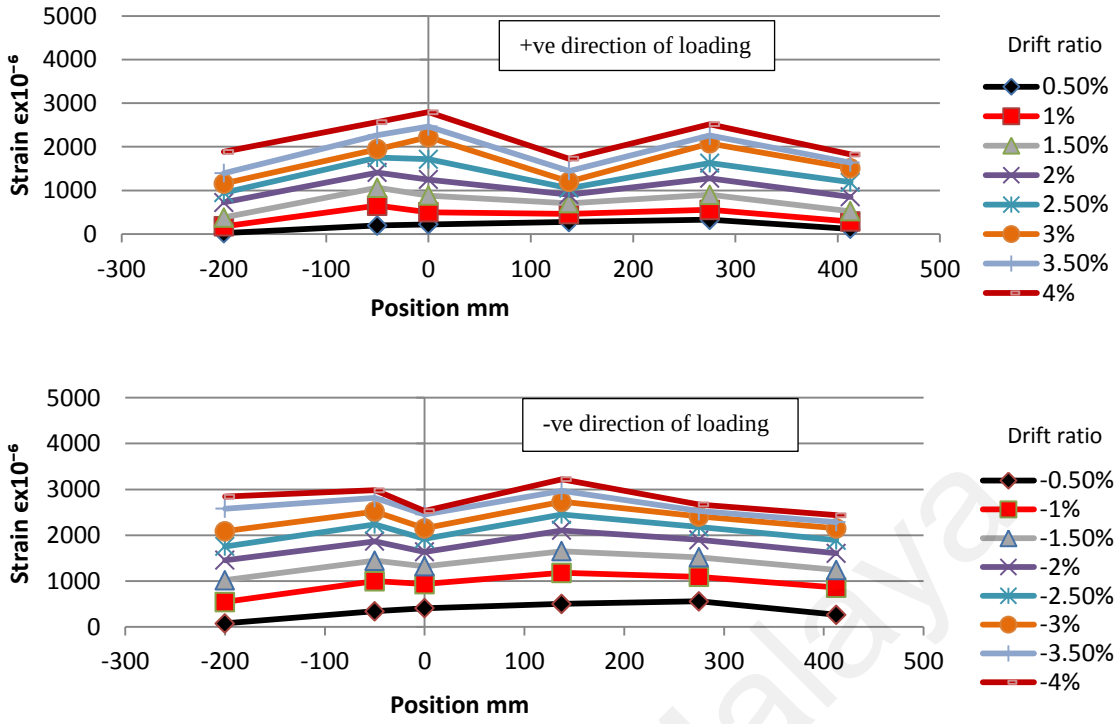

Figure 4.113: Strain distribution along beam longitudinal steel bars for PE_2 specimen

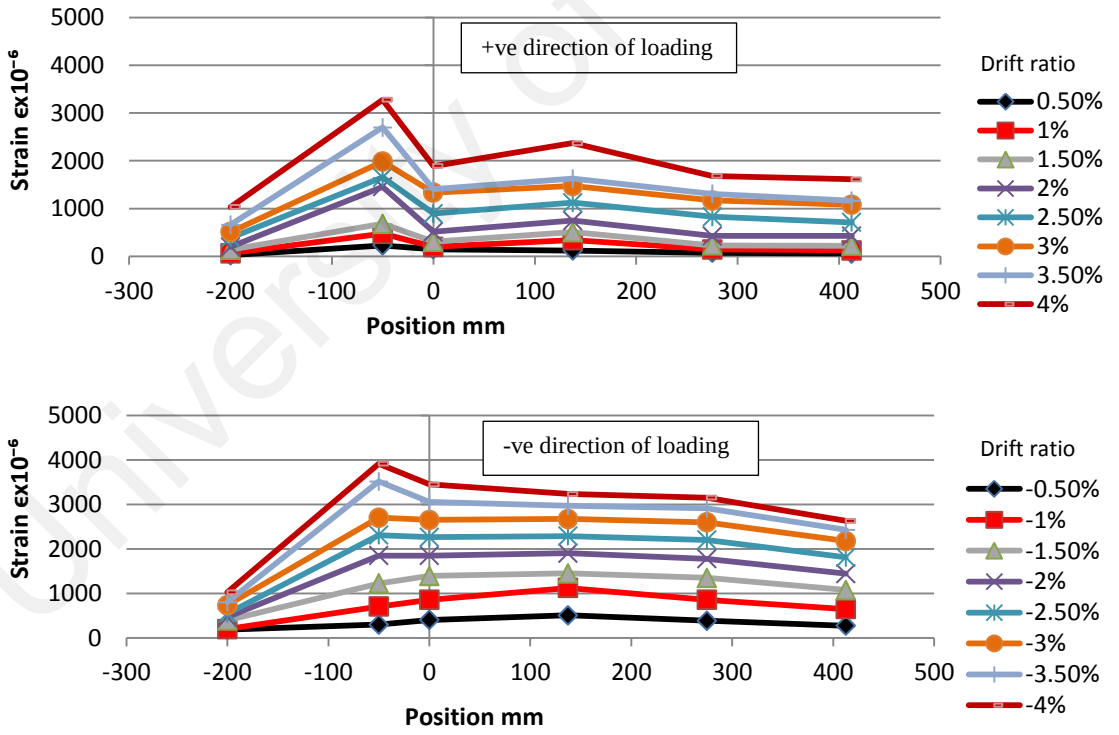

Figure 4.114: Strain distribution along beam longitudinal steel bars for PE_3 specimen

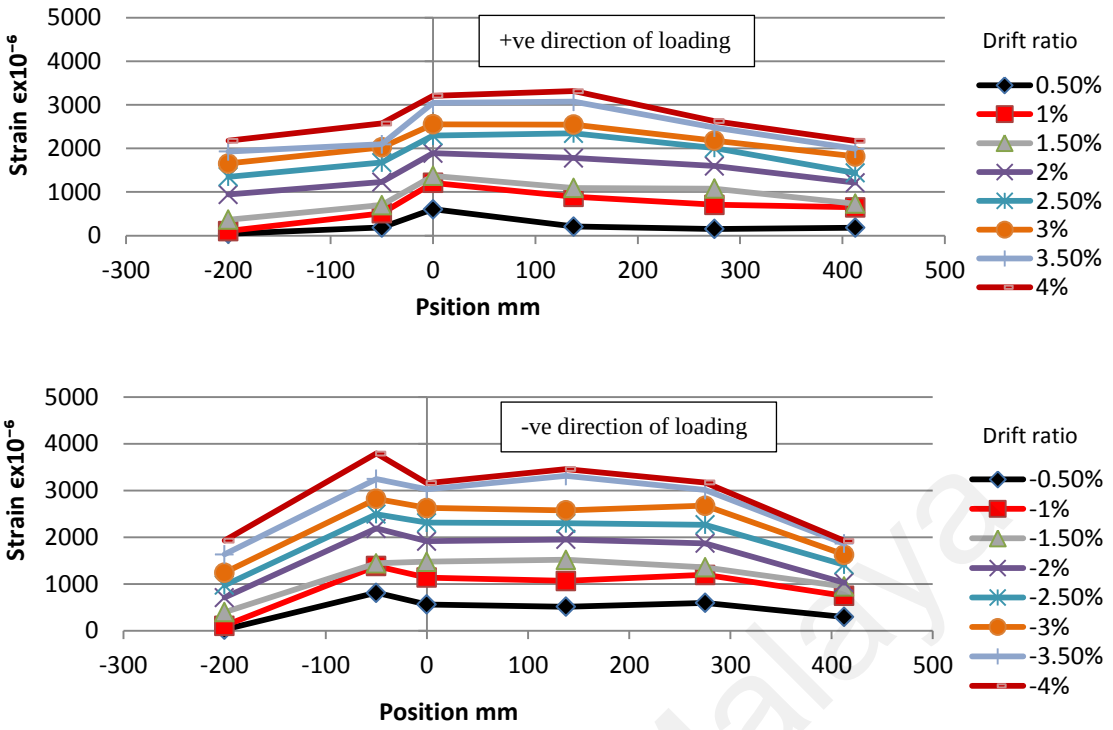

Figure 4.115: Strain distribution along beam longitudinal steel bars for PE_4 specimen

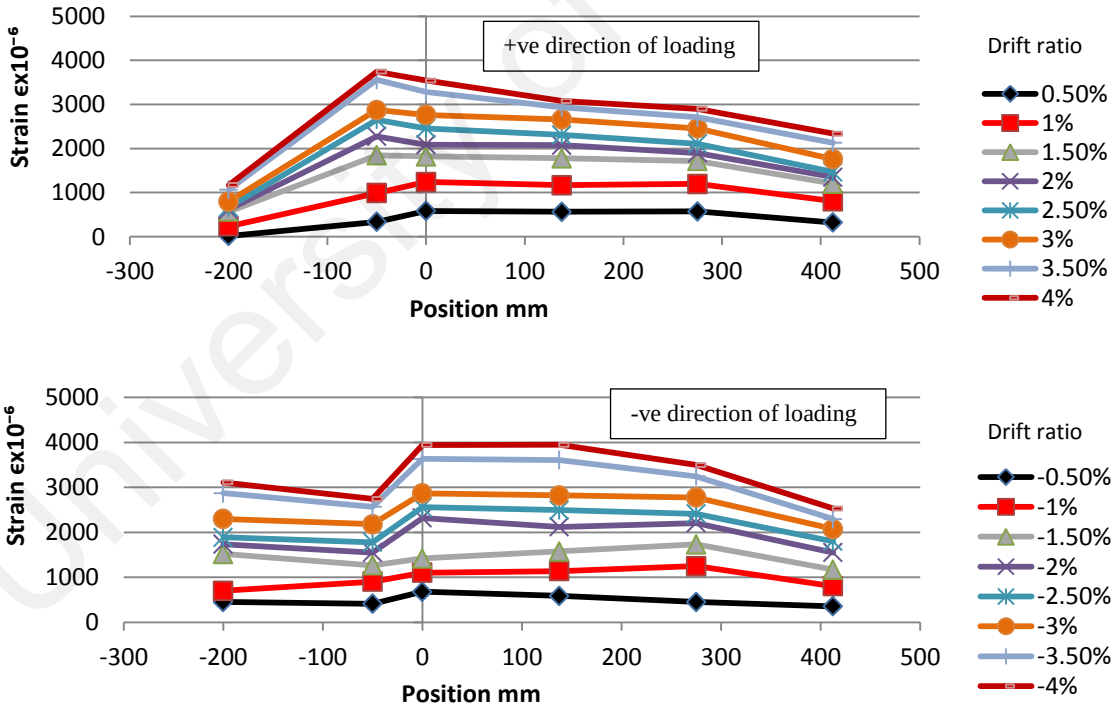

Figure 4.116: Strain distribution along beam longitudinal steel bars for PE_5 specimen

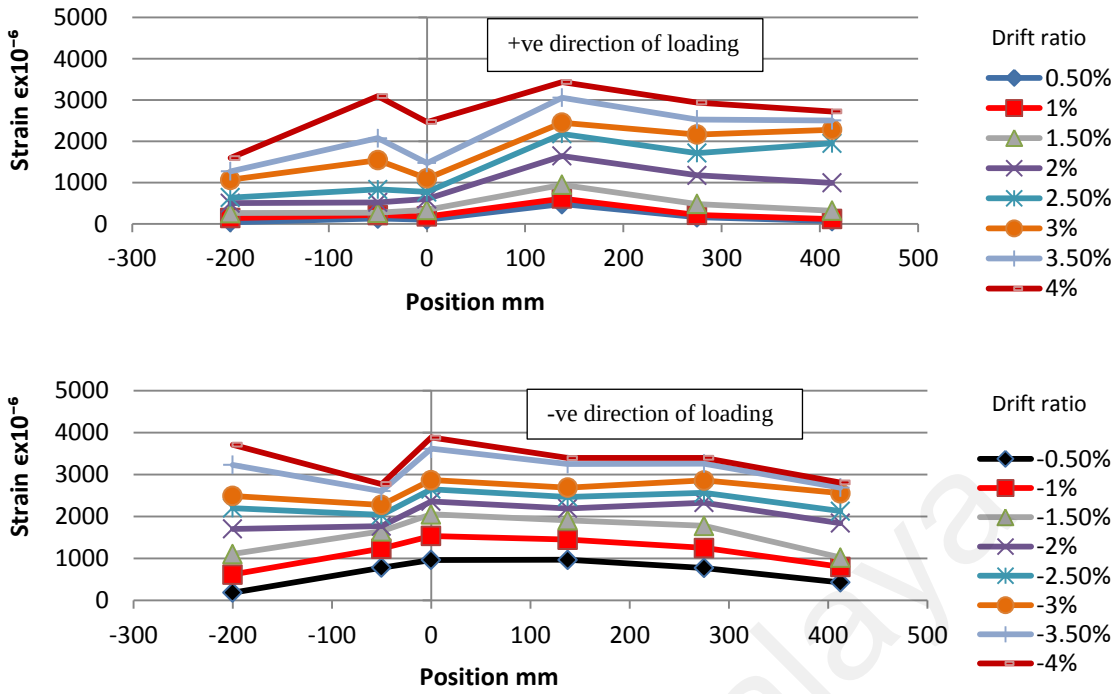

Figure 4.117: Strain distribution along beam longitudinal steel bars for PE_6 specimen

5. The distribution of the longitudinal steel bars strain values for the ECC-PE specimens is more uniform compared to the distribution of the corresponding values for the ECC-PVA specimens.

4.4.10 Cumulative energy absorption

For the same size and reinforcement details of structures, the cumulative energy absorption capacity from the early stage of loading until failure is a function to the ductility of the structure. As reported in the literature (Yuan et al., 2013; Zhang et al., 2015), the amount of absorbed energy is calculated from the areas encompassed by the hysteresis loops of load–deflection relationship, which is the whole energy absorbed by the structure (Zhang et al,2015). In this section, the absorbed energy was evaluated for the joint zone only and directly from the moment–rotation loops.

a) Effect of lateral steel hoops in normal concrete (NC) joints

For NC_1 and NC_2 specimens, the behavior of the cumulative energy absorption curves is identical until the stage 3% of the drift ratio, as shown in Figure 4.118. After this stage, the amount of energy absorption starts to increase in the NC_2 joint due to the effect of lateral steel hoops in the joint zone while the cumulative energy absorption curve in the NC_1 specimen starts to deviate and descends indicating the failure of joint at 4.5% of drift ratio. The increase in the cumulative energy absorption of NC_2 specimen until failure is 64.6% (as shown in Figure 4.119) more than the corresponding value of cumulative energy absorption for NC_1 which denotes higher ductility of NC_2 specimen.

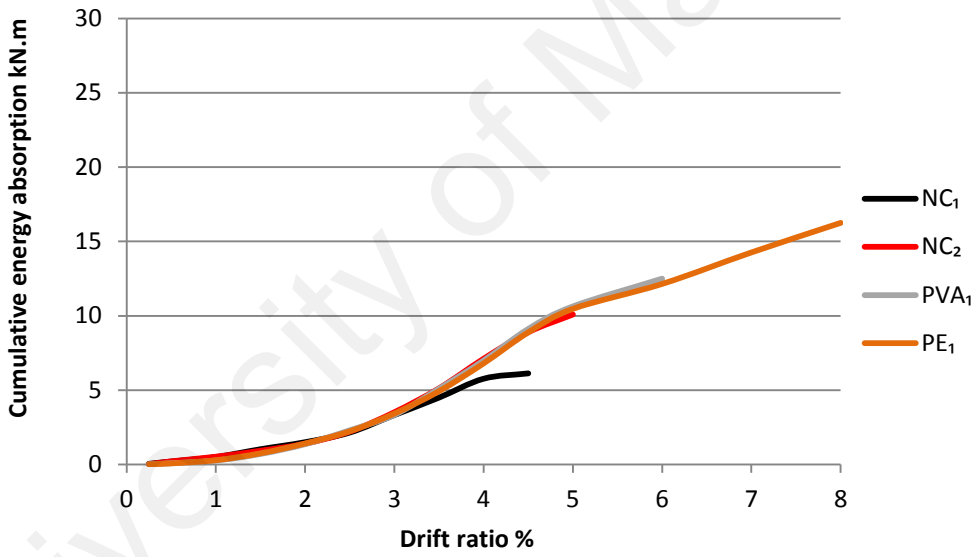

Figure 4.118: cumulative energy absorption in NC_1, NC_2, PVA_1 and PE_1 specimens

b) Effect of the ECC inclusion in the joint zone

Based on Figure 4.118, an infinitesimal amount of increase was in the cumulative energy absorption of the NC_1 and NC_2 joints more than in the PVA_1 and PE_1 joints at the early stages of loading until the drift ratio of 1.5% owing to the higher E modulus for the NC_1 and NC_2 joints. After the 1.5% drift ratio stage, the polymer fibers in the

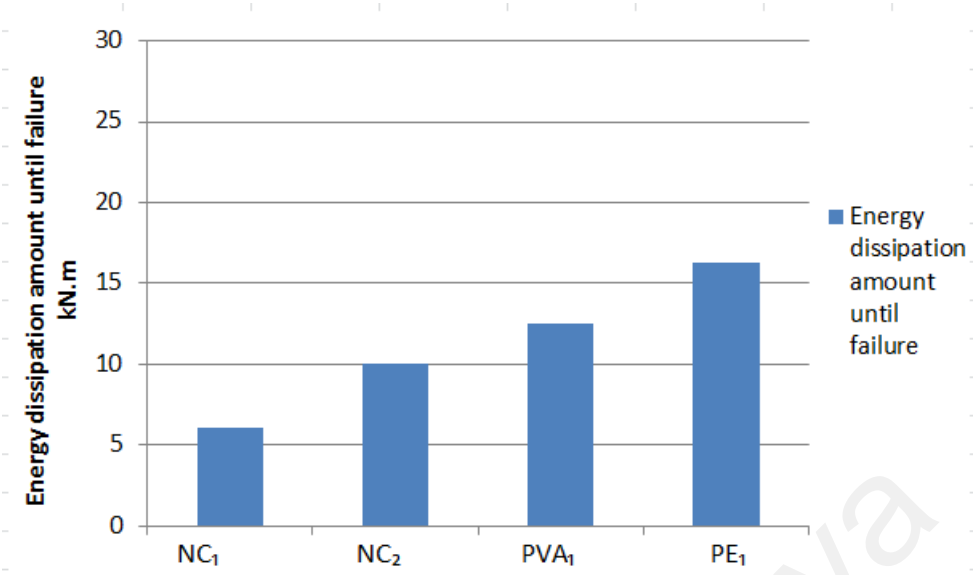

Figure 4.119: Effect of the ECC inclusion in the joint on the energy absorption capacity

ECC start to bridge the cracks and arrest them. This characteristic leads ECC to improve its tensile strength, shear strength, ductility, energy absorption capacity, and to minimize the pinching effect of hysteresis loops in beam-column joints. Figure 4.119 indicates a significant increase in the cumulative energy absorption value of the PVA_1 and PE_1 joints at failure, compared to the corresponding value for the NC_2 joint about of 24% and 61%, respectively.

c) Effect of type of ECC inclusion in the joint zone

Figure 4.120 showed identical behavior of the cumulative energy absorption for the PVA_2, PE_2, PVA_3 and PE_3 joints until the drift ratio of 1.5% owing to the almost similar E modulus for the both types of ECC mix. After the 1.5% drift ratio, the cumulative energy absorption curve for the joints start to deviate each one from the other depending on the nature of fibers bridging mechanism and the bond developed on the interfacial surface of the fibers and the surrounding ECC mix. Eventually, the ductility level of the joints is estimated from the cumulative energy absorption value at failure. Based on Figure 4.121, there is a significant increase in the cumulative energy absorption for the

PE_2 joint compared to the corresponding value for PVA_2 joint of about 37.3%. In addition, another increase in the cumulative energy absorption value was observed for PE_3 joint over the corresponding value of the PVA_3 joint of about 17.8%.

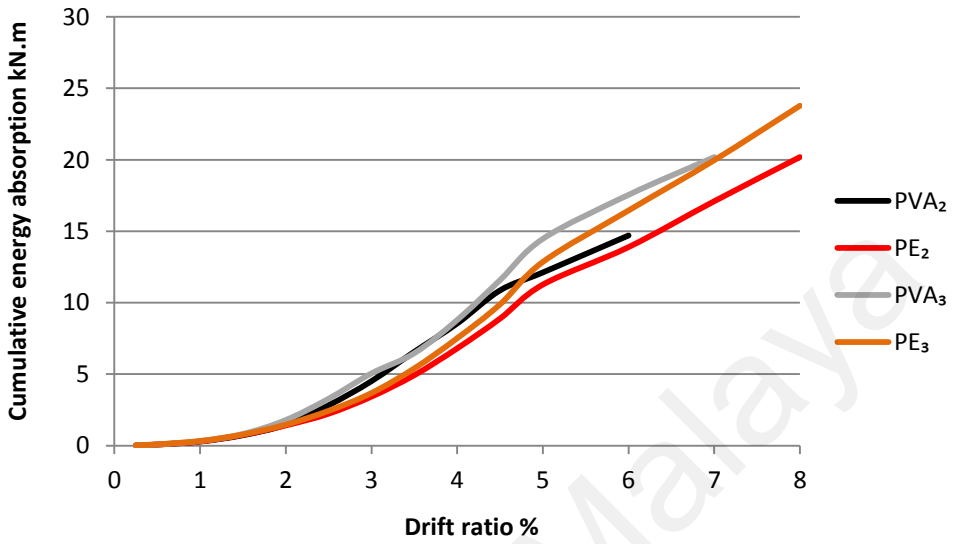

Figure 4.120: Cumulative energy absorption amount at failure for the PVA_2, PE_2, PVA_3 and PE_3 joints

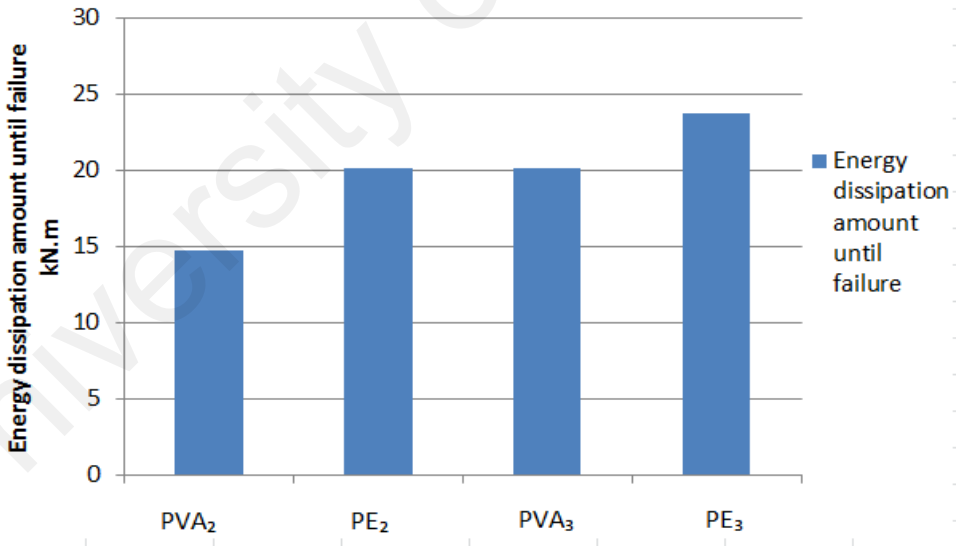

Figure 4.121: Effect of type of ECC in the joint zone on the cumulative energy absorption

d) Effect of the polymer fibers reinforcing index

Figures 4.122a and 4.122b show identical behavior of the cumulative energy absorption for both groups of ECC-PVA, and ECC-PE joints until the drift ratio of 1.5%. After the

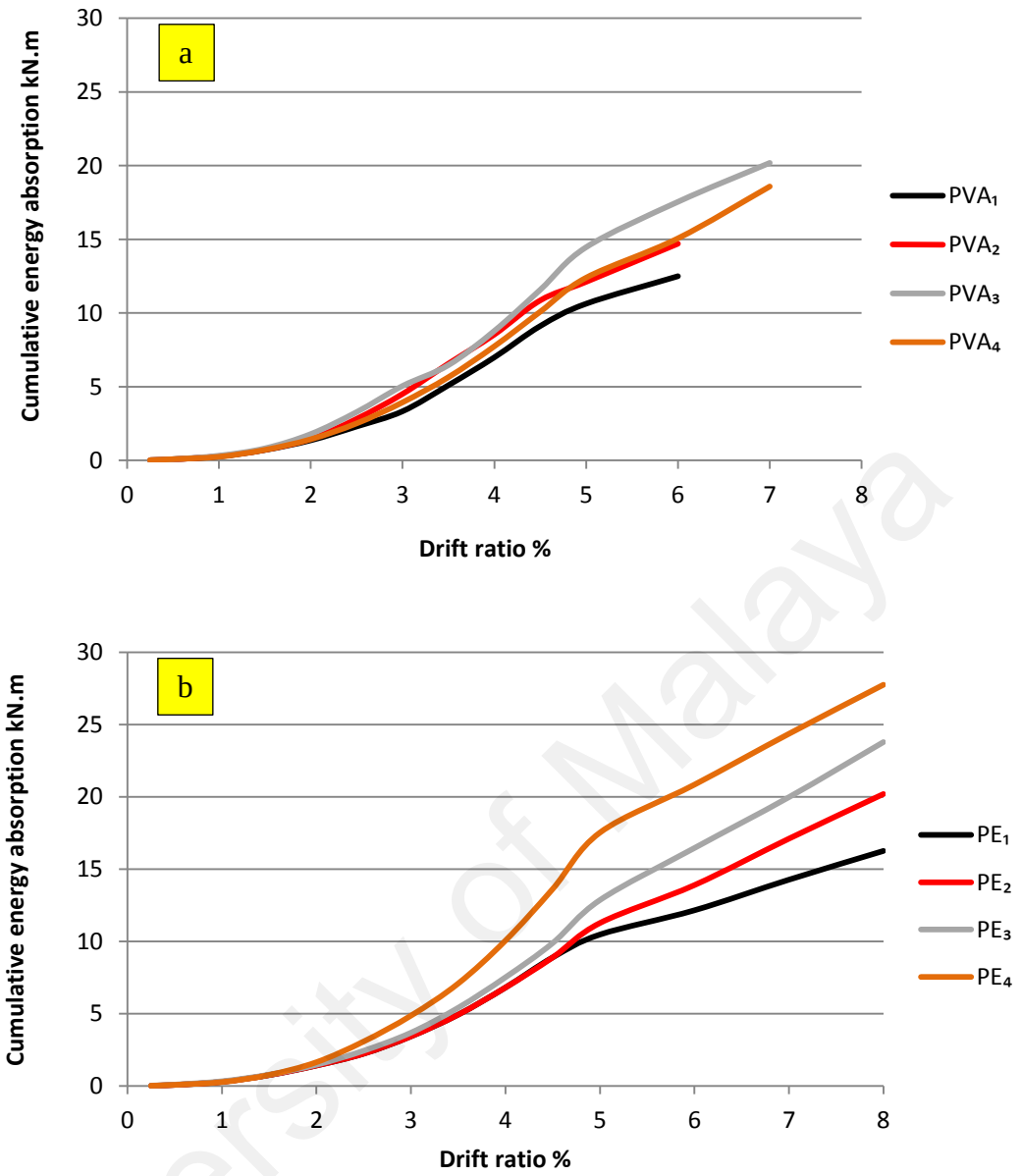

Figure 4.122: Cumulative energy absorption results for (a) PVA_1, PVA_2, PVA_3 and PVA_4 joints (b) PE_1, PE_2, PE_3 and PE_4 joints

1.5% drift ratio, the cumulative energy absorption curve for each specimen starts to separate each one from the other depending on the nature of fibers bridging mechanism and the interfacial bond developed on the interface of the fibers and the surrounding ECC. As shown in Figure 4.123, the PVA_2, PVA_3 and PVA_4 joints showed an increase in the cumulative energy absorption at failure over the corresponding value of the PVA_1 joint about 17.6, 61.5 and 48.7%, respectively. The reduced value for PVA_4 joint is due to the high fiber content in the ECC which led to a non- homogenous dispersion of the

fibers. Similarly, as shown in Figure 4.123, the PE_2, PE_3 and PE_4 joints showed an increase in the cumulative energy absorption at failure over the corresponding value of PE_1 joint of about 24.2, 46.3 and 70.7%, respectively. A linear fit is suggested to analyze the cumulative energy absorption results with high correlation coefficient, as shown in Figure 4.123.

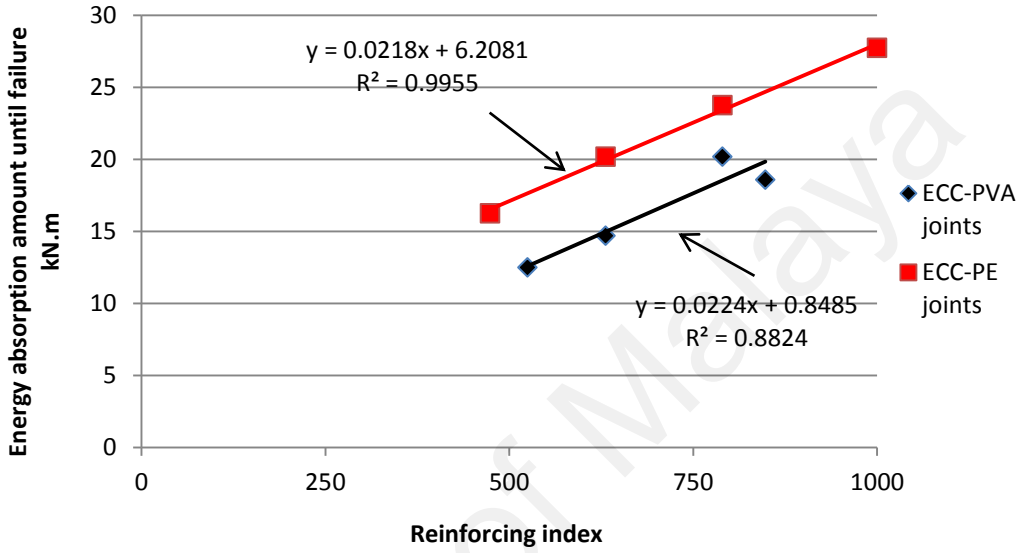

Figure 4.123: Effect of reinforcing index on the Cumulative energy absorption of PVA and PE joints

e) Effect of the lateral steel hoops inclusion in ECC joint zone

Figures 4.124a and 4.124b show the effect of lateral steel hoops inclusion in the joint zone on the behavior of cumulative energy absorption for both PVA and PE joints. As shown in Figure 4.125, the PVA_5 and PVA_6 joints (including 1 and 2 steel hoops) showed an increase in the cumulative energy absorption at failure over the corresponding value for the PVA_2 joint (no steel hoops in the joint) of about 52.4 and 61.8%, respectively, due the effect of lateral steel hoops in the joint zone. Similarly, as shown in Figure 4.125, the PE_5 and PE_6 joints (including 1 and 2 steel hoops) showed an increase in the cumulative energy absorption at failure over the corresponding value for the PE_2 joint about 20.2 and 25.1%, respectively due to the effect of steel hoops inclusion in the joint zone.

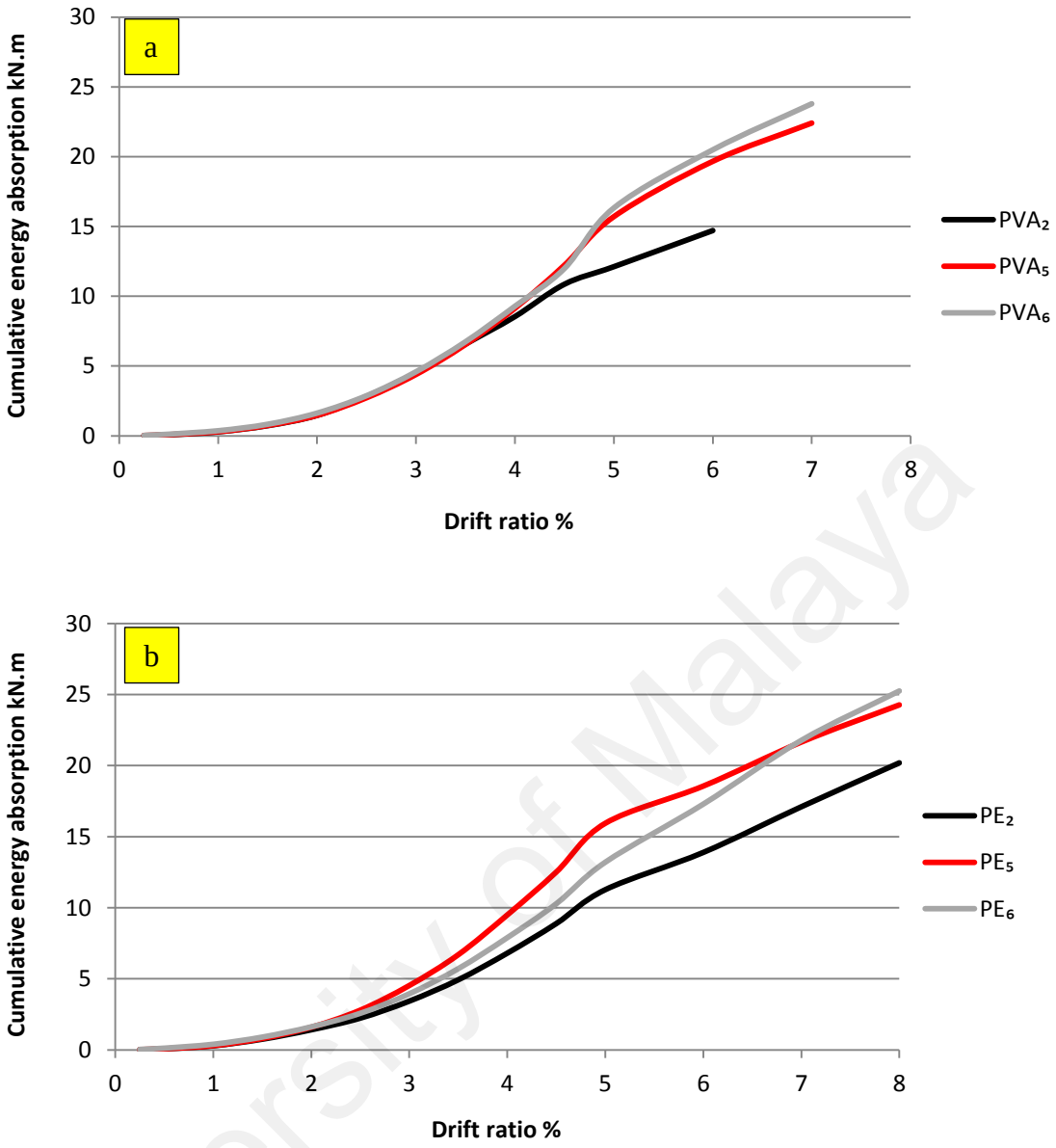

Figure 4.124: Cumulative energy absorption behavior for (a) PVA_2, PVA_5 and PVA_6 joints (b) PE_2, PE_5 and PE_6 joints

4.4.11 Stiffness degradation

Stiffness degradation is considered as a function of the ductility and damage tolerance for beam-column joints. The stiffness of any loading cycle is simply evaluated by calculating the slope of the line connecting each point plotted on the positive part of the envelope load-deflection curve with the analogous point plotted on the negative part of the envelop curve, as shown in Figure 3.19 (Shannag and Alhassan, 2005). By fitting

suitable lines for the data which are collected from the slope results, it is observed that the absolute value for the slope of the fit line is a function of the stiffness

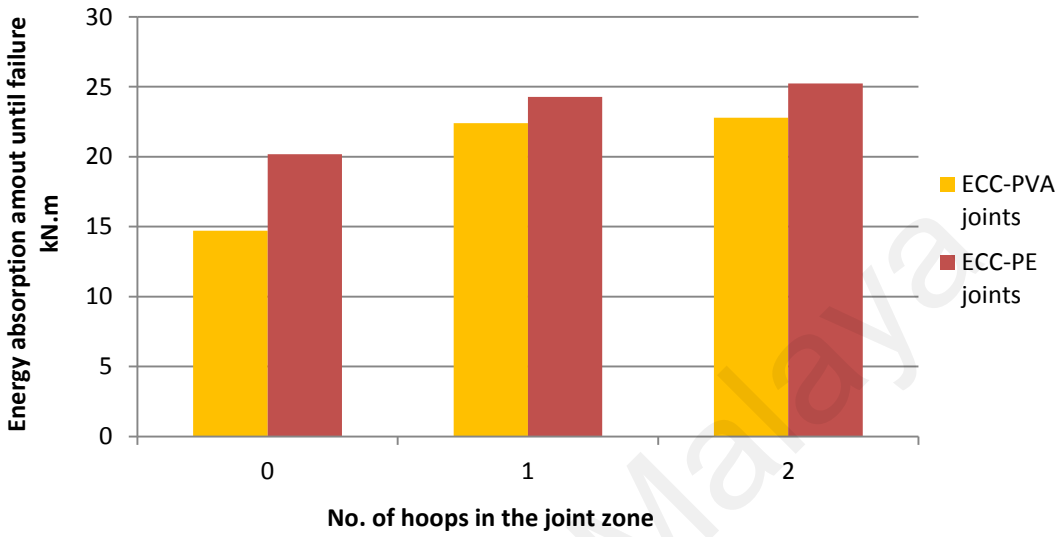

Figure 4.125: Effect of the lateral steel hoops inclusion in the joint zone on the cumulative energy absorption of PVA and PE joints

degeneration rate of the specimen. The slope of the fit line represents the rate of decrease for the fit line which means the rate of stiffness degradation for the specimen; the lesser rate of decrease for the fit line, the better ductility and damage tolerance. Referring to the Figures from 4.126 to 4.139, the rates of stiffness degradation for beam-column specimens are collected from the figures mentioned above and listed in Table 4.5.

a) Effect of lateral steel hoops in NC joints

Referring to Figures 4.126 and 4.127, and Table 4.5, the rate of stiffness degradation for NC_2 is 52.5% lesser than the corresponding rate for NC_1 specimen, which denotes better ductility and damage tolerance for NC_2 specimen than NC_1 specimen.

b) Effect of the ECC inclusion in the joint zone

Based on Figures 4.128 to 4.139, the rate of stiffness degradation for the ECC-PVA and ECC-PE joints are shown in the Table 4.5. The average of the rate of stiffness degradation values for the PVA joints is 0.252 while the corresponding average value for the PE joints is 0.155. The average of the rate of stiffness degradation values for the PVA joints is lesser than the corresponding value for the NC_2 specimen of about 6%

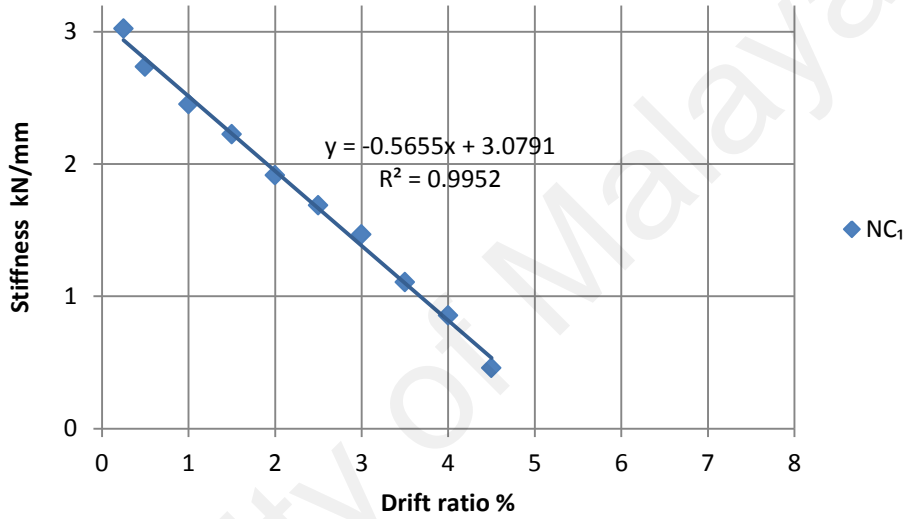

Figure 4.126: Stiffness degradation of NC_1 specimen

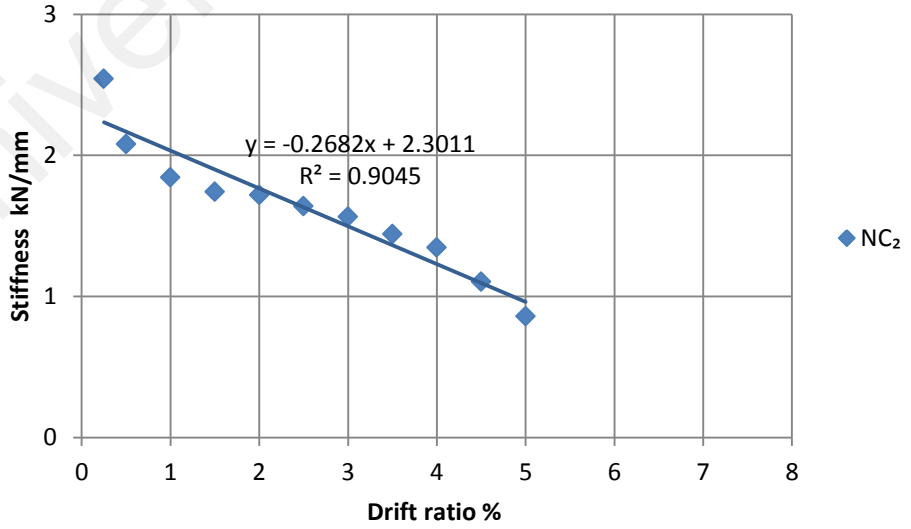

Figure 4.127: Stiffness degradation of NC_2 specimen

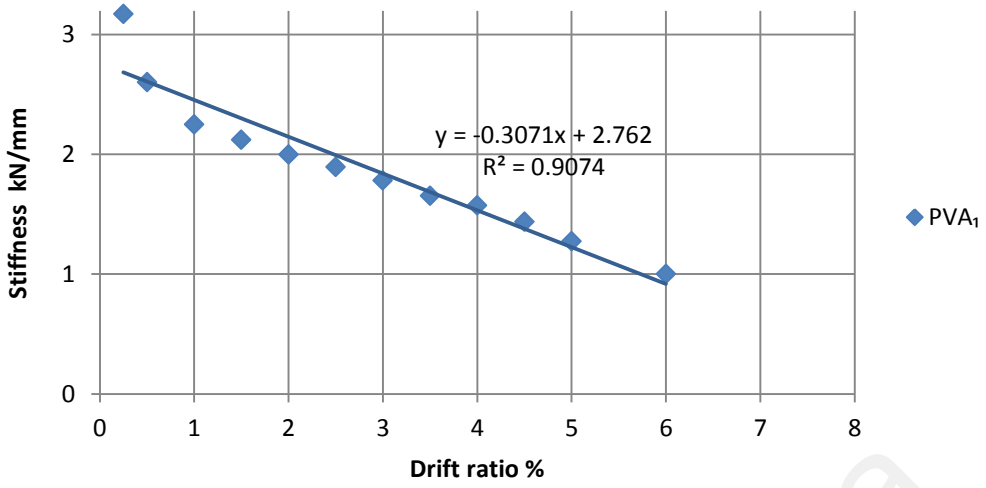

Figure 4.128: Stiffness degradation of PVA_1 specimen

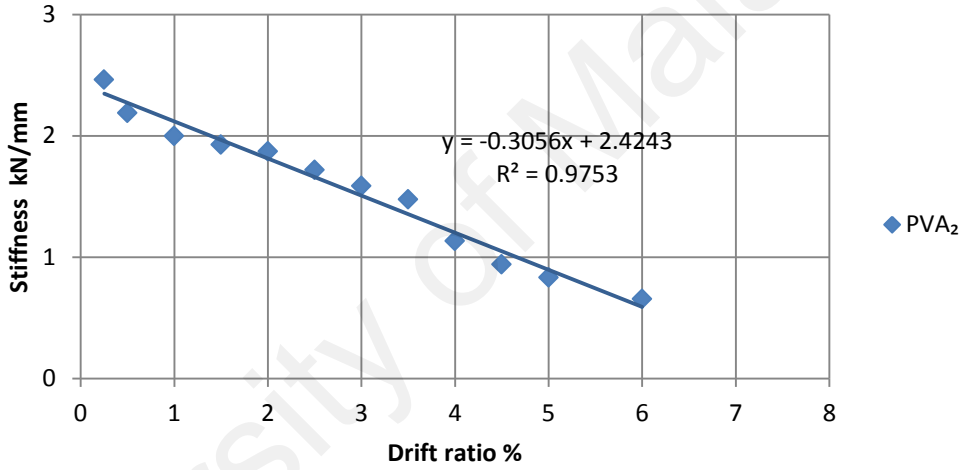

Figure 4.129: Stiffness degradation of PVA_2 specimen

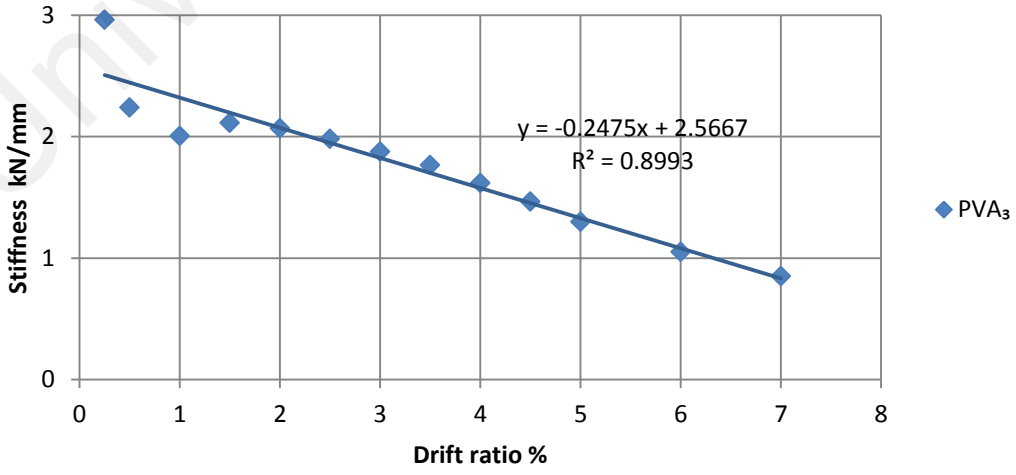

Figure 4.130: Stiffness degradation of PVA_3 specimen

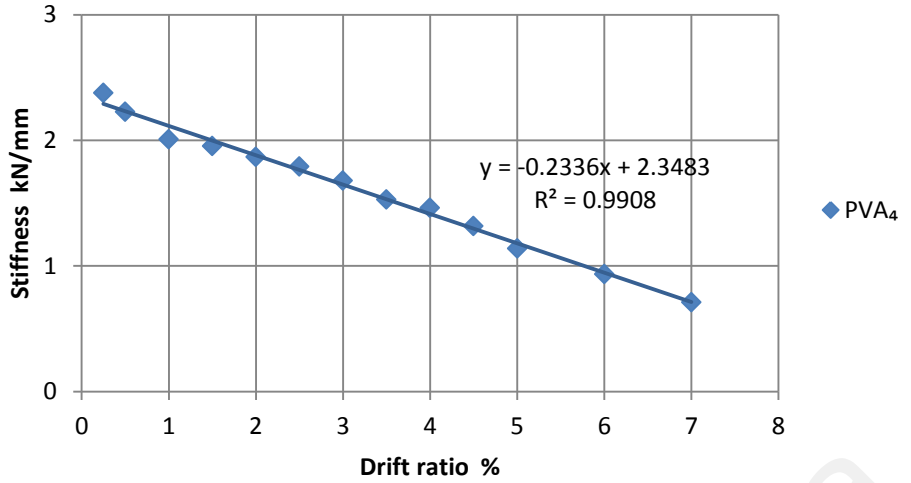

Figure 4.131: Stiffness degradation of PVA_4 specimen

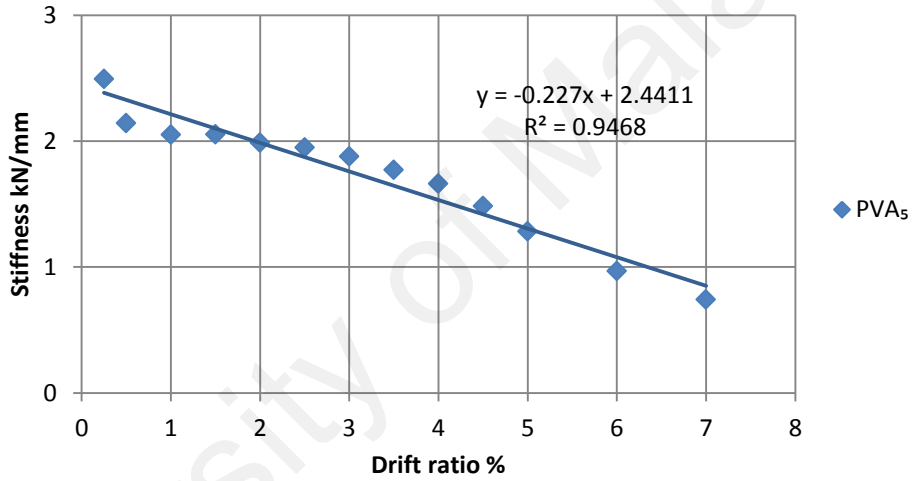

Figure 4.132: Stiffness degradation of PVA_5 specimen

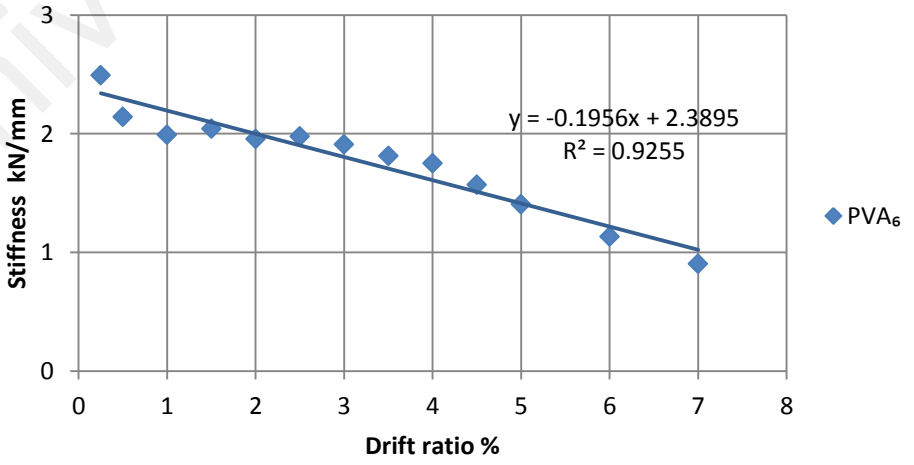

Figure 4.133: Stiffness degradation of PVA_6 specimen

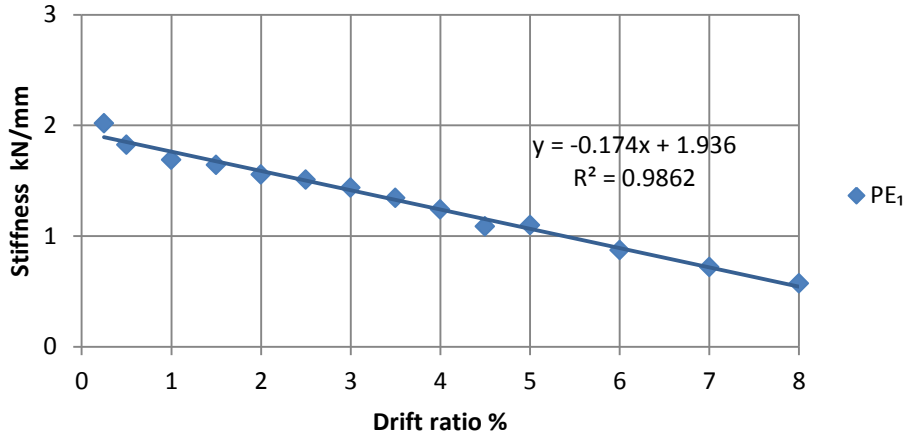

Figure 4.134: Stiffness degradation of PE_1 specimen

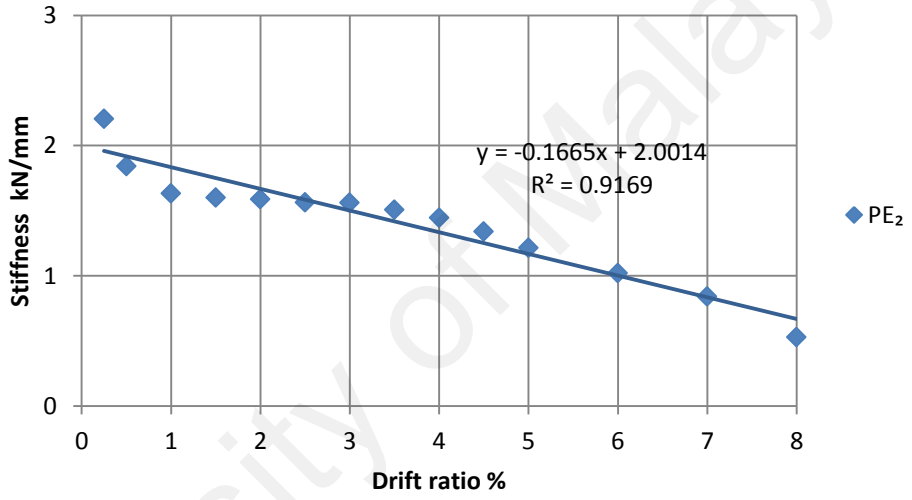

Figure 4.135: Stiffness degradation of PE_2 specimen

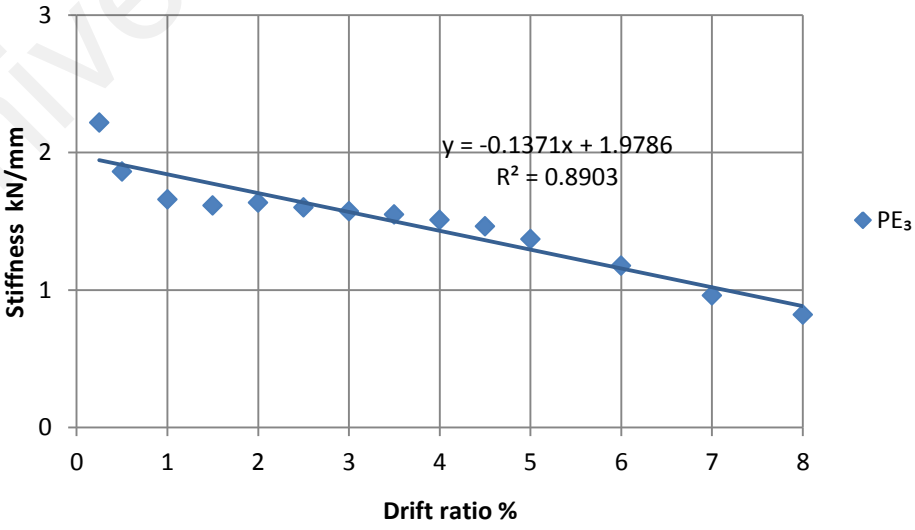

Figure 4.136: Stiffness degradation of PE_3 specimen

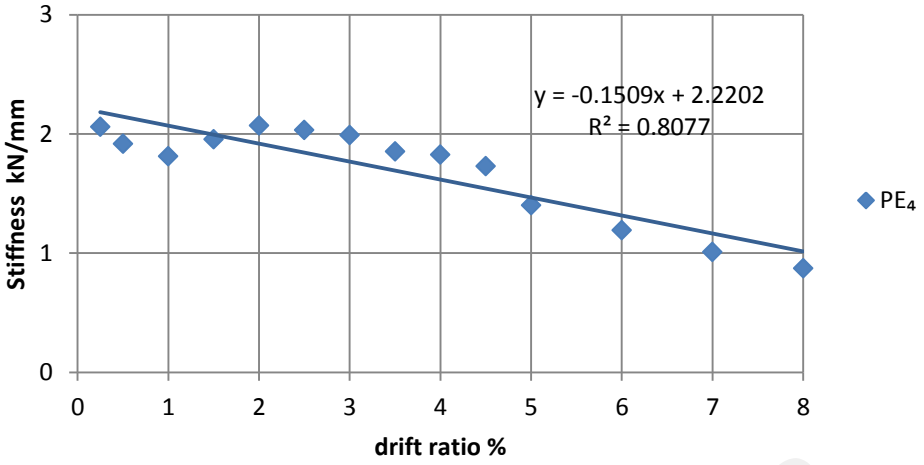

Figure 4.137: Stiffness degradation of PE_4 specimen

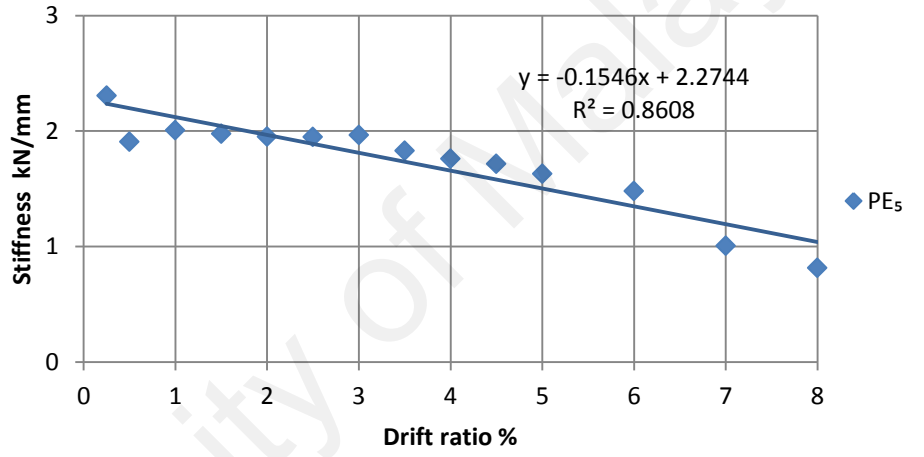

Figure 4.138: Stiffness degradation of PE_5 specimen

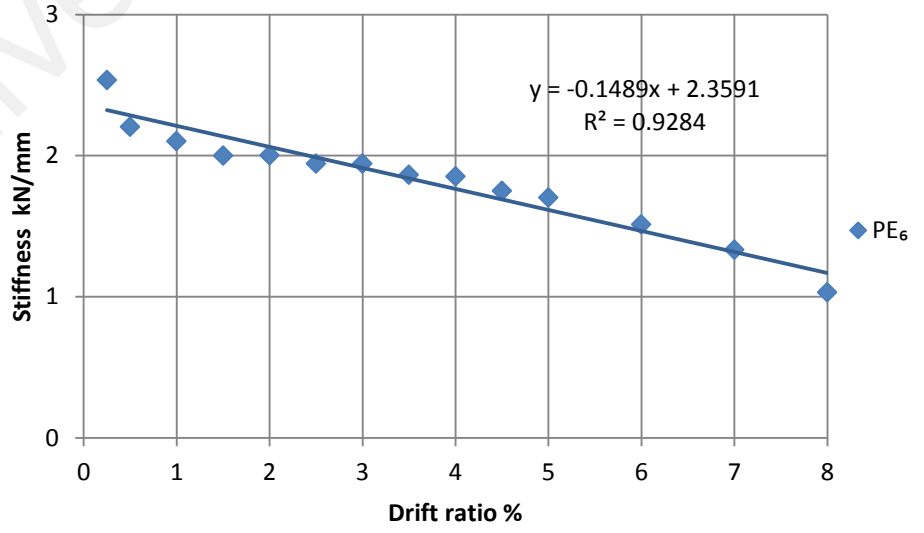

Figure 4.139: Stiffness degradation of PE_6 specimen

Table 4.5: Stiffness degradation rate of beam-column joint specimens

S	Specimen	Rate of stiffness degradation	Remarks
1	NC_1	0.5656	
2	NC_2	0.2682	
3	PVA_1	0.3071	Average value for all PVA specimens = 0.252
4	PVA_2	0.3056	
5	PVA_3	0.2475	
6	PVA_4	0.2336	
7	PVA_5	0.2270	
8	PVA_6	0.1956	
9	PE_1	0.174	Average value for all PE specimens = 0.155
10	PE_2	0.1665	
11	PE_3	0.1371	
12	PE_4	0.1509	
13	PE_5	0.1546	
14	PE_6	0.1489	

While the average of the rate of stiffness degradation values for the PE joints is lesser than the corresponding value for NC_2 specimens of about 46%. It is concluded that the performance of the both kinds of ECC joints is better than the performance of designed NC joint.

c) Effect of type of ECC inclusion in the joint zone

Figure 4.140 shows the effect of ECC-PVA and ECC-PE on the stiffness degradation of beam column joint. The PE_2 specimen showed a rate of stiffness degradation of about 45.5% lesser than the corresponding rate for PVA_2 specimen. In addition, the rate of stiffness degradation for the PE_3 specimen is about 44.6% less than the corresponding rate for PVA_3 specimen. Moreover, the average value of the rate of stiffness degradation values for the PE joints is lesser than the corresponding average value for PVA specimens of about 38.5%. It is concluded from the previous results that the performance of the ECC-PE joints is better than the performance of the ECC-PVA joints.

d) Effect of polymer fiber reinforcing index

Figure 4.141 shows the effect of reinforcing index on the stiffness degradation of beam column joint. The PVA_3 and PVA_4 specimens, of R.I equals to 790 and 948, showed a decrease in the stiffness degradation rate less than the corresponding value for the PVA_1 specimen (of R.I equals to 631) of about 19.5 and 24.5%, respectively. In addition, the PE_2 and PE_3 specimens, of R.I equals to 631 and 790, showed a decrease in stiffness degradation rate less than the corresponding value for PE_1 specimen (of R.I equals to 474) of about 4.4 and 21.2%, respectively. The results for both kinds of ECC revealed better performance, in ductility and damage tolerance, for beam-column joint under cyclic loading as the increase in reinforcing index of polymer fibers. Figure 4.141 shows a linear fit for the stiffness degradation results as a function to R.I, for each kind of ECC specimens.

e) Effect of lateral steel hoops inclusion

Figure 4.142 shows the inclusion effect of lateral steel hoops in the joint zone on the stiffness degradation rate. For PVA specimens, the PVA_5 and PVA_6 specimens (of 1 and 2 steel hoops in the joint zone) showed a decrease in the stiffness degradation of

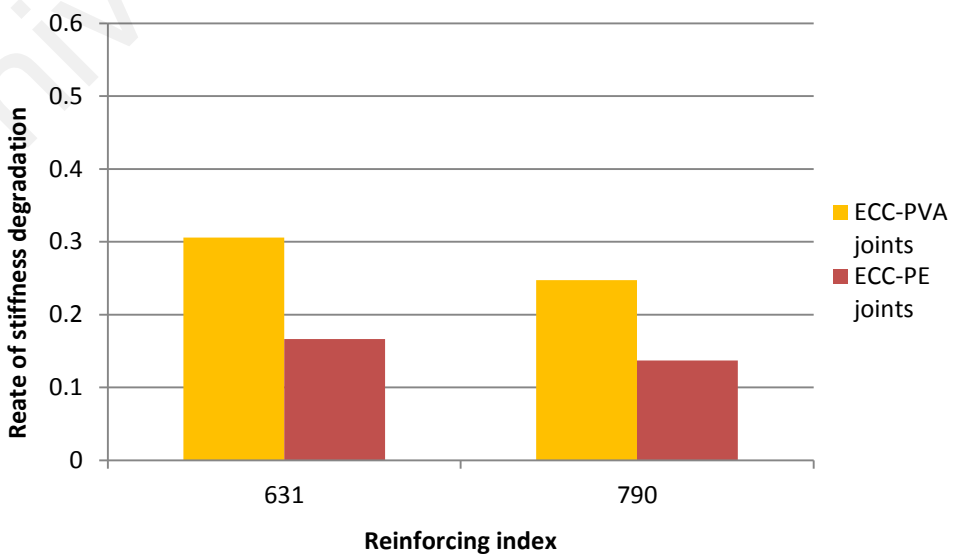

Figure 4.140: Effect of type of ECC on stiffness degradation rate

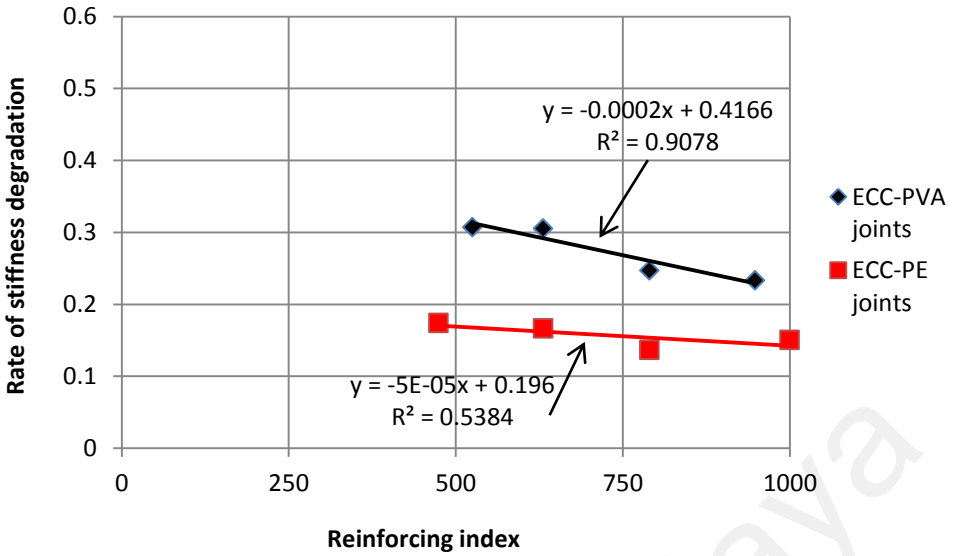

Figure 4.141: Effect of polymer fibers reinforcing index on stiffness degradation rate

about 25.7 and 36% compared to the PVA_2 specimen (without hoops inclusion), respectively. Similarly, the PE_5 and PE_6 specimens (of 1 and 2 hoops in the joint zone) showed a decrease in the stiffness degradation of about 7.2 and 10.5% compared to the PE_2 specimen (without hoops inclusion), respectively. The previous results confirmed that the steel hoops inclusion in the ECC joints improved the ductility and damage tolerance of the beam-column joints.

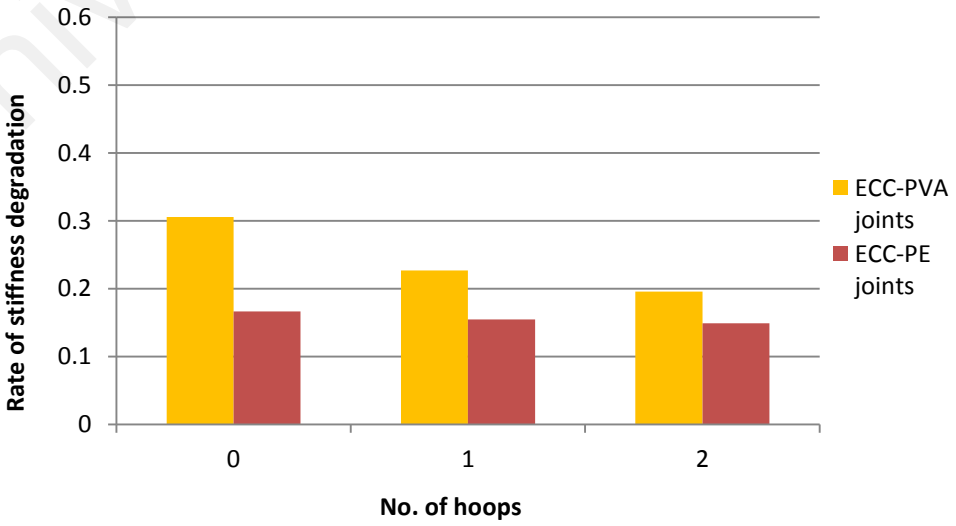

Figure 4.142: Effect of lateral steel inclusion on stiffness degradation rate

4.4.12 Shear strength factor λ

As mentioned previously, λ is a factor proposed by the ACI 352R-02 (352R-02, 2002) to evaluate the nominal shear stresses developed in the Type 2 joint zone. The proposed λ value from the mentioned code for the type of joint is 1. In this study, new values of λ were proposed for ECC joints according to the type of fiber, reinforcing index and the inclusion of lateral steel hoops in the ECC joint zone based on the experimental results. In addition, the value is also evaluated for NC joint, with and without the lateral steel hoops inclusion in the joint zone, as shown in Table 4.6. The ultimate shear capacity V_j is estimated from Equation 3.6 shown in Section 3.4.9. The shear strength of beam-column joint is calculated from Equation 3.18 shown in Section 3.4.16. Finally, λ value was evaluated at the ultimate capacity stage of loading.

a) Effect of lateral steel hoops in normal concrete (NC) joints

As shown in Table 4.6 and Figure 4.143, the λ value for the NC_1 joint is about 7.6% less than 1, which is unable to satisfy the Type 2 joint provisions according to ACI 352R-02 due to the absence of lateral steel hoops in the joint zone. In addition, the λ value for the designed NC joint (NC_2) is 8.3% greater than 1 which successfully satisfied the ACI code provision due to the lateral steel hoops inclusion in the joint zone based on the ACI code design.

b) Effect of the ECC inclusion in the beam-column joints

Figure 4.143 shows the effect of the ECC inclusion in the joint zone on λ value. As shown in the Table 4.6, the inclusion of ECC in the joint zone with the least value of reinforcing index and with the absence of the steel hoops successfully satisfied the Type 2 joint provision according to ACI 352R-02. The PVA_1 joint, with R.I equal to 525,

achieved a λ value equals to 1, while the PE_1 joint, with R.I equal to 474, showed an increase in λ value of about 4.8% greater than 1.

Table 4.6: Evaluation of shear strength factor λ

S	Specimen	Ultimate shear capacity V_i kN	Shear strength of beam-column joint f_j N/mm²	Cylindrical compressive strength of concrete or ECC N/mm²	$\sqrt{f_c'}$	Calculated shear strength factor $\lambda = f_j / \sqrt{f_c'}$	Increase* or decrease** in λ value %
1	NC_1	287	6.753	53.44	7.310	0.924	-7.60
2	NC_2	346	8.141	56.56	7.521	1.083	8.30
3	PVA_1	335	7.882	61.12	7.818	1.008	0.80
4	PVA_2	358	8.424	60.21	7.760	1.086	8.60
5	PVA_3	425	10.000	57.35	7.573	1.320	32.0
6	PVA_4	384	9.036	55.61	7.457	1.212	21.2
7	PVA_5	432	10.165	58.22	7.630	1.332	33.2
8	PVA_6	456	10.729	62.02	7.875	1.362	36.2
9	PE_1	358	8.424	64.64	8.04	1.048	4.80
10	PE_2	395	9.294	63.88	7.992	1.163	16.3
11	PE_3	456	10.729	60.68	7.790	1.377	37.7
12	PE_4	470	11.059	61.29	7.829	1.413	41.3
13	PE_5	512	12.047	62.67	7.916	1.522	52.2
14	PE_6	544	12.800	58.82	7.669	1.669	66.9

*Compared to the ACI 352R-02 provisions
**The decrease shown in negative value

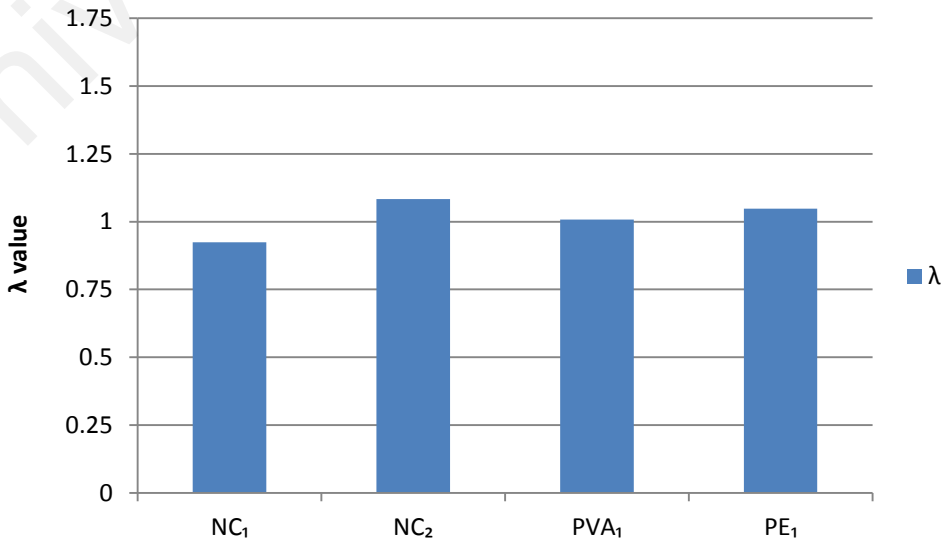

Figure 4.143: Effect of ECC inclusion in joint zone on λ value

c) Effect of type of ECC inclusion in the joint zone

Figure 4.144 shows the effect of type of ECC inclusion in the joint zone on λ value. As shown in Table 4.6, the PVA_2 joint achieved an increase of about 8.6% in λ value, while the PE_2 joint achieved an increase of 16.3% in λ value. The comparison between the PVA_2 and PE_2, with similar R.I equals to 631, shows that the λ value for the PE_2 joint is greater than the corresponding value for the PVA_2 joint of about 7.1%. In addition, an increase in λ value of about 32 and 37.7% was achieved for the PVA_3 and PE_3 joints, of the similar R.I equals to 790, respectively. Moreover, an increase in λ value was observed for the PE_3 joint of about 17.8% over the corresponding value of PVA_3 joint. It is drawn that the ECC-PE inclusion in the joint zone is significantly more effective than the ECC-PVA inclusion.

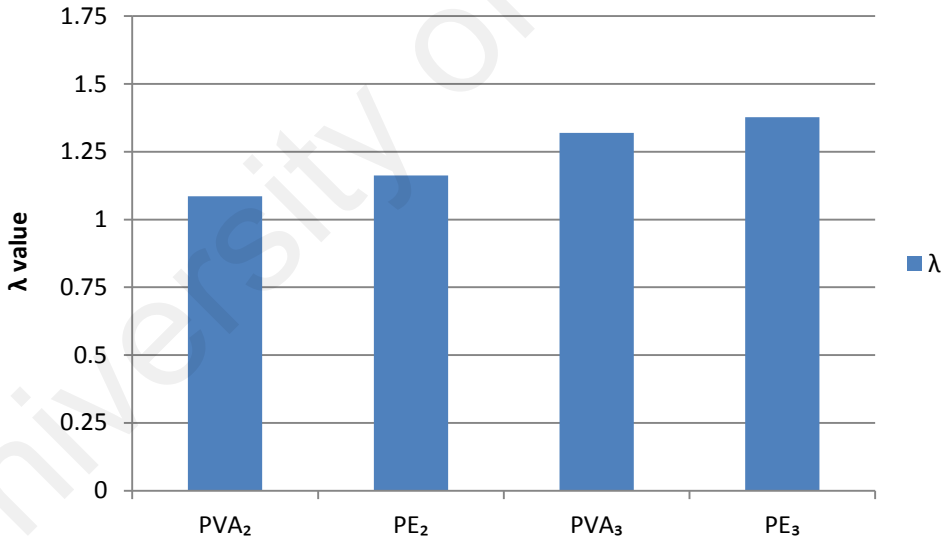

Figure 4.144: Effect of type of ECC in joint zone on λ value

d) Effect of polymer fibers reinforcing index

Figure 4.145 shows the effect of polymer fiber reinforcing index on the λ value. As shown in Table 4.6, an increase in λ value was observed for PVA_4 and PE_4 joints, of about 21.2 and 41.3%, respectively. For PVA group of joints, an increase in the λ value was observed for the PVA_2, PVA_3 and PVA_4 joints over the corresponding value of the

PVA_1 joint of about 7.7, 31 and 20.2%, respectively. In addition, the drop in the increase value for PVA_4 is due to the non-uniform dispersion of PVA fibers in the fresh ECC mix. For PE group of joints, an increase in λ value was observed for the PE_2, PE_3 and PE_4 joints over the corresponding value of PE_1 joint of about 11, 31.4 and 34.8%, respectively. Moreover, Figure 4.145 shows the liner fit relation is more suitable for the λ value as a function to the R.I for each type of PVA and PE fibers, as indicated:

λ_{PVA}= 0.0006*R.I + 0.739 applicable for R.I ≥ 525 (Equation 4.1)

λ_{PE}= 0.0007*R.I + 0.716 applicable for R.I ≥ 474 (Equation 4.2)

The linear fit is a significant finding to estimate the λ for ECC exterior beam-column joints with the variation of R.I for each type of polymer fiber.

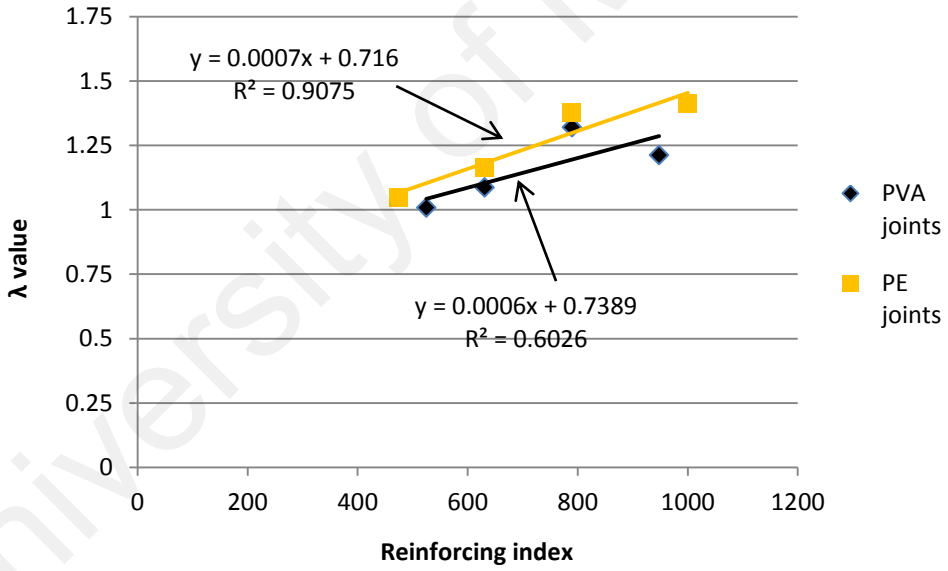

Figure 4.145: Effect of reinforcing index on λ value in ECC-PVA and ECC-PE joint zone

e) Effect of lateral steel hoops inclusion in ECC joints

Figure 4.146 shows the effect of lateral steel hoops inclusion on the λ value. As shown in Table 4.6, an increase in λ value was observed for the PVA_5, PVA_6, PE_5 and PE_6 joints of about 33.2%, 36.2%, 52.2% and 66.9%, respectively. For PVA group of joints,

a significant increase in the λ value was observed for the PVA_5 and PVA_6 joints (with 1 and 2 steel hoops inclusion) over the corresponding value of PVA_2 joint of about 22.7% and 25.4%, respectively. For PE group of joints, a noticeable increase in the λ value was observed for the PE_5 and PE_6 joints over the corresponding value of PE_2 joint of about 30.9% and 43.5%, respectively. It is clear there is a noticeable increase in the λ value with one hoop inclusion for both types of joint. However, the increase in λ value for the joints with two hoops inclusion over the corresponding value of the joints with one hoop inclusion was about 2.3% and 9.6% for PVA and PE joints, respectively, which is insignificant. Table 4.7 indicates a summary for the significant findings of beam-column joints.

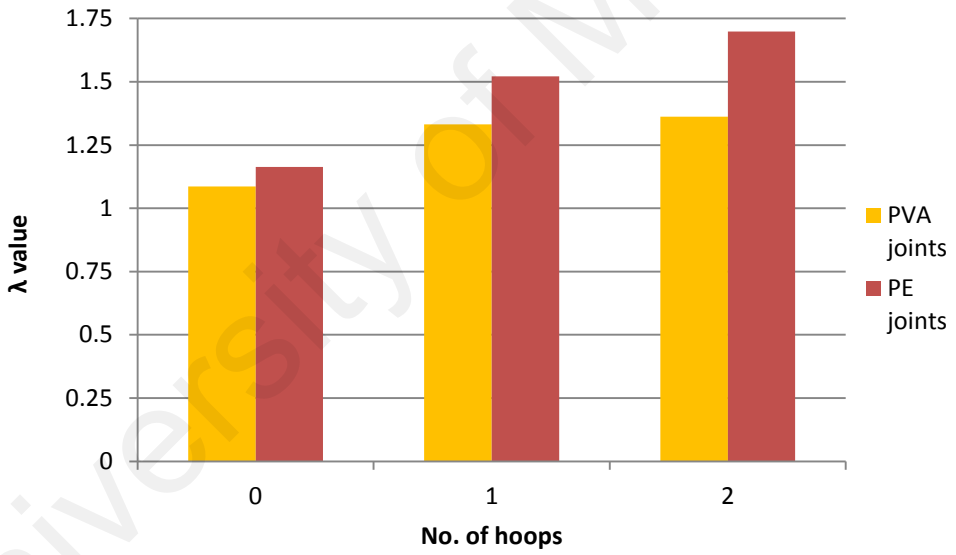

Figure 4.146: Effect of the lateral steel hoops in the ECC-PVA zone ECC-PE joint zone.

f) The effectiveness of fiber amount on λ value

As shown in Table 4.6, the increase in λ value of the PVA_2 joint at ultimate capacity is about 8.6%. A sudden increase in λ value was observed in PVA_3 joint of about 32% which denotes a significant effectiveness of PVA joints at R.I > 631. Similarly, the PE_1 joint showed an increase in λ value of about 4.8%, when a sudden increase in λ value

was observed for PE_2 joint of about 16.3%. The significant effectiveness of the PVA-RECS15-12mm fibers in beam-column joints was observed at 2.5% of fiber content while the corresponding effectiveness for the PE-4800D fibers was observed at 2% of fiber content with high factor of safety. The use of PE-1600D with 2% in the beam-column joints is more reliable than the PE-4800D due to the higher increase in λ value. However, this kind of fiber is more costly.

It is worthwhile to mention that the usage of ECC-PVA or ECC-PE in the joint zone instead of designed normal concrete joint gives better and more reliable results. It allows for ease of fabrication by eliminating the use of lateral steel hoops and get rid of the casting difficulties in the joint zone.

Table 4.7: Summary of results for beam-column joints

	Effect of				
	lateral steel hoops in NC specimens	ECC inclusion in the joint zone	type of ECC in the joint zone	polymer fibers reinforcing index	lateral steel hoops inclusion in ECC joint zone
Load-deflection relationship	Pinching effect of NC_1 due to brittle failure. Wider hysteresis loops for NC_2 due to moderate ductility	Loops behaviour for ECC specimens is much better than the behaviour in NC_2 with wider and more regular loops	Loops behaviour in PE joints is much better than the behaviour for PVA joints due to better ductility and damage tolerance	Improved loops behaviour in PVA_3 and PVA_4 compared to the PVA_1 and PVA_2 with reduced pinching effect	Significant loops behaviour with better ductility for ECC joints with 1 or 2 hoops compared to ECC joint without hoops
Load-deflection envelope	Better ultimate load capacity for NC_2 of about 20% higher than NC_1 with wider area under the envelope curve	The area under the envelope curve for ECC specimens is wider than the area in NC_2 due to better ductility	The area under the envelope curve for PE specimens is greatly wider than the area for PVA specimens	For PE specimens, the area under the envelope curve is gradually increased by the increase in the reinforcing index	Significant increase in the area under the envelope curve for ECC joints with 1 or 2 hoops compared to ECC joint without hoops
Ultimate shear capacity	Shear capacity in NC_2 is improved of about 20.6% compared to the shear capacity in NC_1 joint	The PE joints are much better effective than PVA joints in resisting the shear forces	PE_2 and PE_3 joints improved the shear capacity of about 10.3% and 7.2% compared to PVA_2 and PVA_3, respectively	the ultimate shear capacity for ECC joints increased with the increase in the reinforcing index of fibers	Significant increase in the shear capacity for ECC joints with 1 or 2 hoops compared to ECC joint without hoops
Moment-rotation relationship	Wider loop area and better spread of loop was observed for the NC_2 joint compared to NC_1 joint	loops for ECC joints are wider and better spread than the loops in NC_2 joint	Significant behavior of loops for PE joints with wider area of loops and more spread compared to PVA joints	Positive effect of the reinforcing index increase on the loops behavior of the ECC joints. reduced effect of pinching	Better regularity and reduced effect of pinching for ECC joints with 1 or 2 hoops compared to ECC joint without hoops
Moment-rotation envelope	Better moment capacity, deformation and ductility for NC_2 joint compared for NC_1 joint	Noticeable increase in the rotation value for the ECC joints compared to NC_2 joint	significant increase in the rotation value for the PE joints compared to the PVA joints	Positive effect of reinforcing index on the moment capacity and rotation value in ECC joints	Noticeable increase in the moment capacity and rotation value joints with 1 or 2 hoops compared to ECC joint without hoops
Principal strain	The highest value of the maximum principal strain results in NC_1 joint and reduced values of principal strains in NC_2	Higher ductility of PE_1 results in higher principal strains compared to NC_2 and PVA_1, with lowest results for NC_2	Significant increase in the principal strains for the PE specimens compared to the PVA specimens, respectively	The increase in reinforcing index shows higher values of principal strains for ECC joints due to the improved ductility	The inclusion of 1 or 2 hoops in ECC joints showed the highest result of the principal strains compared to the joint without hoops
Shear deformation	Excessive amount of shear rotation angle for NC_1 joint at early stage while a reduced value for NC_2 was observed	higher shear rotation for PE_1 joint compared to NC_2 and PVA_1 due to the better ductility	PE joints showed a noticeable increase in shear rotation angle compared to PVA joints	The shear rotation angle increased in the ECC joints as the increase in the reinforcing index	An increase in shear angle is observed for the inclusion of 1 or 2 hoops in ECC joints compared to the joints with 0 hoop
Cumulative energy absorption	After 3% of drift ratio, the energy absorption starts to increase in the NC_2 joint over the NC_1 due the effect of lateral steel hoops in the joint zone	Significant increase in the energy absorption value of the ECC joints compared to NC_2 is observed after 1.5% of drift ratio	Significant increase in the energy absorption for the PE joints is observed compared to PVA joints after 1.5% of drift ratio	Significant increase in energy absorption as the increase in the reinforcing index is observed for ECC joints after 1.5% drift ratio	Remarkable increase in in the energy absorption with the inclusion of 1 or 2 hoops in ECC joints compared to the joint without hoops
Stiffness degradation	The rate of stiffness degradation for NC_2 joint is lesser than NC_1 52.5% which denotes better ductility and damage tolerance for the NC_2	Better performance for ECC joints compared to EC_2 attaining lesser rate of stiffness degradation for PVA and PE joints	Better performance for PE joints compared to PVA joints attaining lesser rate of stiffness degradation of about 38.5%	Better performance for ECC joints indicating lesser rate of stiffness degradation as the increase in the reinforcing index	The inclusion of 1 or 2 hoops in ECC joints showed a decrease in the stiffness degradation and improved the ductility and damage tolerance of joint
Shear strength factor λ	The NC2 successfully satisfied the ACI provisions indicating a λ greater than 1 while a value lesser than 1 for NC_1 joint	The PVA_1 joint achieved a λ value equals to 1, while the PE_1 joint showed an increase of 4.8%	Significant increase in λ value is observed for PE joints compared to the PVA joints	Noticeable increase in λ value is observed for ECC joints as the increase in reinforcing index	Remarkable increase in λ value is observed with the inclusion of 1 or 2 hoops in the ECC joint zone

CHAPTER 5: CONCLUSIONS AND RECOMMENDATIONS

5.1 Conclusions

1. For estimating the flexural behaviour, deformation and toughness characteristics of ECC slabs and identifying some active kinds of polymer fibers which are suitable for the production of ECC, the following conclusions are drawn

   a. For the ECC PE and ECC PVA slabs, by increasing the reinforcing index value, the peak load value at post cracking also increased. There was a significant increase in the peak load value of the ECC PE slabs compared to the ECC PVA slabs due to the superior performance of the PE fibers in the bonding and failure mechanism. Moreover, the behavior of the ECC PP slabs was similar to plain concrete, which showed a flexural strength equal to zero for all the fiber contents used.

   b. For all types of ECC slabs tested in this study, the highest value of ultimate load deflection and deflection at failure was recorded for the ECC PE slabs, which showed the highest ductility among all the types of ECC slab without any sudden failure. For the ECC PVA slabs, by increasing the reinforcing index, the ultimate load deflection and deflection at failure values increased and improved the ductility of slabs. The highest value for deflection at failure recorded for ECC PVA slabs was considerably smaller than the highest value recorded for the PE slab. The reduced value for deflection indicated the lower ductility of the PVA slabs compared to the PE slabs. For the ECC PP slabs, no improvement in ductility was observed due to the small interfacial bonding of

fibers with the cement matrix. Thus, the ECC PP slabs behaved like plane concrete.

c. The toughness indices I_5, I_{10}, I_{20}, I_{30} and I_{40} analyzed in ECC PVA slab results show that they increase as the reinforcing index increases. The rate of increase in toughness index also increases as the type of toughness index varies from I_5 to I_{40}. In addition, the toughness indices I_5, I_{10}, I_{20}, I_{30}, I_{40}, I_{50}, until I_{100} evaluated in ECC PE slab increase when the reinforcing index increases. The rate of increase in toughness index also increases when the type of toughness index varies from I_5 to I_{100}. Besides, the increase in ductility, flexural toughness and energy absorption capacity for both kinds of ECC would be intrinsically activated starting from I_{20} and upwards especially at higher values of reinforcing indices.

d. The toughness indices computed for both ECC PVA and ECC PE slabs with reinforcing indices higher than 632, exceed the limitations which are particularly allocated for elastic-perfectly plastic materials. However, the values computed satisfy the definition stated in ASTM C 1018 of observed range of toughness indices I_5, I_{10} and I_{20} for fibrous concrete.

2. For evaluating the direct tensile stress-strain relationship for ECC using two kinds of polymer fibers, the following conclusions are drawn:

a. For the ECC PE and ECC PVA I–shaped samples, by increasing the reinforcing index value, the ultimate stress capacity at post cracking also increased. In addition, the increase in the ultimate stress corresponding to higher reinforcing index dropped due to the high amount of PVA or PE fibers incorporated in fresh ECC led to the irregular dispersion of polymer fibers. In addition, the PE

samples showed an improvement in the ultimate stress at post cracking compared to the PVA samples of about 55% and 18.9% for the same reinforcing index of 474 and 790, respectively.

b. The PE I-shaped samples showed a remarkable improvement in the strain value at post cracking compared to the PVA samples of about four and 2.7 times the value for the PVA samples based on the same reinforcing index of 632 and 790, respectively.

3. For identifying the mode of failure, crack propagation, moment and shear capacity; evaluating the deformation characteristics, rotation, principal strain of beam-column joint zone and the strain of beam longitudinal steel bars, the following conclusions are drawn:

a. At the final stages of loading, the cracks in the normal concrete joint NC_1 (with no lateral reinforcement at the joint zone) propagated and severely widened within the joint zone. Splitting of the concrete was observed in the joint zone and a part of the concrete was crushed indicating a brittle shear failure in the joint. For normal concrete joint NC_2, (with lateral reinforcement inclusion at the joint zone) the cracks propagated regularly and simple splitting in some parts of the joint zone with no crushing in the concrete is observed indicating a shear failure of moderate ductility. In contrast, the main cracks in ECC-PVA joints (for R.I $\geq$631) developed in the joint zone and subdivided into smaller branches forming a dense network of tiny cracks with reduced spacing and width of cracks associated with a ductile mode of failure owing to the high performance of the ECC. Besides, all ECC-PE joints showed highly dense network of tiny cracks with infinitesimal crack spacing and width indicating

higher ductile mode of failure compared to PVA joints with no splitting, crushing, or damage in the ECC joint was observed.

b. The pinching effect was obvious because of the brittle mode of failure, high rate of drop in ultimate load capacity in the NC_1 specimen and the smaller area of hysteresis loops. The pinching effect in NC_2 joint is lesser with wider area of hysteresis loops. The loops area was wider and more organized in the ECC specimen than the loops in both NC_1 and NC_2 specimen, which has the reduced effect of pinching.

c. Generally, the PE joints showed higher capacity of load, moment and shear compared to the PVA joints with identical reinforcing indices of about 8.5%. Moreover, the rotation value for PE joints is higher than the corresponding value for PVA joints of an average about 47% and 25% at ultimate and failure stage, respectively.

d. The highest principal strain value was for NC_1 joint due to the brittle mode of failure and the severity of premature cracks in the joint zone. For the joints with ductile mode of failure, the PE joints indicated higher principal strain values than the values for PVA joints due to the denser cracks propagated in the PE joint zone than the cracks in PVA joints, which denotes better ductility and damage tolerance.

e. For NC_1, it is observed a fluctuation in the strain distribution along the longitudinal steel bars due to the premature cracks occurred in NC_1 with widening of the cracks in early stages of loading. For NC_2 joint, better distribution in the strain along the steel bars was observed due to better load distribution in the beam and joint zone. Due to the high performance and

perfect ductility of ECC, the ECC specimens were able to regulate and reduce the strain values in the steel bars and transfer the yielding point of steel bars to the later stage of loading.

4. For estimating the energy absorption ability and stiffness degradation of beam-column joint to identify the ductility and damage tolerance of the joint, the following conclusions are drawn:

    a. The results revealed that the cumulative energy absorption value for NC_2 is higher than the value for NC_1 of about 64.6% and the cumulative energy absorption value for PVA_1 and PE_1 joints is higher than the NC_2 joint of about 24% and 61%, respectively. In addition, the energy absorption value for PE joints is higher than the value for PVA joints at an average of about 35% which reveals better ductility and damage tolerance for PE joints.

    b. The stiffness degradation rate for NC_2 specimen is 52.5% lesser than the corresponding rate for EC_1 specimen. The average value of stiffness degradation rate for PVA and PE joints is lesser than the corresponding value for NC_2 joints of about 6% and 46%, respectively, while the mean value of stiffness degradation rate for PE joints is lesser than the value for PVA joints of about 28.5%.

5. For evaluating the shear strength factor (λ) for beam-column joint and compare it to the factor proposed by the ACI 352 R-02 to evaluate the permissible shear stresses developed in the Type 2 joint zone.

    a. The λ value for NC_1 is about 7.6% less than 1, which is unable to satisfy the Type 2 joint provision according to ACI 352R-02 due to the absence of lateral

steel hoops in the joint zone while the λ value for the NC_2 joint is about 8.3% greater than 1 which successfully satisfied the ACI code provision due to the lateral steel hoops inclusion in the joint zone.

b. The usage of ECC-PVA or ECC-PE in the joint zone instead of designed normal concrete joint gives better and more reliable results. It allows for ease of fabrication by eliminating the use of lateral steel hoops and getting rid of the casting difficulties in the joint zone. Moreover, the usage of ECC in the seismically designed structures can excessively improves the ductility and damage tolerance of joints giving higher factor of safety under seismic excitations.

5.2 Significant findings and contribution

1. Regarding toughness and direct tension characteristics of ECC, the following contributions are drawn:
   a. A new definition is stated for each of ECC PVA and ECC PE materials based on the present results extends the ASTM C1018 definition of fibrous concrete.
   b. The effect of reinforcing index in both direct tension I-shaped PVA specimens and flexural slabs has shown different behavior of strain-hardening. Unlike the cut-off point in the direct tension for ECC-PVA (which equals to 527), the cut-off point in flexure slabs is set at reinforcing index equals to 421. For ECC-PE mixtures, the findings reveal identical behavior in strain hardening. The cut-off point for ECC PE direct tension I-shaped samples is apparent at the reinforcing index of 474 similar to the slabs.

2. Regarding beam-column joint strength and deformation characteristics:

    a. For ECC-PVA or ECC-PE beam-column joint, with no lateral steel hoops in the joint zone, a noticeable increase in ultimate load, moment and shear capacity, ductility and damage tolerance was observed compared to the designed normal concrete joint (NC2).

    b. All the PVA and PE joints comply with the ACI 352R-02 provisions of Type 2 joint. The λ value for PVA joints ranged from 1.01 to 1.36 while for PE joints ranged from 1.05 to 1.67.

5.3 Recommendations for future research

In this study, several main objectives were addressed. However, some recommendations are proposed for research candidature such as:

1. Analytical model by using finite element analysis is the essential supplementary work for the third stage experimental work is required to find an approach for evaluating the experimental results of ECC exterior beam-column joints.

2. The third stage of project should be conducted on the ECC interior beam-column due to the great importance of this kind of joint in the frame structures.

3. Using hybrid of polymeric fibers of PVA and PE in stage 1 and 2 of the project with different volume ratios and find the best ratios which present ECC achieving the main definition of strain hardening. The production of hybrid ECC may present promising results of ECC characteristics and cost effective aspect.

REFERENCES

352R-02, A.-. (2002). Recommendations for Design of Beam-Column Connections in Monolithic Reinforced Concrete Structures *Joint ACI-ASCE Committee 352*. United States of Amareca: American Concrete Institute, ACI 352.

Alva, G. M. S., El Debs, A. L. H. C., & El Debs, M. K. (2007). An experimental study on cyclic behaviour of reinforced concrete connections. *Canadian Journal of Civil Engineering, 34*, 565-575.

B/525 Technical Committee, B. a. c. e. s. (1997). British Standard for the design and construction of reinforced and prestressed concrete structures. *BS 8110*. United Kingdom: Standards Board BSI.

Bakir, P. G., & Boduroglu, H. M. (2002). A new design equation for predicting the joint shear strength of monotonically loaded exterior beam-column joints. *Engineering Structures, 24*(8), 1105-1117.

Bakir, P. G., & Boduroglu, M. H. (2002). *Parametric studies on cyclically loaded exterior beam-column joints*. Paper presented at the Proceedings of the Sixth International Conference on Computational Structures Technology, Stirlingshire, Scotland, UK.

Balaguru, P., Narahari, R., & Patel, M. (1992). Flexural toughness of steel fiber reinforced concrete. *ACI Materials Journal., 89*(6), 541-546.

Banthia, N., & Trottier, J. F. (1995). Test methods for flexural toughness characterization of fiber reinforced concrete: some concerns and a proportion. *ACI Materials Journal., 92*(1), 48-56.

Batson, G., Jenkins, E., & Spatney, R. (1972). Steel fibers as shear reinforcement in beams. *American Concrete Institute Journal & Proceedings, 69*(10), 640-645.

Bayasi, Z., & Gebman, M. (2002). Reduction of Lateral Reinforcement in Seismic Beam-Column Connection via Application of Steel Fibers. *ACI Structural Journal, 99*(6).

Bedirhanoglu, I., Ilki, A., Pujol, S., & Kumbasa, N. (2010). Behavior of deficient joints with plain bars and low-strength concrete. *ACI Structural Journal, 107*(3), 300-310.

Bonacci, J. F., Alcocer, S. M., Cagley, J. R., LaFave, J. M., Paultre, P., Criswell, M. E., . . . Wyllie, L. A. J. (2002). Recommendations for Design of Beam-Column Connections in Monolithic Reinforced Concrete Structures: American Concrete Institute, ACI 352R-02.

C1018, A. (1997). Standard test method for flexural toughness and first-crack strength of fiber reinforced concrete *ASTM C1018, Standards for Concrete and Mineral Aggregates* (Vol. 04.02, pp. 528-535). United States: American Society for Testing Materials, ASTM.

Case, J., & Chilver, A. H. (1971). *Strength of materials and structures*. London: Edward Arnold.

Chen, C.-C., Suswanto, B., & Lin, Y.-J. (2009). Behavior and strength of steel reinforced concrete beam–column joints with single-side force inputs. *Journal of Constructional Steel Research, 65*(8-9), 1569–1581.

Chen, Z., Yang, Y., & Yao, Y. (2013). Quasi-static and dynamic compressive mechanical properties of engineered cementitious composite incorporating ground granulated blast furnace slag. *Materials and Design, 44*, 500-508.

Cheung, P. C., Pauiay, T., & Park, R. (1993). Behaviour of beam-column joints in seismically-loaded RC frames *The Structural Engineer*, *71*(8), 129-138.

Chutarat, N., & Aboutaha, R. S. (2003). Cyclic response of exterior reinforced concrete beam-column joints reinforced with headed bars— experimental investigation. *ACI Structural Journal, 100*(2), 259-264.

Craig, R. J., Mahadev, S., Patel, C. C., Viteri, M., & Kertesz, C. (1984). Behavior of joints using reinforced fibrous concrete. *ACI Special Publication, 81*, 125-168.

Engindeniz, M. (2008). *Repair and strengthening of pre-1970 reinforced concrete corner beam-column jointsusing CFRP composites.* (PhD), Georgia Institute of Technology, UMI dessertation publishing.

Fanella, D. A., & Naaman, A. E. (1985). Stress-strain properties of fiber reinforced mortar in compression. *ACI Journal Proceedings, 82*(4), 475-483.

Filiatrault, A., Ladicani, K., & Massicotte, B. (1994). Seismic Performance of Code-Designed Fiber-Reinforced Concrete Joints. *ACI structural Journal, 91*(5), 564-571.

Fischer, G., & Li, V. C. (2002). Effect of matrix ductility on deformation behaviour of steel reinforced ECC flexural members under reversed cyclic loading conditions. *" ACI structural Journal., 99*(6), 781-790.

Fischer, G., & Li, V. C. (2003). Deformation behavior of fiber-reinforced polymer reinforced engineered cementitious composite (ECC) flexural members under reversed cyclic loading conditions. *ACI Structural Journal., 100*(1), 25-35.

Fischer, G., Wang, S., & Li, V. C. (2003, October 13-15). *Design of Engineered Cementitious Composites (ECC) for processing and workability requirements.* Paper presented at the Proceedings of International Symposium on Brittle Matrix Composites 7, Warsaw, Poland.

Fujii, S., & Morita, S. (1991). Comparison Between Interior and Exterior R/C Beam-Column Joint Behavior. *ACI Special Publication, 123*, 145-166.

Ganesan, N., Indira, P. V., & Abraham, R. (2007). Steel fiber reinforced high performance concrete beam-column joints subjected to cyclic loading. *Journal of Earthquake Technology, technical Note, 44*(3-4), 445-456.

Ganesan, N., Indira, P. V., & Sabeena, M. V. (2014). Behaviour of hybrid fiber reinforced concrete beam–column joints under reverse cyclic loads. *Materials & Design, 54*, 686-693. doi: 10.1016/j.matdes.2013.08.076

GençOğlu, M., & Eren, I. (2002). An experimental study on the effect of steel fiber reinforced concrete on the behavior of the exterior beam-column joints subjected to reversal cyclic loading. *Turkish Journal of Engineering and Environmental Sciences, 26*, 493-502.

Ha, G.-J., Kim, J.-K., & Ching, L. (1992). Response of reinforced high-strength concrete beam-column joints under load reversals. *Magazine of Concrete Research, 44*(160), 175-184.

Hanson, N. W., & Connor, H. W. (1967). Seismic resistance of RC beam-column joints. *Journal of the structural division, ASCE, 93*(5), 533.

Hegger, J., Sherif, A., & Roeser, W. (2003). Nonseismic design of beam-column joints. *ACI Structural Journal, 100*(5), 654-664.

Hemmati, A., Kheyroddin, A., Sharbatdar, M., Park, Y., & Abolmaali, A. (2016). Ductile behavior of high performance fiber reinforced cementitious composite (HPFRCC) frames. *Construction and Building Materials, 115*, 681–689.

Henager, C. H. (1977). *Steel Fibrous, Ductile Concrete Joints for Seismic-Resistant Structures*. Paper presented at the Symposium on Reinforced Concrete Structures in Seismic Zones, San Francisco, 1974.

Hwang, S. J., & Lee, H. J. (1999). Analytical Model for Predicting Shear Strengths of Exterior Reinforced Concrete Beam-Column Joints for Seismic Resistance. *ACI Structural Journal, 96*(5), 846-858.

Hwang, S. J., Lee, H. J., Liao, T. F., Wang, K. C., & Tsai, H. H. (2005). Role of Hoops on Shear Strength of Reinforced Concrete Beam-Column Joints. *ACI structural journal, 102*(3), 445-453.

Jiuru, T., Chaobin, H., Kaijian, Y., & Youngcheng, Y. (1992). Seismic behavior and shear strength of framed joint using steel-fiber reinforced concrete. *Journal of Structural Engineering, ASCE, 118*(2), 341-358.

Kamada, T., & Li, V. C. (2000). The effects of surface preparation on the fracture behavior of ECC/concrete repair system. *Cement & concrete composites, 22*, 423-431.

Kim, Y. Y., Li, V. C., & Kong, H. J. (2003, 16-18 June, 2003). *Development of sprayable engineered cementitious composites.* Paper presented at the 4th International Workshop High Performance Fiber Reinforced Cement Composites, Ann Arbor, Michigan, USA.

Kong, H. J., Bike, S. G., & Li, V. C. (2003a). Constitutive rheological control to develop a self-consolidating engineered cementitious composite reinforced with hydrophilic poly(vinyl alcohol) fibers. *Cement & Concrete Composites, 25*(3), 333-341.

Kong, H. J., Bike, S. G., & Li, V. C. (2003b). Development of a self-consolidating engineered cementitious composite employing electrosteric dispersion/stabilization. *Cement and Concrete Composites, 25*(3), 301-309.

Kotsovou, G., & Mouzakis, H. (2012). Exterior RC beam–column joints: New design approach. *Engineering Structures, 41*, 307–319.

Krenchel, H., & Stang, H. (1989). *Stable microcracking in cementitious materials.* Paper presented at the Proceedings 2nd international symposium on brittle matrix composites (BMC-2), Cedzyna, Poland.

Kuang, J. S., & Wong, H. F. (2006). Effects of beam bar anchorage on beam–column joint behaviour. *Proceedings of the institution of civil engineers, ICE- Structures & Buildings, 159*, 115-124.

Kuang, J. S., & Wong, H. F. (2011). Effectiveness of Horizontal Stirrups in Joint Core for Exterior Beam-Column Joints with Nonseismic Design. *Procedia Engineering, 14*, 3301–3307.

Lee, H.-J., & Yu, S.-Y. (2009). Cyclic response of exterior beam-column joints with different anchorage methods. *ACI Structural Journal, 106*(3), 329-339.

Li, B., & Kulkarni, S. A. (2010). Seismic Behavior of Reinforced Concrete Exterior Wide Beam-Column Joints. *Journal of Structural Engineering , ASCE, 136*(1), 26-36.

Li, M., & Li, V. C. (2006). Behavior of ECC/ concrete layered repair system under drying shrinkage conditions. *Restoration of Buildings and Monuments, 12*(2), 143-160.

Li, M., & Li, V. C. (2012). Rheology, Fiber Dispersion, and Robust Properties of Engineered Cementitious Composites. *Materials and Structures, 46*(3), 405-420.

Li, V. C. (1993). From Micromechanics to Structural Engineering – The Design of Cementitious Composites forCivil Engineering Applications. *Structural Engineering and Earthquake engineering, Japan Society of Civil Engineers, 10*(2), 37-48.

Li, V. C. (1998). Engineered cementitious composites for structural applications. *Journal of materials in civil engineering, ASCE, 10*(2), 66-69.

Li, V. C. (2002). Advances in ECC research. *Material Science to Application- A Tribute to Surendra P. Shah* (Vol. SP-206, pp. 373-400): ACI Bookstore.

Li, V. C. (2003). On engineered cementitious composites (ECC). A review of the material and its applications *Journal of Advanced Concrete Technology 1*(3), 215-230.

Li, V. C. (2006). Bendable concrete minimizes cracking and fracture problems. *Technology Advances, MRS Bulletin.* (Vol. 31, pp. 862). MRS Bulletin.

Li, V. C. (2008). Engineered cementitious composites (ECC) – material, structural, and durability performance *Concrete Construction Engineering Handbook*: CRC Press.

Li, V. C., & Kanda, T. (1998.). Engineered cementitious composites for structural applications. *Innovations Forum in ASCE J. Materials in Civil Engineering, 10*(2), 66-69.

Li, V. C., & Wang, S. (2002). Flexural behaviors of glass fiber-reinforced polymer (GFRP) reinforced engineered cementitious composite beams. *ACI Materials Journal-American Concrete Institute., 99*(1), 11-21.

Liao, W. C., Chao, S. H., Park, S. Y., & Naaman, A. E. (2007, 10-13 July). *Self-consolidating high performance fiber reinforced concrete: SCHPFRC* Paper presented at the Fifth International Workshop on High Performance Fiber Reinforced Cement Composites (HPFRCC 5) Mainz, Germany.

M.D. Lepech, & V.C. Li. (2008). Large scale processing of Engineered Cementitious Composite. *ACI Materials Journal., 105*, 358-366.

Maalej, M., & Li, V. C. (1994). Flexural Strength of Fiber Cementitious Composites. *Journal of materials in civil engineering, ASCE, 6*(3), 390-406

Maalej, M., & Li, V. C. (1995). Introduction of strain-hardening engineered cementitious composites in design of reinforced concrete flexural members for improved durability. *ACI Structural Journal., 92*(2), 167-176.

Mady, M., El-Ragaby, A., & El-Salakawy, E. (2011). Seismic Behavior of Beam-Column Joints Reinforced with GFRP Bars and Stirrups. *Journal of Copmosites for Construction, 15*(6), 875-886.

Mady, M., Hasaballa, M., El-Ragaby, A., & El-Salakawy, E. (2011). *Effect of Reinforcement Detailing on the Behavior of GFRP-RC Beam-Column Joints*. Paper presented at the Advances in FRP Composites in Civil Engineering. Proceedings of the 5th International Conference on FRP Composites in Civil Engineering (CICE 2010), Beijing, China.

Megget, L. M., & Park, R. (1971). Reinforced concrete exterior beam-column joints under seismic loading. *New zealand Engineering, 26*(11), 341-353.

Merriam, G., Merriam, C., & Webster, N. (2015). *Merriam-Webster Dictionary*: Encyclopædia Britannica Online. .

Minard, A. (2009). Bendable concrete heals itself-just add water. National Geographic News. National Geographic. from http://news.nationalgeographic.com/news/2009/5/090505-self-healing-concrete.html

Mishra, D., K. (1995). *Design of pseudo strain-hardening cementitious composites for a ductile plastic hinge.* (Ph.D PhD thesis), University of Michigan, Michigan. (9527701)

Murty, C. V. R., Rai, D. C., Bajpai, K. K., & Jain, S. K. (2003). Effectiveness of Reinforcement Details in Exterior Reinforced Concrete Beam-Column Joints for Earthquake Resistance. *ACI Structural Journal, 100*(2), 149-156.

Naaman, A. E. (1985). Fiber reinforcement for concrete. *Concrete International, 7*(3), 21-25.

Naaman, A. E. (2007, 10-11 December). *High performance fiber reinforced cement composites: classification and applications.* Paper presented at the Cement Based Materials and Civil Infrastructure, NED University of Engineering and Technoloigy, Karachi, Pakistan.

Naaman, A. E., & Reinhardt, H. W. (1996). *Characterization of High Performance Fiber Reinforced Cement Composites—HPFRCC*. Paper presented at the High

Performance Fiber Reinforced Cement Composites 2 (HPFRCC 2), Proceedings of the Second International RILEM Workshop, Cachan Cedex, France.

Neela, S. (2010). *Flexural behaviour of balast FRB bar reinforced concrete members with and witout polypropylene fiber*. (MSC MSC thesis), Akron, Akron, Ohaio, USA.

NZS3101, C. D. C. P. f. t. S. C. (2006). New Zealand Concrete Structures Standard. *The Design of Concrete Structures.* New Zealand: Standards New Zealand.

Pakotiprapha, B., Pama, R. P., & Lee, S. L. (1974). Mechanical properties of cement mortar with randomly oriented short steel wires. *Magazine of Concrete Research, 26*(86), 3-15.

Pan, J. L., Yuan, F., Luo, M., & Leung, K. Y. (2012). Effect of composition on flexural behavior of engineered cementitious composites. *Science China Technological Science., 55*(12), 3425-3433.

Park, S. (2010). *Experimental and Analytical Studies on Old Reinforced Concrete Buildings with Seismically Vulnerable Beam-Column Joints* (PhD), University of California, Berkeley UMI dessertation publishing.

Park, S., & Mosalam, K. M. (2010). *Analytical and experimental study on RC exterior beam-column joints without transverse reinforcement* Paper presented at the 5th International Conference on Earthquake Engineering (5ICEE), Tokyo Institute of Technology, Tokyo, Japan.

Park, S., & Mosalam, K. M. (2012). Analytical Model for Predicting Shear Strength of Unreinforced Exterior Beam-Column Joints. *ACI Structural Journal, 109*(2), 149-159.

Parker, D. E., & Bullman, P. H. M. (1997). Shear strength within reinforced concrete beam-column joints. *The Structural Engineer, 75*(4), 53-57.

Parra-Montesinos, G., & Wight, J. K. (2000). Seismic response of exterior RC column-to-steel beam connections. *Journal of Structural Engineering, ASCE, 126*(10), 1113-1121.

Perumal, P., & Thanukumari, B. (2011). Behavior of M_{60} concrete using fiber cocktail in exterior beam-column joint under reversed cyclic loading. *Asian Journal of Civil Engineering (Buildind and Housing). 12*(2), 255-265.

Qudah, S., & Maalej, M. (2014). Application of Engineered Cementitious Composites (ECC) in interior beam–column connections for enhanced seismic resistance. *Engineering Structures, 69*, 235-245.

Rajagopalan, K., Parmeswaran, V. S., & Ramaswamy, G. S. (1974). Strength of SFRC beams. *Indian Concrete Journal, 48*(1), 17-25.

Rathod, J. D., Mistry, A. R., & Patodi, S. C. (2010). A comprehensive study of mechanical properties of steel fiber reinforced ECC. *international journal of earth sciences and engineering, 3*(3), 302-311.

Reinhardt, H. W., Krüger, M., & Große, C. U. (2003). Concrete prestressed with textile fabric. *Journal of Advanced Concrete Technology, 1*(3), 231-239.

Sarsam, K. F., & Al-Azzawi, Z. M. K. (2010). Shear capacity of high-strength fiber reinforced concrete beam-column joints. *Engineering & Technology Journal, 28*(6), 1253-1266.

Sarsam, K. F., & Phipps, M. E. (1985). The shear design of in situ reinforced concrete beam-column joints subjected to monotonic loading. *Magazine of Concrete Research, 37*(130), 16-28.

Shakya, K., Watanabe, K., Matsumoto, K., & Niwa, J. (2012). Application of steel fibers in beam–column joints of rigid-framed railway bridges to reduce longitudinal and shear rebars. *Construction and Building Materials, 27*, 482-489.

Shao, Y., & Shah, S. P. (1997). Mechanical properties of PVA fiber reinforced cement composites fabricated by extrusion processing. *ACI Materials Journal, 94*(6), 555-564.

Singh, S. P., Singh, A. P., & Bajaj, V. (2010). Strength and flexural toughness of concrete reinforced with steel-polypropylene hybrid fibers. *Asian Journal of Civil Engineering (Building and Housing), 11*(4), 495-507.

Sood, V. K., & Gupta, S. P. (1987). Behavior of steel fibrous concrete beam-column connections. *ACI Special Publication, 105*, 437-474.

Sravana, P., Rao, P. S., & Sekhar, T. S. (2010). *Flexural behaviour of glass fiber reinforced self compacting concrete slabs.* Paper presented at the 35th "coral" Anniversary Conference on Our World in Concrete & Structures., Singapore.

Sutoyo, D. (2009). *Hysteretic characteristics of wood-frame structures under seismic motions.* (Ph.D), California Institute of Technology, USA.

Swaddiwudhipong, S., Lu, H. R., & Wee, T., J. (2003). Direct tension test and tensile strain capacity of concrete at early age. *Cement and Concrete Research, 33*(12), 2077–2084.

Swamy, R. N., Mangat, P. S., & Rao, C. V. S. K. (1974). The mechanism of fiber reinforcement of cement matrices. *Fiber Reinforced Concrete, American Concrete Institute, SP-44*, 1-28.

Thamilselvi, P. D. (2012). Behaviour of Exterior Beam Column Joints using SIFCON. *International Journal of Engineering Research & Technology (IJERT), 1*(5).

Tsonos, A. G., Tegos, I. A., & Penelis, G. G. (1992). Seismic Resistance of Type 2 Exterior Beam-Column Joints Reinforced with Inclined Bars *ACI Structural Journal, 89*(1), 3-12.

Wallace, J. W. (1997). Headed reinforcement a viable option. *Concrete International, 19*(12), 47-53.

Wallace, J. W., Mcconnell, S. W., Gupta, P., & Cote, P. A. (1998). Use of headed reinforcement in beam-column joints subjected to earthquake loads. *ACI structural journal, 95*(5), 590-606.

Wang, S., & Li, V. C. (2003, June 16-18, 2003). *Lightweight engineered cementitious composites (ECC).* Paper presented at the 4th International Workshop on High Performance Fiber Reinforced Cement Composites, Ann Arbor, Michigan, USA.

Ward, R. J., & Li, V. C. (1991). Dependence of flexural behaviour of fiber reinforced mortar on material fracture resistance and beam size. *Construction & building materials journal., 5*(3), 151-160.

Wong, H. F., & Kuang, J. S. (2008). Effects of beam–column depth ratio on joint seismic behaviour. *Proceedings of the institution of civil engineers, ICE- Structures & Buildings, 161*, 91-101.

Yuan, F., Pan, J., Xu, Z., & Leung, C. K. Y. (2013). A comparison of engineered cementitious composites versus normal concrete in beam-column joints under reversed cyclic loading. *Materials and Structures, 46*(1-2), 145-159.

Yurdakul, O., Avşar, O., & Kilinç, K. (2013). Application of Different Rehabilitation and Strengthening Methods for Insufficient RC Beam-Column Joints. *Advanced Materials Research, 688*, 222-229.

Zhang, R., Matsumoto, K., Hirata, T., Ishizeki, Y., & Niwa, J. (2015). Application of PP-ECC in beam–column joint connections of rigid-framed railway bridges to reduce transverse reinforcements. *Engineering Structures, 86*, 146-156.

Zheng, W., Kwan, A. K. H., & Lee, P. K. K. (2001). Direct Tension Test of Concrete. *ACI Materials Journal, 98*(1), 63-71.

APPENDICES

Appendix A: Structural analysis of beam-column joint

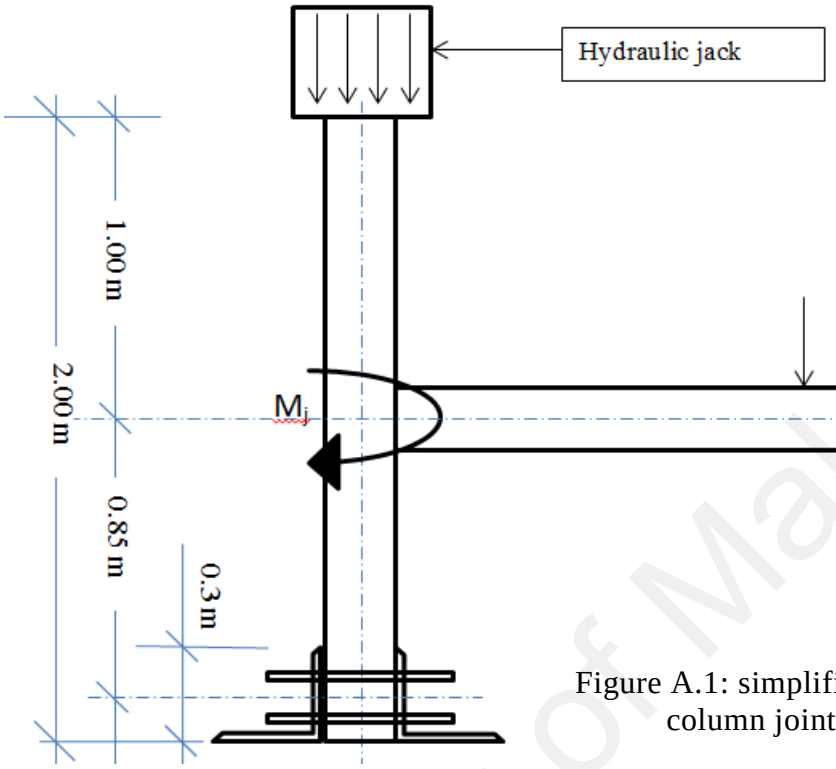

Figure A.1: simplified diagram of beam-column joint under loading

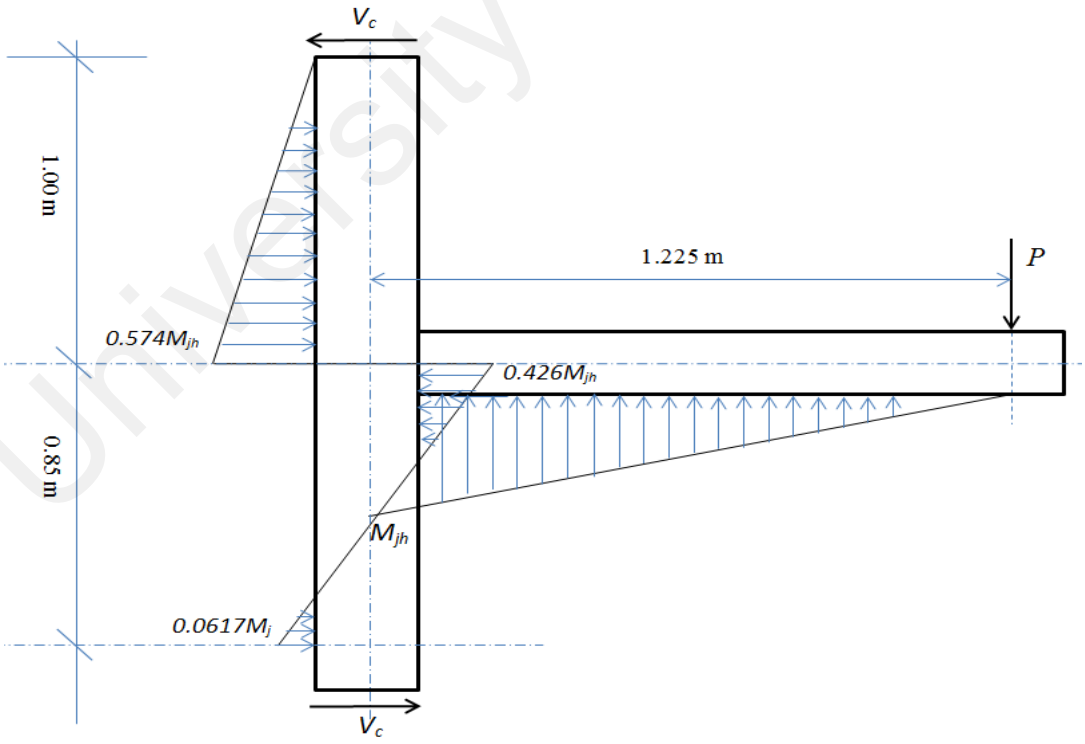

Figure A.2: Free body diagram of beam-column joint and load distribution

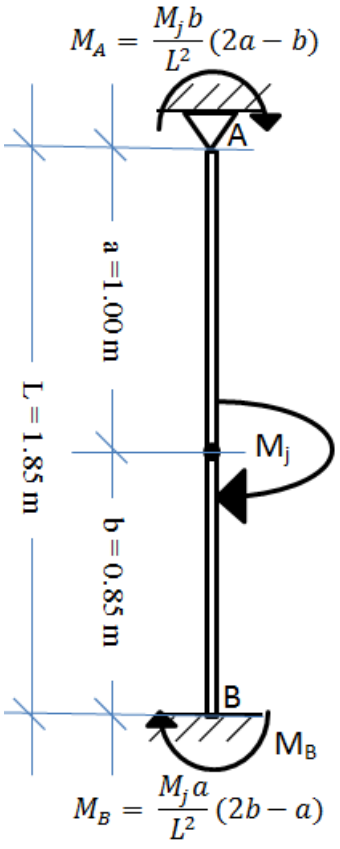

$$M_A = \frac{M_j b}{L^2}(2a - b)$$

$$M_A = 0.2856 M_j$$

$$M_B = \frac{M_j a}{L^2}(2b - a)$$

$$M_B = 0.2045 M_j$$

Figure A.3: Free body diagram of column and moment values at the inflection points

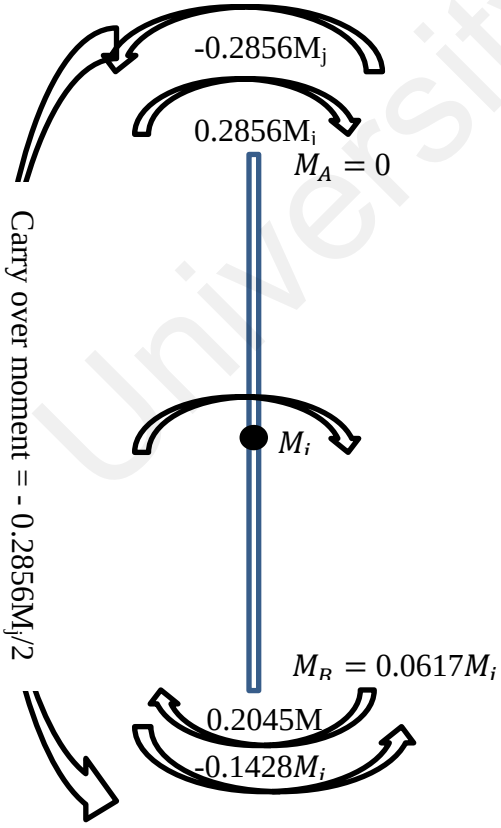

∵ Point A is hinge

∴ M_A should be equal to zero

A moment equals to $0.2856 M_j$ and in opposite direction to moment M_A should be added in point A

Figure A.4: Moment distribution analysis for beam-column joint

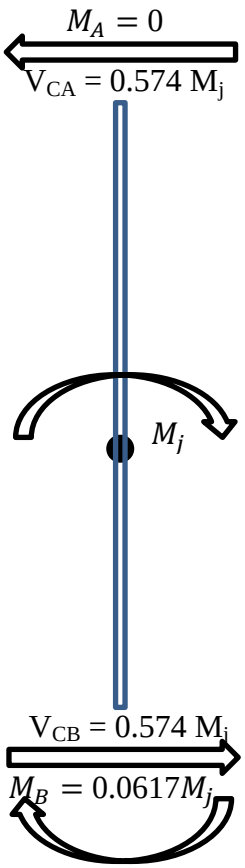

$V_{CA} = V_{CB} = 0.574 M_j$

$M_B = 0.0617 M_j$

Figure A.5: Final result for moment distribution analysis

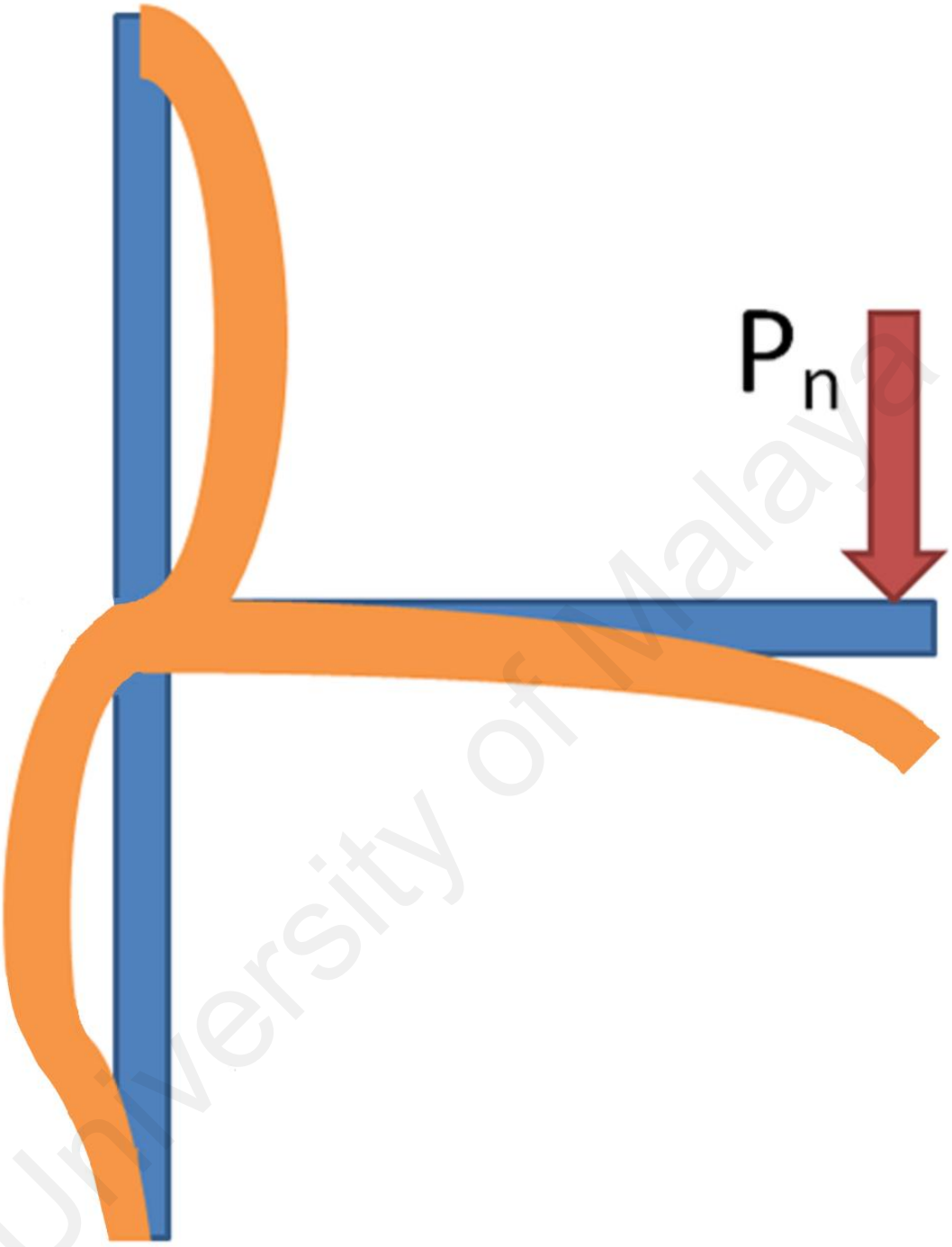

Figure A.6: Deformed shape of beam-column specimen

Appendix B: Determination of fiber diameter

Denier (d): Is defined as the mass in grams per 9000 meters.

1 denier = 1 gram per 9000 meters

1 denier = 1000 milligrams (mg) per 9000 m

1 denier = 0.1111 mg/m

$\emptyset$ is the diameter of fiber ($\boldsymbol{\mu}$m)

ρ is the specific gravity of the fiber

$$\emptyset = \sqrt{\frac{444.4 * d}{\pi * \rho}}$$

Dtex (dx): Is defined as the mass in grams per 9000 meters.

1 dtex = 1 gram per 10000 meters

1 dtex = 1000 milligrams (mg) per 10000 m

1 dtex = 0.1 mg/m

$$\emptyset = \sqrt{\frac{400 * dx}{\pi * \rho}}$$

Table B.1: Determination of fiber diameter for different polymer fibers

Type of fiber	Grade of fiber	Denier, d dpf	Specific gravity	Dtex, dx	Diameter. $\emptyset$ $\boldsymbol{\mu}$m
PVA	RECS15	-	1.3	15	38
PP	Mono-Tuf	15	0.91	-	48
PE	4800D	10	0.97	-	38
PE	1600D	4	0.97	-	24

Appendix C: Properties of materials and reinforcement in beam-column specimens

Table C.1: Mechanical properties of NC, ECC and reinforcement spacing in beam-column specimens

S	Specimen	$f_c^{'}$ MPa	E_c MPa	Main reinforcement	Stirrups in beam	Ties in column	Lateral steel hoops inclusion
1	NC_1	53.44	35	(2Ø16 + 1Ø12) at top and bottom	Ø10@100 c.c	Ø10@100 c.c	-
2	NC_2	56.56	37		Ø10@50 c.c	Ø10@50 c.c	4Ø10
3	PVA_1	61.12	25.5	(2Ø16 + 1Ø12) at top and bottom	Ø10@100 c.c	Ø10@100 c.c	-
4	PVA_2	60.21	24.5				-
5	PVA_3	57.35	25				-
6	PVA_4	55.61	22.4				-
7	PVA_5	58.22	26.3				1Ø10
8	PVA_6	62.02	24.7				2Ø10
9	PE_1	64.64	31				-
10	PE_2	63.88	27				-
11	PE_3	60.68	25.9				-
12	PE_4	61.29	23.5				-
13	PE_5	62.67	28.2				1Ø10
14	PE_6	58.82	25.8				2Ø10

Table C.2: Mechanical properties of longitudinal steel bars used in beam-column specimens

bars diameter Ø	Yield strength f_y MPa	Tensile strength MPa	E_s GPa
16	544	680	
12	504	628	200000
10	505	623	

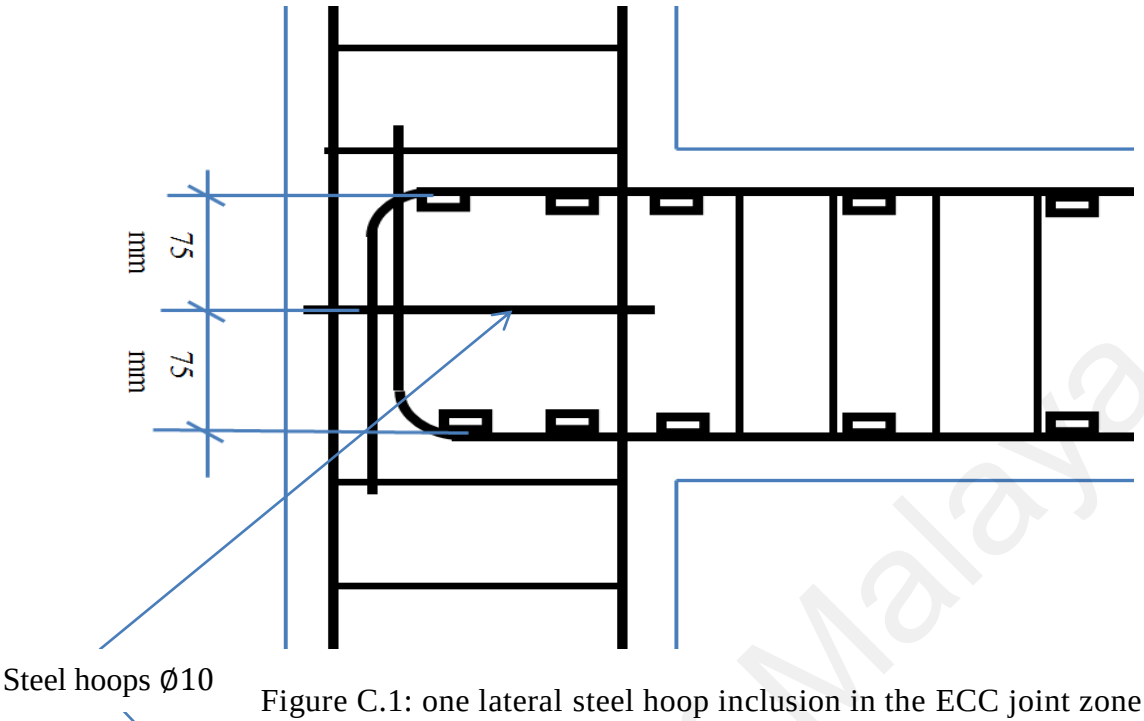

Figure C.1: one lateral steel hoop inclusion in the ECC joint zone

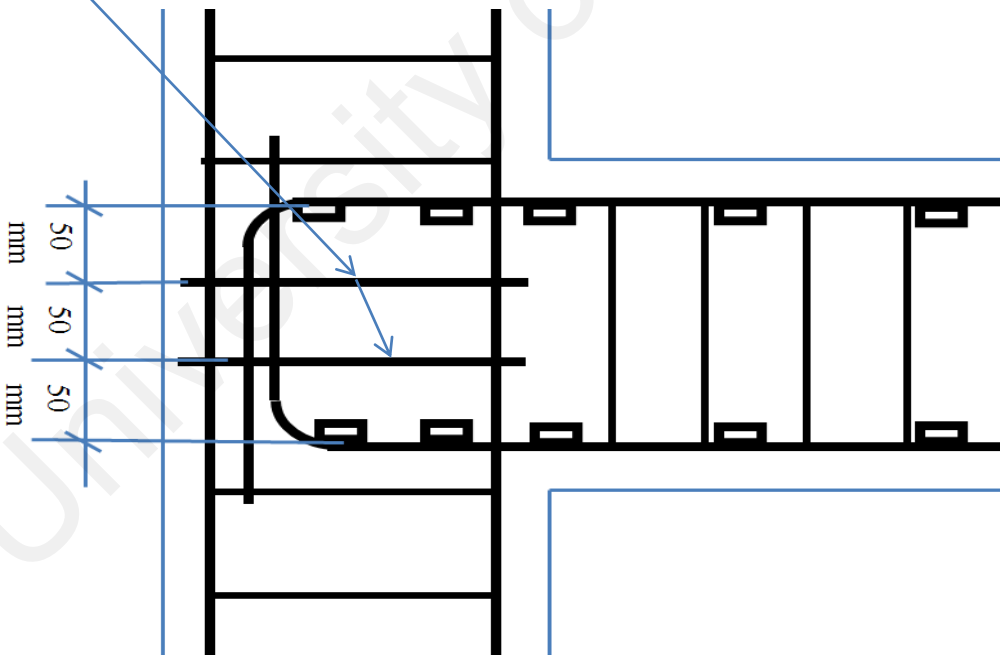

Figure C.2: Two lateral steel hoops inclusion in the ECC joint zone

Appendix D: Determination of principal strains and shear deformation angle

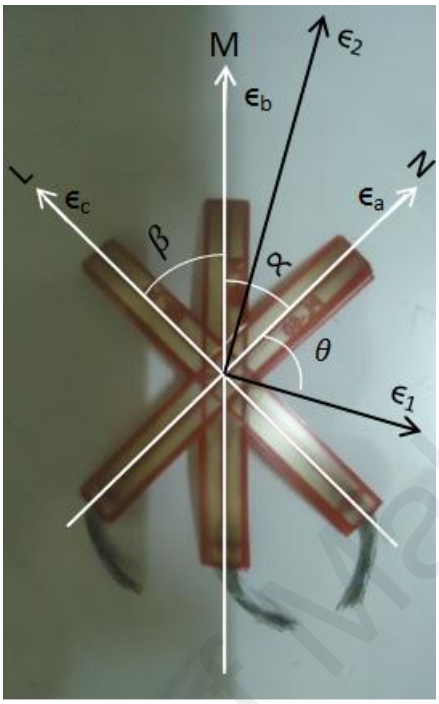

Figure D.1: Principal strains in a two-dimensional system

D.1 Principal strains

ϵ_1 and ϵ_2 are the principal strains in a two-dimensional system, as shown in Figure D.1. The following equation is applicable for the system above.

$$\epsilon = \frac{1}{2}(\epsilon_1 + \epsilon_2) + \frac{1}{2}(\epsilon_1 - \epsilon_2)\cos 2\theta \qquad \text{Equation D.1}$$

We have the direct strains ϵ_a, ϵ_b, ϵ_c in directions inclined at θ, $(\theta + \propto)$ and $(\theta + \propto + \beta)$ to ϵ_1 are:

$$\epsilon_a = = \frac{1}{2}(\epsilon_1 + \epsilon_2) + \frac{1}{2}(\epsilon_1 - \epsilon_2)\cos 2\theta$$

$$\epsilon_b = = \frac{1}{2}(\epsilon_1 + \epsilon_2) + \frac{1}{2}(\epsilon_1 - \epsilon_2)\cos 2(\theta + \propto)$$

$$\epsilon_b = = \frac{1}{2}(\epsilon_1 + \epsilon_2) + \frac{1}{2}(\epsilon_1 - \epsilon_2)\cos 2(\theta + \propto + \beta)$$

Equations D.2

In the experimental test, we have a rosette strain gauge of $\propto = \beta = 45^o$, as shown in Figure D.1, equations D2 become:

$$\epsilon_a = = \frac{1}{2}(\epsilon_1 + \epsilon_2) + \frac{1}{2}(\epsilon_1 - \epsilon_2)\cos 2\theta$$

$$\epsilon_b = = \frac{1}{2}(\epsilon_1 + \epsilon_2) - \frac{1}{2}(\epsilon_1 - \epsilon_2)\sin 2\theta$$

$$\epsilon_b = = \frac{1}{2}(\epsilon_1 + \epsilon_2) - \frac{1}{2}(\epsilon_1 - \epsilon_2)\cos 2\theta$$

By eliminating θ from the equations above, ϵ_1 and ϵ_2 will be the roots of the following equation:

$$\epsilon^2 - (\epsilon_a + \epsilon_c)\,\epsilon + [\epsilon_a\epsilon_c - \frac{1}{4}(2\epsilon_b - \epsilon_a - \epsilon_c)^2] = 0$$

where

$$\epsilon_1 \text{ and } \epsilon_2 = 0.5\,(\epsilon_a + \epsilon_c) \pm \sqrt{(\frac{\epsilon_a + \epsilon_c}{2})^2 - [\epsilon_a\epsilon_c - \frac{1}{4}(2\epsilon_b - \epsilon_a - \epsilon_c)^2]}$$

D.2 Shear deformation angle

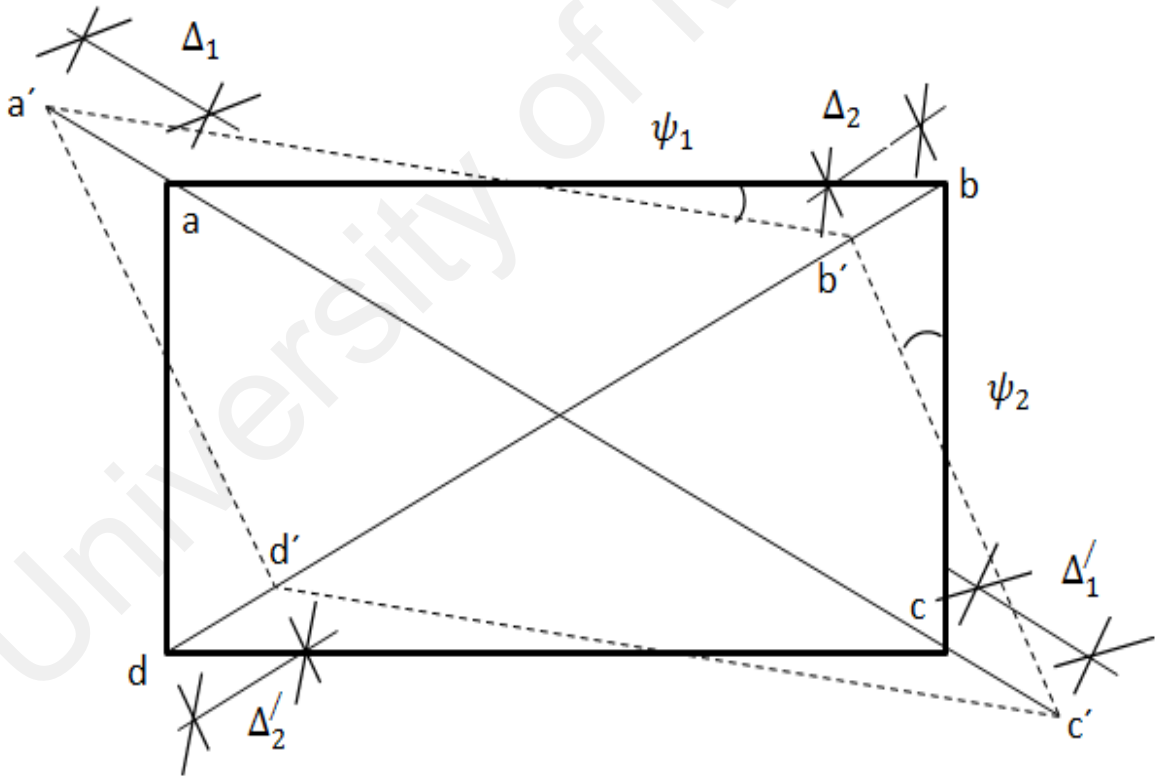

Figure D.2: Shear deformation in beam-column joint

From the triangles, as in Figure D.2, we have the following relation

$$\tan(\psi_1) = \frac{|\Delta_1^{/} + \Delta_2^{/}| * \sin(\phi)}{2(dc)} + \frac{|\Delta_1 + \Delta_2| * \sin(\phi)}{2(dc)}$$

From small angle theory will get:

$$\tan(\psi_1) = \psi_1$$

$$\psi_1 = \frac{|\Delta_1^{/} + \Delta_2^{/}| * \frac{bc}{bd}}{2(dc)} + \frac{|\Delta_1 + \Delta_2| * \frac{bc}{bd}}{2(dc)}$$

$$\psi_1 = \frac{|\Delta_1 + \Delta_1^{/}| * (\mathrm{bc})}{2(dc)(ac)} + \frac{\left|\Delta_2 + \Delta_2^{/}\right| * (\mathrm{bc})}{2(dc)(bd)}$$

$$\epsilon_{ac} = \frac{|\Delta_1 + \Delta_1^{/}|}{(ac)} \quad , \quad \epsilon_{bd} = \frac{|\Delta_2 + \Delta_2^{/}|}{(bd)}$$

$$\psi_1 = \epsilon_{ac} \frac{bc}{2dc} + \epsilon_{bd} \frac{bc}{2dc}$$

$$\psi_1 = (\epsilon_{ac} + \epsilon_{bd}) \frac{bc}{2dc}$$

For ψ_2, the equation will be as follows:

$$tan\ (\psi_2) = \frac{|\Delta_1^{/} + \Delta_2| * \sin(\beta)}{2(bc)} + \frac{\left|\Delta_1 + \Delta_2^{/}\right| * \sin(\beta)}{2(bc)}$$

From small angle theory will get:

$$\tan(\psi_2) = \psi_2$$

Following the same procedure above to determine ψ_2 will get:

$$\psi_2 = (\epsilon_{ac} + \epsilon_{bd}) \frac{dc}{2bc}$$

$$\gamma_{sh} = \psi_1 + \psi_2 = (\epsilon_{ac} + \epsilon_{bd}) \frac{bc}{2dc} + (\epsilon_{ac} + \epsilon_{bd}) \frac{dc}{2bc}$$

$$\gamma_{sh} = (\epsilon_{ac} + \epsilon_{bd})\left(\frac{bc}{2dc} + \frac{dc}{2bc}\right)$$

$$\gamma_{sh} = \left(\frac{(ab)^2 + (bc)^2}{2(ab)(bc)}\right)(\epsilon_{ac} + \epsilon_{bd}) \qquad \text{Equation D.3}$$

Appendix E: Published papers

1. Said, S. H., & Razak, H. A. (2016). Structural behavior of RC engineered cementitious composite (ECC) exterior beam–column joints under reversed cyclic loading. *Construction and Building Materials, 107*, 226–234.

2. Said, S. H., & Razak, H. A. (2015). The effect of synthetic polyethylene fiber on the strain hardening behavior of engineered cementitious composite (ECC). *Materials and Design, 86*, 447-457.

3. Said, S.H., Razak, H. A., & Othman, I. (2015). Strength and deformation characteristics of engineered cementitious composite slabs with different polymer fibers. *Journal of Reinforced Plastics and Composites, 34*(23), 1950-1962. doi:10.1177/0731684415607393

4. Said, S. H., Razak, H. A., & Othman, I. (2015). Flexural behavior of engineered cementitious composite (ECC) slabs with polyvinyl alcohol fibers. *Construction and Building Materials, 75*, 176-188.